UNIVERSITY OF STRATHCLYDE

DEPARTMENT OF CIVIL ENGINEERING

Influence of desiccation fissuring on the stability of flood embankments

by

Marcin Zieliński

A thesis presented
in fulfilment of the requirements
for the degree of Doctor of Philosophy

2009

This thesis is the result of the author's original research. It has been composed by the author and has not been previously submitted for examination which has led to the award of a degree.

Glasgow, 2009-09-29

Signed: 

This Thesis is dedicated to my mother and my brother.

ABSTRACT

It has been known since studies carried out by Cooling and Marsland for the 1953 North Sea Floods that desiccation fissuring of clay fill can play a major role in the failure of flood embankments under overflow conditions. However, very little scientific research has been carried out into the onset of desiccation fissuring in flood embankments and the potential failure mechanisms. To overcome this shortage of information, field and laboratory studies have been carried out into the desiccation fissuring of clay fill for flood embankments. The preliminary results confirmed that desiccation fissuring occurs to a depth of typically 60 cm within the outer surface of a flood embankment constructed from clay fill and can occur within 2 years of construction. The critical condition occurs when desiccation creates an interconnected network of sub-vertical and sub-horizontal fissures that increases the mass permeability of the fill material similar to that of coarse sand or gravel and hence allows rapid seepage of flood water through the surface layer of the embankment (crest and sides slopes).

The aim of the thesis is to investigate the influence of desiccation fissuring on the stability of flood embankments. In particular, the main objectives of this thesis are as follows:

1. Survey of flood embankments in UK constructed from clay fill to determine the extent and nature of desiccation fissuring.
2. Construction and investigation of the behaviour of macro-scale embankment model subjected to desiccation processes.
3. Investigation of the innovative, non-invasive geophysical technique for desiccation cracking detection.
4. Investigation of the embankment model behaviour under different flooding conditions.

ACKNOWLEDGEMENTS

First and foremost I would like to thank my supervisor Dr. Philippe Sentenac for his support, interest and enthusiasm for my research. Without his guidance, assistance and freedom he gave me during the period of this work I would not have been able to produce the thesis in its present form. I am most grateful that the work I have carried out with him will be of great benefit for my future career in geotechnical engineering.

I would also like to thank Prof Mark Dyer for his supervision at the University of Strathclyde. Special thanks go to Dr. Marcelo Sanchez at the University of Strathclyde for his financial support to carry out a specific study at the UPC, Barcelona and Dr. Enrique Romero at the UPC, Barcelona for his comments and assistance.

The research presented in this thesis was funded by Flood Risk Management Consortium (FRMRC), EPSRC (grant GR/S76304/01) and scholarship from the Faculty of Engineering at the University of Strathclyde. I would also like to thank Delta-T (UK) for their technical support during my study. The funding and collaboration of all parties is gratefully acknowledged.

Special thanks go to my friends in the Department: Gráinne, Harald, Gerry, Gavin, Andrzej, Daniela, David, John, Derek, Marco, Antonio and Urs for making my time special. With special thanks to Gráinne for her advice and for raising very detailed problems at all the time.

To my family, my mother and brother: thank you very much for your endless support and encouragement.

TABLE OF CONTENTS

TABLE OF FIGURES

TABLE OF TABLES

THESIS LAYOUT

Presented thesis is divided in two parts: (i) Part 1 – Scientific background and field studies; (ii) Part 2 – Laboratory studies and physical modelling. Both parts of presented research consist of the following chapters: Part 1 – Chapter 1 to Chapter 3, Part 2 – Chapter 4 to Chapter 8. In the four remaining chapters, discussion, conclusions, remedial measures and the future work are discussed.

In **Chapter 1** as an introduction, the current scientific understanding of the stability of flood defences is presented. This is followed by the overview of the failure mechanisms observed in the past and historical background of the failures that were related to desiccation fissuring.

In **Chapter 2** the importance of soil suction in desiccation cracking is discussed. In order to provide a better understanding of the nature of desiccation cracking and its propagation, the state variables for saturated and unsaturated soil mechanics are described. Direct and in-direct measurements as well as generation of soil suction are presented in order to understand their importance in soil mechanics.

Chapter 3 presents results from field investigations in UK which were undertaken during this research. A detailed survey, carried out in 2006 for two embankments (historic and newly constructed) at Humber Estuary in Thorngumbald is described. Findings and results are then compared with these carried out by Dyer (2005) and described by Cooling and Marsland after North Sea Flood in 1953.

In **Chapter 4** a short description of the soil origin used in this research is followed by detailed investigation of soil properties used for construction of the macro-scale embankment model. The methodology that was implemented for the state-of-the-art embankment model construction is explained. Finally, the characteristic of the environmental chamber that was constructed above embankment model is presented.

Chapter 5 describes the capabilities and technical specifications of different sensors (moisture content probes, tensiometers, Relative Humidity & temperature sensor,

rain gauge, miniature resistivity array) and measuring techniques that were used in presented research.

In **Chapter 6** an innovative non-invasive geophysical method that was used for detection of desiccation cracking is described. The few case studies that can be found in the literature are reviewed. Pilot studies are presented in order to investigate and present the capabilities of the miniature resistivity array. The preliminary results show that presented and implemented method can be used for cracking detection.

Chapter 7 describes the methodology and the experimental procedure which was used in the first phase of the experiment. The desiccation sequence was carried out in three separate procedures in order to investigate the embankment behaviour under different weather conditions:

- one weekly precipitation and drying of the embankment model at constant temperature (carried out for 6 weeks);
- two weekly precipitations and drying of the embankment model at constant temperature (carried out for 4 weeks);
- extremely dry conditions at constant temperature without precipitation (carried out for 5 weeks).

In **Chapter 8** the flooding experiment (second phase), is described. This experiment was carried out in order to investigate behaviour of the desiccation cracked embankment subjected to flooding conditions. Experimental results showed that internal seepage through the rubbilised zone was taking place. This is in the good agreement with the findings presented by Marsland and Cooling (1958). It was also found, that the embankment can be still resilient to flood loadings even when it is highly and deeply fissured.

Chapter 9 provides discussion about the outcomes that have been gained from this research.

In **Chapter 10** it is proposed to use one of the remedial methods in order to prevent embankments from desiccation fissuring and to remediate embankments which are already cracked.

Chapter 11 summaries the main conclusions reached in the previous chapters and gives recommendations for future research.

In **Chapter 12** recommendations for future work are given.

PUBLICATIONS

A part of this thesis has led to three journal publications four conference papers and four research reports.

Journal publication I: Zielinski, M., Sentenac, P., McCloskey, G., Dyer, M., (2009) Desiccation cracking detection using resistivity array. Under review. ICE Proceedings. Geotechnical Engineering, GE-D-09-00068.

Journal publication II: Dyer, M.R., Utili, S., Zielinski, M., (2009). Field study into fine desiccation fissuring at Thorngumbald. ICE Proceedings. Water Management. June 2009, Issue WM3, pp. 221-232.

Journal publication III: Sentenac, P., Zielinski, M., (2009),Clay fine fissuring monitoring using miniature geo-electrical resistivity arrays. Journal of Environmental Geology. DOI:10.1007/s12665-009-0017-5 online.

The journal publications are appended at the end of this thesis. The full list of the publications (journal, conference and research reports) is presented in Chapter 14.

Another two journal papers are planned to be published in Journal of Geotechnical and Geoenvironmental Engineering (ASCE) and ICE Proceedings - Geotechnical Engineering.

INTRODUCTION

There are some 35 000 km of estuarine and river flood embankment in the UK with an annual budget of approximately £30 million spent on the maintenance and new construction (NADNAC, 2004). The majority of these flood embankments are located in England and Wales and constructed using traditional methods over the last century or more, and the effective performance of these embankments during extreme flood events is critical for sustainable flood management. In practice the construction of flood embankments can be highly variable across the country and prone to deterioration for a number of reasons such as (a) desiccation fissuring (b) animal infestation (c) surface erosion and d) long term settlement. The tendency for earth embankments to deteriorate with time is of particular concern because climate change and the increasing occurrence of extreme flood events along with the effects from dryer summers and wetter winters are expected to impose a greater hydraulic load on the flood embankments.

One of the deterioration processes known to have an adverse effect on the stability of flood defences is desiccation fissuring. Early work by Cooling and Marsland (1954) for the 1953 North Sea Flood identified desiccation fissuring a major contributory case for embankment collapse. This conclusion was corroborated in more recent work by Dyer and Gardener (1996) and Dyer et al. (2009). Based on this, presented research was undertaken to improve technical understanding about the onset and adverse effects caused by desiccation fissuring and how better that could be managed.

The results from field observations showed that desiccation fissuring occurs to a depth of typically 60 cm within the outer surface of a flood embankment constructed from clay fill and can occur within 2 years of construction. In some other cases it has been seen that cracking can penetrate embankments to a depth of 1 m. The critical condition occurs when desiccation creates an interconnected network of sub-vertical and sub-horizontal fissures that increases the mass permeability of the fill material to

that of coarse sand or gravel and hence allows rapid seepage of flood water through the surface layer of the embankment (crest and side slopes).

Instead of leading to an increase of pore water with a corresponding reduction of effective stress as proposed by Marsland and Cooling (1954), high rates of seepage can potentially lead to localised erosion of the upper rubbilised zone and internal erosion of the embankment (Dyer et al., 2009).

The laboratory work presented in this study consisted of investigating the soil properties used for the construction of the embankment model, the measurements of soil moisture content and suction profiles, the investigation of Soil Water Characteristic Curve, a geophysical survey and visual observation of the onset of desiccation cracking.

This study has also assessed the resilience of the embankment made of stiff clay ("Boulder clay"), subjected to the seepage and overflow conditions.

This experimental research had the aim to investigate the behaviour and performance of laboratory embankment. Hence, it may or may not represent field behaviour.

OBJECTIVES

As stated before, these studies were divided into two parts and the objectives for both parts are presented below.

In particular the main objectives of the first part of this research were as follows:

- Survey of two flood embankments (historical and new) in Thorngumbald constructed from clay fill to determine the extent and nature of desiccation fissuring.
- Survey of 9 desiccation cracked embankments in UK constructed or reconstructed from different clay fills.

The second part of the project, which is mainly based on the laboratory studies, examined the effects of fine fissuring of clay fills on the geotechnical stability and breach initiation of flood embankments on the macro-scaled embankment model constructed in the laboratory and subjected to different weather conditions. It also introduced an innovative non-invasive geophysical technique for desiccation cracking detection.

In particular, this laboratory study had the following objectives:

- monitoring of the extent of fine fissuring on the examined embankment model using visual observation,
- measuring changes in moisture content profile during: dry, wet and extremely dry conditions,
- measuring changes in suction profile during: dry, wet and extremely dry conditions,
- investigating Soil Water Characteristic Curve for given soil and comparing the results obtained from four different measuring and empirical methods,
- investigating a non-invasive geophysical method for cracking initiation and detection,
- investigating the use of soil instrumentation to detect the extent of desiccation fissuring,

- monitoring the behaviour of fissured embankment model under flooding conditions using visual observation and geophysics,
- monitoring failure of the embankment subjected to overtopping conditions using visual observation with suction and moisture content measurements.

In addition to these objectives, remedial measures are proposed in order to minimise the extent of fissuring.

PART 1- SCIENTIFIC BACKGROUND AND FIELD STUDIES

CHAPTER 1

1. CURRENT SCIENTIFIC UNDERSTANDING

1.1. STABILITY OF FLOOD EMBANKMENTS

1.1.1. INTRODUCTION

Flood embankments essentially act as low-level dams for short retention periods. For the majority of the time, the embankments are only exposed to low hydraulic heads and remain largely unsaturated. However, during flood events embankments need to withstand a rapid rise in water level on the outward face, along with the corresponding changes to internal water pressure (and potential seepage) driven by the higher hydraulic gradients. The increase in head on the embankment may be further exaggerated by low head overtopping, and even the use of temporary flood barriers on the crest of the embankment.

The main purpose of fluvial and estuarial flood embankments is to constrain and direct the passage of floodwater along a river valley or estuary. This may occur in a river channel where the bank carrying capacity of a river channel has been enhanced through the construction of flood embankments along both banks.

1.1.2. OVERVIEW OF THE TYPES OF FLOOD EMBANKMENTS AND FILL MATERIALS

There are several variations of flood embankments. A detailed review is given in the report by HR Wallingford (2004) on "Reducing the risk of embankment failure under extreme conditions". In some cases the flood capacity of a river channel is enhanced further by the construction of flood embankments set back from the river channel to incorporate part of the floodplain to form a so-called two-staged channel. There are

also perched river channels, where the flood capacity has been enhanced through the construction of flood embankments along both banks and the water level permanently remains higher than local ground level. This occurs where river channels and flood embankments have been progressively raised over long periods and/or settlement has taken place such as in the Fens of East Anglia caused by consolidation of underlying peat stratum. Another variation is a flood-retention reservoir constructed for flood attenuation as well as in some cases water supply, recreation and power generation. These reservoirs are constructed to retain water typically behind an impermeable barrier, which is similar to a flood embankment.

Having identified the different types of flood embankments that can exist, the principal form of flood embankment is shown in Figure 1.1. The main features include (a) an embankment body that provides the mass obstruction against flood water, (b) the toe of the embankment on both the outward or inward embankment faces, (c) the inward face of the embankment exposed directly to water, (d) the outward face on the landward side not normally directly exposed to flood water, (e) the crest at the top of the embankment that is typically flat and (ideally) several metres wide, (f) a drainage ditch also known as a 'soke' or 'delph' ditch excavated close to the inward toe of the embankment, (g) surface protection sometimes termed revetment in the form of vegetation (e.g. grass), manmade material (e.g. concrete) or a combination of different materials. The drainage ditches known as 'soke' ditches or 'delph' ditches are used to drain any seepage and control water levels through the embankment.

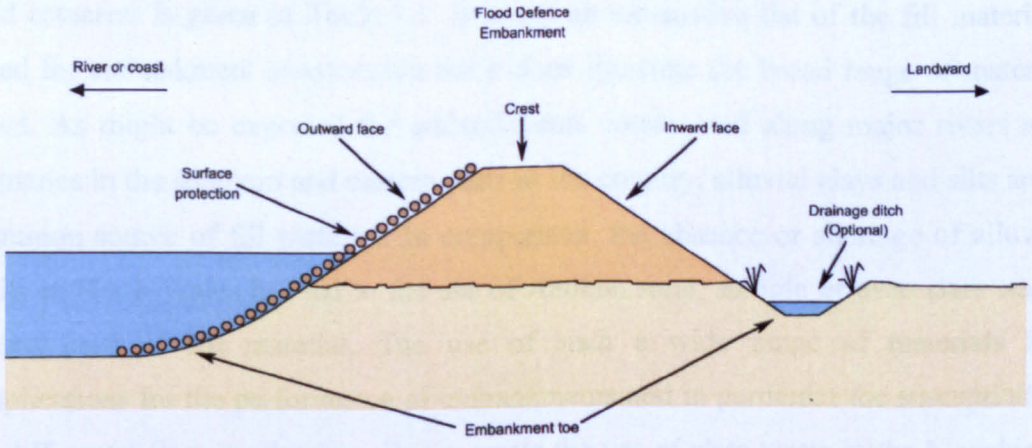

Figure 1.1 Typical flood embankment (after HR-Wallingford, 2004).

Accurately predicting the performance of flood embankments and understanding potential breach initiation mechanisms under these extremes in loading is difficult. This is further compounded by the long lengths of flood embankment that exist to protect rivers, estuaries and coastlines which make a comprehensive condition assessment of all embankments logistically difficult to implement. Nevertheless knowledge about the type of fill material used to construct embankments and the method of the construction does allow the performance of the embankment to be analysed using principles of soil mechanics and engineering geology.

Many embankments are relatively old structures that have evolved over decades or even centuries from original constructions. In contrast with the modern construction of embankments for highway and dam projects using heavy earth compaction equipment, many flood embankments have been built using low cost traditional techniques. These traditional methods have often evolved to suit local sources of fill material, which have been excavated from surface deposits or retrieved from river sediments. As a result, the construction of flood embankments can be highly variable across the country, which can affect the performance and potential failure mechanism for embankments.

A review of traditional earthwork materials used to construct flood embankments (Dyer and Gardener, 1996) found a wide range of soils and rocks used as fill material depending on the local geology and particularly the superficial deposits. A list of the earthwork materials used to construct flood embankments along several major rivers and estuaries is given in Table 1.1. It is not an exhaustive list of the fill materials used for embankment construction but it does illustrate the broad range of material used. As might be expected for embankments constructed along major rivers and estuaries in the southern and eastern parts of the country, alluvial clays and silts are a common source of fill material. In comparison, the absence or shortage of alluvial soils in North Wales has led to the use of Aeolian sand, shingle or even slate waste being used as fill material. The use of such a wide range of materials has implications for the performance of embankments and in particular the susceptibility to different failure mechanism. For example the use of slate waste in the Mawddach

estuary has resulted in high seepage rates through flood embankments with the risk of piping failure. Likewise the use of sand and shingle for the construction of flood embankments at several other estuaries along the west coast of Wales has resulted in high seepage rates that cause flooding of adjacent roads. In contrast the use of highly plastic clays in the Anglian Region has led to fine fissuring, which has increased internal seepage and reduced resistance to erosion from overtopping. Apart from local geology, other waste materials used as sources of fill material include colliery spoil, demolition material and blast furnace slag.

Table 1.1 Typical earthwork materials used for flood embankment construction in England and Wales (HR-W 2004 and Dyer 2005).

Region	**Typical Earthwork Materials**
Anglian	
Ouse Washes &Forty Foot Drain	Kimmeridge Clay& Fluvial Sediments (Silts)
Thameside Marshes	London Clay /Thanet Sand/ Alluvium (Clays)/ Hoggin (Clayey Sand)
Southern	
R Ouse	Chalk & Alluvium (Silty Clay)
R Rosher	Wealden Clay & Alluvium (Silty Clay)
Midlands	
R Severn (Argae)	Alluvium (Silty Clay)
North West	
R Wyre (Preesall)	Morainic Drift
R Duddon (Haverigg)	Estuarine Alluvium (Sand)
R Gowy	Alluvium (Silt)
North East	
R Aire (Upper and Lower)	Alluvium
R Calder,	Alluvium
R Don/Dearne/Rother	Colliery Spoil & Alluvium (Silts, Clays)
Wales	
Borth Estuary	Peat
Mawddach Estuary	Slate Waste and Quarry
Porthmadog	Sand & Quarry Overburden
Dyssyni Estuary,	Sand and Shingle
Wentlooge Levels	Alluvium (Silty Clay)

In comparison modern flood embankments are typically constructed in layers using standard compaction specification (Specification for Highway Works – Earthworks, Series 6000). In cases where the fill material is considered to be too permeable, a less permeable core is incorporated into the construction. In practice, an impermeable core is not often used, even where highly permeable fill materials such as quarry

waste or sand is used (such as in North Wales). Nevertheless it would be feasible to design the core to prevent unacceptable internal seepage and inundation of water behind an embankment that could pose a threat to the long-term stability. For example, the core may be built from a more impervious local material, probably with higher clay content, or could be formed by steel sheet piling or construction of a concrete, asphaltic concrete or cement bentonite cut-off wall. In some situations (typically in the Netherlands, Germany and Denmark), sand embankments are protected by a layer of clay beneath the revetment surface layer. In effect, the embankment has a porous but stable core that is coated by an impermeable layer of clay and then protected by some form of surface layer such as vegetation.

Stability of the embankment may be enhanced through the use of geotextiles to provide longer-term surface protection, increased face stability or to provide temporary support whilst vegetation is established. Where embankments are being placed on soft ground or where the width of the base of the embankment is restricted by lack of space, alternative materials can be considered which may be either of lower density and/or of increased shear strength. This may simply be a question of providing reinforcement with geotextiles or geogrids to an embankment of otherwise traditional construction. However, lightweight materials such as polystyrene blocks or tyre bales can also be used with appropriate precautions (such as wrapping the new materials with heavy-duty impermeable membranes and / or careful consideration of internal drainage).

1.1.3. FAILURE MECHANISMS FOR FLOOD EMBANKMENTS AND HISTORICAL BACKGROUND

The unpredictable and violent nature of a breach means there is often little evidence available about the exact cause and mechanism that led to the catastrophic failure of an embankment. As a result, there is a shortage of well-documented case studies of embankment failures. Nevertheless a recent review of recorded flood embankment failure can be found in Dyer (2005).

One of the few notable studies of flood embankment failures is the paper on 1953 North Sea Floods by Cooling and Marsland (1954) with subsequent studies into the

role of fine fissuring on failure of embankments carried out later by Marsland and Cooling (1958) and Marsland and Randolph (1978). During the the North Sea floods in 1953 extensive damage to the coastal defences of the East Coast of the UK was caused by an abnormal tide surge. A series of investigations were carried out including field surveys and laboratory testing of the mechanical properties of the soil, where the most serious damage to embankments occurred. The majority of investigated embankments were located along the Thames estuary, which were built on soft marsh clay. The post-mortem investigation revealed that the embankments, where seepage failure of a different type occurred, were constructed of highly shrinkable soft clay (Cooling and Marsland, 1954). Further investigation showed that the type of material used for construction was strongly linked with those modes of failures which are related to a highly permeable outer layer of the embankment (Marsland 1957).

A second notable study worth mentioning is the failure of a flood embankment at Crayford Marshes due to hydraulic uplift pressures beneath the embankment done by Marsland and Randolph (1978), Hird et al. (1978) and later by Padfield and Schofield (1983). In the case of the North Sea floods, Cooling and Marsland (1954) reported that the remains of a breach were often just blocks of clay thrown some considerable distance away from the embankment, and in many cases the cause of failure was attributed to desiccation fissuring of the embankment that led to significant seepage of overflow flood water into the embankment. A late full-scale study carried out by Marsland and Cooling (1958) and Marsland (1968) showed that the seepage of flood water into the crest of the test embankment led subsequently to a progressive collapse of the back slope.

Although there are several geotechnical factors that can affect the performance of a flood embankment, the individual factors can be divided into two main groups depending on whether the hazard develops in the founding layers or the embankment itself. A simple guide to the range of hazards and risks that can occur is shown in Figure 1.2 taken from the Dutch Rijkswaterstaat (1990).

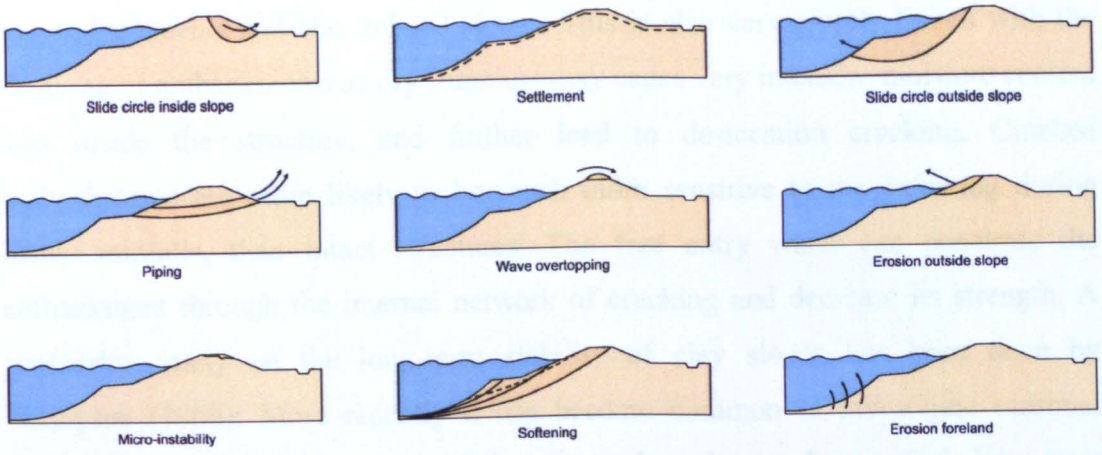

Figure 1.2 A selection of typical failure mechanisms (after TAW, 1990).

Figure 1.2 is based on a general understanding of geotechnical processes involved with embankment performance supported by case histories about embankment failures during the last 50 years, including the 1953 North Sea Floods. This assessment of the geotechnical factors affecting the performance of embankments shows that hazards stemming from the founding strata could potentially result in excessive settlement, deep seated slope instability, large scale lateral movement, excessive under seepage or hydraulic uplift pressures. In comparison, the hazards emanating from the embankment itself are identified as surface or toe erosion (outward and inward faces), excessive internal seepage and shallow slope instability. Some of these hazards are short term such as global instability due to construction on soft clays whilst others would be long term caused, for example, by fine fissuring resulting in excessive internal seepage, which would lead to potential internal erosion or instability of the inward face. This range of failure modes does not however consider the effects of deterioration such as desiccation fissuring (Konrad and Ayad, 1997; Stark and Hisham, 1997; Aubeny and Lytton, 2004 and Picarelli et al., 2006) or animal burrowing as well as surface instability of the outward face due to overtopping / overflow conditions.

Furthermore, it is also worth to mention another type of failure trigger, when the awareness about the infrastructure embankments is rising up due to the climate change. Global climate change will generate more extreme climate input conditions (and new long-term conditions for any given embankment, however old), (Hudacsek

et al., 2009). Seasonal weather variations will be causing irreversible changes within the embankments and clay related slopes. This is also very closely linked with the fissuring of embankments as dry summers may cause very intensive moisture content loss inside the structure, and further lead to desiccation cracking. Cracked embankments are more likely to be much more sensitive to the softening during heavy rainfalls, than intact structures. The free entry water can penetrate the embankment through the internal network of cracking and decrease its strength. A pioneering study on the long-term stability of clay slopes has been done by Skempton (1960). More recently it has become common to investigate seasonal changes in the moisture content of clay slopes in order to observe their long term behaviour (Take and Bolton, 2001; Take and Bolton, 2002; Smethurst et al., 2006; Hudacsek and Bransby, 2008; Zielinski et al., 2008).

Lastly, one of the causes of embankment failure is seepage of flood water through or under an embankment. In the worst case, this can lead to collapse and breach formation of the structure. This may be accompanied by overtopping, which of course increases the seepage flow. However, especially in its early stages, the volume of water lost from internal seepage is often relatively small and the problem is sometimes ignored. If left untreated, finer particles of soil will be washed out of the embankment or the embankment's foundation by the flow. Thus, the problem is one of progressive deterioration; as the soil becomes more permeable, the flow rates increase and as a result, more particles of soil are eroded. Seepage will also increase the likelihood of slip failure as a result of changes to the piezometric regime within the embankment, causing a softening of the fill materials or increasing the uplift pressures beneath an embankment toe. This is well illustrated in Figure 1.3. The first image of Figure 1.3 shows a steady state seepage through a uniform flood embankment of coarse grained fill. In the second image, it is possible to visualise the localised seepage through the desiccated clay fill. In the third image, it is shown seepage through animal burrow holes leading to erosion. Finally the last image shows seepage beneath the embankment itself through channels, lenses or strata of highly permeable soil that can lead to erosion and / or piping.

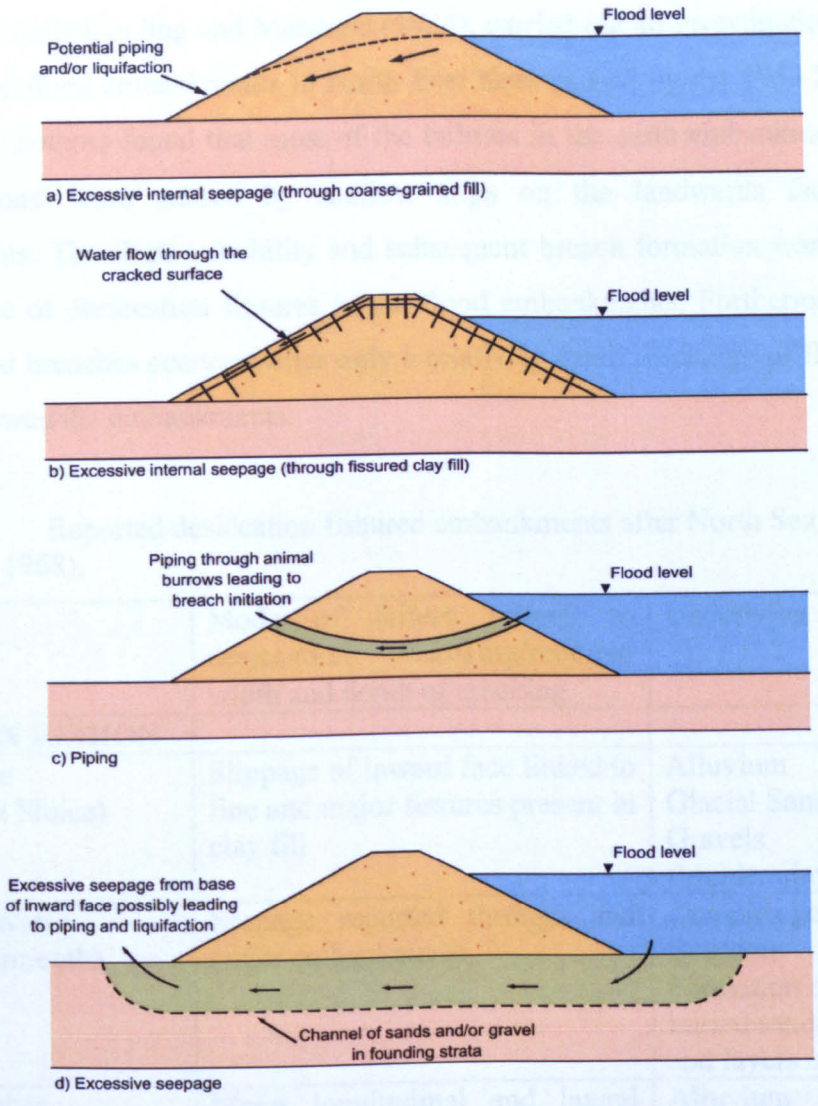

Figure 1.3 Seepage and piping through or under a flood embankment (modified from HR-Wallingford, 2004).

One of the factors that can lead to an increased likelihood of excessive internal seepage is the formation of fine desiccation fissures. This was highlighted in the early work by Cooling and Marsland (1954) and later studies by Marsland and Cooling (1958), Marsland (1968). These studies showed that the annual process of drying and wetting could transform the relatively homogeneous clay fill into a rubblised slope (Dyer et al., 2009). These fissures have the effect of increasing the permeability in a shallow zone beneath the surface of the crest and side slopes embankment.

In the 1953 study Cooling and Marsland (1954), carried out an investigation into the breaching of flood embankments in North East Kent caused by the 1953 North Sea Floods. The authors found that most of the failures in the earth embankments along the east coast were caused by shallow slips on the landwards face of the embankments. The slope instability and subsequent breach formation was linked to the presence of desiccation fissures in the flood embankments. Furthermore it was reported that breaches occurred after only a relatively small discharge of flood water had overflowed the embankments.

Table 1.2 Reported desiccation fissured embankments after North Sea Flood (Marsland, 1968).

Region	Mode of failure related to desiccation cracking/reported width and depth of cracking	Underlying Geology
ANGLIAN REGION		
River Alde (near Ham Sluice)	Slippage of inward face linked to fine and major fissures present in clay fill	Alluvium Glacial Sands and Gravels Boulder clay
Breydon Water (Great Yarmouth)	Seepage reported through and under embankments	Complex geology of Breydon Formation containing buried sand channels and layers of peat
Ouse Washes	Major longitudinal and lateral cracking of new embankment	Alluvium Peat
THAMES REGION		
Easington (East Yorkshire)	Washing away of the cracked upper layer with the exposition of intact clay core	No evidence
Crayford Marshes (Coryton, Essex)	Seepage through fissured zone followed by slippage of the outward face	Alluvium Peaty clay Brown silty clay Soft grey clay with bands of peat
East Tilbury (Essex)	No evidence about instability, widely fissured embankment (60-125 mm wide, 0.9-1.5 m depth),	Alluvium Marsh clay
Cabborns Farm, Stanford Lee Hope Marshes (Essex)	No evidence about stability, 50 mm wide cracks to a depth of 0.9-1.2 m	Alluvium Marsh clay

Benfleet to Hadleigh, (Essex)	Breached in several places, 12-20 mm wide cracks to a depth 0.3-0.6 m	Alluvium Marsh clay
Norpits, South side of the River Crouch, (Essex)	Severely breached, 38 mm wide cracks at the surface, 1.15 m deep	Alluvium Very soft to soft clay
Scrapsgate, Isle of Sheppey (Kent)	No evidence about instability, no cracks seen from the surface, extensive system of fine cracks revealed after trial trench excavation, 3-6 mm wide vertical cracks to a depth 1.1 m	Alluvium Marsh clay
Middle Stoke, Isle of Grain (Kent)	No evidence about instability, reported shrinkage cracking in the upper back slopes to a depth 1.1m	Very soft sticky silty clay
North Grain Wall, Isle of Grain (Kent)	Embankment very badly damaged during North Sea Flood (1953), rebuilt later in 1953, inspection of the clay in trench showed that upper clay was still intact, underlying clay was cracked to a depth of 1.4 m,	Alluvium

Table 1.2 presented above shows the evidence of fissured embankments that were reported after the North Sea Flood by Marsland (1968) during his study. It was found that desiccation fissuring often ran to a depth of 0.9 – 1.4m and in some cases transformed the upper layer of the embankment into a rubblised zone (highly fissured zone due to loss of moisture as a result of desiccation). In a rubblised zone, the permeability of the soil dramatically increases allowing water to seep through the structure without even reaching the crest of the embankment. Lumps of clay may form during desiccation, which can then be undercut by seeping water and washed away as the embankment erodes.

Figure 1.4 below shows a possible failure mechanism proposed by the authors in which the water level is not sufficient for overtopping, but seepage through the upper fissured zone initiates a slip in the landward face and eventually results in breaching.

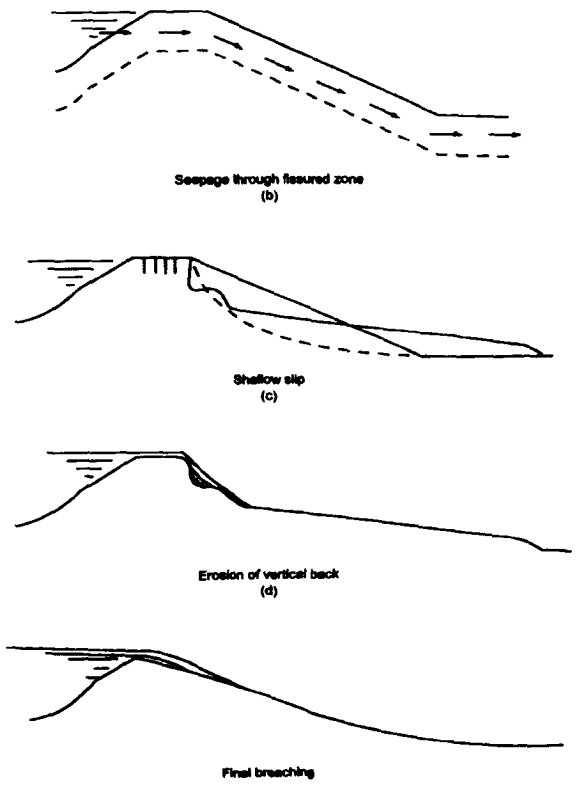

Figure 1.4 Development of a breach caused by fissuring (after Cooling and Marsland, 1954).

In the later full-scale cofferdam studies Marsland and Cooling (1958) and Marsland (1968) reported that flood water seeped directly into the desiccated crest of the flood embankment without reaching the back slope of the structure. This rapid ingress of flood water was followed within minutes by a progressive collapse of the back slope that lead to breach formation. The slope instability was attributed by the authors to a reduction in effective stress brought about by the ingress in flood water and corresponding increase in pore water pressure.

In these earlier studies the detrimental effects of desiccation fissuring was attributed to increase seepage during overflow condition with a corresponding increase in pore pressure that led to slope instability of the outward face. More recent soil studies by Dyer (2005) have suggested a different mode of failure. Instead of causing an increase in pore pressure, it is proposed that the network of shallow desiccation fissures allows a critical hydraulic head to be generated beneath the outward slope that led to the uplift of the desiccated blocks of rubblised fill material as shown in Figure 1.5. This alternative failure mode depends on hydraulic continuity between the embankment crest and outward slope to allow a critical hydraulic head to be

developed for uplift to take place. This kind of failure can take place only in the case, when the water is confined inside the cracking network with no outlet.

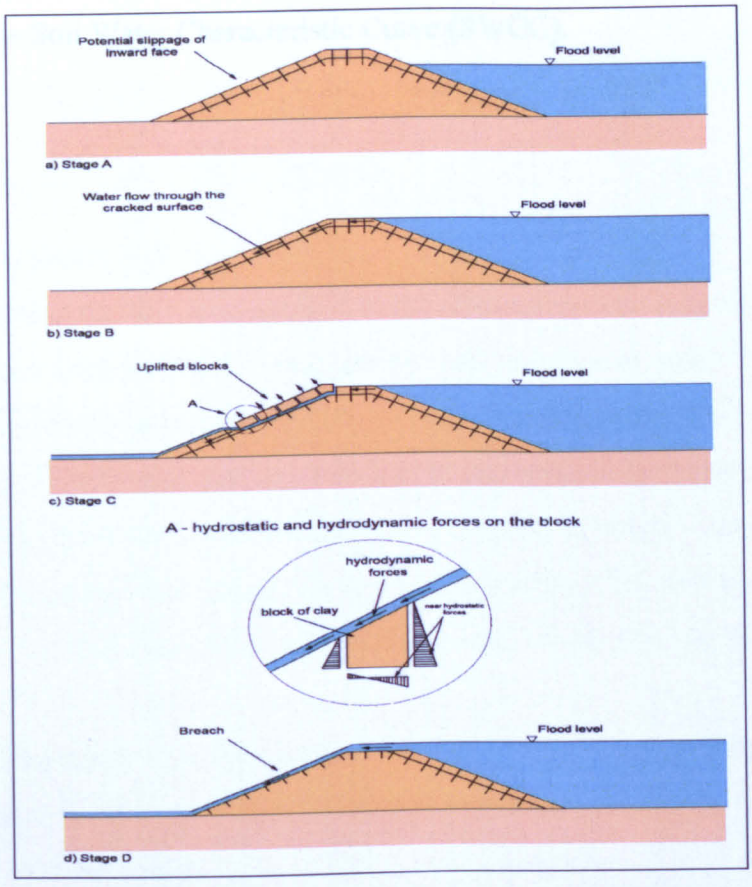

Figure 1.5 Proposed failure mechanism with breach formation of uplifted clay blocks (Dyer et al., 2009).

The dramatic failure events which occurred during of the North Sea Floods revealed how widespread desiccation fissuring is in clayey embankment structures in the UK. In summary fine desiccation fissuring has in the past been recognized as being one of the main cause of embankment breaching. In practice however, it can be difficult to detect desiccation fissuring, particularly if the surface vegetation is well developed. Even if cracking near the surface is observed, it will not be possible to determine the depth to which the cracking penetrates without careful excavation and inspection.

There is also very little scientific literature about the processes of fine fissuring and crack formation. It is not yet known quantitatively how different factors govern fissure growth, frequency, depth and orientation. As a first step towards developing a sound engineering understanding a review of desiccation cracking is presented in the next Chapter along with an introductory explanation of unsaturated soil mechanics.

An extensive literature survey about all available methods for measuring soil suction was carried out in order to highlight the most reliable tools that can be used for determining the Soil Water Characteristic Curve (SWCC).

CHAPTER 2

2. UNSATURATED SOIL MECHANICS AND DESICCATION FISSURING

2.1. BACKGROUND

In order to understand the development of the desiccation cracking with associated failures a basic background of unsaturated soil mechanics must be possessed. Unsaturated soils are mainly controlled by desiccation process. In particular, this process is governed by soil suction, which is dependent on the moisture within the soil through the soil water characteristic curve. Hence, the accurate prediction of the desiccation state of soil was needed. Thus, in recent years, it has become increasingly important for methods capable of measuring or controlling suction efficiently to be developed.

Soil is used extensively as a fill material (i.e. earth-works such as road, railway and flood embankments and earth dams) and the unsaturated condition of the fill will crucially affect its behaviour.

Although many of the soils encountered in geotechnical engineering practice are unsaturated, for example surface layers of natural deposits and all compacted earthworks, soil mechanics has developed with a bias towards the fully saturated state. This approach has been adopted because it is vastly easier to measure the properties of soils containing only one fluid phase (i.e. either air or water) than that of soils containing two fluid phases (i.e. both air and water). The primary justification for the assumption is that the approach usually is conservative. For instance, the shear strength of water saturated soil is lower than the shear strength of the same soil at the same voids ratio under unsaturated conditions. This is not necessarily the case for flood embankments where the earthworks are constructed with unsaturated soil and subsequently exposed to seasonal drying and wetting cycles as well as extreme hydraulic gradients imposed by flood events. This seasonal drying and wetting is known to lead to the formation of desiccation cracking and fine fissuring in clayey soils with a detrimental effect on the embankment stability.

2.2. STATE VARIABLES FOR SATURATED AND UNSATURATED SOIL MECHANICS

Within the framework of traditional soil mechanics the concept of effective stress plays a key role. In fact, effective stresses describe the state of stress acting on the soil skeleton. According to Terzaghi (1943), they are defined as:

$$\sigma'_{ij} = \sigma_{ij} - u_w \tag{2.1}$$

where σ_{ij} are the *total stresses*, u_w the *water pore pressure* and σ'_{ij} are the *effective stresses* acting in a point.

For unsaturated soils, the physical meaning of the effective stresses remains the same, but two additional factors must be considered: the stress acting through the air phase (i.e. the pore air pressure, u_a) and the difference between the pore air pressure and the pore water pressure, know in literature as matric suction. Therefore according to Bishop (1959), the Terzaghi's classic effective stress equation may be expanded as follows:

$$\sigma'_{ij} = (\sigma_{ij} - u_a) + \chi(u_a - u_w) \tag{2.2}$$

where the differences $(\sigma_{ij} - u_a)$ are referred as the *net normal stresses*, the difference $(u_a - u_w)$ is the *matric suction* and χ is a material variable which vary from zero to one referred as the *effective stress parameter*. When $\chi = 0$, the soil is completely dry ($u_a = 0$), when $\chi = 1$, the soil is fully saturated therefore Eq. (2.2) reduces to Terzaghi's classic effective stress equation for describing the behaviour of saturated soil (Eq. (2.1)).The material variable χ depends on the degree of pore water saturation S:

$$\chi = \chi(S) \tag{2.3}$$

or analogously on the soil moisture content. The effective stress parameter depends on the amount of water in the system. Figure 2.1 illustrates this dependency on saturation for several types of soils.

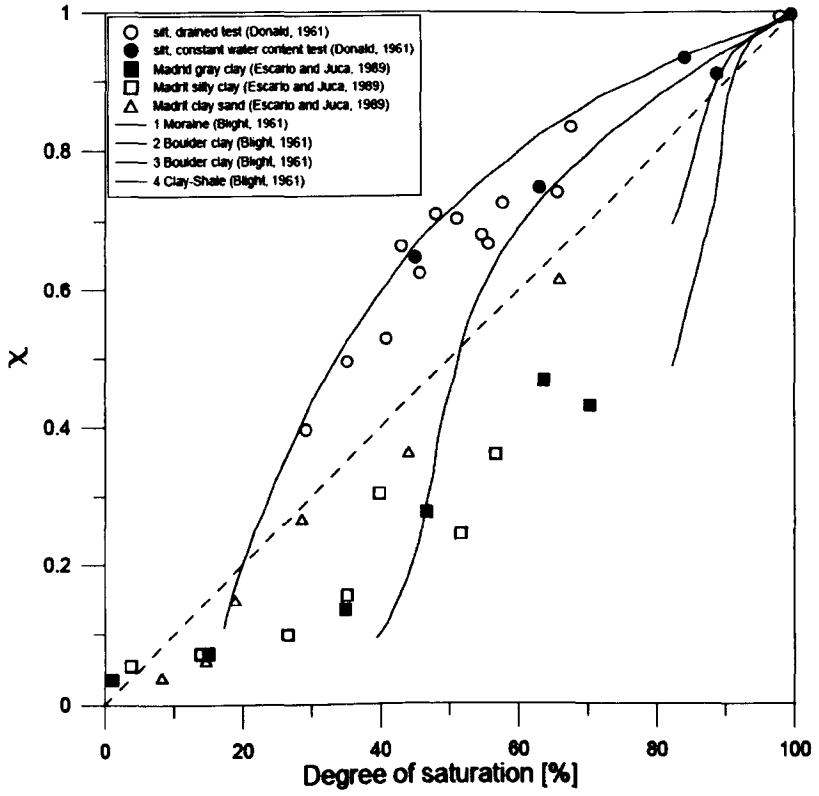

Figure 2.1 Experimental results showing the dependency of Bishop's effective stress parameter on the degree of saturation (after Lu & Likos, 2004).

Tests using Eq. (2.1) have shown that it can produce errors in the results (Jennings and Burland, 1962). Jennings and Burland (1962) appear to be the first to suggest that Bishop's equation did not provide an adequate relationship between volume change and effective stress for most soils, particularly those below a critical degree of saturation (estimated up to 85-90% for clays). They concluded that the factor χ must depend on the current stress and the stress history; hence it is not correlated only to the degree of saturation. Bishop's equation explains the shear strength behaviour but does not explain the volume change behaviour. This is explained by the apparent breakdown of the effective stress principle, as the parameter χ for volume yield differs from that causing shear yield (Coleman, 1962). Therefore Coleman (1962) suggested the use of net normal stresses (σ_{ij} - u_a) and matric suction (u_a-u_w) as stress variables to describe stress-strain relationships. Fredlund and Morgenstern (1977) considered the approach from both experimental and theoretical standpoints and formally proposed the use of net normal stress and matric suction as independent stress variables for unsaturated soil. Studies conducted over the past two

decades have demonstrated renewed interest in Bishop's effective stress approach, but the majority of constitutive models are based on the Fredlund and Morgenstern (1977) independent stress state variable approach. According to this approach, there is not one single effective stress equation for unsaturated soils but rather there exist two sets of stress state variables: $(\sigma_{ij} - u_a)$, net normal stresses and (u_a-u_w), matric suction, that form the most general and fundamental basis for the development of a science for unsaturated soil mechanics (Fredlund, 2006).

The two sets of stress state variables, given above, are the most commonly used with respect to engineering as the net normal stresses can be separated from the change in pore-water pressure. However there are other combinations of variables which could be used to describe the stress state of the soil. These are listed in the Table 2.1.

Table 2.1 Stress state variables for unsaturated soils (after Fredlund and Rahardjo, 1993).

Reference Pressure	Stress State Variables	Compressible phases
Air, u_a	$(\sigma_{ij} - u_a)$ and $(u_a - u_w)$	(u_a)
Water, u_w	$(\sigma_{ij} - u_w)$ and $(u_a - u_w)$	(u_w)
Total, σ	$(\sigma_{ij} - u_a)$ and $(\sigma_{ij} - u_w)$	(σ_{ij})

Therefore, the behaviour of unsaturated soil may be characterised in terms of the following state variables (Fredlund and Morgenstern, 1977):

(i) Total stress relative to the pore air pressure: σ

(ii) Matric Suction: ψ

(iii) Void ratio: e (or specific volume $v = 1 + e$)

where, the total stress is defined as a difference between effective stress σ_{ij} and pore air pressure u_a:

$$\sigma = (\sigma_{ij} - u_a) \tag{2.4}$$

Matric suction is described as a difference between the pore air pressure and pore water pressure,

$$\psi = (u_a - u_w) \tag{2.5}$$

and the void ratio is defined as the volume of voids in a mixture divided by the volume of solids:

$$e = \frac{V_V}{V_S} \tag{2.6}$$

Compression of an unsaturated soil can then take place either by changes in total stress, by changes in matric suction or by a combination of the two. Moreover, soil suction is an important factor in increasing the stresses in the soil to exceed the strength of the soil to initiate fissuring.

A subdivision of the total suction, ψ, of a soil, as proposed by Marshall (1958), is made up of two components, matric suction, (u_a-u_w), and the osmotic suction, π. The most recent version of the equation defining total suction is proposed by Fredlund (2006).

$$\psi = \psi_m + \psi_o \tag{2.7}$$

where the total suction is defined as the summation of matric suction, ψ_m, and osmotic suction ψ_o.

According to Aitchison (1965) total, matric, and osmotic suction may be also qualitatively defined as follows:

"Total suction or free energy of the soil water: In suction terms, it is the equivalent suction derived from the measurement of the partial pressure of the water vapour in equilibrium with a solution identical in composition with the soil water, relative to the partial pressure of water vapour in equilibrium with free pure water.

Matric or capillary components of free energy: In suction terms, it is the equivalent suction derived from the measurement of the partial pressure of the water vapour in equilibrium with the soil water, relative to the partial pressure of the water vapour in equilibrium with a solution identical in composition with the soil water.

Osmotic (or solute) components of free water: In suction terms, it is the equivalent suction derived from the measurement of the partial pressure of the water vapour in equilibrium with a solution identical in composition with the soil water, relative to the partial pressure of water vapour in equilibrium with free pure water."

The total suction of the soil is effect both of these components. Osmotic suction is more influential in unsaturated soils. However osmotic suction is due to the salt content in the pore-water so it is applicable in both saturated and unsaturated soils.

As such osmotic suctions are generally less significant than matric suction and less sensitive to changes in the soil water content, hence a change in matric suction is approximately equivalent to changes in total suction for both saturated and unsaturated soil. So for the fissured soils typical of flood embankments, matric suction is of more interest and the effect of osmotic suction can usually be ignored.

2.3. SOIL SUCTION AND DESICCATION FISSURING

The soil suction induced by desiccation of clay fills leads to the fissuring of clay material by increasing the stresses in the soil until the shear strength is exceeded.

As explained earlier, the total suction, ψ, is made up of two components of matric suction, ψ_m, and osmotic suction, ψ_o. Osmotic suction is due to the salt content in the pore-water, which is applicable in both saturated and unsaturated soils. Since osmotic suctions are generally less significant than matric suction and less sensitive to changes in the soil water content, matric suction is often taken to be equivalent to total suction for unsaturated soil. Hence for fissured soils matric suction is of more interest.

Matric suction, ψ_m, is the difference between air and water pressures. The magnitude of the matric suction is often considerably higher than the magnitude of the net normal stress, $(\sigma\text{-}u_a)$ in normal circumstances. The matric suction, ψ_m, can be expressed using the curvature of the air-water meniscus or contractile skin, r, (see Figure 2.2) by the following equation where σ is surface tension:

$$\varphi_m = \frac{2\sigma}{r} \tag{2.8}$$

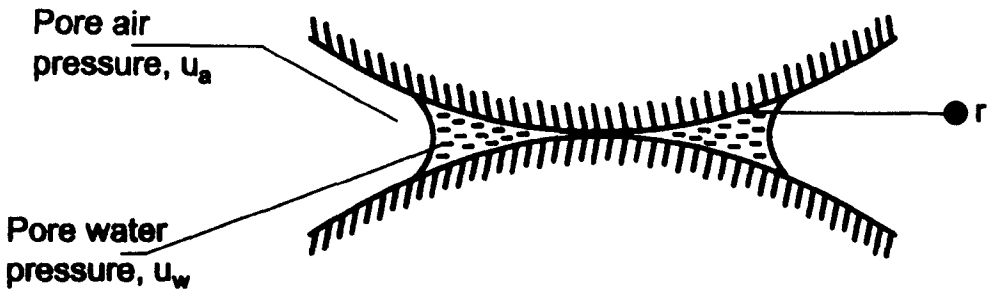

Figure 2.2 Surface tension in the menisci for an unsaturated soil (after Skempton, 1960).

As the matric suction of the soil increases, it reaches the air entry value of the soil. At this stage air can enter the soil and the desaturation process commences. Water is drawn to the surface from the deeper pores via the capillary water columns formed through the menisci. The resulting water loss occurs in the largest pores first. As the suction penetrates deeper, finer and finer pores become desaturated leading to higher matric suction. When the water content reduces significantly, this leads to a decrease in the rate of evaporation and hence a slower increase in the matric suction.

Likewise as the volume of pore water is reduced, the overall volume of the soil decreases due to the rearrangement of soil particles under the matric suction. This leads to density changes and a reduction in permeability. The reduction in the spacing between the particles will reduce the curvature of the air-water menisci and lead to an increase in matric suction. As the soil reaches a dry condition, the matric suction will tend to a limiting value of typically 620-980 MPa as the water content approaches 0% (Fredlund, 1964).

2.4. DESICCATION AND CRACK PROPAGATION IN CLAY SOILS

The desiccation and rearrangement of soil particles into a denser structure creates shear strains between soil particles. At the same time, negative pore water pressures or matric suction is generated in the soil, which both strengthen the intact soil and lead to tensile stress due to the soil contracting. However the tensile force due to the matric suction can readily exceed the lateral confining pressure. When this happens vertical cracking or fissuring develop below the horizontal surface. The tensile strength of the soil depends on its material properties and past stress history. Plastic clays contain more water than leaner sandier clays and therefore experience larger volumetric contractions on drying. Higher plasticity clays however can have a greater effective cohesion (c') and greater tensile strength (σ_t) but this is offset by higher volumetric change and higher suctions that leads to fissuring.

Fissures typically propagate from the soil surface downwards from the drying surface; where the matric suctions are usually greatest and stresses due to self-weight are minimal (Morris, 1992). As desiccation proceeds, they propagate downwards

under the influence of matric suction in a direction perpendicular to that of the maximum tensile stress. Cracks can be assumed to occur when the horizontal stress at the tip of a crack exceeds the tensile strength of the soil (Morris et al., 1992). For soils of a smaller particulate size, the tensile stress required to propagate a crack within them is larger than required in for example sands with larger particle size. This is counter balanced as described before by the capillary model as the matric suction is larger in soils with smaller particle size.

Fissures are generally vertical or sub-vertical, although a few are horizontal and propagate inwards from initial vertical cracks leading to a separation of the upper desiccated layer from the layer below. This will reduce the stability of embankments greatly as the blocks will not be fully joined to the soil below so they can easily part under fairly little through flow.

Experiments have shown that one key factor that controls the onset of fissuring is the rate of evaporation and relative humidity, since soils in relatively dry atmospheres loose water quicker by evaporation (Coleman, 1962). The rate of evaporation affects whether fissuring occurs; observations have shown that extensive cracking occurred in soil specimens dried at a relative humidity of 3% whilst no cracks developed in specimens dried in a relative humidity of 43% (Kayyal, 1995).
Of course desiccation cracking is widespread in nature and can be observed readily in such places as mud flats. As water is lost from the surface layers of soil, tensile forces are set up in uppermost drying surface layer. A saturated soil can relieve these tensile stresses by plastic flow. However when sufficient water has been lost, the soil loses this ability and hence the tensile forces have to be relieved though the formation of shrinkage cracks that break up the surface layer into separate pieces. The restraint necessary for the cracking of the upper surface is provided by the lower strata of soil. When the soil is undisturbed and the drying is natural such as on a mud flat, the cracking will form a regular geometrical pattern. The exact geometry of the polygons formed by the shrinkage cracks depends mainly on the clay mineral composition but also on things such as constitution of the pore fluid (e.g. salt content).

When an initially saturated soil is dried one dimensionally from a horizontal surface (such as the crest of an earth embankment), moisture loss is accompanied by a rearrangement of the soil particles into successively more tightly packed arrangements. Previous studies, carried out by Croney and Coleman (1960), have shown that the void spaces between particles do not remain filled with water indefinitely, but successively larger proportions of air gradually enter the voids as drying takes place. This leads to surface tension effects at soil – air – water interfaces which generate below atmospheric negative pressures (or matric suctions) in the pore water. Matric suctions (defined as the difference between pore-air pressure, u_a and pore-water pressure, u_w) have a significant influence on the cracking process. Matric suctions produce two counteracting effects. First, assuming the degree of saturation is sufficient for the pore water to remain interconnected and pore air is discontinuous; the soil contracts isotropically and produces vertical shrinkage cracks below the horizontal drying surface. Secondly however, the negative pressures of matric suction increase soil strength and resistance to crack formation.

Near the surface where cracking takes place, the magnitude of matric suction varies much more rapidly with environmental changes than the osmotic suction, and hence has a greater bearing on cracking. Therefore this research concentrates only on matric suction.

The in situ soil suction profile may vary from time to time. If there was a constant water table in a natural soil deposit, the matric suction would decrease linearly with depth from a maximum at the ground surface to zero at the phreatic surface. In reality the water table is rarely stable but fluctuates with the seasons, and so more often matric suction decays non-linearly from a maximum at the ground surface to zero at the phreatic surface (see Figure 2.3).

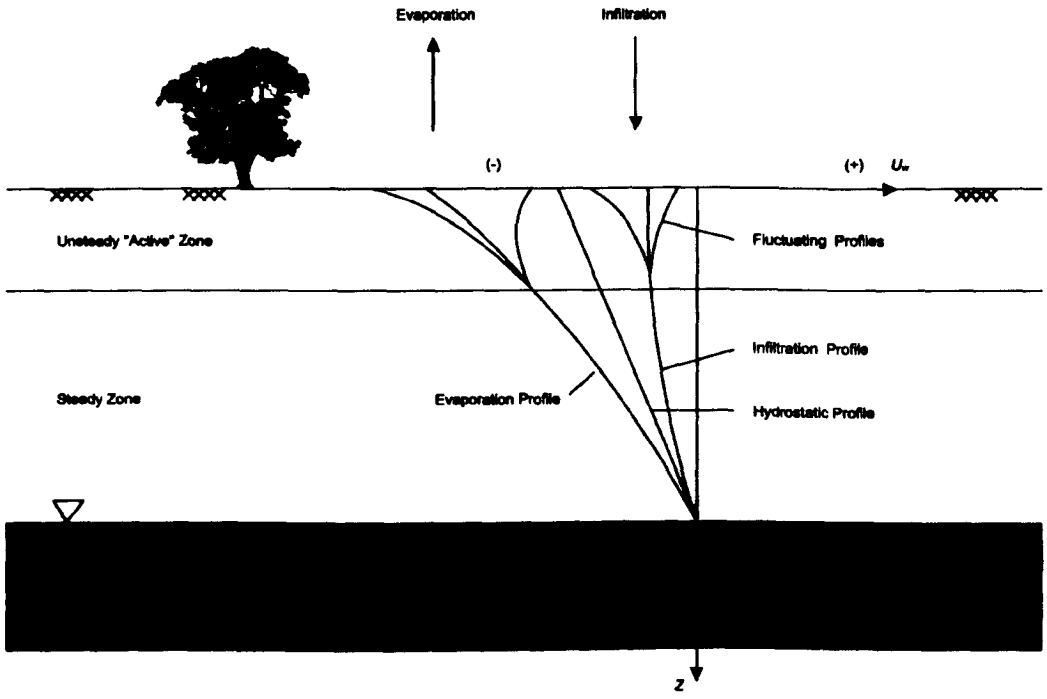

Figure 2.3 Suction regimes and profiles in homogeneous deposit of unsaturated soil under various surface flux boundary conditions (after Lu & Likos, 2004).

It was found by Jennings (1960) and later mentioned by Fredlund and Rahardjo (1993) that the matric suction profile below an uncovered ground surface can be affected significantly by environmental changes. Dry and wet seasons cause variations in the suction profile, particularly to the ground surface (Fredlund and Rahardjo, 1993). It is more likely that the suction profile beneath a covered ground surface is more constant with respect to time than is a profile below an uncovered surface. However, in some cases it is possible that water will slowly accumulate below the covered area on a long-term basis, and consequently cause a reduction in the soil suction.

2.5. INFLUENCE OF THE VEGETATION ON DESICCATION CRACKING

It is very well known that vegetation can have a number of impacts on the infrastructure slopes. Two major effects: (i) mechanical and (ii) hydrological that influence embankments behaviour can be recognised. The increase in embankments stability may be caused by natural reinforcement of roots, whereas water can be extracted from the soil and increase suctions during dry periods (Glendinning et al.,

2009). Decrease in moisture content of the soil caused by vegetation as a result of water extraction leads to volume change of the soil. Hence, shrinkage and cracking of the soil may be observed.
Expansive soils, that are characteristic for semi-arid and arid climates were found to be the most susceptible to the soil volume changes caused by vegetation (Richards, et al., 1983). It is different for Britain's soils where the climate is wet, and these changes are relatively small (Driscoll, 1983).

In the early, very extensive study, Black and Croney (1958) mentioned that in natural soils covered by vegetation, suction varied between zero in the winter and values of 89 kPa near the ground surface during an average summer. Observed increase in suction during the summer in natural soils was mainly due to the transpiration from the vegetation. Where the vegetation was removed, or where it was naturally sparse, observed seasonal change was very small. This brings the conclusion that evaporation from the surface played a limited part in drying soil during dry season.

In the soil surface covered with vegetation, transfer of soil water content to the atmosphere is held by a process called transpiration. Transpiration is caused by a vapour pressure gradient between the leaf cells and atmosphere. Water is extracted from the soil by plant roots and transferred to the transpiring leaves (Ravina, 1983). Thus, where the vegetation is present the soil may dry quicker than the soils where vegetation is sparse. Hence, vegetation can increase shrinkage and soil cracking.

Interestingly Aitchison and Richards (1969) presented empirical methods predicting equilibrium soil suction under structures by carrying out a large field investigation of soil conditions beneath sealed pavement in Australia. The studies showed that soils under a covered area are isolated from rapid environmental changes and tend toward a stable equilibrium moisture distribution. However, the total suction beneath the covered area still showed a variation with climatic conditions, though it was deemed to be insignificant.

As mentioned above, for crack propagation to occur at the surface, restraint from below is required. This restraint is provided by underlying soil strata which are subjected to lower suctions and hence lower suction induced strains.

2.6. DESICCATION AND CRACK PATTERNS

Konrad and Ayad (1997) have presented the results of a field desiccation test in an intact clay deposit at the experimental site of Saint-Alban, Quebec, Canada. Figure 2.4 illustrates schematically the different phases leading to the formation of desiccation cracks in the Saint-Alban intact clay. The suggested mechanisms operative during the first 250 h of evaporation can be described with six main events. Firstly, the initiation of primary cracks under restrained conditions leading to a crack depth of about 5 cm and spacing between 20 and 24 cm occurring before 17 h of evaporation. Secondly, a phase where volume change results in crack opening and the progressive build up of tensile stresses within each polygon and further propagation of the primary cracks consistent with moisture change. Thirdly, the initiation of secondary cracks after about 70 h when tensile stresses reach the tensile strength of the desiccating soil crust and the sudden propagation of these secondary cracks to a depth controlled by the soil's intrinsic properties. The fourth phase leads to differential horizontal strains in a plane at a depth of about 6–8 cm owing to three-dimensional effects. This also results in sub horizontal crack propagation towards the centre of each polygon. The length of the sub horizontal crack is about a third of the polygon size, i.e., 3 to 4 cm. The fifth step corresponds to the initiation and propagation of a new set of vertical cracks in the soil below the horizontal crack. Figure 2.5 shows a schematic description of the mechanisms leading to vertical cracks below the shear plane and formation of a protuberance. Within each polygon, vertical crack surfaces are initiated at a spacing of about one-third of the polygon width. Finally, continued evaporation and volume change leads to the formation of the observed protuberance in each polygon. The crack depth in the soil below the horizontal shear plane is thus reflected by the size of the protuberance and ranges between 4 and 6 cm.

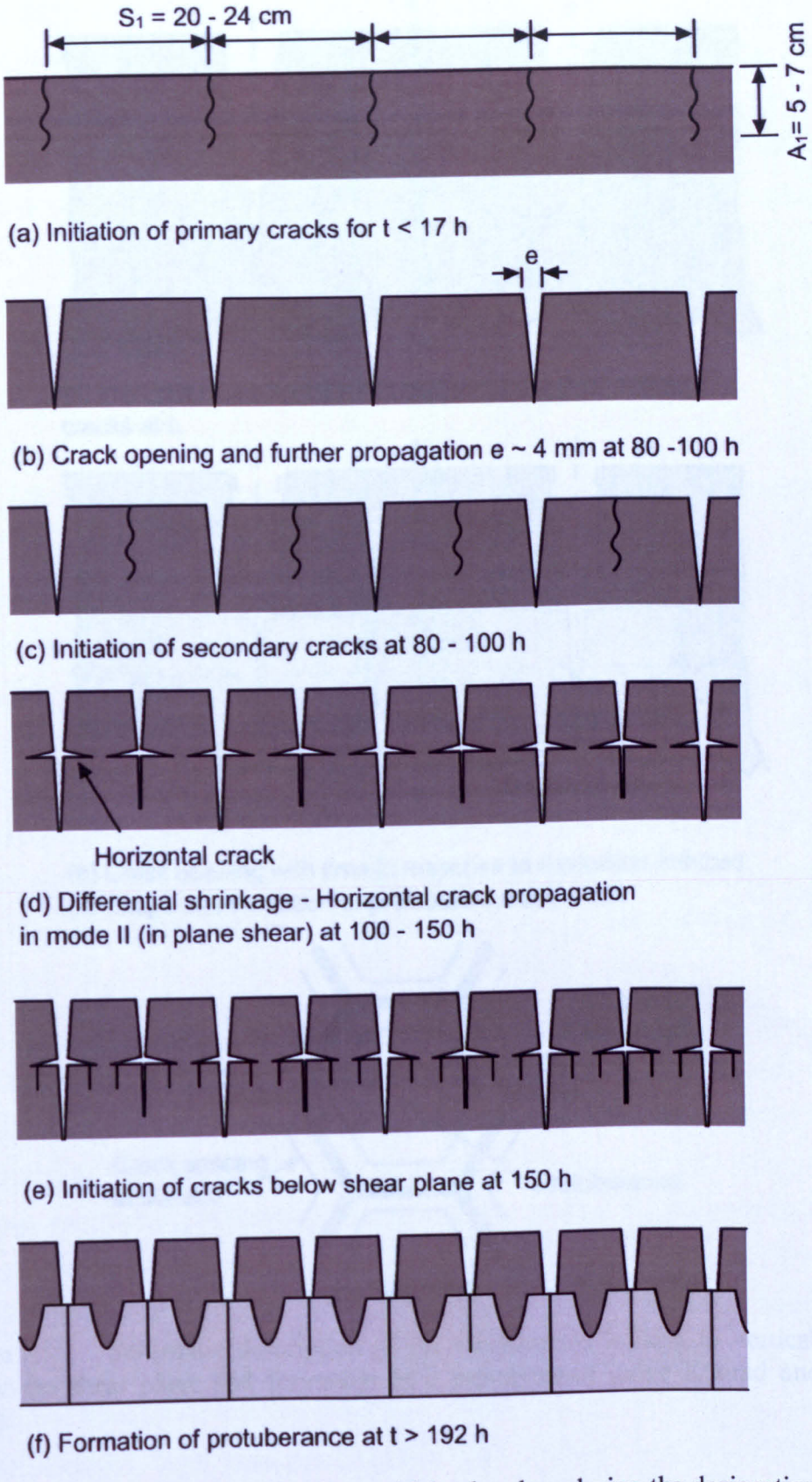

Figure 2.4 Suggested mechanisms which take place during the desiccation of the intact Saint-Alban clay (after Konrad and Ayad, 1997).

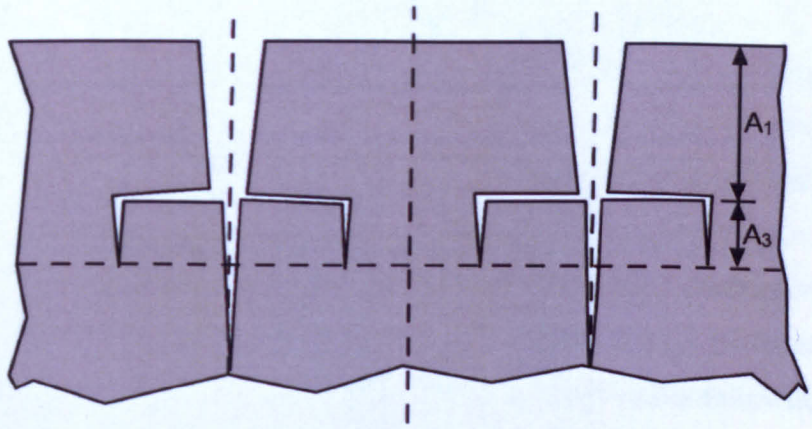

(a) Initiation of crack in the soil below the depth of primary cracks at t_1

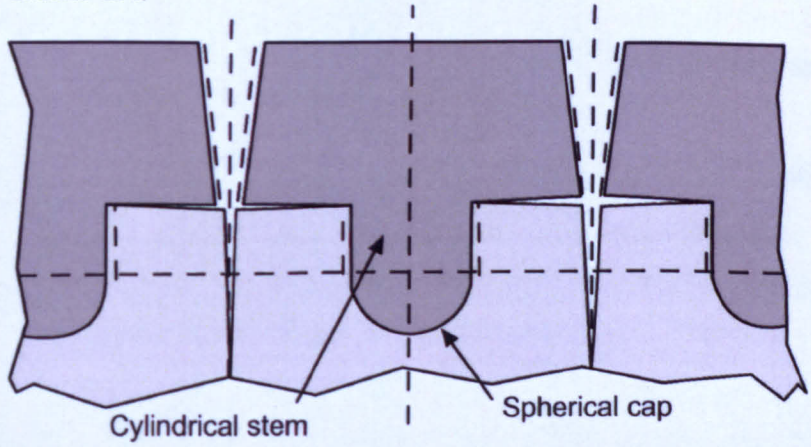

(b) Crack opening with time in response to desication-induced shrinkage and formation of protuberance at $t > $ at t_1

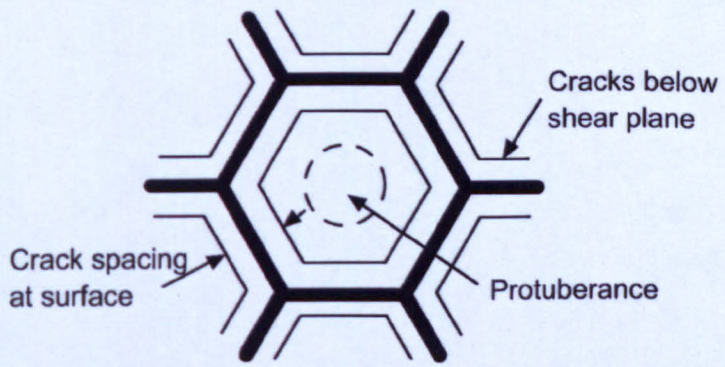

(c) Plan view Not to scale

Figure 2.5 Schematic description of the mechanisms leading to vertical cracks below the shear plane and formation of a protuberance (after Konrad and Ayad, 1997).

2.7. SELF-HEALING OF DESICCATION FISSURES

It is well known that fine-grained soils when exposed to cyclic drying and wetting or freezing and thawing, generally, although not always, experience increases in their hydraulic conductivities as a result of the formation of fissures and cracks that govern the overall permeability of the soils. For non-plastic or very low-plastic soils and for very high plastic and highly active soils, hydraulic conductivities did not change, because of self-healing mechanisms, which during permeation lead to closure of fissures or fractures. Eigenbrod (2003) identified the following three main causes for closure of fractures and cracks in fine-grained soils:

1. Increase in effective stress to levels above the undrained shear strength of the intact soil,
2. Clogging of fractures by particles eroded from the fraction surfaces (Suffusion) during permeation for non- or low plastic soils, and
3. Swelling of the clay particles near the fracture or fissure surfaces in highly swelling clay.

The boundaries between soils that were affected and those that were not affected by self-healing are quantified on the basis of standard classification tests, such as plasticity index and activity, for an initial assessment of their suitability as mineral soil liners.

Eigenbrod (2003) reported that the non plastic or very low-plastic fine grained soils generally will experience closure of fractures induced by freezing during permeation and therefore will not exhibit increase in hydraulic conductivities subsequent to freezing and thawing. However, permeabilities may increase after freeze-thawing cycles in dense silty soils that contain gravel and boulder sized stones. Very highly swelling clays and clay-sand mixtures will not experience increases in hydraulic conductivity subsequent to freeze-thaw cycles if the fractures induced during freeze will close during permeation with water as a result of swelling of the clay along the fracture surfaces. Very high swelling, and thus the potential for self healing, is indicated if the plasticity index of the soil is $I_p > 100\%$ and the activity $A > 3$.

Soils with intermediate to high plasticity of I_p = 10% - 100% and the activities of A < 1.25 generally will experience increases in hydraulic conductivities subsequent to freeze-thaw cycles (unless they are dispersive clays), as the fractures induced during freezing will stay open during permeation with water at an overburden stress less than 20 kPa.

For the soils with plasticities Ip > 100% and activities A between 1.25 and 3.0, additional information would be useful to determine the boundary between the clays that experience increases in hydraulic conductivities during freeze-thaw and that do not. In addition, flow-conditions and thus the hydraulic conductivities in unsaturated fractures soils are not known and need to be investigated.

2.8. MEASUREMENT AND GENERATION OF SOIL SUCTION

The importance of the effective stress concept in soil mechanics was first highlighted by Terzaghi in 1925. In the later study Bishop (1960) has summarised the development of the concept of effective stress and has considered the theoretical aspects of the principle in detail (Mitchell, 1962). Two years later Mitchell (1962) has brought a new view on Bishop's theory and raised the completely new aspect in geotechnical engineering. His new concept shows the engineering significance of the components of pore water pressure.

Pore water pressure plays a major role in saturated and unsaturated soil mechanics. Pore water pressure can be divided into: (i) positive pore water pressure and (ii) negative pore water pressure (suction). Both of these pressures are related to different mechanical soil behaviours and can be responsible for different soil states and failures.

Failures related to positive pore water pressure are more likely to occur in wet climates as shallow slips (Aubeny and Lytton, 2004), where the increasing pore water pressure reduces the strength of the soil.

Failures related to negative pore water pressure are more related to the extremely arid, arid and semi-arid climates where the annual evaporation exceeds annual

precipitation. Evapotranspiration also plays some role as it causes consolidation and desaturation of the soil mass. Most of the failures that are occurring in unsaturated soils are closely linked with desiccation cracking (Stark and Eid, 1997). When expansive unsaturated soils are subjected to wetting, (ie. a reduction in suction) significant volume changes can occur (swelling). Some of the soils present extreme swelling or expansion when wetted, and some show the significant loss in shear strength upon wetting. Changes in negative pore water pressure, due to heavy rainfalls are the main cause for many of slope failures. This indicates the importance that the negative pore water pressure has in controlling mechanical behaviour in unsaturated soils.

There is huge evidence in engineering records about the methods of controlling negative pore water pressure (suction). It can be found that many of them have been developed in the last 50 years when knowledge about unsaturated soils has expanded. In engineering practice, there are two ways to measure soil suction: (i) direct measurements, (ii) indirect measurements. Recently, a deterministic method was also considered as an additional method for obtaining the value of soil suction. Techniques and devices that are widely used at the moment are presented in Table 2.2, which contains also the range of measurements.

Table 2.2 Techniques and devices used for soil suction determination.

Method	Device	Suction Range	Reference
indirect	Pressure plate	100-1500 kPa	Richards 1941, Gardner 1956, Croney and Coleman 1960, Reginato and van Bavel 1962, Fredlund 1964, Fredlund and Rahardjo 1993, Navaneethan et al. 2005
indirect	Filter paper	20-5000 kPa	Gardner 1937, McKeen 1981, McKeen 1985, Crilly and Chandler 1993, Chandler et al. 1995, Likos and Lu 2002, Likos and Lu 2003
indirect	WP4*	1-60 MPa	Leong 2003, Leong 2007, Cardoso et al. 2007
deterministic	MIP**	-	Purcell 1949, Regab et al. 1982, Prapaharan et al. 1985, Aung 2001

direct	Tensiometer	0-200 kPa	Croney 1958, Croney and Coleman 1960, Penman 1956, Gourley and Schreiner 1996, Ridley and Wray 1996, Ridley et al. 1998
direct	HS Tensiometer***	1-1500 kPa	Ridley 1993, Guan 1996, Guan and Fredlund 1997, Meilani et al. 2002, Take and Bolton 2004

* Chilled-mirror dew-point psychrometer (WP4 Dewpoint PotentiaMeter)

** Mercury Intrusion Porosimetry

*** High Suction Tensiometer

The axis translation technique (Hilf, 1956) is a commonly used method for measuring and generating suctions in soil specimens. The technique involves placing a sample of soil on a ceramic porous disc (Figure 2.6) with the pore water in the soil in contact with the water in the ceramic filter, which is at atmospheric pressure under the plate. The soils samples are then subjected to air pressures inside a chamber and the pore-air pressures in the soil allowed equilibrating with applied air pressure. The pore-water pressure is consequently forced out of the sample through the ceramic filter. This positive translation of the pore-air pressure allows the pore-water pressure in the sample to be referenced against the positive applied air pressure.

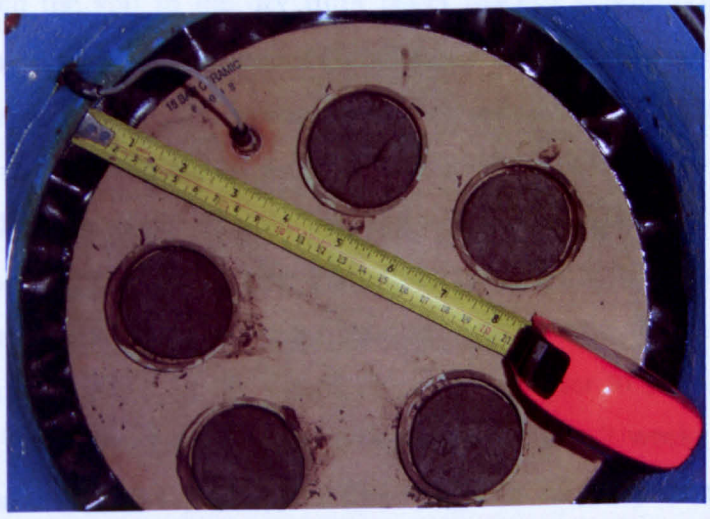

Figure 2.6 Porous disc with soil samples inside pressure plate extractor.

The axis-translation technique simply translates the origin of the reference for the pore-water pressure from the standard atmospheric to the pressure in the chamber to the applied air pressure. However, this technique contains some limitations and has been criticised in recent years (Delage et al. 2008). The main limitations are the

following: (i) the technique is not representative for field conditions where air pressure is under atmospheric conditions, (ii) it is still not clear how the air pressurisation process affects the water when water is held by adsorption mechanism, (iii) the application of the technique at nearly saturated states when the continuous gaseous are not present is not straightforward.

The filter paper method is an inexpensive and relatively simple laboratory technique from which total suction and matric suction can be measured (Bulut et al., 2001). The technique was developed by Gardner (1937), but has not been used by engineers for many years, until McKeen (1981) found it to be useful for studies on airport pavement sub-grades and swelling potential in expansive soils. In recent years the method was revived and found to provide very promising and reliable measurements of soil suction. The method is very low cost making it suitable for routine testing in research laboratories and engineering practice. The principle of the method is based on the assumption that the filter paper will come in to equilibrium with the soil that has a specific suction. Equilibrium can be reached in two ways: by liquid or vapour exchange between soil and the filter. The process of exchange continues until the water flow from the soil to the dry filter paper reaches equilibrium. The method involves placing a circular filter paper (Whatman nr. 42) between two soil samples. This requires a good contact between the filter paper and soil samples. Thus, the surface where the paper is placed must be as smooth as possible. It is suggested to avoid putting the filter paper directly between soil samples (Bulut et al., 2001). For this reason two sacrificial filter papers (Whatman nr. 1) are usually placed below and above the filter used for determining suction. The sample then is sealed using wax/cling film and placed in the sealed container in order to prevent evaporation (Chandler and Gutierrez, 1986). Usually, the period of 1 to 2 weeks is required for the equalisation. After this period, the filter paper is carefully removed from the sample and the measurement of the filter paper moisture content is taken.

A good correlation between the filter paper gravimetric moisture content (w_p) and the sample suction (p_k) can be calculated from the calibration work reported by Chandler and Gutierrez (1986) and Crilly and Chandler (1993):

$$\log_{10} p_k = \begin{cases} 4.84 - 0.0622 w_p & w_p < 47\% \\ 6.05 - 2.48 \log_{10} w_p & w_p > 47\% \end{cases} \quad (2.9)$$

In summary, to emphasize the effectiveness of this method it is worth mentioning that this method was proposed by Crilly and Chandler (1993) and later by Chandler et al. (1995) as a robust method for determining the state of desiccation in clay soils.

Another apparatus used to measure the soil suction are high range psychrometers. The working principle of the WP4 psychrometer is based on the measurement of the relative humidity of the air inside a small sealed chamber (Cardoso et al., 2007). When the equilibrium is reached in the chamber, the relative humidity of the air inside the chamber is equal to the relative humidity of the soil sample. The relative humidity can be expressed as:

$$RH = \frac{p}{p_0} \quad (2.10)$$

where p is the equivalent suction derived from the vapour pressure, in equilibrium with the soil water, and p_o is the saturation vapour pressure, at the same temperature in equilibrium with free pure water. For given relative humidity the total suction ψ, can be expressed by the psychrometric law (Fredlund and Rahardjo, 1993):

$$\psi = -\frac{RT\rho_w}{M_w} \ln(RH) \quad (2.11)$$

where, R is the gas constant (8.314 J/(mol K)), T is the absolute temperature, M_w is the molecular mass of water (18.016 kg/kmol) and ρ_w is the density of pure water (998kg/m^3 at 20°C).

The measurements taken by psychrometers in some cases can be affected by some variables and factors. It is important to take readings at constant temperature of the measurement environment in thermal equilibrium with the soil sample (Cardoso, et al. 2007).

The Mercury Intrusion Porosimetry MIP was developed to determine the total pore spaces and pore-size distribution in the porous solids (Diamond, 1970; Juang and Holtz, 1986a). The Washburn equation (11) (Washburn, 1921) is used to calculate an absolute pressure p which is applied to a non-wetting liquid (mercury) in order to enter the empty pores (Romero and Simms, 2008).

$$p = -\frac{n\sigma_{Hg}\cos\theta_{nw}}{x} \tag{2.12}$$

where σ_{Hg} is the surface tension of mercury (σ_{Hg} =0.484 N/m at 25°C), θ_{nw} is the contact angle between mercury and the pore (usually taken between 139° and 147° for clay minerals (Diamond, 1970)).

The principle of Mercury intrusion is to find the pore-size distribution which relates to the volume of intruded pores to the pressure required for intrusion (Romero and Simms, 2008).

The sample used for the MIP test requires the removal of water that is contained in the small pores and prevents the entry of mercury. This type of treatment can be done by dehydration process chosen from one of the following techniques: air-drying, oven-drying, freeze-drying or critical-point-drying. A good review of these techniques was provided by Delage and Pellerin (1984). In the case when the sample is sensitive to heat-drying, it is suggested to use freeze-drying technique, especially at high moisture contents (Ahmed et al., 1974). Freeze-drying process eliminates the surface tension forces caused by air-water interfaces, by manipulating the temperature and pressure conditions. Hence, there is no shrinkage during drying process which can disturb the sample. A 1 cm^3 cube sample is required for freeze-drying process in order to maximize the heat transfer (Romero and Simms, 2008).

MIP was previously used by the number of researchers to determine the Soil Water Characteristic Curve, SWCC, (Prapaharan et al., 1985; Romero, 1999, Romero et al., 1999, Aung et al., 2001). The mercury intrusion process is similar to air-intrusion during the desorption path of the soil water characteristic curve (SWCC). Thus, the entry of the mercury is equivalent to the removal of the water by the non-wetting front of air advance being intruded. The volume of not intruded pores, are used to evaluate the water content or degree of saturation corresponding to matric suction (Romero and Simms, 2008). Water is generally held in the soils at low suctions, due

to the capillarity, and at high suctions by adsorption on particle surfaces (Romero et al., 1999; Romero and Simms, 2008).

There are four main limitation of the MIP: (i) pores isolated by surrounding solids are not measured (this porosity is not significant in soils), (ii) bigger pores which are accessible through the smaller ones are not measured until the smaller pores are penetrated, (iii) entry to the smallest pores can be limited by the capacity of the apparatus (non-intruded porosity), (iv) maximum pore size may not be detected due to the limit of the minimum practical pressure of the apparatus (non-detected porosity). Following this, when the soil sample is intruded by mercury, the intruded void ratio does not represent the void ratio of the sample.

Despite the limitations, the method was found to be reliable for the derivation of the matric suction-water content relationship at the low-suction range (Romero and Simms, 2008).

Alternatively tensiometers were developed to measure directly the negative pore-water pressure that exists in the soil so that the matric suction could be measured directly out in the field, or laboratory. First, well recorded suction measurements using tensiometer were described by Croney et al. (1958) and Croney and Coleman (1960). Although, the structure of the tensiometer has evolved over the years, the principles of its functioning have been unchanged.

A tensiometer is basically a piezometer that has been re-designed and specifically modified to measure pore water tension (Ridley et al., 2003b). The negative pore water pressures are due to the water tension in the air-water menisci in an unsaturated soil. The direct measurement of the matric suction overcomes the problems and assumptions of the other techniques, as the ambient air pressure remains atmospheric. So the pore-air pressure within the soil is atmospheric at the surface being measured. However, in practice when the tensile stress is applied to the water inside the tensiometer, it can cause the air entry into the reservoir (Ridley et al., 2003b). When the air enters the reservoir, the measured tension of water does not represent the suction in the soil. This phenomenon is called cavitation and has been investigated by number of researchers (Harrison and Blight, 2000; Tarantino and Mongovì, 2001; Tarantino, 2003; Take and Bolton, 2004).

Tensiometers can be applied to many geotechnical related concepts. Over the years they were used as practical tools for measuring suction of the soil in the laboratory (Ridley, 1993; Guan, 1996; Guan and Fredlund, 1997; Muraleetharan and Granger, 1999; Take and Bolton, 2001; Wendling and Meiβner, 2001; Yoshida and Adachi, 2001; Take and Bolton, 2002a; Take and Bolton, 2002b; Meilani et al., 2002; Vatsala and Srinivasa Murthy, 2002; Ridley et al., 2003b; Tarantino and Mongiovì, 2003) and in situ applications (Croney et al., 1958; Croney and Coleman, 1960; Wu et al., 1993; Gourley and Schreiner, 1995; Cui et al., 2008; Ridley et al., 2004.; Smethurst et al., 2006; Trandafir and Gomi, 2008).

Ridley and Burland developed high suction tensiometers at Imperial College during the 1990's (Mongiovi and Tarantino, 2003). These small electric piezometers used a ceramic intake filter that was placed closely to the stiff diaphragm of the transducer or strain gauge, leaving a volume of only $3mm^3$ as the water reservoir. It was shown to be able to read values of negative pore water pressures up to the air entry value of the ceramic filter (1500kPa). Once equilibration between the soil and the measuring systems is achieved, water in the tensiometer will have the same negative pressure as the pore-water pressure in the soil, allowing the matric suction to be read directly. The deflection of the diaphragm can be calibrated to the pressure in the water reservoir and hence the water pressure in the soil sample.

It needs to be borne in mind that tensiometer saturation is an important part of the test because if the filter is sufficiently saturated, higher negative pore-water pressures can be measured without cavitation taking place. The maximum measurable suction is controlled by:

- the growth of pre-existing gas bubbles,
- the air entry value of the filter,
- the nucleation of vapour bubbles or release of air trapped in surface crevices.

As the filters are saturated under high pressures when they become under high suction if any of the above mechanisms happen they will lead to the separation of the fluid in the water reservoir from the fluid in the pores of the soil. After this, any increase in the suction causes the gas to expand rapidly within the water reservoir

next to the strain gauge preventing any further readings to be taken, this is know as cavitation of the tensiometer. The cavitation of tensiometers is one of the limiting factors in their performance. The resistance to cavitation has been improved by the investigation of ceramic filter saturation techniques.

In summary, tensiometer becomes the only one available device at the moment to measure the soil suction directly in the soil. It makes tensiometer a very robust tool and shows its potential in unsaturated soil mechanics.

It should be noted that there are other methods of controlling or measuring soil suction (e.g. pyschrometers, osmotic control of matric suction), however those presented are some of the most commonly used methods in current engineering practice.

Four of the techniques discussed above were used in the research presented herein: (i) filter paper, (ii) WP4, (iii) MIP and (iv) tensiometer.

2.9. SOIL WATER CHARACTERISTIC CURVE

The relationship between soil suction and soil water content is given as the soil water characteristic curve (SWCC) or water retention curve (WRC), (Williams, 1982). This curve describes the thermodynamic potential of the soil water stored in the macro and micro pores with respect to the suction. When the soil contains a relatively small amount of water, the pore water potential is significantly reduced relative to free water, thus producing relatively high soil suction. When the soil contains a relatively big amount of water, the difference between the pore water potential and the potential of free water decreases, thus the soil suction is low. When the potential of pore water is equal to the potential of free water, the soil suction is equal to zero. This happens when the amount of water contained in the soil is close to 100%. Clay soils are capable of sustaining significant suction over a wide range of water content.

A typical SWCC using degree of saturation versus matric suction is presented below.

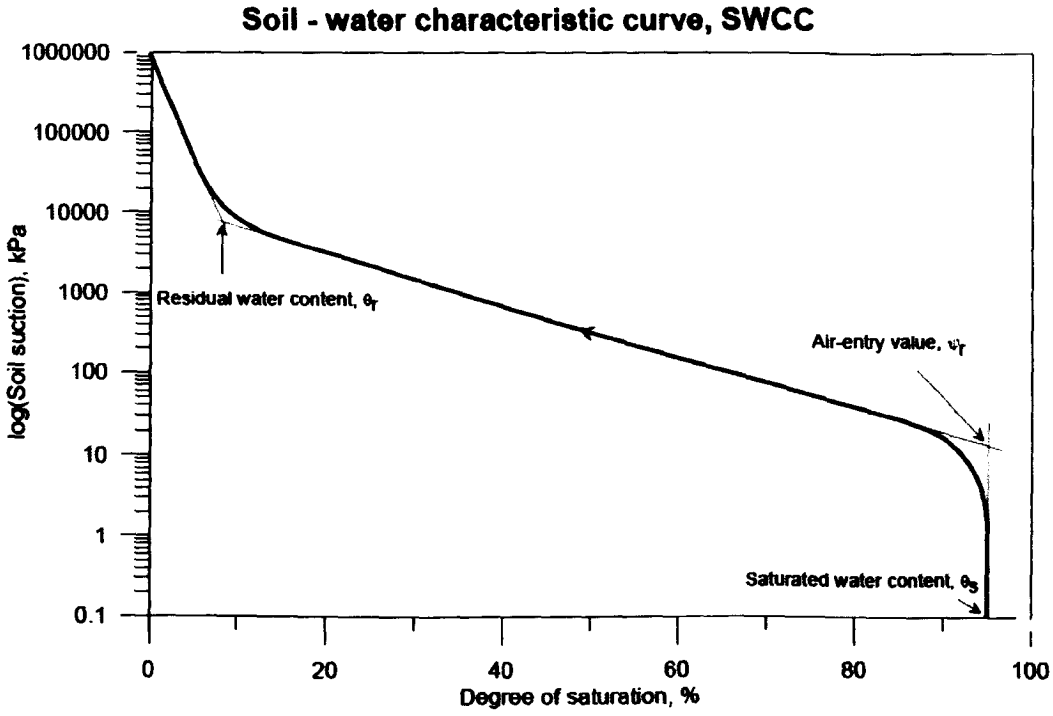

Figure 2.7 A typical Soil Water Characteristic Curve (after Leong and Rahardjo, 1997).

The air-entry value, ψ_r, is the value of matric suction where air starts to enter the largest pores in the soil. The residual water content, θ_r, is the water content where a large suction is required to remove additional water from the soil. The saturated water content, θ_s, is the water content contained by the soil in the pores at its maximum saturation state. The saturated moisture is equivalent to porosity, φ.

The Soil Water Characteristic Curve can be also determined experimentally (Simms and Yanful, 2001) using one of the techniques described in the previous paragraph or from in-situ measurements. It can be also estimated from the particle size distributions (Gupta and Larson, 1979; Fredlund et al., 1997), pore size distribution (Simms and Yanful, 2001; Simms and Yanful, 2002) or from mechanical properties of soils (Ghosh, 1980).

The SWCC can be also derived using an empirical procedure (Fredlund and Xing, 1994). The van Genuchten (1980) equation is commonly used (Fredlund and Xing, 1994; Leong and Rahardjo, 1997; Tinjum et al., 1997; Sivakumar and Gartung, 2001; Zhou and Yu, 2004) for estimating the SWCC.

$$\Theta = \frac{(\theta - \theta_r)}{(\theta_s - \theta_r)} = \left[\frac{1}{1+(\alpha\psi)^n}\right]^m \tag{2.13}$$

where, Θ is the effective saturation (or normalized water content), θ, θ_r, θ_s are the volumetric water content at suction ψ, and a, n, m are constant fitting parameters for the relationship.

The above equation can be also expressed in the following way for given values of, θ_r, residual moisture content and, θ_s, saturated moisture content:

$$\theta = \theta_r + \frac{(\theta_s - \theta_r)}{[1+(\alpha\psi)^n]^m} \tag{2.14}$$

Seasonal variations in climatic conditions affect the water retention in soils; as a result they swell and shrink. During the dry spells the shrinkage of soils is commonly associated with the formation of cracks. There is however still a lack of knowledge about desiccation cracking created under natural conditions. Hence, a field survey across Britain was carried out in order to gather the informations about existing embankments affected by desiccation cracking. Nine field inspections are presented in the next Chapter.

CHAPTER 3

3. FIELD STUDIES ON DESICCATION FISSURING

3.1. INTRODUCTION

It is very important in the engineering practice to make sure that the theory is always followed by the experimental confirmation. All assumed concepts must be verified in order to understand, clarify and to confirm them by observations and measurements. Hence, this chapter describes all the findings that have been achieved during site investigations and laboratory studies.

Field studies have been carried out across UK on different clay embankments to validate the assumption that desiccation fissuring transforms the upper layer of the embankment into the rubbilised zone (Cooling and Marsland, 1954; Dyer et al. 2009).

The first phase of the project has involved a field study of fine fissuring at an historic and new flood embankment at Thorngumbald near the city of Hull on the north shore of the Humber Estuary. The second phase has involved a field study of 8 embankments in UK which were indicated by the Environment Agency inspectors as desiccated fissured embankments.

3.2. SITE DESCRIPTION -THORNGUMBALD

A satellite photograph of the historic flood embankment is shown in Figure 3.1 with the alignment of the new flood embankment drawn. The historic flood embankment was replaced by a new flood embankment in 2003 in order to create salt marshes. The field study has involved the excavation of trial pits to expose desiccation fissuring beneath the crest and side slopes of the embankments along with soil sampling for later laboratory analysis and on site double ring infiltrometer tests. The site visits to Thorngumbald were undertaken in 2003, 2005 and 2006. The results of the field study are reported as follows.

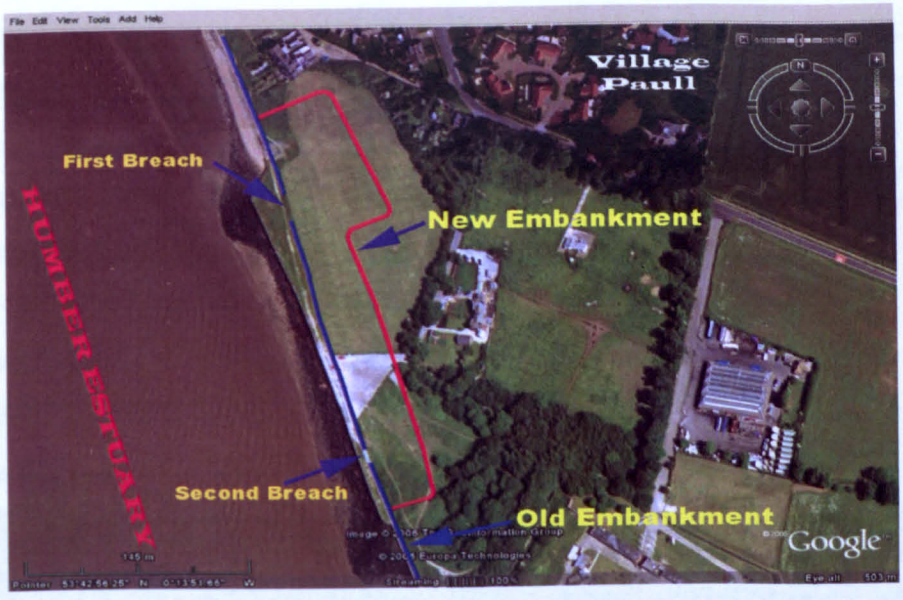

Figure 3.1 Satellite photograph of historic flood embankment at Thorngumbald (source: Google Earth).

3.3. FIELD STUDY ON DESICCATION FISSURING AT THE HISTORIC FLOOD EMBANKMENT IN 2003

The initial field study (Dyer, 2004; Dyer et al., 2009) involved the excavation of trial trenches into the historic flood embankment (Figure 3.2) to expose desiccation fissures in the clay fill material.

Figure 3.2 Historic flood embankment at Thorngumbald.

Four trial trenches were excavated into the crest and landward slope of the flood embankment using a hydraulic back-actor with the final portion excavated by hand to minimise disturbance and expose the fissures. Disturbed and undisturbed soil samples were taken from the trenches for laboratory analysis. In addition, undisturbed samples were taken using a U_{100} sampling tube pushed into the side and base of the trench and then excavated. Visual inspection of the trenches revealed extensive fissuring of desiccated clay fill to a depth of approximately 600 mm below the crest height of the embankment in each excavation. A photograph of one side of the trench is shown in Figure 3.3.

Figure 3.3 Desiccation fissures observed in trial trench at Thorngumbald flood embankment at an approximate depth of 600 mm below crest level (after Dyer et al. 2009).

It appears from the trial pits that the pattern of desiccation fissures can be divided into two zones. There is an upper zone where the fissures extend perpendicular to the drying surface and then terminate with a horizontal set of fissures that give a two dimensional array of fissures. In comparisons the lower set of fissures extends vertically from the horizontal fissures and terminates in intact soil. These zones are called A and B in Figure 3.4. This simple classification of desiccation fissuring means that there appears to be an upper surface zone of fill material that has been

rubblised into a two dimensional network of fissures that significantly increase the mass permeability of the fill material and so allow water to readily flow through and along that portion of the embankment. This should result in a much greater infiltration of water into the surface of the flood embankment and potentially lead to collapse of the back slope. This interpretation matches the observations made by Marsland and Cooling (1958) for a full-scale cofferdam test, where the overflow of flood water was diverted into the crest of the test embankment.

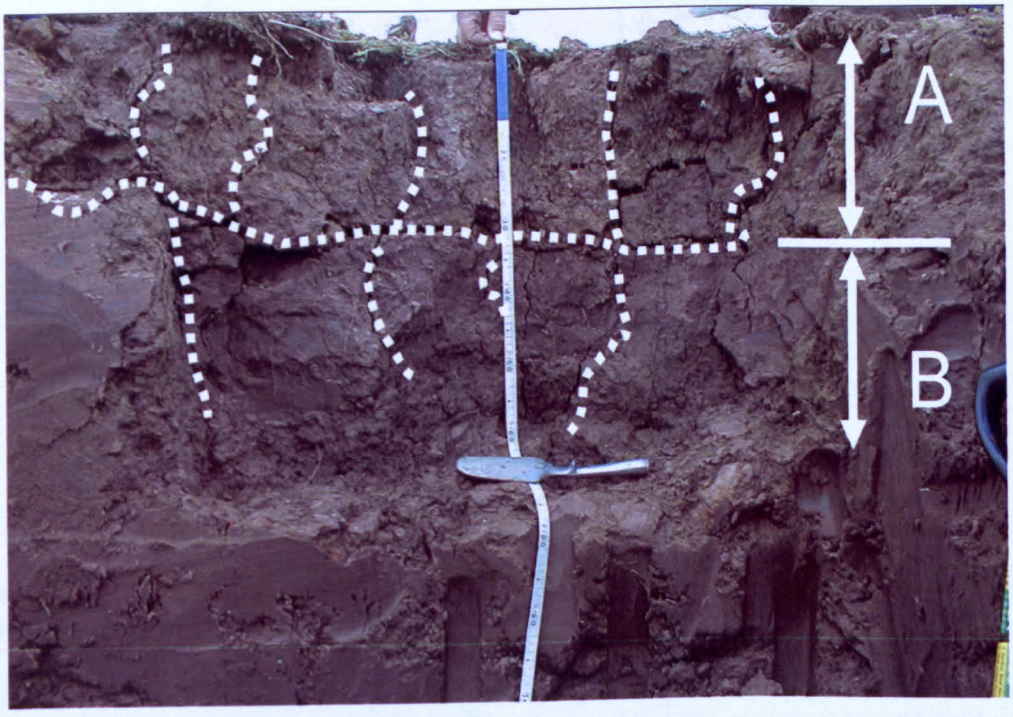

Figure 3.4 Proposed division of desiccation fissures into two zones: A and B (after Dyer et al., 2009).

In addition to visual record of desiccation fissuring the material properties of the disturbed soil samples were measured to determine in-situ moisture content as shown in Figure 3.5. The corresponding shrinkage, plastic, and liquid limits for the clay fill were determined to be 14, 25, and 49% respectively (Dyer, 2007). The plastic and liquid limits were measured according to BS 1377-2:1990. Whilst the shrinkage limit (SL) was determined by measuring the volumetric change in a bath of mercury as described by Akroyd (1964).

The moisture content profile clearly shows that the highly fissured clay fill within the top 500 mm has dehydrated towards the shrinkage limit of 14%. Whereas, below a

depth of typically 500 mm the in-situ moisture content vary between the shrinkage and plastic limits. This distinct change in moisture content agrees with the visual inspection of the trial trenches that show a well defined zone of desiccation. At greater depth the moisture content increases to approximately 30%.

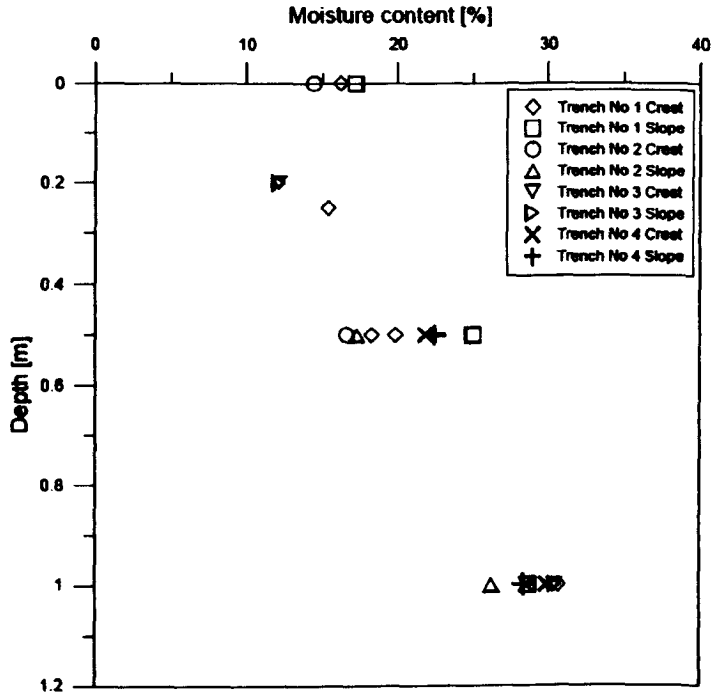

Figure 3.5 Moisture content profiles in trial trenches excavated below crest of embankment (after Dyer et al., 2007).

3.4. FIELD STUDY ON DESICCATION FISSURING AT THE HISTORIC FLOOD EMBANKMENT IN 2006

During the second field survey of the historic embankment in 2006, one trial trench was hand excavated into the crest (1.0 m x 1.0 m) to a depth of 1.0 m. Deep fissures were observed to a depth of 1.0 m below crest level (Figure 3.6). The extent of the fissuring was so pronounced that the widths of the fissures were measured at 10 cm intervals as shown in Figure 3.7. However the network of fissures was different from the first survey. In this latter trial trench the fissures are not connected into a two dimensional network but instead tended to be single deep fissures that would allow the seepage of water into the depth of the embankment but not lateral flow beneath the surface of the embankment slope, which could lead to slope instability or slope erosion.

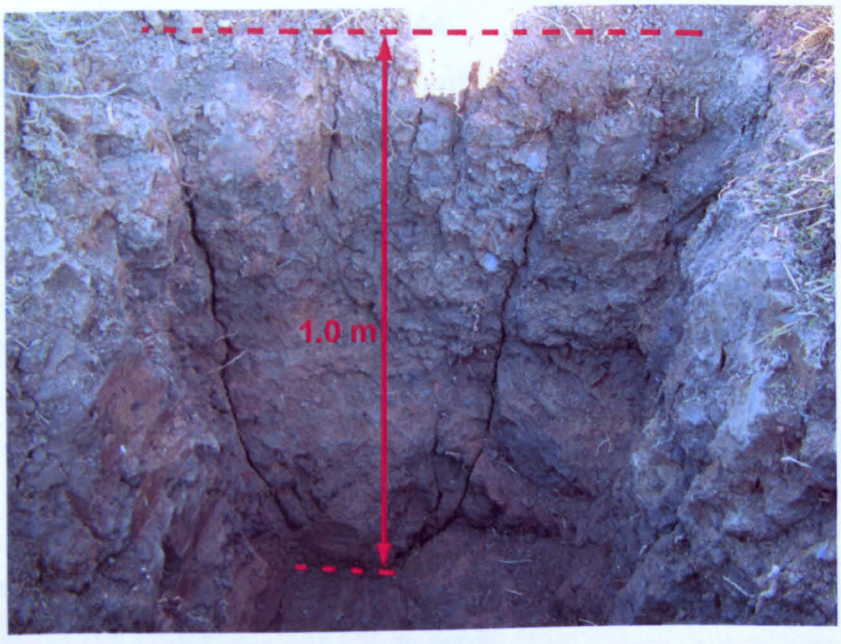

Figure 3.6 Desiccation fissures observed in trial trench in historic embankment (Dyer et al., 2009).

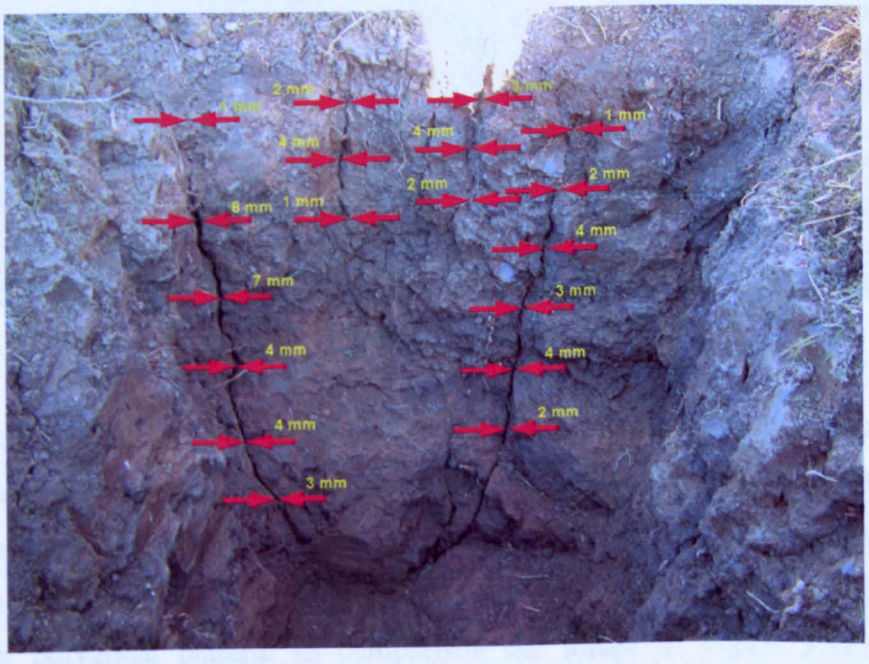

Figure 3.7 Corresponding width of desiccation fissures in historic flood embankment (Dyer et al., 2009).

3.5. FIELD STUDY ON DESICCATION FISSURING AT THE NEW FLOOD EMBANKMENT IN 2006

The new flood embankment (Figure 3.8) built in 2003 was constructed from locally excavated alluvial clays extracted from a borrow pit in the area of the new salt marshes. The results again are presented as a series of photographs of desiccation fissures along with measurements of fissure width and spacing and also double ring infiltrometer measurements.

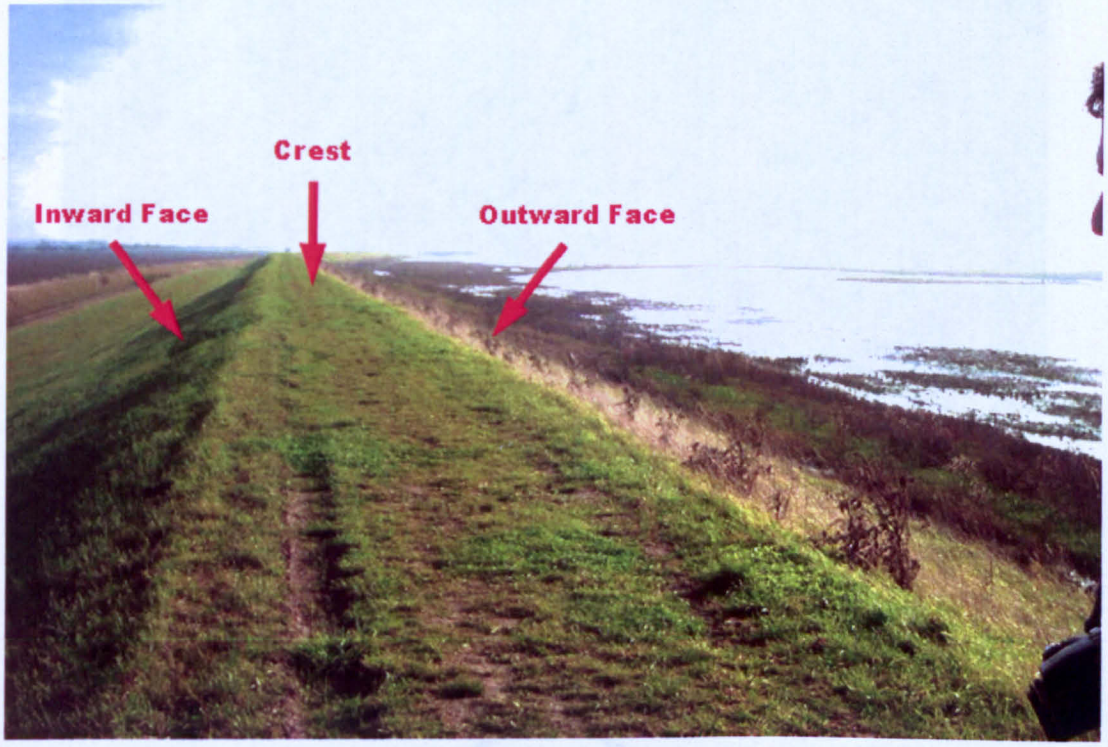

Figure 3.8 New flood embankment at Thorngumbald.

The field survey of the new embankment in 2006 identified desiccation fissures along the crest of the embankment as shown in Figure 3.9 and Figure 3.11. The image in Figure 3.9 shows a polygonal pattern of fissures that are characteristic of desiccation cracking. Figure 3.10 shows the sketch of measured dimensions for one particular polygonal pattern. In comparison the image in Figure 3.11 shows a pronounced longitudinal crack that is more characteristic of differential movement. The widths of the polygonal desiccation fissures varied from 5 mm to 25 mm and were generally found where the embankment lacked a healthy grass cover, for the reasons explained earlier in Chapter 1.

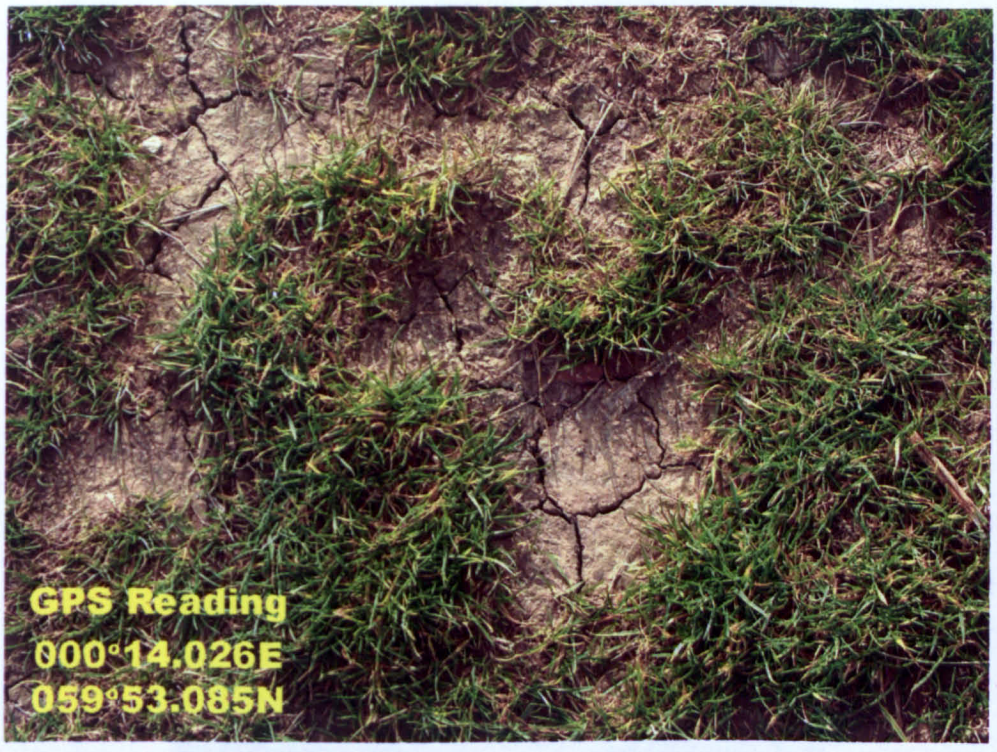

Figure 3.9 Pattern of desiccation cracks observed on the crest of the new embankment (2006).

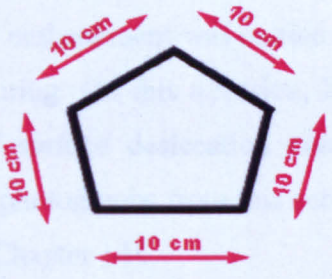

Figure 3.10 Sketch of desiccation fissures on the crest of the new embankment.

Figure 3.11 Pattern of desiccation and differential fissures observed along crest of new embankment (2006).

This survey of the new flood embankment was carried out to obtain more data on the presence of desiccation fissuring. On this occasion, hand excavated trial pits were used to track the depth of surface desiccation cracks beneath the crest of the embankment. A selection of photographs from this survey visit in November 2006 is presented in the Annex - A (Chapter 14).

A characteristic polygonal pattern of desiccation fissures was observed on the crest of the new embankment as shown in Figure 3.12.

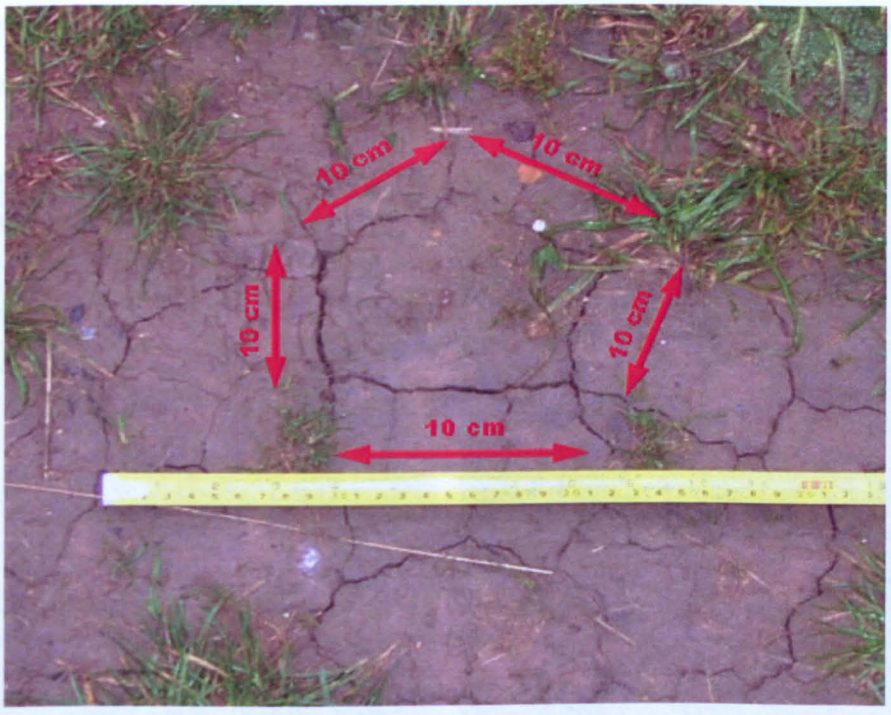

Figure 3.12 Polygonal pattern of fissures observed on the crest.

These fissures appeared to be more pronounced where grass cover was bare or absent (see Figure 3.13).

Figure 3.13 Photograph of surface desiccation fissuring on crest of new embankment prior to hand excavation (2006).

The underlying network of desiccation fissures revealed by the hand excavated trial trench is shown in Figure 3.14.

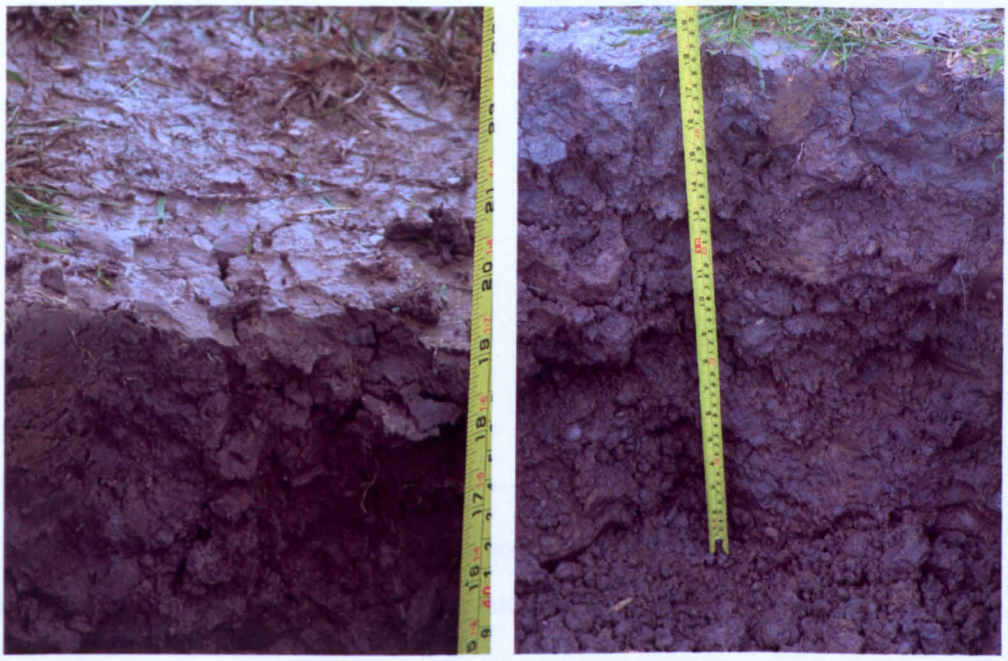

Figure 3.14 Photographs of hand excavated trial pit showing the network of desiccation fissures beneath the crest of the new embankment (2006).

In Figure 3.15 the gravimetric moisture content is plotted for the examined trial pit. In this case, all the tested zone is cracked. Considering the variation of moisture content with depth, shift can be noted for the readings taken from the 0.1-0.3 m deep region against a linear trend of the other values. This shift is also noticeable in the previous investigations run in 2003 (see Figure 3.5). According to the literature, a non linear profile in terms of water content vs. depth can be perfectly reasonable (Cameron and Walsh, 1984). The plastic and liquid limits, measured according to BS 1377-2:1990, are shown in Table 3.1.

The plastic and liquid limits averaged over the examined layers are 29 %and 57 % respectively. Therefore, the clay fill forming the embankment is below its plastic limit and likely close to its shrinkage limit.

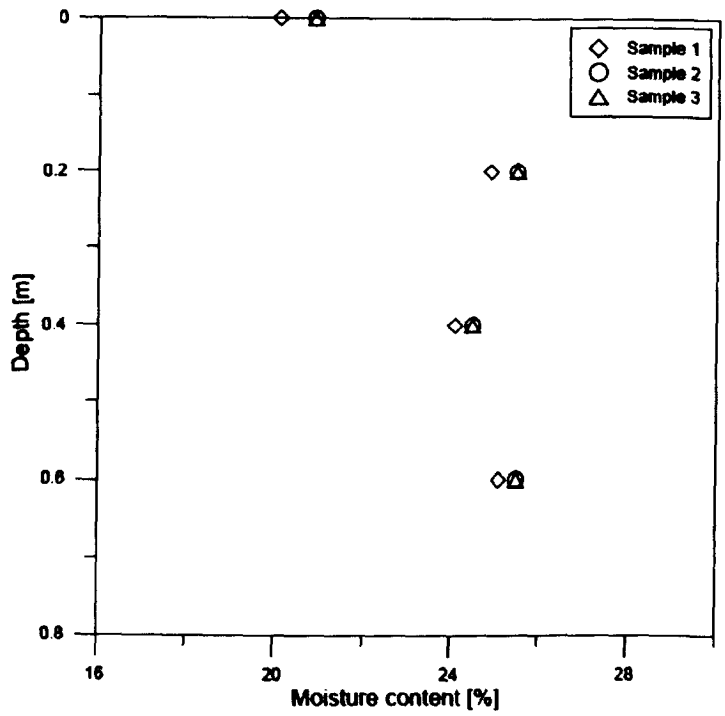

Figure 3.15 Moisture content profile below crest of new embankment.

Table 3.1 LL, PL and PI measured for samples taken at new embankment.

Depth [m]	0.0-0.1 m	0.1-0.3 m	0.3-0.5 m	0.5-0.6 m
LL, ω_L [%]	59.10	59.05	55.20	54.99
PL, ω_P [%]	29.50	28.76	29.08	28.15
PI, I_P [%]	29.60	30.29	26.12	26.84

LL – Liquid Limit
PL – Plastic Limit
PI – Plasticity Index

3.6. DOUBLE RING INFILTROMETER TEST RESULTS

Double ring infiltrometers are often used in the field to measure the infiltration rates of natural soil deposits, re-compacted soil liners and amended soils such as soil-bentonite and soil-lime mixtures (Daniel, 1989; Sai and Anderson, 1990; Benson et al., 1994; Trast and Benson, 1995; Benson et al., 1997). The most common field test is conducted using a sealed double ring infiltrometer (see Figure 3.16).

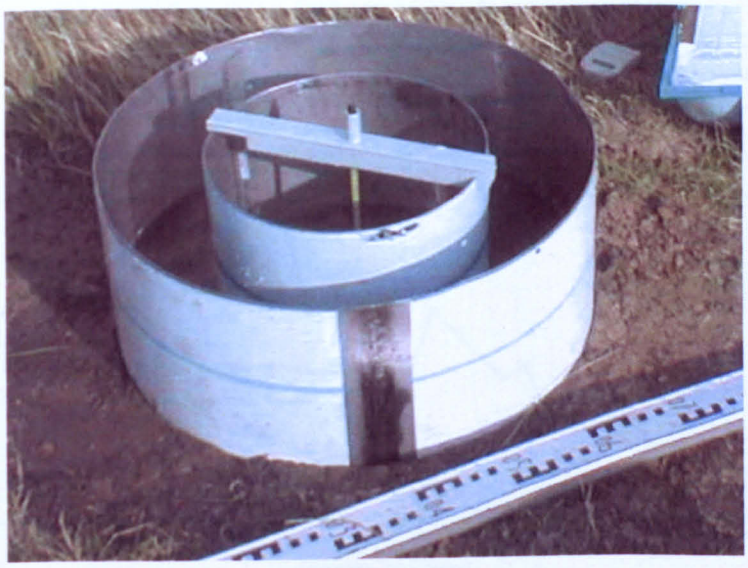

Figure 3.16 Double ring infiltrometer apparatus.

The hydraulic conductivity can be calculated based on the measured infiltration rate for a known hydraulic gradient assuming that the suction head at the wetting front is zero. Two other important assumptions are homogenous soil and seepage beneath the inner ring is one-dimensional. The former assumption is indeed satisfied since the embankment is made by a uniform clay fill. Concerning the latter assumption, the use of a double ring has been conceived in order to guarantee a vertical flux within the inner ring. This aspect is important since the horizontal permeability for a clay material can be much higher than the vertical one, up to two orders of magnitude, therefore if the water flow has a horizontal component, even small, this can lead to a big overestimation of the real vertical permeability.

Double ring infiltrometer tests were carried out in the field to measure the effect of fissuring on the mass permeability of the clay fill in 2003 (Dyer et al. 2007). The initial double ring infiltrometer tests were carried on the crest of the historic embankment without any excavation. The metal rings of the infiltrometer supplied by ELE International measured 320/570 mm in diameters. The rings were driven approximately 10 mm into the ground surface to provide a seal (see Figure 3.16). In Figure 3.17 is shown the infiltration rate recorded on the historic embankment. The water seepage decreases quite rapidly in time and the resulting mass permeability is comparable to that typical of sand.

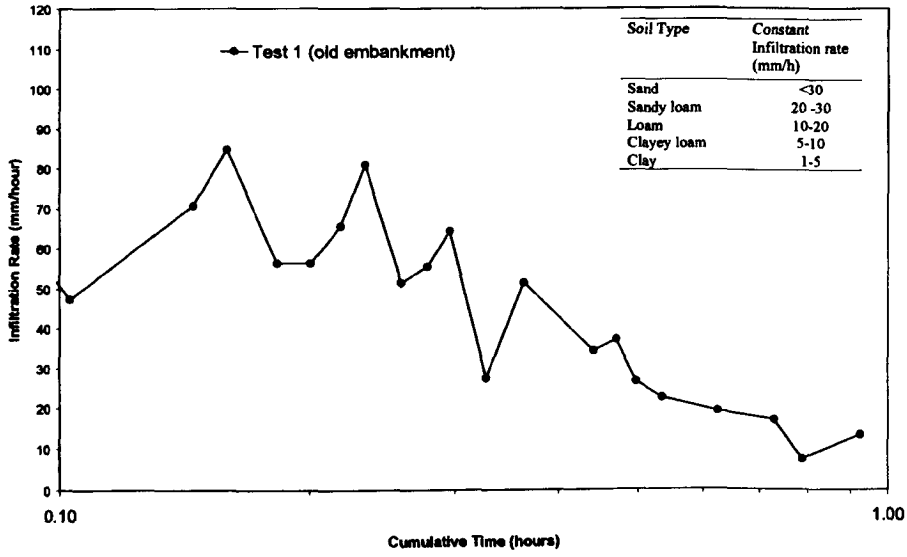

Figure 3.17 Infiltration rate vs. time from the double ring infiltrometer test run on a non-fissured zone in the historic embankment (after Dyer et al., 2009).

Initial attempts to measure the rate of infiltration on the new embankment proved unsuccessful. The water drained away too rapidly to allow any meaningful readings to be taken. Nevertheless, the observation did concur with the behaviour of full-scale cofferdam tests carried out by Marsland and Cooling (1958). The investigators reported that water overtopping the crest failed to reach the landward side because the water drained into the crest of the trial embankment too rapidly, which led within a matter of minutes to the progressive collapse of the landward face eventually resulting in a breach. In Figure 3.18 the infiltration rate from the second double ring infiltrometer test is shown. This rate is 3 orders of magnitudes higher than typical rates for clayey soils. This remarkable difference can only be explained by considering the presence of cracks which cause water seeping down in the embankment much faster (see Figure 3.19). The presence of cracks radically changes the bulk permeability of the soil making the clay fill as much permeable as gravel.

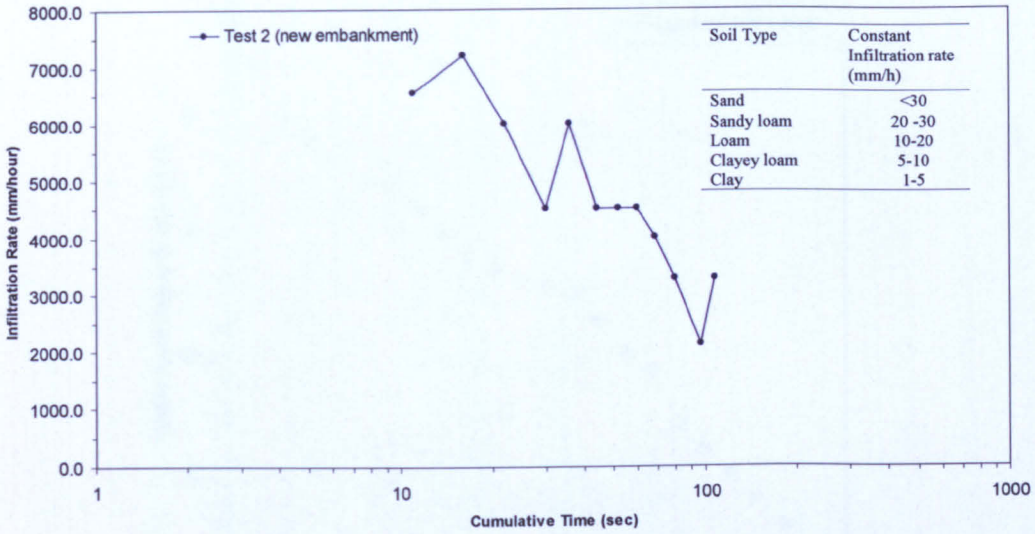

Figure 3.18 Infiltration rate vs. time from the double ring infiltrometer test run on a fissured zone in the new embankment (after Dyer et al., 2009).

Figure 3.19 Surface crack pattern within the inner ring.

In 2006, different experiments were carried out to measure infiltration rates within the historic embankment. First a trial trench 1m x 1m wide, 1 m deep was excavated, then water from big tanks was poured in to the hole. The water seeped down because of the presence of cracks. The flow rate of the water seeping through the cracks was recorded at regular time intervals. In Figure 3.20 the water level in the hole is plotted against time. According to the Figure 3.20, it can be noted that the filtration rate of water is not constant in time, but is initially high and then decreases progressively.

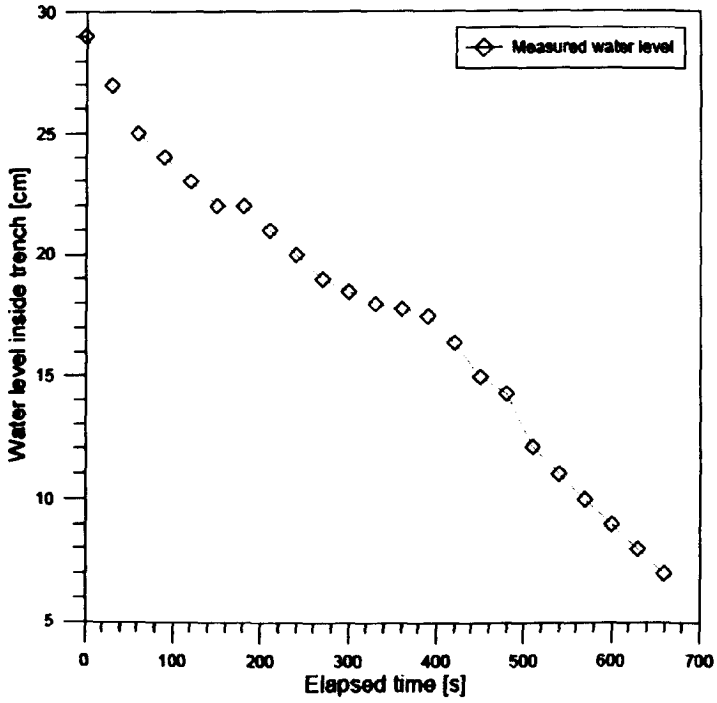

Figure 3.20 Water filtration test inside the trench.

The experiment had also the objective of identifying any potential outlet point for the water through the embankment side slope. In fact, the occurrence of outflow of water from the side slope would indicate the presence of strongly interconnected cracks through which water can massively percolate. In order to detect any outflow of water from the side slope, a large grassy area was cut away (see Figure 3.21).

According to the visual observation ran during the experiment there was no evidence of any spillage of water from the side slope examined. Therefore, it can be inferred that the crack network was not so extended to let water flow through the side slope.

Figure 3.21 Observed area along the inland side embankment.

3.7. ADDITIONAL FIELD OBSERVATIONS ON DESICCATION FISSURING IN UK

In 2007 additional embankments were visited across UK in order to study the nature of desiccation cracking on different fills. The map of visited places is presented in Figure 3.22 followed by a short description of the investigated embankments.

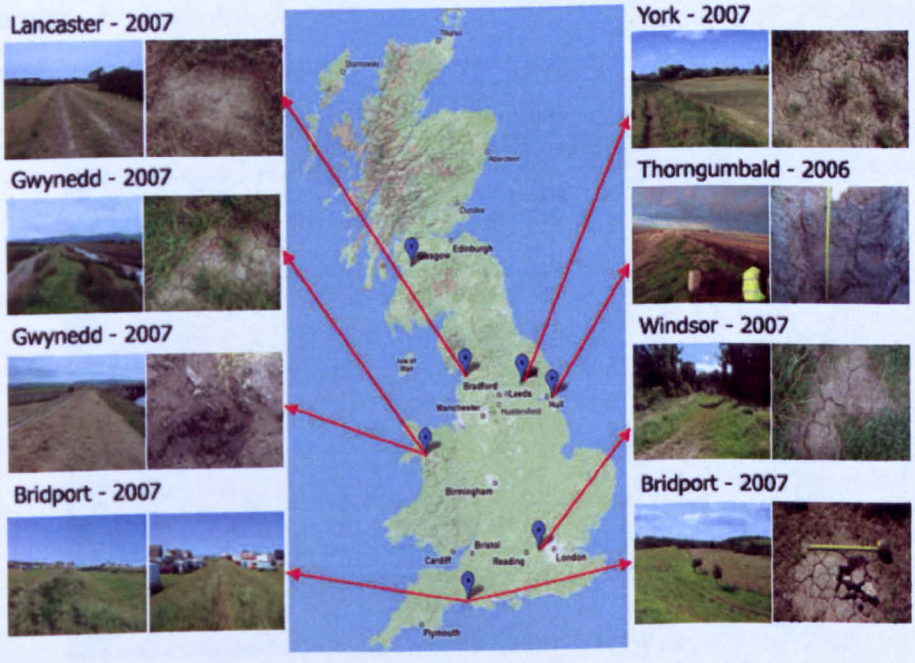

Figure 3.22 Investigated places of fissured embankments in 2007.

3.8. SITES DESCRIPTION

3.8.1. YORK

The embankment investigated in York is located along the River Ouse (Figure 3.23). The embankment is 2 km long, 4.0 m high with about 2 m wide crest. It was found that this embankment was in the worst condition among all the inspected embankments.

Figure 3.23 Embankment along River Ouse.

The embankment was heavily vegetated and was maintained only on one side by the local farmer. It was revealed that the embankment was intensively affected by animals burrowing (see Figure 3.24).

Figure 3.24 Observed animals burrowing.

In the places where there was a lack of vegetation or vegetation was sparse, desiccation cracking was present (see Figure 3.25).

Figure 3.25 Desiccation cracking observed in York.

It was decided to dig a trial trench in one of the places where the cracking was so pronounced in order to investigate its depth and pattern. Only few very tiny and shallow vertical cracks were found (Figure 3.26) with no signs of interconnected cracking network. Most of the visually observed cracks were only superficial with a depth of 1-2cm.

Figure 3.26 Cracks observed inside the trial trench.

On one side of the trench an animal hole was found (Figure 3.27), just a few centimetres below the crest surface. This confirmed the visual assumption about existing defects of embankment body caused by animals burrowing.

Figure 3.27 Animal burrowing close to the crest surface.

3.8.2. WINDSOR

The embankment visited at Windsor is located along the River Thames (Figure 3.28). The embankment is about 1 km long, 3.0 m high with about 1.5 m wide crest and it is connected along half of its length with the concrete wall constructed on the back of the industrial estate.

Figure 3.28 Embankment along Thames River at Windsor.

After the visual inspection of embankment it was decided to carry no further investigation as the observed cracking seemed to be only superficial (Figure 3.29) without any signs of deep penetration.

Figure 3.29 Superficial cracking observed at Windsor embankment.

3.8.3. BRIDPORT

Two embankments were visited in Bridport. The first embankment was newly constructed (1 km long, 6.0 m high with 2.0 m wide crest) in order to create the water reservoir (Figure 3.30).

Figure 3.30 Embankment along reservoir, Bridport.

The second embankment inspected in Bridport is located along the Brit estuary (Figure 3.31). This embankment is about 2 km long, 1.5 m high with 1 m wide crest.

Figure 3.31 Embankment along Brit estuary, Bridport.

In both cases presented above, only a few places with desiccation cracking could be found. However, as mentioned before, cracking occurred in the locations with lack of vegetation (Figure 3.32). Cracking was not pronounced where the embankment was covered by grass.

Figure 3.32 Desiccation cracking observed at Bridport embankment.

3.8.4. GWYNEDD

Two flood defence schemes were visited in Gwynedd (Wales). The first embankment situated along the River Resr (Figure 3.33). The embankment is about 4 km long, but only about 1 m high with the crest width of about 0.8 m.

Figure 3.33 Embankment along River Resr.

The second embankment in Gwynedd is located along the Dovey estuary (Figure 3.34).

Figure 3.34 Embankment along Dovey estuary, Gwynedd.

This embankment is about 3 km long, approximately 3.8-4.5 m high, with a 2 m wide crest. The embankment was carefully investigated as the visual inspection revealed wide superficial cracks. The trial trench excavation showed that the cracks were due to the soil washed away between the pebbles (Figure 3.35). It was discovered from the history of this embankment that a mixture of soil with pebbles was used for the restoration after breaching of the existing embankment in 1976 and after the 1997 overtopping when the embankment was topped up to increase its height.

Figure 3.35 Pebbles mixed with top soil with some visible loose material.

3.8.5. LANCASTER

The Lancaster embankment was the last flood defence inspected during the 2007 survey. The embankment is the part of new flood prevention scheme for the city of Lancaster. This flood prevention scheme, along the river Lune, involves various flood prevention structures including concrete walls, earth structures. The inspection of one section (Figure 3.36) was carried out a few months after its completion.

A 4 m high, 2 km long with 3 m wide crest, embankment was constructed with clay-cement mixture in order to increase its strength.

Figure 3.36 Flood embankment along River Lune, Lancaster.

Just a few months after completion, tiny cracks were observed on the surface (Figure 3.37).

Figure 3.37 Cracks visible on the crest surface, Lancaster.

These cracks were superficial cracks, and did not seem to be interconnected desiccation cracks. However, in order to examine the embankment's behaviour over the period of a few months, a 1m deep trial trench was excavated (Figure 3.38).

Figure 3.38 Trial trench excavated at Lancaster embankment.

No signs of vertical and horizontal cracking could be found from the excavation. The visual observation of the embankment body from the trench, confirmed its homogeneity and integrity.

In summary, in many cases, cracking of the embankments is neglected by the engineers as it is difficult to detect it on the surface covered by rough grass or vegetation. Some other potential and dangerous symptoms of embankments instability can also be ignored or wrongly interpreted, i.e.: tension cracking along the slope due to the settlement or bulges on the landward side due to the increase of pore water pressure in underlying strata.

The purpose of presented field survey was to extent the knowledge about different crack pattern which is not only related to the conditions inside the embankments, but also to their locations, weather conditions, shapes and type of the fill material. There is very little evidence provided about desiccation cracked embankments. Hence, the creation of such a database is vital for the practitioners to have a vision of the risk of embankments fissuring that may become more frequent due to the climate change.

Under the field conditions the crack pattern observed during this survey was associated with a long-term behaviour as the weather conditions could not be controlled. Hence, the laboratory model under fully controlled environment could give a valuable insight into the process of desiccation cracking creation and their growth. The next Chapter presents the construction of the embankment model along with the description of the soil classification and the experimental set-up.

PART 2- LABORATORY STUDIES AND PHYSICAL MODELLING

CHAPTER 4

4. EXPERIMENTAL TESTING

4.1. CONSTRUCTION OF MACRO-SCALE EMBANKMENT MODEL

4.1.1. INTRODUCTION

The past research on the desiccation cracking of flood embankments which has been presented in Chapter 1 has shown that under natural conditions embankments constructed from local alluvium or clayey soils always tend to crack when dry period occurs for a long time. It has been found that during drying process interconnected network of cracking can occur on the upper layer of flood defence and moreover it can progressively affect defence construction to a depth of 1.0 m.

First of all a literature survey was necessary to recognise the number of parameters and monitoring methods applied to embankments and slopes.

A huge number of laboratory studies have been done in order to investigate soils cracking. Furthermore, the behaviour of embankments has been investigated by many researchers. Most of the field based research focussed on measuring the moisture content and pore water pressures during different seasons. Ridley et al., (2003a) investigated pore water pressure changes in the highway embankments using different measuring devices and tried to find the best available method for direct measurements. Ng et al., (2003) carried out experiment on a cut slope in order to investigate the performance of an unsaturated expansive soil subjected to artificial rainfall. Smethurst et al., (2006) looked at seasonal changes in pore water pressures and changes in the moisture content at different depths in a grass-covered cut slope in London Clay. Experiments, performed by Take and Bolton (2002) investigated the

effect of seasonal moisture changes on clay slopes using micro-scaled centrifuge model.

One major question rises before the experiment: How to replicate the cracking under laboratory conditions and how to obtain a similar extent of cracking to the one observed by Cooling and Marsland (1954)?

Desiccation cracking occurs when the soil is subjected to drying, but how the structure behaves when it is cracked and when the extreme conditions (dry summers and wet winters) occur, is not fully understood.

Weather conditions are very complex and consist of many different phenomena. It is difficult to replicate them under laboratory conditions, therefore the use of artificial sources was considered in order to approach field conditions. Due to climate change, extreme conditions should be applied to the experimental set-up in order to obtain results within the optimum range of measurements.

4.2. ORIGIN OF THE MATERIAL

To investigate the effect of desiccation cracking on the stability of flood embankments, a macro-scale embankment model was constructed in the laboratory concrete flume and contained inside an environmental chamber.

The highest priority in this experiment was to find the natural source of clay which could be used for the construction and for further experimental work. It has been also considered, to use the same type of material which was used for the real embankments.

At the same time of this study, a new embankment was constructed in Galston, on the south-west from Glasgow as a part of flood prevention scheme in Ayrshire.

The first in-situ inspection of the clay used from a local quarry, has indicated a very high tendency of desiccation cracking (Figure 4.1).

Figure 4.1 State of desiccation cracking indicated in the quarry.

On site measurements of undrained shear strength were carried out in four different places of the quarry using hand vane tester. The results which are presented below in the Table 4.1, were analysed in accordance to BS 8004:1986 and the clay was identified as stiff clay.

Table 4.1 Measured undrained shear strength.

Ref.	Undrained shear strength	Consistency in accordance with BS5930	Field indication
-	[kN/m^2]		
1	121	stiff	Cannot be moulded in the fingers
2	133	stiff	"
3	152	stiff	"
4	146	stiff	"

4.3. GEOTECHNICAL CLASSIFICATION TESTS

4.3.1. INTRODUCTION

Some disturbed soil samples were taken from the quarry in order to investigate soil properties. Due to a large content of boulders in clay, this clay is called Boulder Clay. A number of geotechnical tests have been carried out in order to characterise the properties of the clay used in this study:

- particle size distribution analysis
- specific gravity of soil particles
- Atterberg limits
- linear shrinkage tests
- compaction test
- soil water characteristic curve tests
- pore size distribution analysis

The first two tests were carried out to describe disturbed characteristics of a Boulder Clay (apparent particle size, grain specific gravity). Consistency tests (Atterberg limits), are more representative of a remoulded state, obtained for a mixture at a water content greater than the plastic limit. Linear shrinkage tests are representative for soils of low plasticity including silts and clays, where the percentage of linear shrinkage of a soil is obtained. The compaction test refers to the compacted state of the soil at different moisture contents. The two remaining tests, which are presented in the following sections, refer mainly to the characterisation of the different artificially prepared soil packings used in this research.

4.3.2. SOIL CHARACTERISATION AT DISTURBED STATE

The particle size distribution, both wet/dry sieve analysis and sedimentation processes (BS1377-2:1990) have been done for the basic understanding of the nature of the soil. Combined dry/wet sieving is used for the soil where both clays and gravels are present. Soil is previously washed through the set of sieves in order to wash the clay and silts from sand and gravels. Furthermore, the standard procedure is applied for dry sieving to separate fractions from 63 mm down to a size of 63 μm. The sedimentation analysis (hydrometer) is effective for separating smaller fractions

from 63 μm down to a size of about 1.2 μm. Soil that is previously pre-treated for organic and calcareous matter should be dispersed and sieved. It can be seen on Figure 4.2, that the soil used in this research has about 50% of gravels and sand in its content. It appears from the sedimentation test that Boulder clay is mainly composed of silts with a small content of clay (5 % particles < 2 μm).

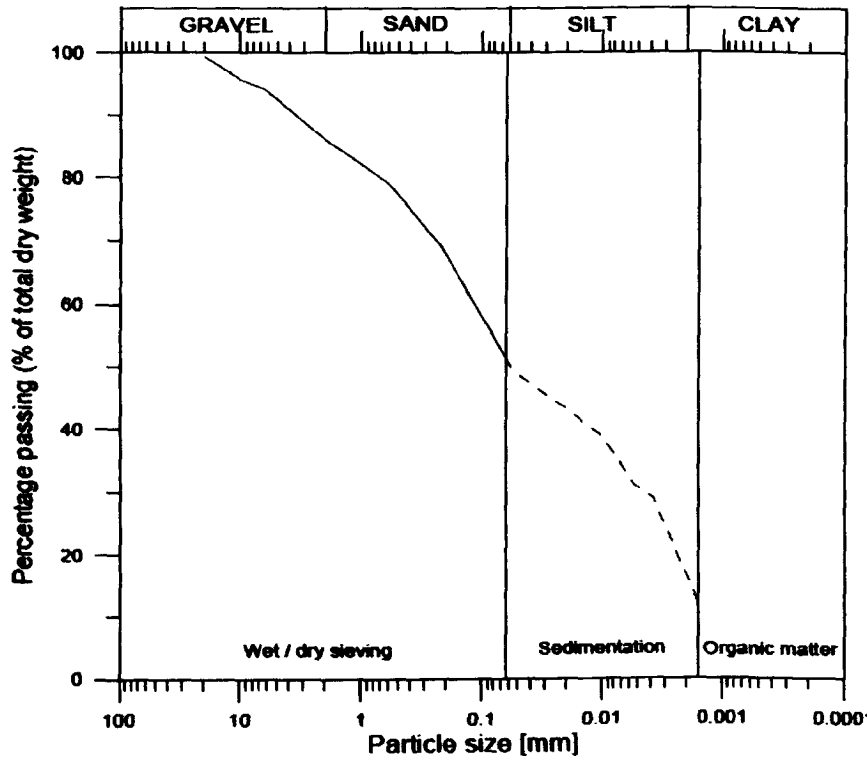

Figure 4.2 Particle size distribution curve.

In order to measure the specific gravity of soil particles, density bottles have been used (BS1377-2:1990). It was decided that due to a high fraction of particles >2 mm, two tests will be performed to measure the specific gravity for particles < 2mm and particles >2mm. The measured specific gravity for both samples is given in Table 4.2.

4.3.3. CONSISTENCY LIMITS (ATTERBERG LIMITS)

The liquid limit and plastic limit are the most useful tests in identifying and classifying fine-grained cohesive soils (BS1377-2:1990). These laboratory performed tests enable clays to be classified and to understand other various properties related to them. The condition of the clays depends on their moisture content related to

plastic and liquid limit. This relation can be expressed by the plasticity index. The liquid limit of the soil used was measured using a cone penetrometer. The plastic limit was determined using the standard rolling method. The results for both tests are given in Table 4.2.

Table 4.2 Soil properties of Boulder clay.

Property	Value
Natural Moisture Content *MC*: %	17.91*
Optimum Moisture Content *OMC*: %	11.50
Linear shrinkage *LS*: %	10.13*
Liquid Limit *LL*: %	35.75*
Plastic Limit *PL*: %	16.40*
Plasticity Index I_D: %	36.20*
Maximum Dry Density ρ_d: Mg/m^3	1.95
Specific gravity (<2 mm) ρ_s: Mg/ml^3	2.65*
Specific Gravity (>2 mm) ρ_s: Mg/ml^3	2.77*

*Average from 3 independent tests

4.3.4. COMPACTION TEST

The compaction test (BS1377-4:1990) is used to provide the information about the soil density that can be used to control compaction procedures on site. From the compaction test the following information can be obtained for compacted fill material:

(i) relationship between dry density and moisture content for compactive effort

(ii) the value of optimum moisture content at which the maximum dry density can be achieved

(iii) the value of maximum dry density achieved for used compactive effort.

The compaction test has been done using a British Standard compaction mould with 27 blows (2.5 kg rammer) applied to three layers of soil (BS1377-4:1990). The estimated compaction curve is plotted in Figure 4.3. Two arrows on axis X and axis Y indicate the optimum moisture content (OMC) at which the maximum dry density (MDD) will be achieved.

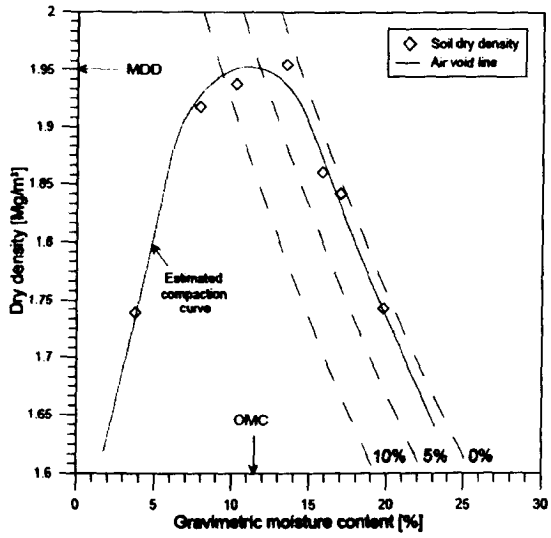

Figure 4.3 Soil compaction test on Boulder clay.

4.3.5. Assessment of Desiccation of Clay - Soil Water Characteristic Curve

The relationship between the matric suction and soil moisture content (Soil Water Characteristic Curve) was determined using three techniques described in Chapter 2. It is worth mentioning that each technique requires a different size of sample. Moreover, samples are relatively small in comparison to the mass of the soil in-situ. The following procedures have been applied for each particular technique.

4.3.5.1. Filter Paper Method

The filter paper method is commonly used for determining the Soil Water Characteristic Curve. In this method a circular filter paper (Whatman nr. 42) is placed between two soil samples (see Figure 4.4). A direct contact is required between the filter paper and soil samples. Additionally, two sacrificial filter papers (Whatman nr. 1) are usually placed below and above the filter. The sample then is wrapped by a cling film and placed into a tightly sealed container for a period of 1 to 2 weeks (see Figure 4.5 and Figure 4.6). This time is required, as the filter paper has to come to the equilibrium with soil. The filter is then carefully removed from the sample and the measurement of the filter paper moisture content is taken. Two filter paper tests have been carried out in order to study the water retention curve of soil used in this research. In the first test, eleven samples were compacted at different dry unit weights and at different moisture contents. In the second test two samples were

compacted at the desired dry unit weights (γ_d=18.62 kN/m^3 and γ_d=17.25 kN/m^3) and at constant moisture contents of 14.6% and 18.8% respectively. The filter papers were removed from the samples after one week and the soil suction measurements were taken, whereas the filter papers were replaced in the samples used for the second test. Moreover, before placing the new filter paper samples were exposed to atmosphere for about 4 hours in order to initiate drying. Prior to this operation, samples were carefully weighted and measured in order to calculate the moisture content and volume change after drying. The samples were then sealed again and placed inside containers for another week. It can be clearly seen in Figure 4.7 that the same desorption path is followed by results obtained from both tests.

Figure 4.4 Filter paper placed on the soil sample.

Figure 4.5 Sample wrapped in cling film.

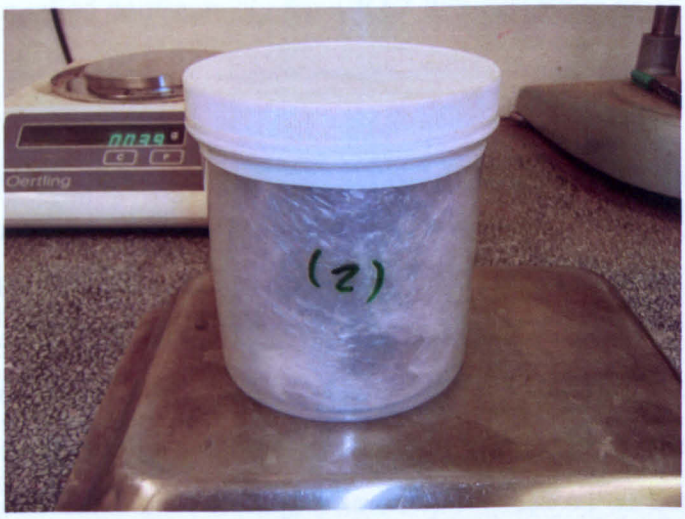

Figure 4.6 Sealed plastic container.

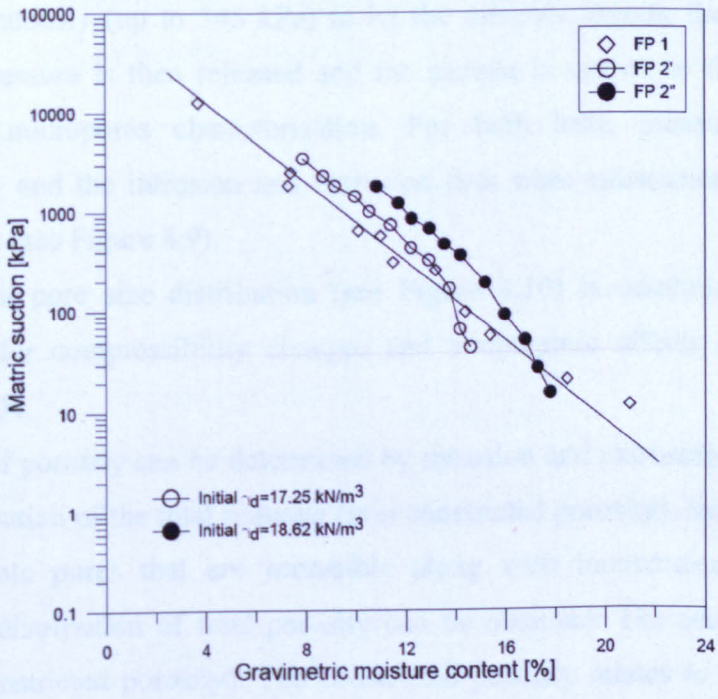

Figure 4.7 SWCC for filter paper.

4.3.5.2. Micro Intrusion Porosimetry

MIP test was carried out at UPC in Barcelona using Autopore IV 9500 porosimeter to examine the pore structure of the soil sample prepared at saturation state. The equipment consists of two operating units: low pressure filling apparatus from approximately 0.67 kPa to 345 kPa measuring macropores with apparent pore diameter from 3.6 μm to 360 μm where the sample is degassed under vacuum; and

the high pressure station for micropores characterisation, where the high pressure (up to 228 MPa) is applied continuously from 0.67 kPa (apparent pore diameter 0.0055 μm to 6 μm).

The MIP equipment requires dehydrated cubical samples measuring preferably less than 1 cm^3 (limited by the sample holder). A sample was previously prepared and compacted in the oedometer ring at desired dry unit weight (γ_d=16.47 kN/m^3) and at constant water content of 20.03 %. From the compacted sample, a small specimen was carefully trimmed using a penknife into a cube measuring around 10 mm on each side. Subsequently this sample was freeze dried to remove the pore water and then kept in a desiccator until testing. The sample is placed in the sample holder, weighed and mercury is allowed to flow into the sample holder. The pressure is raised continuously (up to 345 kPa) to let the mercury intrude the sample (Figure 4.8). The pressure is then released and the sample is moved to the high pressure station for micropores characterisation. For both tests, pressure was applied continuously and the intrusion and extrusion data were automatically recorded for both stations (see Figure 4.9).

The apparent pore size distribution (see Figure 4.10) is determined by applying corrections for compressibility changes and temperature effects as suggested by ASTM D4404.

Two types of porosity can be determined by intrusion and extrusion cycles. The first is the distribution of the total porosity (non-constricted porosity). Intrusion cycle fills intra-aggregate pores that are accessible along with interconnected pore space. Hence, the distribution of total porosity can be obtained. The second defines free porosity (constricted porosity). The constricted porosity relates to the constrictions formed by clayey bridges and irregular shape of aggregates trapping mercury in the inter-aggregate pores (Romero, 1999).

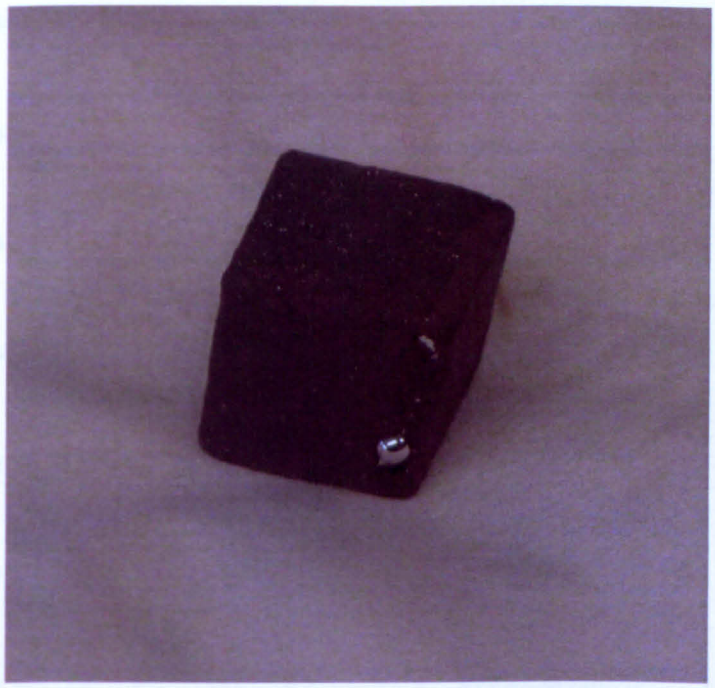

Figure 4.8 Sample intruded by mercury.

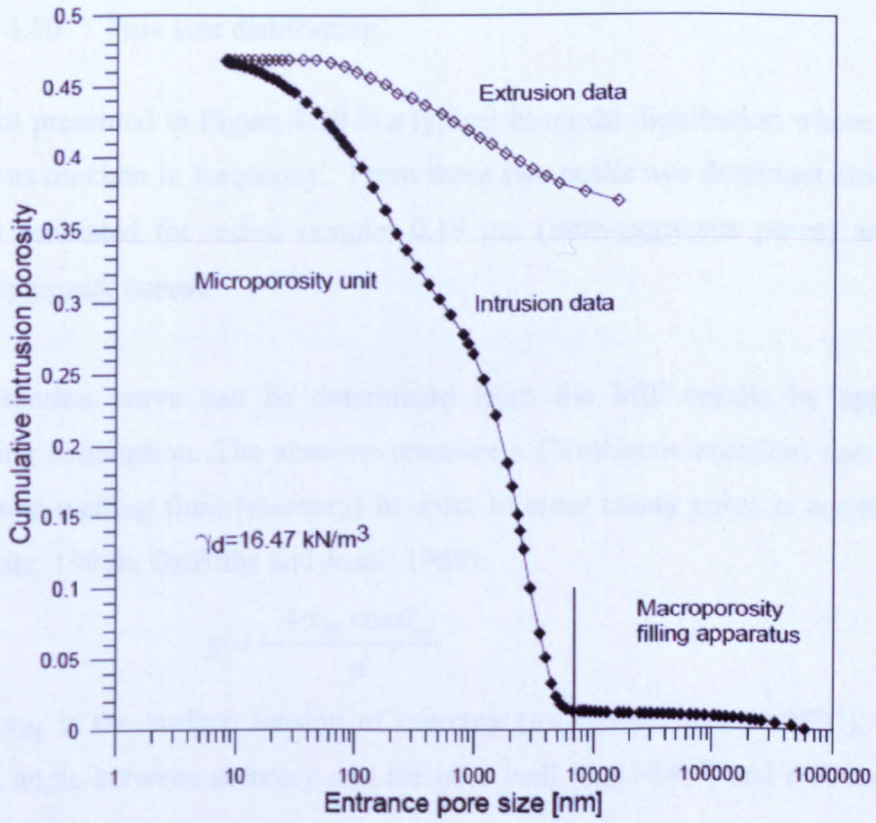

Figure 4.9 Cumulative intrusion porosity.

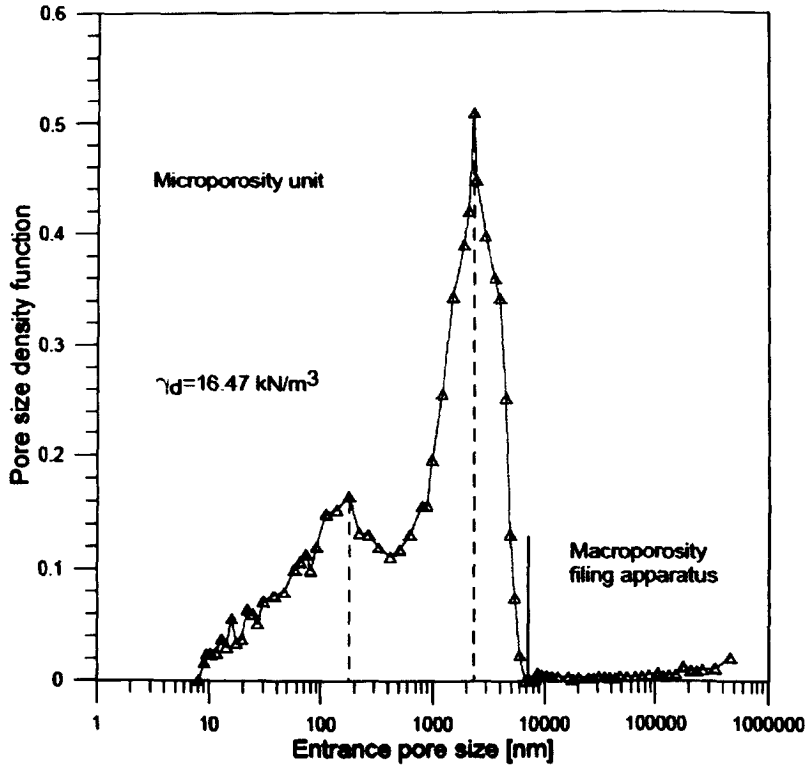

Figure 4.10 Pore size distribution.

The plot presented in Figure 4.10 is a typical bi-modal distribution where two peaks appear as maxima in frequency. From these two peaks two dominant sizes of pores can be estimated for tested sample: 0.19 μm (intra-aggregate pores) and 2.1 μm (inter-aggregate pores).

The retention curve can be determined from the MIP results by applying the following assumption. The absolute pressure p (Washburn equation) that is applied to the non-wetting fluid (mercury) in order to enter empty pores is equal to (Juang and Holtz, 1986b; Griffiths and Joshi, 1989):

$$p = -\frac{4\sigma_{Hg}\cos\theta_{nw}}{d} \tag{4.1}$$

where σ_{Hg} is the surface tension of mercury (σ_{Hg}=0.484 N/m at 25°C), θ_{nw} is the contact angle between mercury and the pore wall (θ_{nw} =140°) and d is the apparent pore diameter.

The injection of non-wetting fluid (mercury) with the contact angle of θ_{nw} =140° is equal to the ejection of water from the pores (desorption curve) by the non-wetting front advance of air with θ_{nw} =180° for the same intruded pores (Romero, 1999):

$$(u_a - u_w) = \frac{4\sigma \cos\theta_w}{d} \tag{4.2}$$

where (u_a-u_w) is the air overpressure or matric suction, σ is the water surface tension (σ=0.072 N/m at 25°C), $cos\theta_w$ is the wetting coefficient for the air-water interface.

By applying Eq. 4.2 to Eq. 4.1, matric suction can be determined:

$$(u_a - u_w) = -\frac{\sigma \cos\theta_w}{\sigma_{Hg} \cos\theta_{nw}} p \approx 0.196p \tag{4.3}$$

The volume of pores not intruded by mercury should be used to determine the water content or degree of saturation that corresponds to the applied air overpressure. The corresponding water content w can be estimated from the following expressions:

$$Sr_{nw} + Sr = 1 \tag{4.4}$$

$$Sr \cdot e = Gs \cdot w \tag{4.5}$$

$$w = \frac{e_{int}}{Gs}(1 - Sr_{nw}) = w_{sat}(1 - Sr_{nw}) \tag{4.6}$$

where Sr_{nw} is the mercury degree of saturation, Sr is the water degree of saturation, e_{int} is the intruded void ratio, Gs is the specific gravity of the soil, and w_{sat} is the saturated water content.

For the saturated moisture content (w_{sat}=22%) the water retention curve SWCC is presented in Figure 4.11.

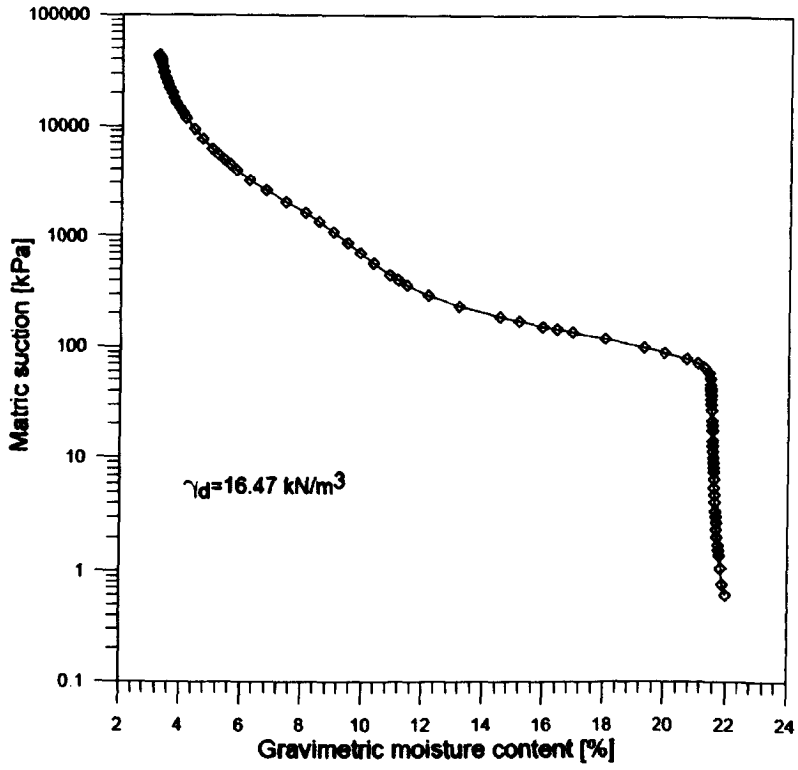

Figure 4.11 SWCC curve determined from MIP test.

4.3.5.3. WP4 – Chilled mirror dewpoint PotentiaMeter

WP4-T uses the chilled-mirror dewpoint technique to measure the water potential of a sample. This technique is much faster and more accurate than pressure plate and filter paper. The WP4 (see Figure 4.12) measures water potential by determining the relative humidity of the air above the sample in a closed chamber that contains a mirror and a means of detecting condensation on the mirror. At temperature equilibrium, relative humidity is a direct measurement of water potential of the sample. In addition, WP4 features an internal fan that circulates the air within the chamber, thus the equilibrium time is reduced to minimum. WP4 can measure the water potential directly within the range from 0 MPa up to -300 MPa. However, it was found that there is a lot of noise below 1 MPa, hence WP4 is used for the measurements from 1MPa upwards.

Figure 4.12 WP4-T Chilled mirror dewpoint PotentiaMeter.

These tests were also carried out at UPC in Barcelona. The sample was prepared and compacted in an oedometer ring at desired dry unit weight (γ_d=17.56 kN/m^3) and at constant water content of 10.0 %. Then the sample was trimmed and sliced into two slices. Both samples were trimmed to the size of sample cup and weighed. The first slice was placed inside the chamber, whereas the second slice was left to air dry in order to find the air dry point. After each measurement, sample is removed and the weighed. The same procedure was applied for an air dried sample.
The suction readings are plotted against the moisture content determined from the difference between the initial and final mass of the sample.

Despite the fact that the initial water content and void ratio for both samples were different, the same drying path was obtained for both samples, as it is presented on Figure 4.13.

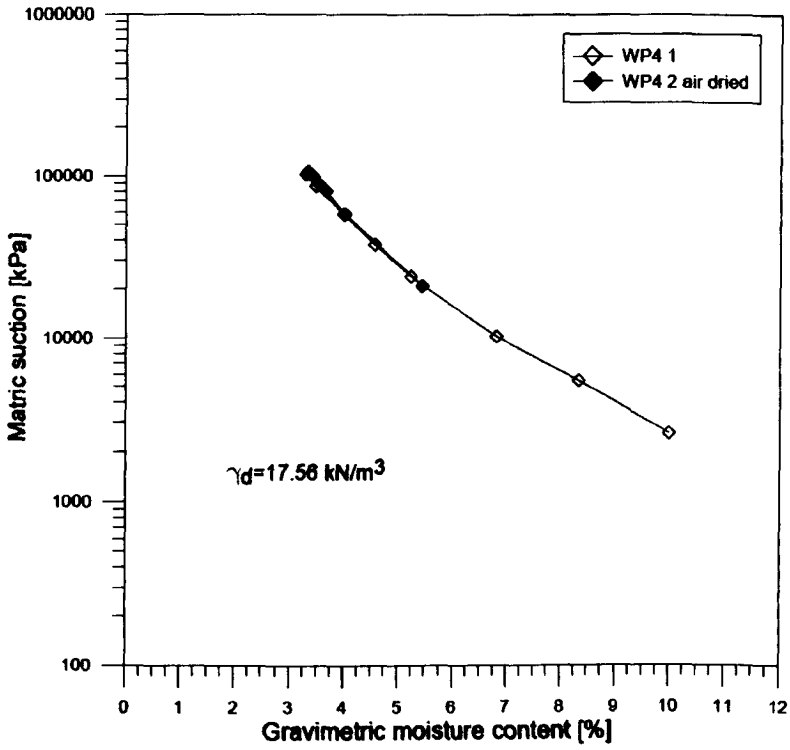

Figure 4.13 SWCC for WP4 test.

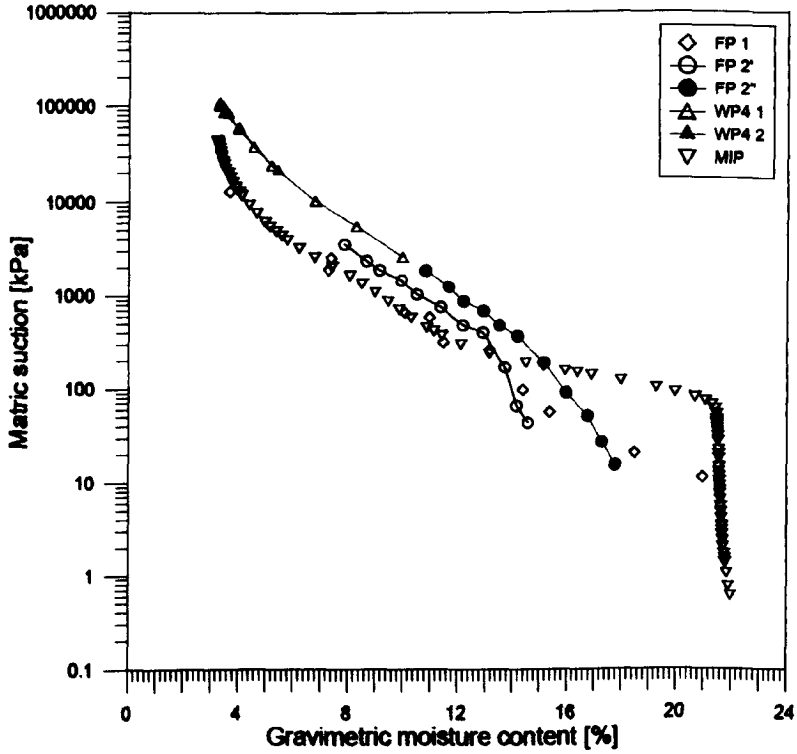

Figure 4.14 SWCC for Boulder clay determined by different techniques.

In Figure 4.14, the relationship between matric suction and gravimetric moisture content is plotted. This graph summarises the results obtained from the three methods that were used to determine Soil Water Characteristic Curve for the soil used. The measurements from the three different techniques closely match the slope of drying curve (desorption curve) that is characteristic for this specific soil.

The initial void ratio and moisture content were found to play a significant role on the soil water characteristic curve (Kawai et al., 2000; Zhou and You, 2005) at low suctions. This trend was also observed for all the presented methods where there was a difference in suction measurements at the initial state for each sample. When the air entry value was reached, this effect seemed to decrease. Hence, the slope of desorption curve was the same. This was in good agreement with the observations made by Zhou and You (2005).

4.4. CONSTRUCTION OF THE EMBANKMENT MODEL

The embankment model has been constructed in the concrete flume where a large amount of water could be supplied in order to simulate the flooding conditions. The concrete channel (1.1 m high, 1.85 m wide and 20 m long) consists of two side windows in its middle part. The intention was to visually observe cracking growth inside the embankment model during desiccation process. The channel was additionally equipped with a water supply system containing the diffuser installed at its end. Figure 4.15, shows the concrete flume where the experimental model was constructed.

Figure 4.15 Concrete flume with diffuser and windows where the model was constructed.

It was decided to build the embankment model in ten 10 cm thick layers to achieve maximum homogeneity and required compaction. Prior to the construction, a cut off barrier was installed in the centre of embankment body (Figure 4.16). Following the cut off installation, a 20 cm thick and 2 m long berm was constructed on the upstream side (Figure 4.17).

Figure 4.16 Installed cut-off barrier.

Figure 4.17 Berm compacted to desired state.

The soil was placed into 12 cm high shuttering and then broken down to smaller lumps (Figure 4.18). Under normal conditions, when the embankments are being constructed in the fields, grid rollers are used to break down the big lumps of the fill material in order to achieve a homogenous product.

Figure 4.18 Soil prepared for compaction (2nd layer).

The moisture content of the soil plays a major role during the compaction process. It is important to control the moisture content during compaction to achieve the maximum required compaction. Moreover, it was found that according to Specification for Highway Works, the soil moisture content for compacted soil should be within the range of 5.8 %-16.5 %. This corresponds to the 95% of maximum dry density estimated from Figure 4.19. Thus, soil samples where taken from each layer in order to measure the moisture content (using a specialised balance which allows rapid determination of the moisture content of a soil sample within 20 minutes) before the compaction was applied. When the moisture content exceeded the estimated range, the soil was left overnight to let the water evaporate. The moisture content was measured again the next day to confirm that the required value was achieved.

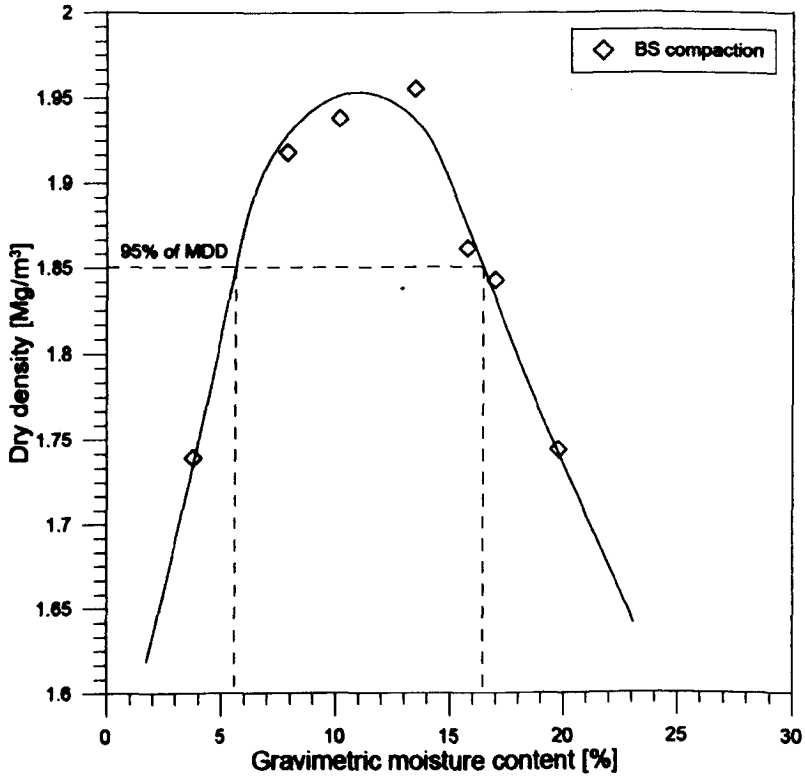

Figure 4.19 95% of maximum dry density estimated from compaction curve.

Due to requirements specified in the Specification for Highway Works, 85 kg heavy vibrating plate was used for compaction (Figure 4.20).

Figure 4.20 85 kg vibrating plate used for compaction.

As mentioned before, the embankment was constructed in 10 layers. The compaction has been split in two parts. Five layers were first compacted in 10cm high layers and the last 5 layers were divided in two parts. In order to investigate the effect of the thickness of the compacted layer on the desiccation process, one half of the embankment was compacted in 10 cm thick layers, and the other half in 5 cm thick layers. Prior to the completion of each 10 cm layer, 5 cm layers were first completed.

Furthermore, to make the best contact between two layers and to avoid the weak surface in between, each layer was scraped using a rake, as it is shown in Figure 4.21. At the end of compaction day, embankment was covered by a plastic sheet in order to prevent any the moisture loss.

Figure 4.22 shows the timescale that was needed for the construction of the experimental set-up.

Figure 4.21 Scraped surface prepared for the next layer placing.

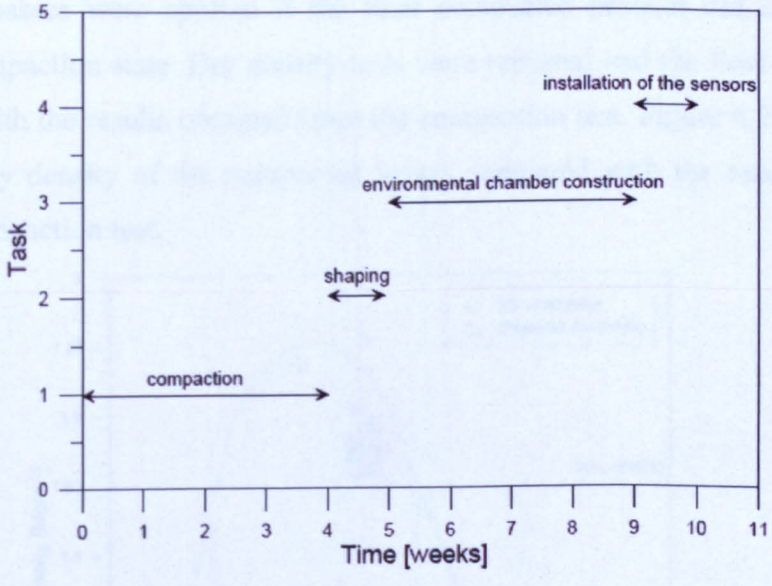

Figure 4.22 Construction timescale.

4.4.1. SOIL COMPACTION PROPERTIES DURING CONSTRUCTION.

To indicate the state of the compaction, dry density tests were carried out. One undisturbed soil sample was taken from each side of the compacted layer using U_{100} steel tubes. The samples were extruded from the tube and the weighted. The volume of each sample was recorded. Figure 4.23 shows an extruded sample.

Figure 4.23 U_{100} sample taken from compacted layer.

Additional passes were applied if the final compacted product did not meet the required compaction state. Dry density tests were repeated and the final results were compared with the results obtained from the compaction test. Figure 4.24, shows the measured dry density of the compacted layers compared with the results obtained form the compaction test.

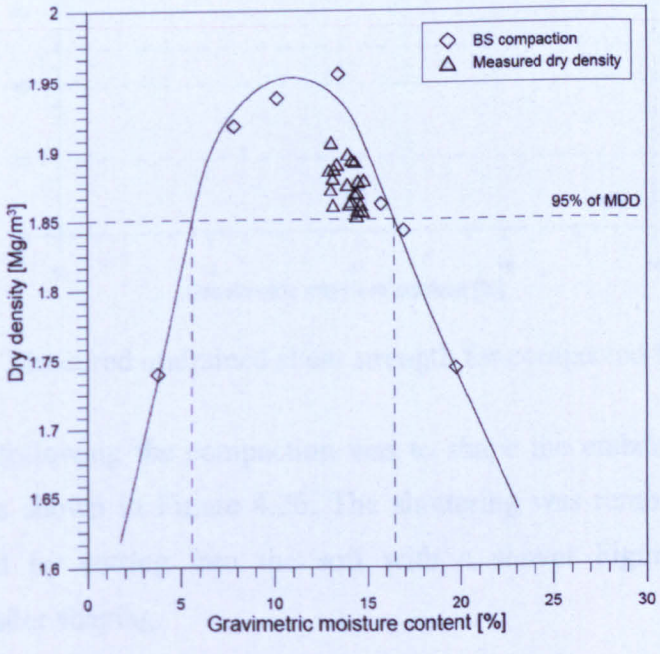

Figure 4.24 Dry density measured for compacted layers.

In order to provide a good compaction product, the shear strength of the soil had to be measured in a randomly chosen 6-9 points (for each compacted layer). The measurements were taken during the construction phase using hand vane tester (H-60 Field Inspection Vane Tester - ELE Manual) and the undrained shear strength was calculated. The measured undrained shear strength varied in the range of 64-96 kPa, with the moisture content ranging from 13.0 % to 14.87 % (see Figure 4.25).

The final achieved consistency has been classified to be Firm and mostly Firm to Stiff (BS 5930:1999). This meets the compaction state required by Specification for Highway Works – Earthworks, Series 6000. This also confirmed that the compaction procedure was appropriate. The construction was designed according to required standards.

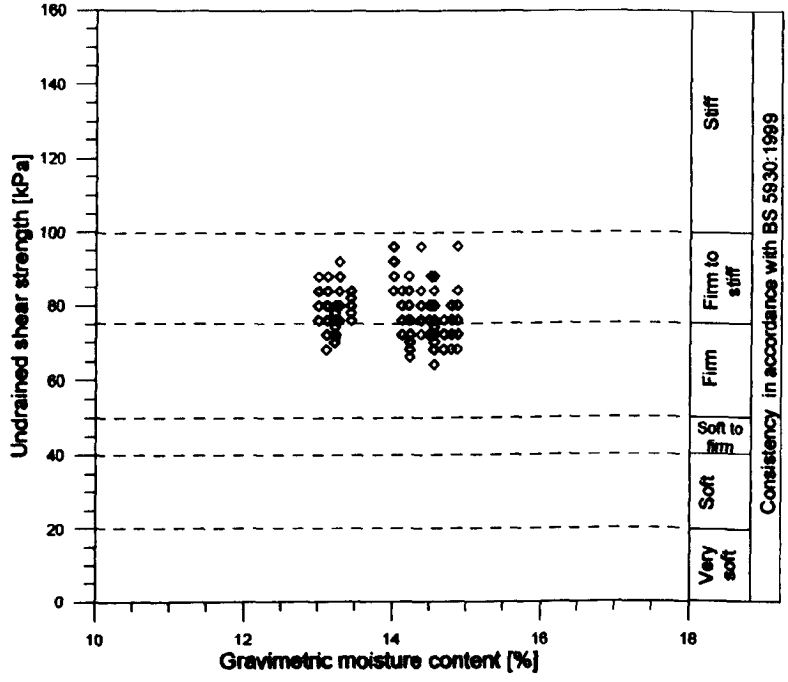

Figure 4.25 Measured undrained shear strength for compacted layers.

The last step following the compaction was to shape the embankment to designed dimensions, as shown in Figure 4.26. The shuttering was removed and the slopes were prepared by cutting into the soil with a shovel Figure 4.27 shows the embankment after shaping.

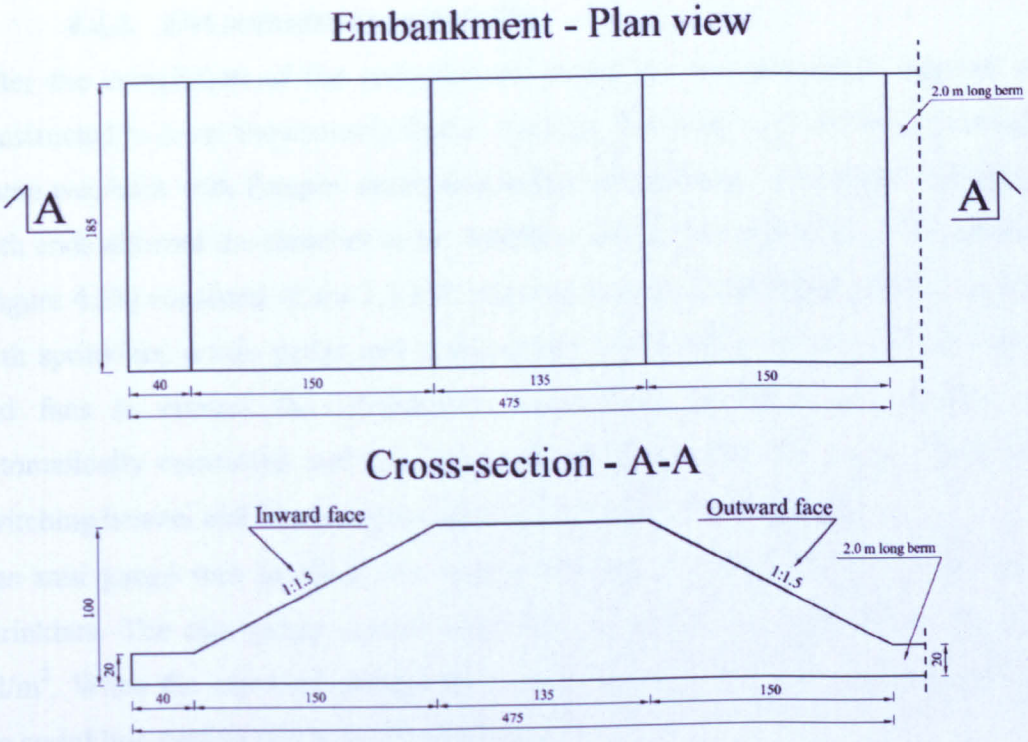

Figure 4.26 Plan view and cross-section of the embankment model.

Figure 4.27 Final shape of the embankment.

4.4.2. *ENVIRONMENTAL CHAMBER*

After the completion of the embankment model, an environmental chamber was constructed to cover the concrete flume. 1m high, 8 m long and 1.85 m wide wooden frame was built with Perspex sheets and sealed with silicone. Two doors installed on both ends allowed the chamber to be ventilated during the experiment. The chamber (Figure 4.28) consisted of six 1.2 kW infra-red heaters, 2 high speed fans, two pipes with sprinklers, a rain gauge and a thermostat which was coupled with the heaters and fans to control the temperature inside. The whole heating system was automatically controlled and was based on the thermostat and relays which were switching heaters and fans until the adjusted temperature was reached.

The rain gauge was installed 1 m above embankment body in the same line as sprinklers. The rain gauge remote controller was set to a precipitation rate of 55 ml/m^2. When the expected precipitation was achieved, an alarm was triggered and the sprinkling system had to be closed manually.

Figure 4.28 Environmental chamber with embankment and installed sensors.

In summary, the geotechnical tests presented in this Chapter characterised the geotechnical parameters of clay (Liquid Limit, Plastic Limit, Plasticity Index, linear shrinkage, specific gravity, maximum dry density and optimum moisture content) used for the construction of the embankment model. Additionally, three non-

conventional geotechnical tests were carried out to predict the trend of the water flow within unsaturated soil in respect to suction through the Soil Water Characteristic Curve (SWCC). Although the size of the samples was different for each test, a good agreement was achieved and the same slope of desorption curve was obtained.

The construction of the embankment model was carried out according to the Specification for Highway Works which at the moment is the only existing standard in UK where these types of the earth works are specified.

The environmental chamber required more design as these types of facilities are not commercially available.

The next Chapter provides an overview about the instrumentation used for monitoring the evolution of the embankment as well as ambient parameters.

CHAPTER 5

5. MEASURING EQUIPMENT

5.1. INTRODUCTION

This chapter is introducing the type of instrumentation used on the embankment model in order to observe its behaviour during the experimental period. The measuring equipment included: moisture content sensors, tensiometers, Relative Humidity (RH) and temperature sensors, rain gauge and miniature resistivity. Their working principles and the installation procedure are described.

An excellent overview of the advantages and limitations of the measuring methods in applied soil mechanics has been provided by Peck (1969). A similar approach has to be applied to unsaturated soil problems in order to increase the confidence in the application of unsaturated soil theories. Moreover, the measurements must be reliable and reveal the significant phenomena in detail. The matric suction, moisture content and soil electrical resistivity are the measurements that can provide information on unsaturated soil behaviour. Hence, civil engineers must have access and consider the use of devices that will provide adequate tools in engineering design (Fredlund, 2006). Furthermore, they must ensure that these devices have a sufficient accuracy for engineering purposes.

5.2. MOISTURE CONTENT PROBES – TDR'S

Measurements of gravimetric moisture content provide a reference for the amount of water contained in a soil. They are very important and can play a major role in the assessment of the soil behaviour. However, this method is intrusive, destructive and not satisfactory even if, it provides direct and quick measurements. Time domain reflectometry sensor (TDR) consists of 4 metal rods which should be inserted into soil during measurements. An electrical pulse is sent to the end of the rods (and returns) and the results provide a measure of the dielectric constant of the soil. The dielectric property is dependent on the amount of water in the soil and the measurement can be converted to the gravimetric water content (Fredlund, 2006). Figure 5.1 shows an example of TDR probe used in the experiment.

Figure 5.1 Example of TDR probe used in the experiment (after Delta-T).

A specific calibration curve for the soil needs to be used to achieve the proper accuracy of the measurements. The example of the calibration curve is shown in Figure 5.2. In some cases the salt content in the pore water may affect the moisture content measurements, this may need to be considered if the equipment is used in estuarial environments, but is not significant in laboratory measurements.

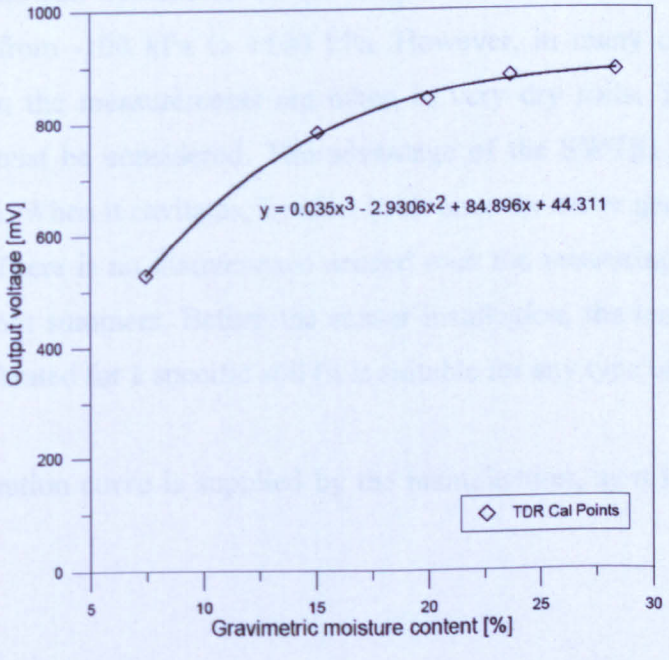

Figure 5.2 Specific calibration curve for Boulder clay.

5.3. SOIL WATER TENSION SENSOR – SWTS 1

Generally, the most preferred measurements in unsaturated soil mechanics are the measurements of matric soil suction. Over the years, there has been a significant increase in development of sensors and devices, particularly related to the measurement of soil suction in the agronomy or agriculture-related disciplines (Dane and Topp, 2002). Moreover, these sensors have been also successfully applied in geotechnical related problems especially unsaturated soil mechanics (Croney et al., 1958; Croney and Coleman, 1960; Ridley, 1993; Wu et al., 1993; Gourley and Schreiner, 1995; Guan, 1996; Guan and Fredlund, 1997; Muraleetharan and Granger, 1999; Take and Bolton, 2001; Wendling and Meiβner, 2001; Yoshida and Adachi, 2001; Take and Bolton, 2002a; Take and Bolton, 2002b; Meilani et al., 2002; Vatsala and Srinivasa Murthy, 2002; Ridley et al., 2003b; Tarantino and Mongiovì, 2003; Ridley et al., 2004.; Smethurst et al., 2006; Cui et al., 2008; Trandafir and Gomi, 2008).

The SWTS 1 tensiometer compromises three direct different measurements. It can measure the following: (i) suction of the unsaturated soils, (ii) positive pore water pressure in saturated soils, (iii) and it can also measure the temperature of the water contained in the soil considered as the temperature of the soil. The range of the sensor varies from -100 kPa to +100 kPa. However, in many cases this range is exceeded when the measurements are taken in very dry soils. Thus, high suction tensiometers must be considered. The advantage of the SWTS1 sensor is its self-refilling option. When it cavitates, it refills itself once the water gets inside the sensor after rainfall. There is no maintenance needed over the measuring period especially after dry and hot summers. Before the sensor installation, the tensiometer does not need to be calibrated for a specific soil (it is suitable for any type of soil).

A single calibration curve is supplied by the manufacturer, as it is shown in Figure 5.3.

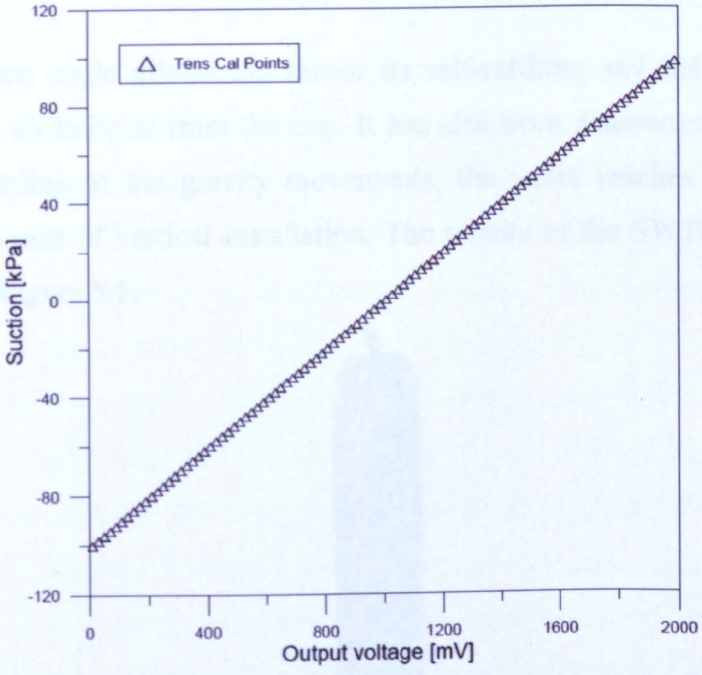

Figure 5.3 Single calibration curve for tensiometer - SWTS1.

The sensor can be installed either downwards or upwards but it has to be inserted at an angle and in the position where the water flow is not disturbed by the tensiometer (see Figure 5.4). The ideal angle for the air removal from the ceramic cup is 25° to 65° from the vertical line (Tensiometer TS1 - UMS Manual). Hence, the correction offset needs to be applied to the measurements.

Figure 5.4 Downwards installation at a specific angle (after UMS).

The installation angle allows the sensor its self-refilling and helps to completely removing the air bubbles from the cup. It has also been discovered, that during the rainfall, according to the gravity movements, the water reaches the ceramic cup faster than in case of vertical installation. The picture of the SWTS1 tensiometer is presented on Figure 5.5.

Figure 5.5 SWTS 1 tensiometer (after UMS).

To ensure the most reliable readings of the sensor, a good contact between the ceramic cup and the soil must be provided. Thus, it is suggested to inject the slurry paste of the same soil inside the augered hole to fill up the space between the sensor body and the soil. The full procedure of installation is described in the final section of this Chapter.

5.4. SOIL WATER TENSION SENSOR – T4E

The water movements in soils are depending on the soil water tension. The water will always move from a point of higher potential to a point of lower potential (UMS Manual). The most of the soil water movements are taking place when the small water tensions are occurring. Tensiometers are the best sensors which allow direct and very precise measurements of the water tensions. In the homogenous soils not

only precipitation and evaporation affect the process of water movement. The texture, particle size distribution, cracks, compaction, roots and air voids, also should be considered. Due to these heterogeneities the soil water tension may vary and change dramatically especially when the soil is cracked. In general, the purpose of use the tensiometers, is to measure the soil water tension respectively of matrix potential. Presented tensiometer, can measure the pore water pressure from +100kPa (positive pore water pressure) to -85kPa (suction of the soil). If the soil is drier than -85kPa, tensiometer gets dry and cavitates and needs to be refilled before the soil is moist again. Water contained in the soil has a contact with the tensiometer through the ceramic cup which is porous and lets the water get inside the cup. This creates an ideal interface between both soil and water. The pressure transducer inside the ceramic cup gives direct and continuous measurements of water tension. The reference pressure is measured through membrane installed on the cable. Chosen T4e is equipped with two capillary tubes (refilling tubes) and can be refilled in the field without removing it from the soil. Figure 5.6 shows the T4e tensiometer used in this study.

Figure 5.6 Soil water tensiometer sensor - T4e (after UMS).

The T4e tensiometer must be installed with following the procedure described in the previous paragraph. The installation angle must be applied and a good contact

between ceramic cup and the soil must be ensured. The calibration curve, (Figure 5.7) for the T4e tensiometer is supplied by the UMS manufacturer (T4e tensiometer - UMS Manual), and the sensor does not need to be calibrated for specific soils.

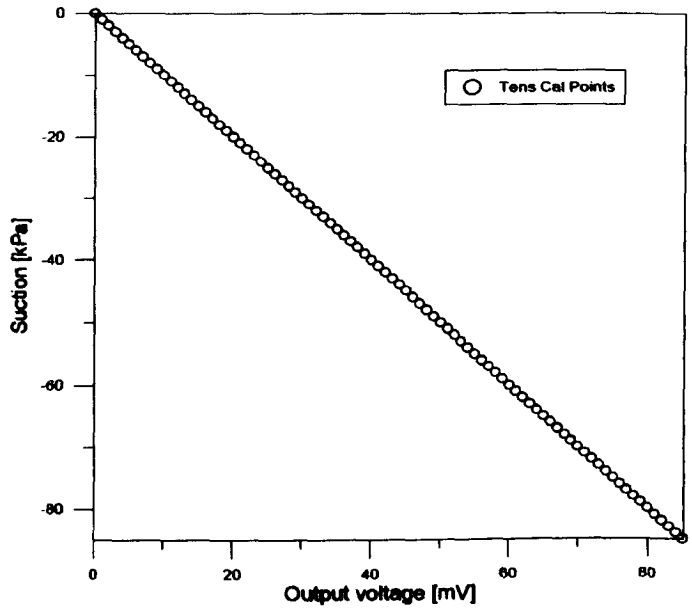

Figure 5.7 Single calibration curve for tensiometer – T4e.

Four of these tensiometers were installed on the upstream slope of the embankment model. The full procedure that was used for the installation is described in the final section of this Chapter.

5.5. RELATIVE HUMIDITY & AIR TEMPERATURE SENSORS – RHT2NL

The RHT2nl sensor compromises two independent sensors: Relative Humidity and air temperature transducer which are housed in the radiation shield. The transducers provide two output signals for the RH and air temperature. The RHT2nl sensor gives high precision measurements with the output range 0 to 100% for relative humidity and -50°C to 150°C for air temperature. These sensors are design to work as part of the weather station, but when needed, they may work independently when plugged into the Data Logger. Figure 5.8 shows a picture of the sensor used.

Figure 5.8 Picture of RHT2nl sensor in the solar radiation shield (after Delta-T).

Both sensors give very accurate and direct measurements and do not need to be calibrated before use. The calibration curve is supplied by manufacturer.

5.6. RAIN GAUGE

The Oregon Scientific Wireless Rain Gauge contains an automatic self-emptying rain cup and the indoor gauge module (Figure 5.9).

Figure 5.9 Oregon Scientific Wireless Rain Gauge with self-emptying rain cup and the indoor gauge module.

The rain cup communicates with the gauge module through the wireless which displays the precipitation amount in mm/m^2.

5.7. MINIATURE RESISTIVITY ARRAY

The miniature resistivity array is a geoelectrical tool using the ARES (Automatic Resistivity System) earth meter equipment purchased from the company Gf Instruments (see Figure 5.10). The ARES earth meter comprises the 1100 V – 2 A – 300 W transmitter coupled with T-piece which allows connection of multi-electrode cable sections and cables for current and potential electrodes.

Figure 5.10 ARES earth meter (after Gf Instruments).

The resistivity measurements can be used for many applications, such as: ground water explorations, geotechnical investigations, monitoring of dams and embankments, environmental studies, pollution plumes mapping, geological surveys, mineral prospecting, archaeology, detection of caves, marine, borehole and cross-hole measurements.

The electrical resistivity method measures the apparent bulk electrical resistivity by sending current into the ground through current electrodes that are pushed in the ground surface. The difference of the electrical potential between the potential electrodes is then measured. The amount of current measured in Amperes and the potential difference measured in Volts is used to calculate the apparent resistivity (ohm-meters) at the midpoint of the array of the electrodes. A schematic working principles of Wenner resistivity array is presented in Figure 5.11.

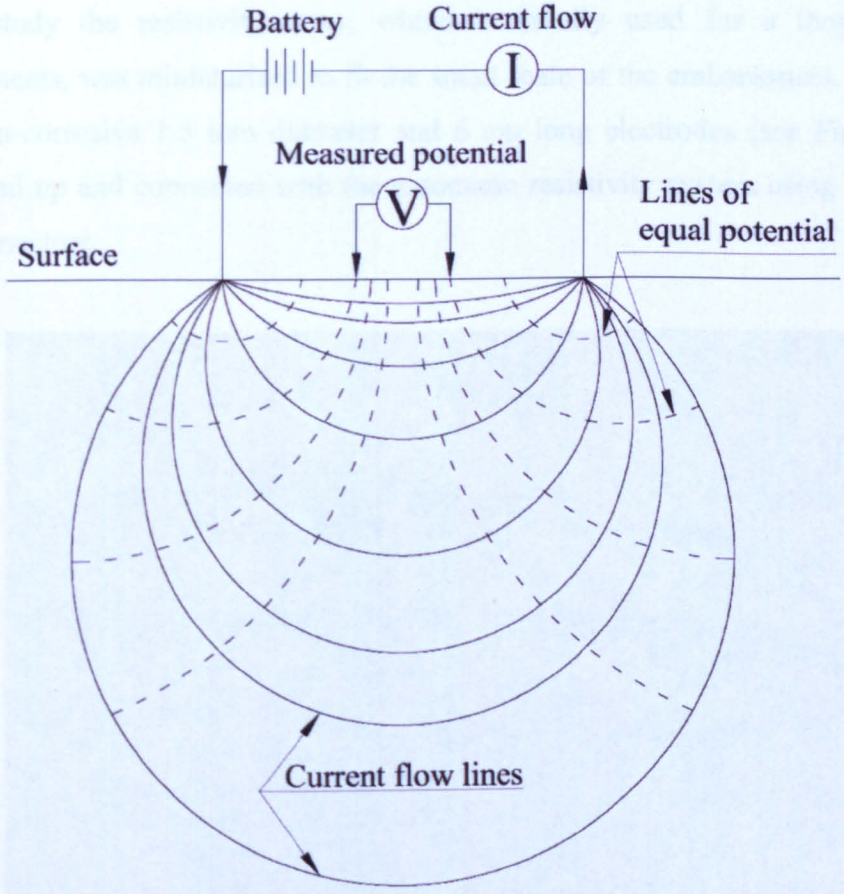

Figure 5.11 Wenner resistivity array.

The map of apparent resistivity measurements can be obtained using the inversion model provided by Res2Dinv Software. Figure 5.12 shows an example how the resistivity measurements are inversed into a contour map.

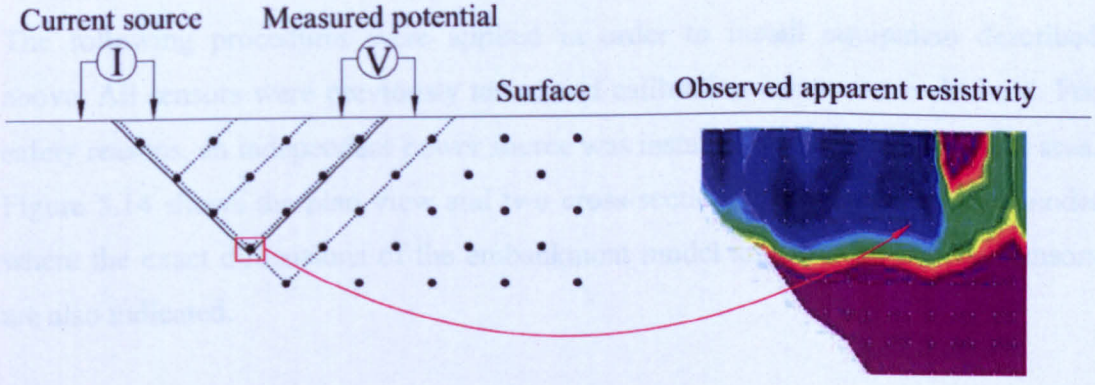

Figure 5.12 Resistivity measurements inverted into contour map.

In this study the resistivity array, which is usually used for a long distance measurements, was miniaturised to fit the small scale of the embankment. Two sets of 48 non-corrosive 1.5 mm diameter and 6 cm long electrodes (see Figure 5.13) were wired up and connected with the automatic resistivity system using double 24 ways connectors.

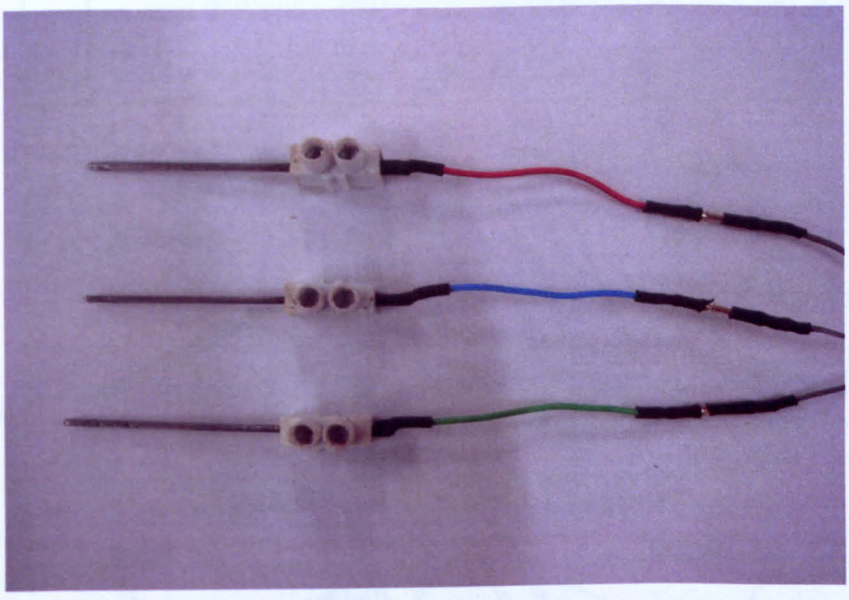

Figure 5.13 Non-corrosive electrodes mounted in block terminals.

The installation procedure which was applied to this equipment is described in the next section.

5.8. INSTALLATION PROCEDURES

The following procedures were applied in order to install equipment described above. All sensors were previously tested and calibration curves were obtained. For safety reasons, an independent power source was installed close to experimental area. Figure 5.14 shows the plan view and two cross-sections of the experimental model where the exact dimensions of the embankment model and locations of the sensors are also indicated.

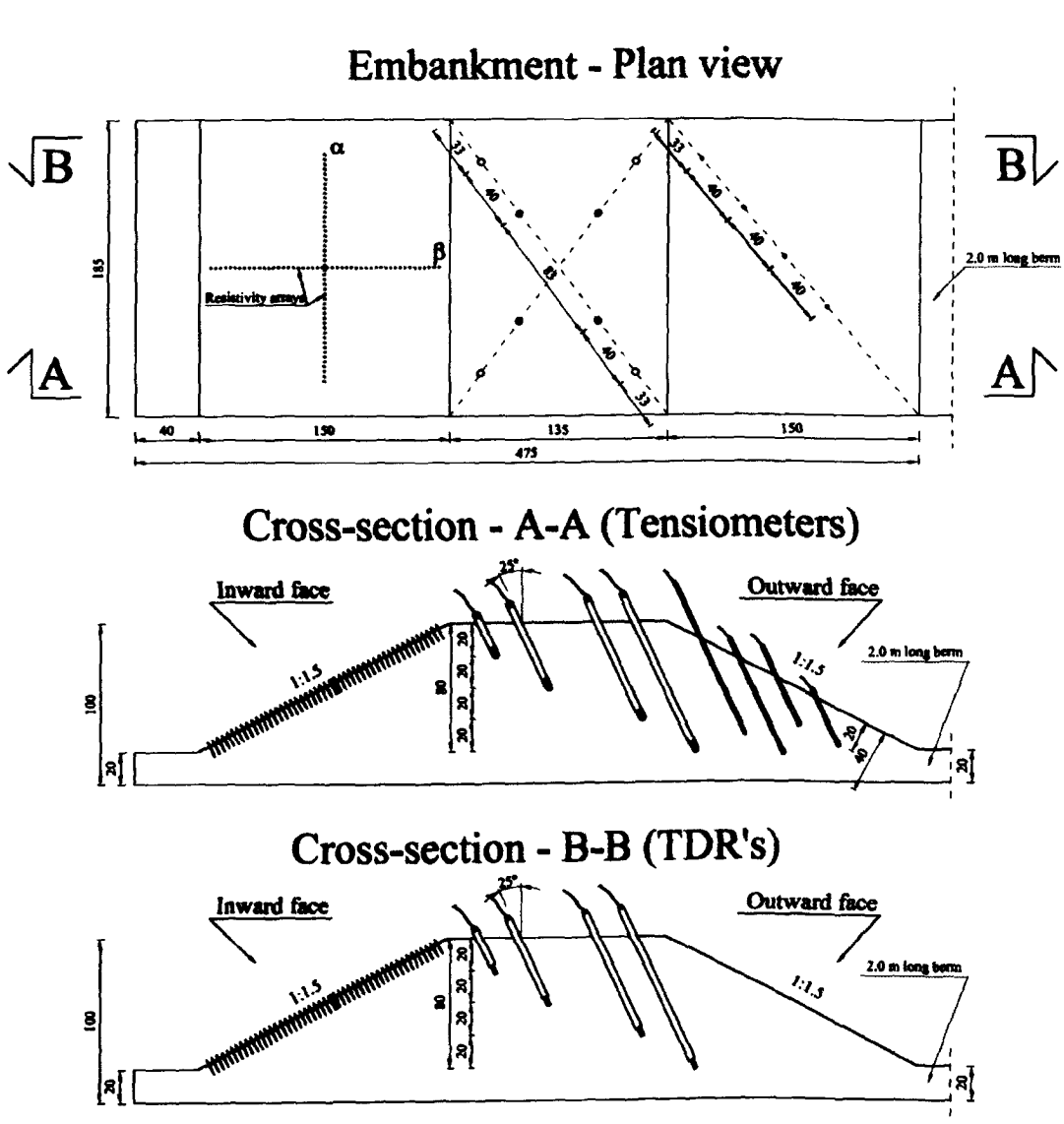

Figure 5.14 Plan view and the cross-sections of the experimental model.

5.8.1. Moisture Content Probes

Four moisture content probes (TDR's) were installed on the crest of the embankment model at four different depths (0.2 m, 0.4 m, 0.6 m, 0.8 m), (see Figure 5.14). Sensors were installed in the previously drilled holes using an auger and a steel angle supporter in order to ensure that the same installation angle of 25 ° is applied (see Figure 5.14 and Figure 5.15).

Figure 5.15 Supporting steel angle with the auger.

After the hole was augered, the soil samples were taken from the bottom of the hole and the undrained shear strength was measured using a Vane Tester (see Figure 5.16 and Figure 5.17).

Figure 5.16 Sample taken from the bottom of the hole.

Figure 5.17 Field inspection vane tester for undrained shear strength measurements.

Each sensor was inserted inside the hole and pushed into the soil until the steel rods were fully covered by the soil. The same distance was kept between the sensors on both sides of the embankment with a larger space left in its central part (Figure 5.18). Following the insertion of the sensors, the soil was compacted around their shafts.

Figure 5.18 TDR probes installed on the crest.

5.8.2. *SWTS1 TENSIOMETERS*

SWTS 1 tensiometers were supplied with their ceramic cups covered with small plastic bottles filled with water in order to prevent their desaturation. However, to ensure that they were fully refilled with water, additional automatic refilling was carried out. The sensors were attached to the racks with their ceramic cups immersed into glass containers with de-aired water (Figure 5.19). A 10V power supply was connected and the sensors were left overnight to refill themselves automatically.

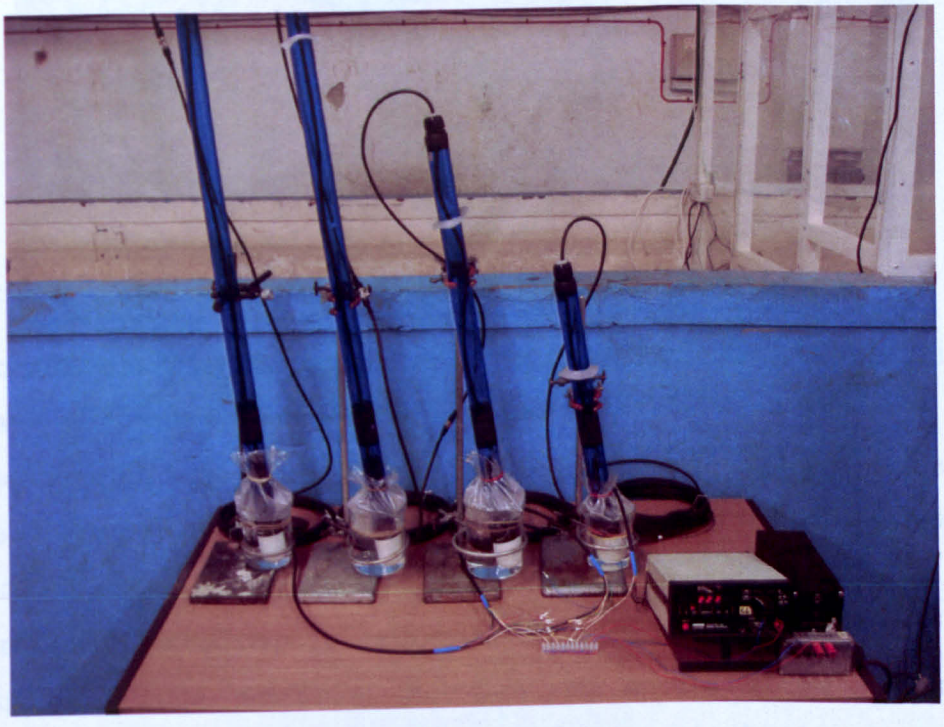

Figure 5.19 Tensiometers during refilling procedure.

After refilling, the tensiometers were removed from the water and immediately transferred into a container with the slurry paste of the same soil used for the embankment model (Figure 5.20).

Figure 5.20 Ceramic cup covered with the slurry paste.

It is important to cover the ceramic cup of the tensiometer after it is removed from the water, as the sensor must be free of entrapped air.

Four tensiometers were installed on the crest of the embankment model at the same depths as the moisture content probes (0.2 m, 0.4 m, 0.6 m, 0.8 m). The opposite section was chosen for the tensiometers installation in order to have the same reference points for both types of sensors (as shown on Figure 5.14).

A slightly different installation procedure was applied to the tensiometers installation. The same installation angle of 25^{o} was used with the ceramic cups directed to the upstream side of the embankment (see Figure 5.14). The soil samples and undrained shear strength measurements were taken at the bottom of each hole. Additionally, the slurry paste was injected into each augered hole in order to provide a good contact between the soil and the ceramic cup. The silicone tube was filled with a 25% moisture content slurry paste and a flexible pipe was fitted on its end (Figure 5.21).

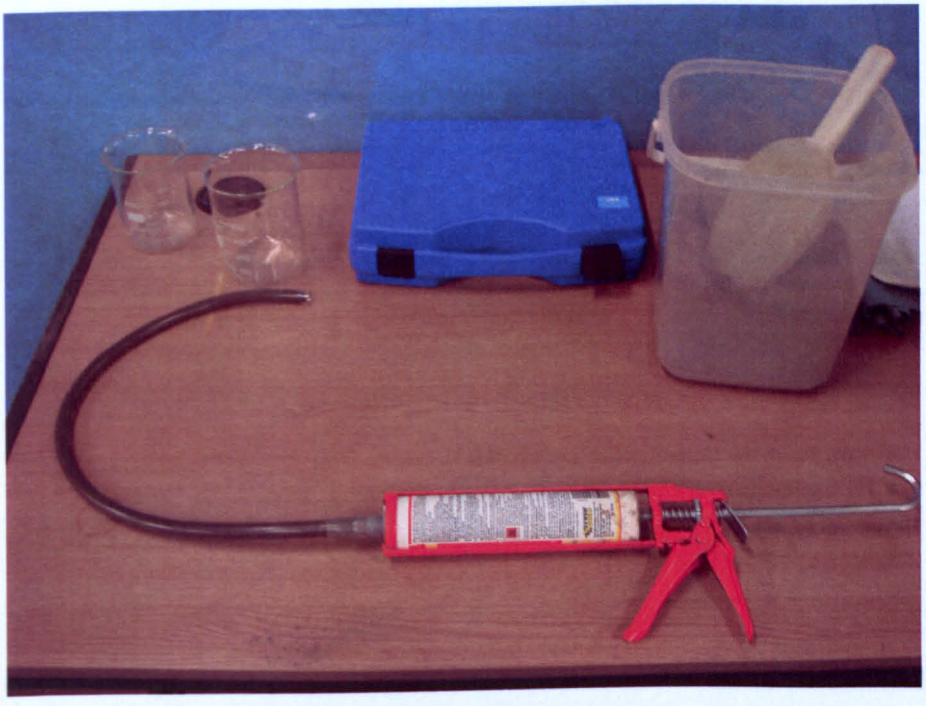

Figure 5.21 Silicone tube with flexible pipe.

A silicone gun (Figure 5.22) was used to push the slurry from the tube and to inject it into the hole on its full depth (Figure 5.23).

Figure 5.22 Injection of the slurry paste using silicone gun and flexible pipe.

Figure 5.23 Slurry paste inside the hole.

Each sensor was pushed carefully and slowly through the slurry paste. The depth required for each sensor was previously marked on the shaft of each sensor (see Figure 5.24).

Figure 5.24 Black mark on the shaft shows the installation depth.

At the same time, the insertion pressure was controlled by the INFIELD 7b Pressure Reading Unit (UMS Manual) (Figure 5.25) in order to ensure that the insertion pressure does not exceed the limit of sensor. Exceeding the pressure range of the sensor, could result in breaking it.

Figure 5.25 UMS INFIELD 7b Pressure Reading Unit used for controlling insertion pressure.

After installation, each tensiometer was disconnected from the INFIELD 7B reading unit and connected to the Delta-T Data Logger that was programmed to take readings every 30 seconds.

5.8.3. T4E TENSIOMETERS

Following the installation on the crest, four T4e tensiometers were installed on the upstream slope in order to investigate the difference between the suction changes on the slope and on the crest of embankment. It was decided that the T4e sensors will be installed at the same depths (two sensors at 0.2 m and two at 0.4 m) as the SWTS 1 tensiometers. Hence, the suction measured on the crest and on the slope could be compared. The same procedure and installation angle was applied, keeping the same distance between the sensors (Figure 5.14 and Figure 5.26).

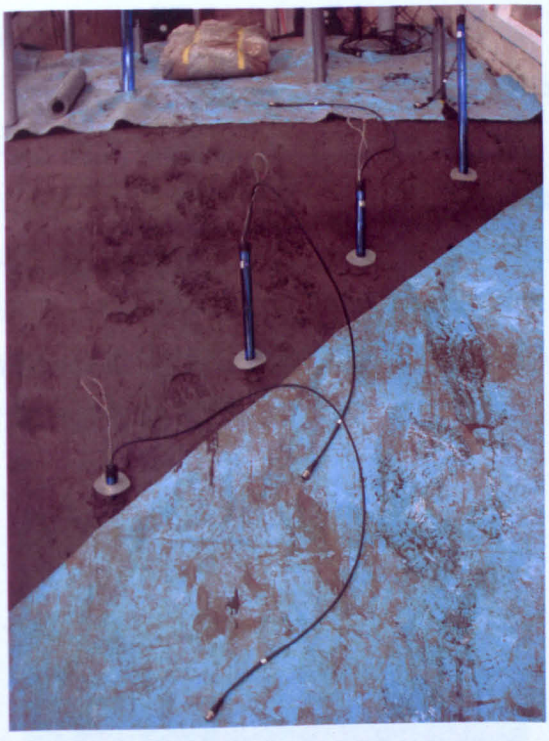

Figure 5.26 T4e Tensiometers installed on the upstream slope.

As these tensiometers were different than the one installed on the crest of the embankment model, they had to be additionally refilled using the manual vacuum pump system (Figure 5.27) in order to ensure that any entrapped air was removed from the system.

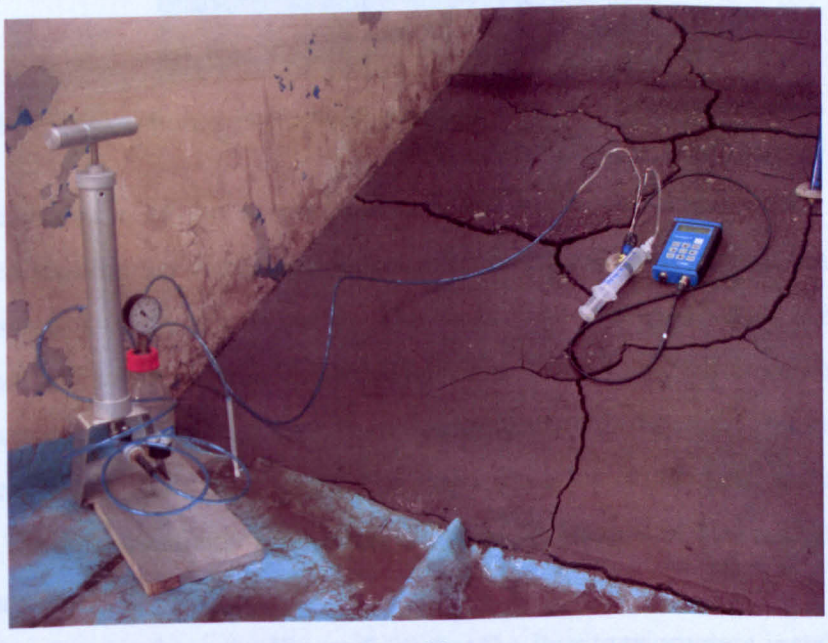

Figure 5.27 Vacuum pump and refilling kit.

Temperature variations and the formation of gas bubbles can cause problems and give false readings in tensiometric measurements. This is due to the expansion effect of the tensiometer shaft and the ceramic cup (Durner and Or, 2005). A study undertaken by Durner and Or (2005) showed that the above ground refilling tubes and the sensors shafts must be protected from heat and solar radiation. Hence, the proper lightning protection has to be considered whenever a system with several sensors and loggers is installed. Therefore, the pipe insulation was used on the bodies of tensiometers and TDR's (Figure 5.28).

Figure 5.28 Tensiometers protected by insulation.

During the insertion of the sensor, the pressure inside the ceramic cup increases. Hence, each tensiometer requires a certain time to get into equilibrium with the pore water pressure that is contained in the soil. The pressure, measured by the tensiometers had to be recorded after installation. From these measurements, it can be easily assumed when the sensor is in equilibrium with the soil. The equalisation time is completed, when there is no significant increase in the pore water pressure and when the measurements are stable. The measurements of the soil suction can then be started.

It can be clearly seen from the Figure 5.29 that the four tensiometers installed on the crest of embankment model, equalised after a few days after the installation.

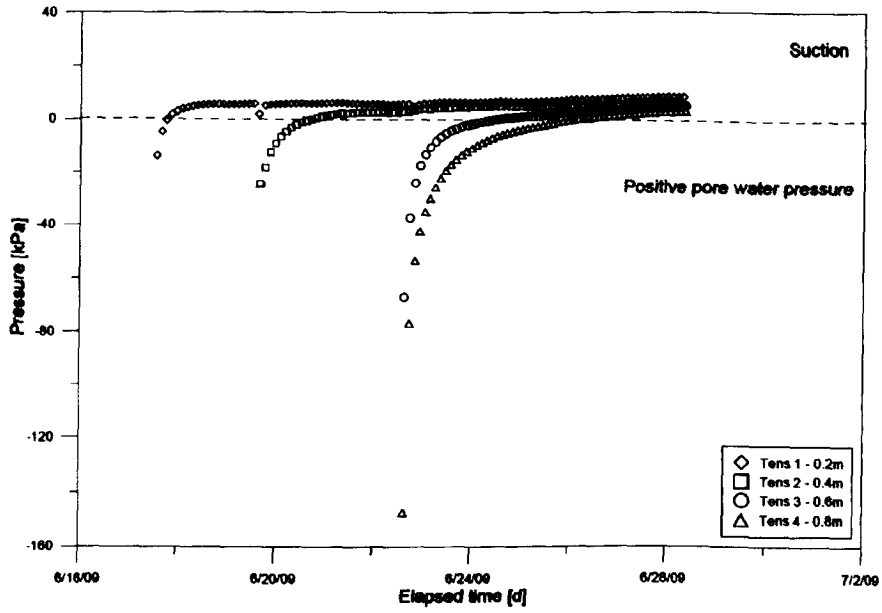

Figure 5.29 Measured pore water pressure after tensiometers installation on the crest.

As mentioned before, the undrained shear strength was measured on the bottom of each installation hole. The measurements are summarised on the Figure 5.30.

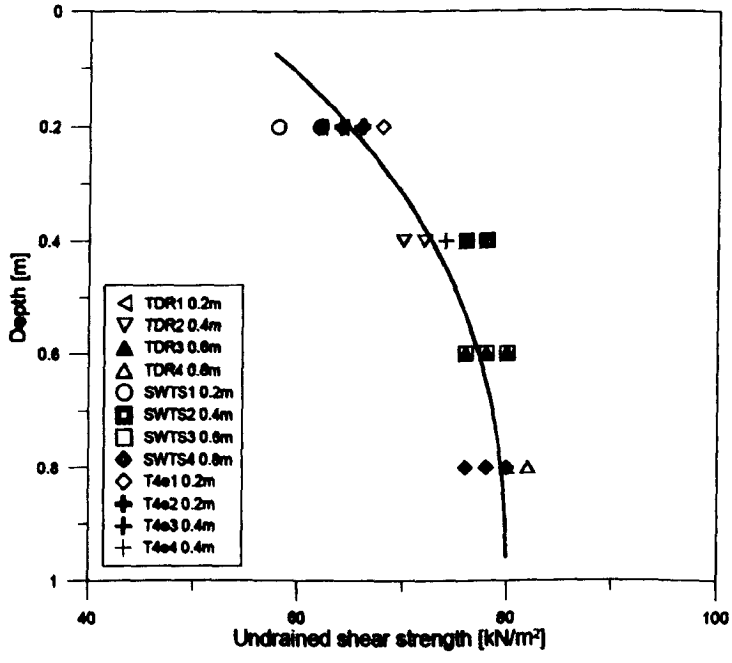

Figure 5.30 Measured undrained shear strength at the sensor level.

It can be seen from the graph that there was an increase of the undrained shear strength with depth. Lower value of the undrained shear strength at the upper

installation level was due to the wetting front of the embankment model after construction. In order to prevent the embankment from the desiccation process the model was frequently wetted prior to sensors installation. Hence, the values of the shear strength in the upper part of the model were found to be lower than at the bottom.

5.8.4. *Relative Humidity and temperature sensor - RHT2nl*

RHT2nl sensors were mounted in the solar radiation shield 1 m above the embankment crest. The bracket of the shield was attached to the frame (see Figure 5.31) and the sensors were connected to the Delta-T Data Logger.

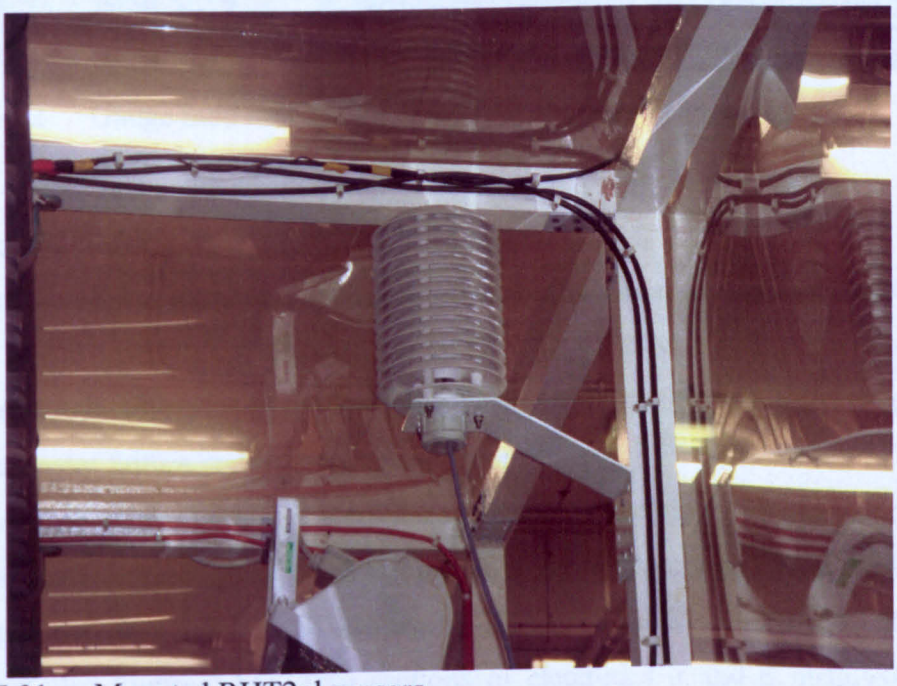

Figure 5.31 Mounted RHT2nl sensors.

5.8.5. *Rain gauge*

The Oregon scientific rain gauge was installed 1 m above the berm level and on the same line as sprinklers in order to catch the maximum rainfall. The rain gauge was mounted on the arm that was attached to the chamber frame (Figure 5.32).

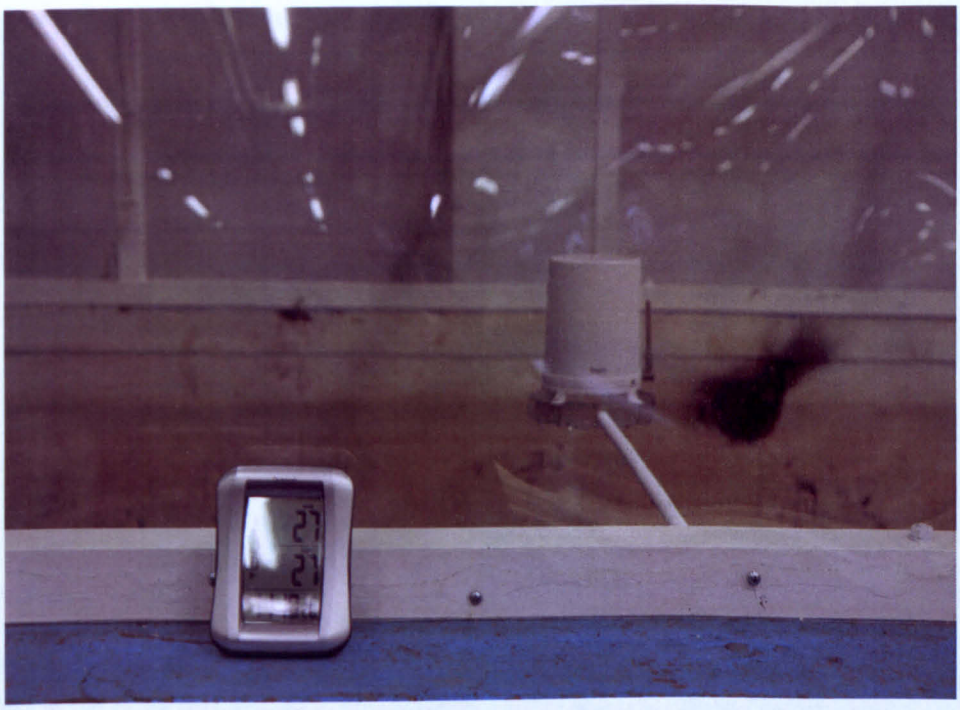

Figure 5.32 Gauge module with the rain cup inside the chamber.

5.8.6. MINIATURE RESISTIVITY ARRAYS

In order to avoid disturbance of a downstream side of embankment model it was decided to use a non-invasive technique for desiccation cracking detection (as shown on Figure 5.14). This part of embankment was used in further study for observation of embankment failure under flooding conditions.

Two miniature resistivity arrays were installed in two directions. 48 electrodes of the first array have been pushed into the soil with a 3.5 cm spacing (Figure 5.33) in the central part across the slope, and another 48 electrodes have been installed along the walls (see also Figure 5.14). Two sections of electrodes α and β installed on the model are presented on Figure 5.34.

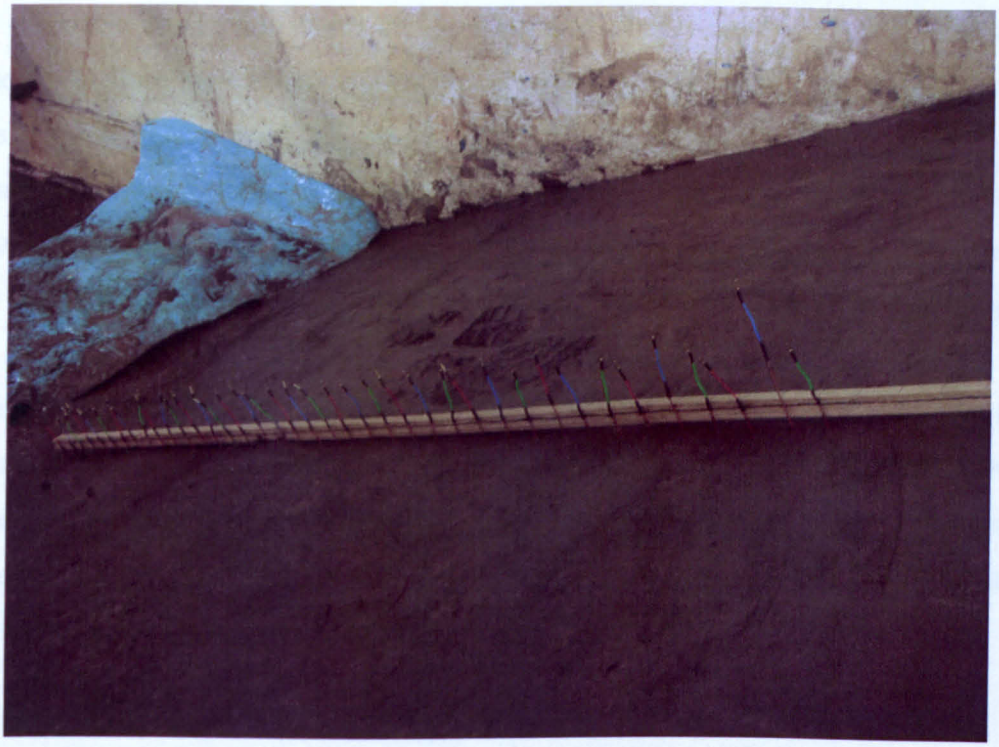

Figure 5.33 Electrodes installed in the central part of the slope.

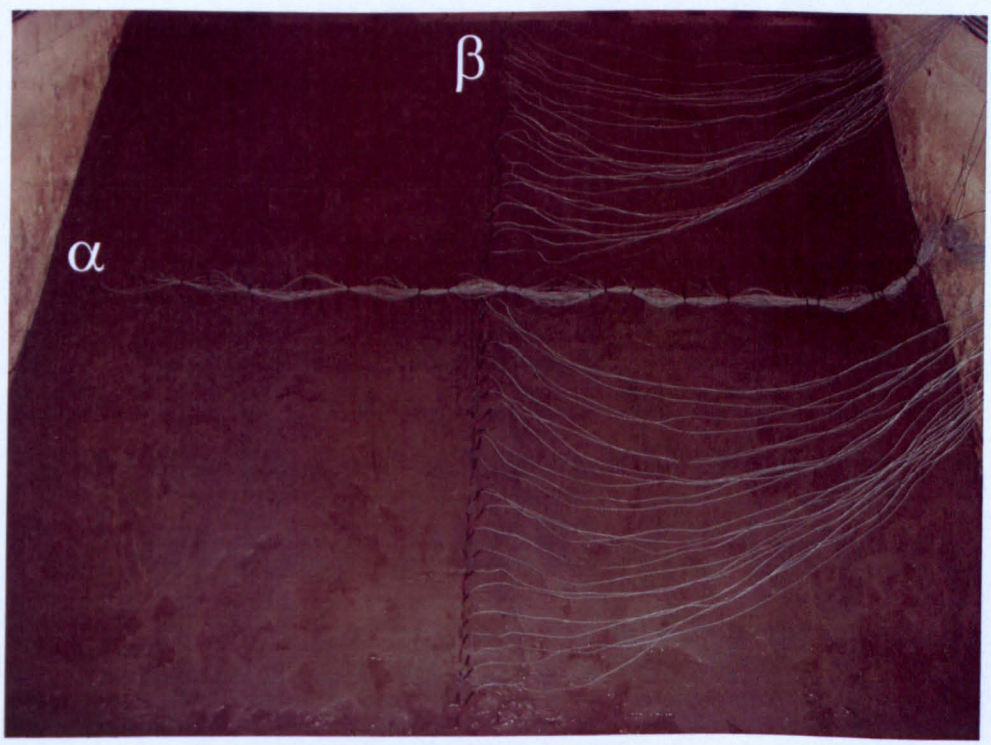

Figure 5.34 Two sections of miniature resistivity arrays.

An extensive description about the equipment has been presented in this Chapter in order to explore their efficiency for the experimental set up. Each particular sensor was carefully examined to assess their suitability for monitoring the model behaviour. Their working principles were described in order to understand how the measurements could be collected and used for further analysis. It was necessary to pay attention to the sensors installation procedure (state of the art) as they are fragile.

The miniature resistivity arrays introduced in this Chapter were used for the first time for such a scaled application. The literature survey given in the next Chapter presents several geotechnical applications using this technique. A pilot test was carried out in order to investigate the use of geophysics for desiccation cracking detection. Preliminary results are also presented.

CHAPTER 6

6. INVESTIGATION OF THE USE OF GEOPHYSICS IN DESICCATION CRACKING DETECTION

6.1. PILOT TEST

6.1.1. INTRODUCTION

One of the aims of the study was to investigate whether geophysical resistivity tests could be a useful tool for detecting the onset and development of desiccation cracking.

Geophysical methods based on miniature resistivity arrays could be the solution as they have proved to be reliable to monitor contaminant transport in soils scaled models in centrifuge experiments (Depountis, 1999). This technique is non-invasive and hence is reducing considerably the disturbance of the soil, improving the accuracy of the measurements.

For the assessment of embankments this technique could be very useful for long term monitoring of clay sealings which are not accessible.

The subsurface soil properties are determined by measuring the distribution of resistivity. The basis of the technique is to pass a direct current through the soil between a pair of electrodes. This process is observed by monitoring the distortion of the equipotentials (assuming the soil to be a homogeneous half-space) using another pair of potential electrodes located at the ground surface (Barker, 1997). This provides a simple, repeatable technique that can be applied where any contrast in electrical conductivity exists in space (or time). The electrical resistivity of compacted clays is closely associated with the moisture content and degree of saturation (McCarter, 1984; Tezel and Özçep, 2003). Moreover, a close relationship between hydraulic conductivity of compacted clays and electrical resistivity can be also found (Abu-Hassanein et al., 1996).

Lataste et al., (2003) used the resistivity technique with a device made of four electrodes spaced out 5 or 10 cm, arranged in a square to study the cracks on a damaged concrete slab. He used a numerical modelling approach rather than an

inversion model showing a qualitative similar disturbance of apparent resistivity right to cracks, for depth or opening variations. On a wider scope at geology level, Nguyen et al., (2005) proposed a methodology to locate automatically limits or boundaries between synthetic faults and layer boundaries in two dimension electrical tomography using a crest line extraction process in gradient images. He found that the method showed poor results when vertical gradients are greater than horizontal ones but otherwise should be systematically used to improve tomography interpretation.

In most of the Geo-electrical surveys the resistivity technique usually involves a computer controlled multi-electrode arrays to give a tomography contour model of the subsurface in two and three dimension (Griffiths and Barker, 1993; Griffiths and Barker, 1994; Olayinka and Weller, 1997; Godio and Bottino, 2001). One of the first team to use miniature resistivity imaging to detect cracks of cm size was Samouëlian et al. (2003). They used porous special electrodes filled with CuSO4 similar to the one currently used for self potential measurements to improve the electrical contact in creating a wet contact with the surrounding dried soil. They created artificially a crack of 2mm width with a saw at varying depths (1, 2, 3, and 4 cm deep) in order to obtain four cracking stages. The highest interpreted electrical resistivity was detected in the top 1.5-cm depth of their soil sample, whereas the crack developed down to 4 cm. The electrical images obtained from these electrodes enabled the detection of structures at the millimetre scale. More recently Tabbagh (2007) developed a new inversion model for assessing and simulating the electrical response and the main physical parameters of cracks in soils. Their model allowed a faster inversion of the experimental results.

As Sjödahl et al., (2008) quoted, the work on monitoring of resistivity on embankments for safety and integrity is not common. In Sweden, a permanent monitoring system was designed at two dams in 1996 and 1999 (Johansson and Dahlin, 1998) and electrical resistivity and SP surveying and monitoring was carried out at the Sädva embankment (Dahlin et al., 2001). Hällby was the first Swedish embankment to get a permanently installed monitoring system of resistivity measurements.

Rather than recreating artificially cracks and improve the inversion model, the present research has focused on the natural apparition of cracks and their direct detection using resistivity arrays and then using viscous tracers.

6.1.2. EXPERIMENTAL SET UP

The same soil as for the embankment construction has been chosen for this pilot test in order to investigate the use of geophysics for cracking detection. 190 kg of clay was oven dried to remove all the moisture and sieved using 20 mm mesh sieves. The sample was mixed with water to obtain 15 % of soil moisture content. It was then left for 24 hours for a curing period. The chosen value of moisture content was within the range of moisture for 95% of maximum dry density, and was close to the natural moisture content measured in the field.

After the soil preparation, a 2.5 kg compaction load was applied to several layers 5 cm deep, over the 1.5m length, 0.25m wide and 0.4m high Perspex tank, secured by 3 steel clamps. The transparency of the Perspex tank allowed checking of the uniformity of the clay compaction.

To identify the soil layers location already known, a miniature resistivity array was adapted to be used with the ARES earth meter equipment purchased from the company Gf instruments. 48 non-corrosive 1.5 mm diameter and 6 cm long electrodes (see Figure 6.1) were wired up and connected with the automatic resistivity system using double 24 ways connectors.

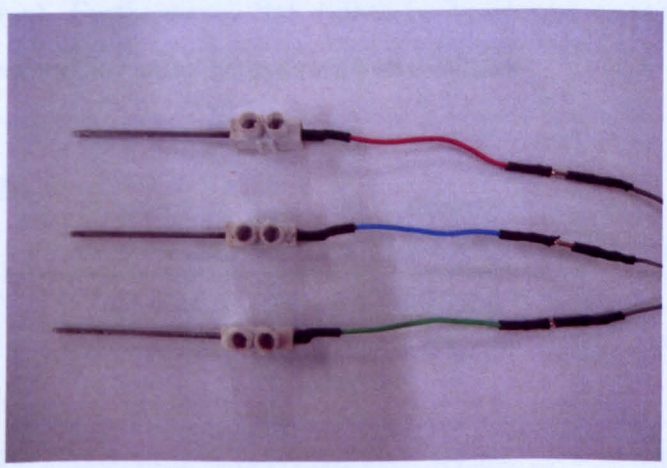

Figure 6.1 Non-corrosive electrodes mounted in block terminals.

The electrodes were pushed 3 cm into the compacted clay keeping a 3 cm spacing between them. To initiate and perform the desiccation and drying process a 1.2 kW infra-red heater was placed 0.9m above the clay surface, as shown in Figure 6.2.

Figure 6.2 Experimental setup with infra-red heater and electrodes installed.

The measurements selected option was a 2 dimensional multi-electrodes resistivity profile. A Wenner-Schlumberger array profiling method as shown on Figure 6.3, was chosen in this study because it is the most sensitive configuration to vertical resistivity changes (horizontal structures) in the soil strata and the groundwater table, and it is also more sensitive than other arrays to the horizontal resistivity changes (vertical structures). Furthermore, the extensive horizontal coverage and greater number of data points than other arrays justified its choice.

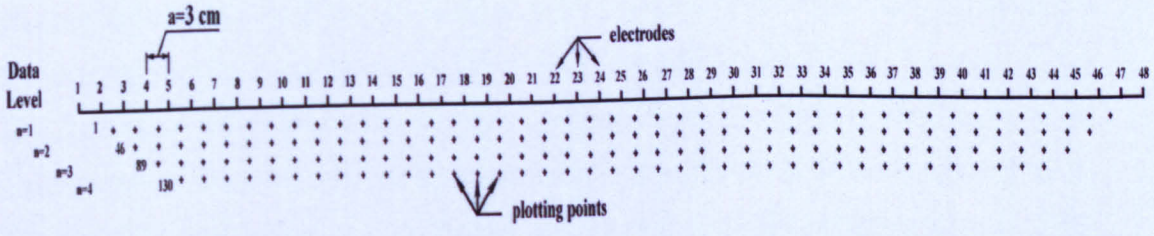

Figure 6.3 Four levels array of plotting points chosen for data analysis.

In the case presented here, only the first four levels and 168 plotting points were chosen for data analysis in relation to the measurements taken outside the physical boundaries (depth) of the flume model, which were identified as high resistivity measurements due to the plastic interferences at the bottom of the Perspex tank.

An experiment was carried out with the flume tank only filled with water with a measured conductivity of 63.2 μs/m to investigate the geometry of outer boundaries and electrodes. Figure 6.4 shows the geo-electrical profile obtained. It can clearly be seen the resistivity artifact due to the bottom Perspex tank boundaries in deep purple and the water in deep blue.

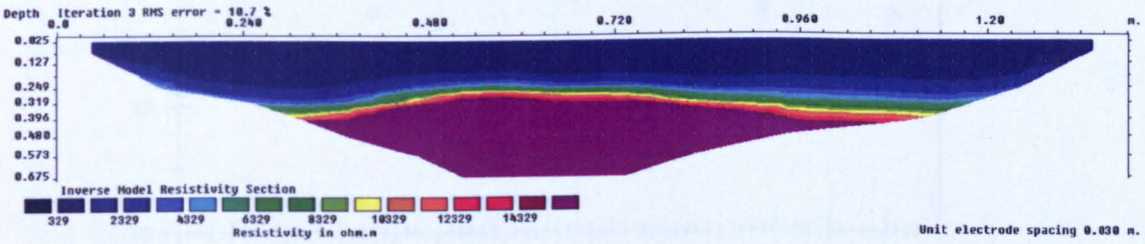

Figure 6.4 Water and tank boundaries resistivity profile, baseline.

6.1.3. EXPERIMENTAL PROCEDURE

The experiments were carried out for twelve days. Every morning the infra-red heater was switched on and left for 6 hours to initiate and perform desiccation cracking. During this drying stage the variations in soil temperature were recorded every hour (see in Figure 6.5). Then the geoelectrical scan was carried out, and the equipment was switched off overnight. The initial temperature of the soil in the morning was recorded at 20 cm depth every day before starting a new drying stage. Each last measurement was taken after drying has been finished.

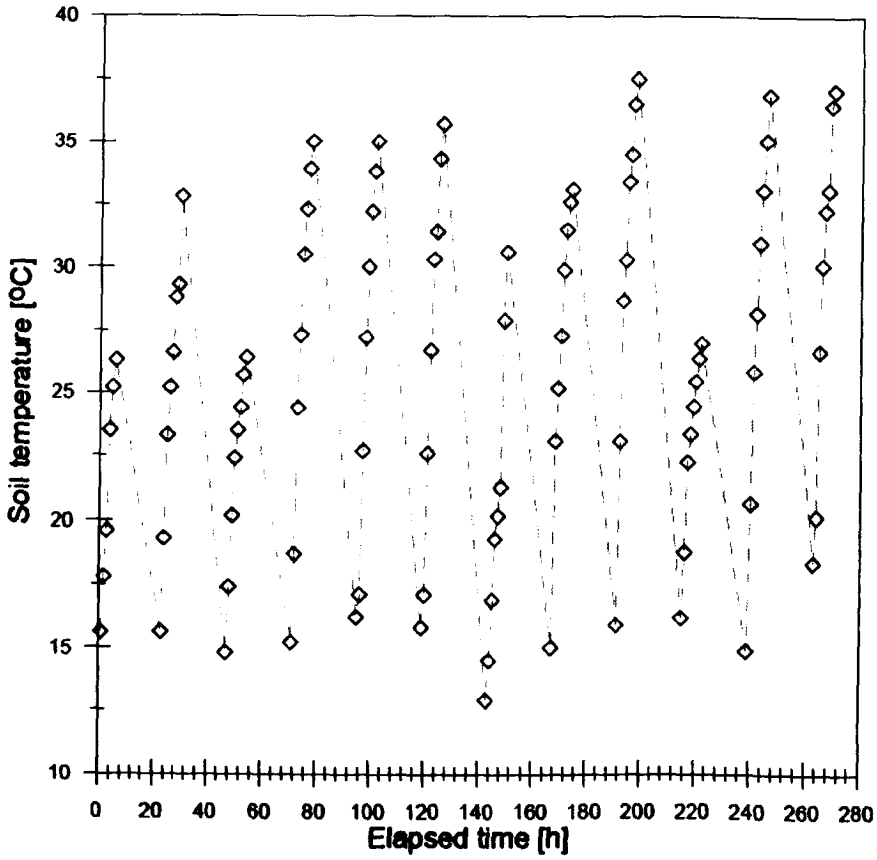

Figure 6.5 Temperature variations for 12 days drying process.

6.1.4. RESULTS AND DISCUSSION

As it was mentioned before, the Wenner-Schlumberger method was used to measure the resistivity changes in the soil during the desiccation process.

The idea of the pilot test was to examine an existing geophysical method that could be used for detection of the desiccation cracking. The final results explored the potential of the resistivity measurements and confirmed that it could be used for the embankment model presented in Chapter 7.

The numbering and detection of vertical crack was the main target taking into account the limitation of the scanning method which was the electrodes geometry as the spacing kept between them was the same as the contact depth into the soil.

The first scan was taken after the clay compaction and before drying in order to confirm that the model was homogenous and was compacted to the expected state. The baseline map presented in Figure 6.6, shows that the compaction was fully achieved and the measured resistivity was in the range of 20-30 ohm*m. This can be

seen as a deep-blue color, which is the resistivity contour obtained after inversion of the experimental measurements.

The temperature was increased from 15.0 °C up to 37.0 °C. The heat generated from the infra-red lamp, generated a temperature of 35.3 °C above the model, similar to a very hot summer day.

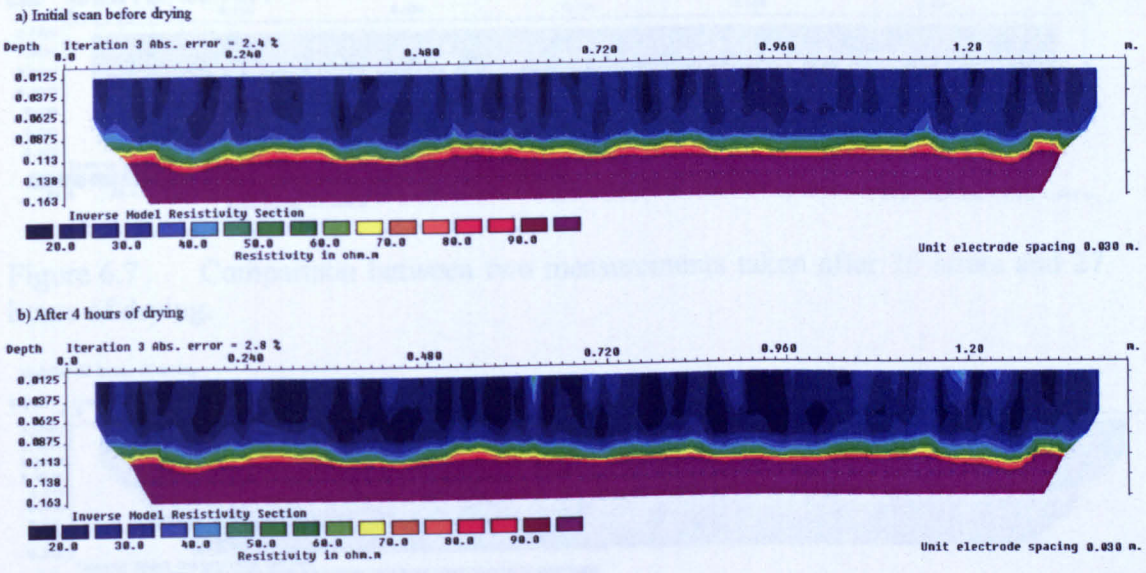

Figure 6.6 Inversed resistivity map taken before drying process and after 4 hours of heating.

The resistivity measurements were taken every morning, before the IR heater was switched on and every afternoon after the drying was finished. Due to the small changes in readings caused by evaporation process only the measurements taken every morning were analyzed.

Figure 6.7 and Figure 6.8 show how the resistivity changed with time and with cracks formation.

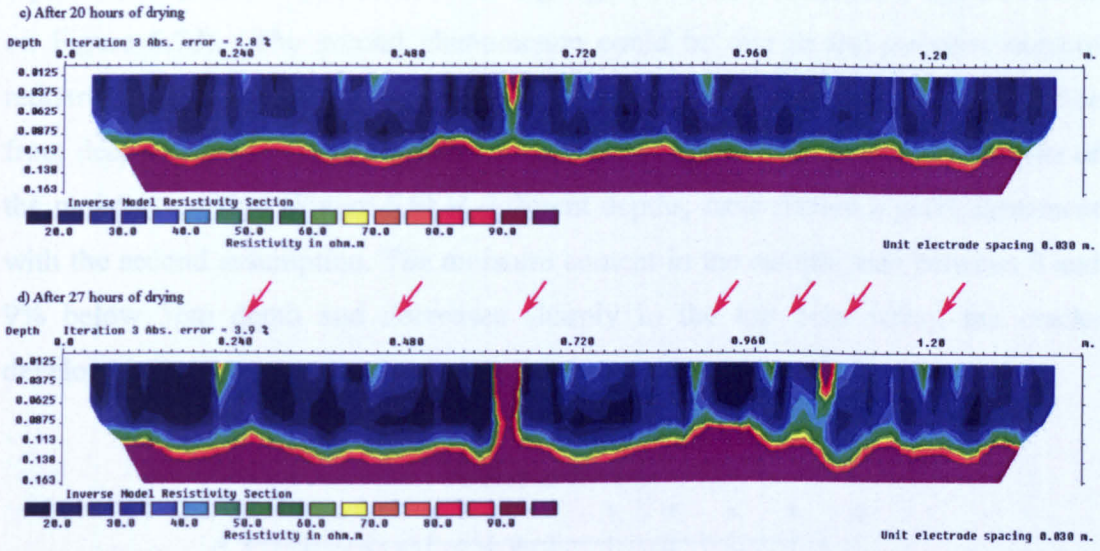

Figure 6.7 Comparison between two measurements taken after 20 hours and 27 hours of drying.

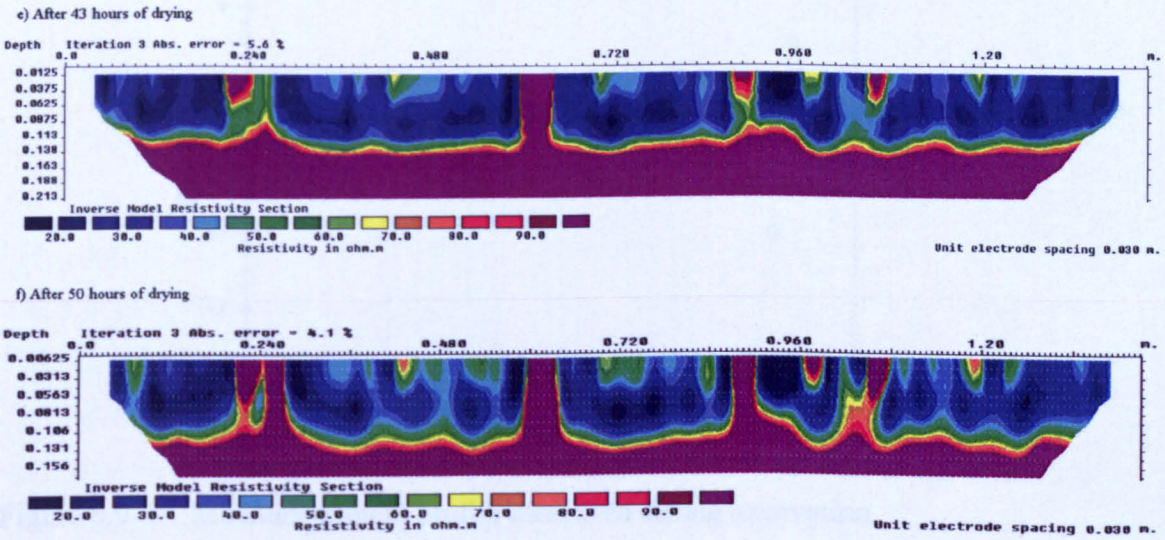

Figure 6.8 Comparison between two measurements taken after 43 hours and 50 hours of drying.

It can be clearly seen on the resistivity profile presented on Figure 6.7c) and Figure 6.7d) that several vertical openings occurred and became wider with time (vertical purple channels indicated by red arrows) corresponding visually to the same vertical cracks location on the laboratory clay sample.

However, it can be explained that during the fast heating process, the decrease in soil resistivity may be due to two phenomenons. The first can be described as micro swelling of the clay and closing up of the cracks caused by evaporating water

represented by the disappearance of the light green vertical afternoon contours shown on Figure 6.7d). The second phenomenon could be due to the moisture content redistribution in the model due to evaporation and the water rising to the surface from deeper regions. A post mortem excavation of the model, and measurements of the moisture content (Figure 6.9) at different depths, have shown a good agreement with the second assumption. The moisture content in the sample was between 8 and 9% below 5cm depth and decreased sharply in the top 5cm where the cracks developed.

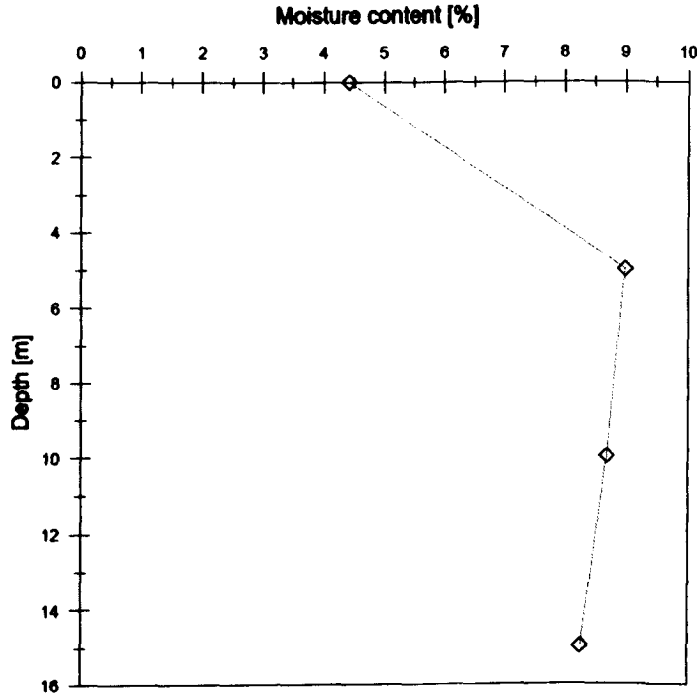

Figure 6.9 Moisture content profile measured during excavation.

The inversed resistivity map, shown on Figure 6.10, has confirmed that the air space created inside the crack should give the high resistivity response in analyzed measurements shown as vertical purple (dark) wide channels. It has to be noted that the photographic picture of the cracks was made of 3 different pictures and was not at the same scale as the resistivity profile. The corresponding location of the cracks was given as an indication.

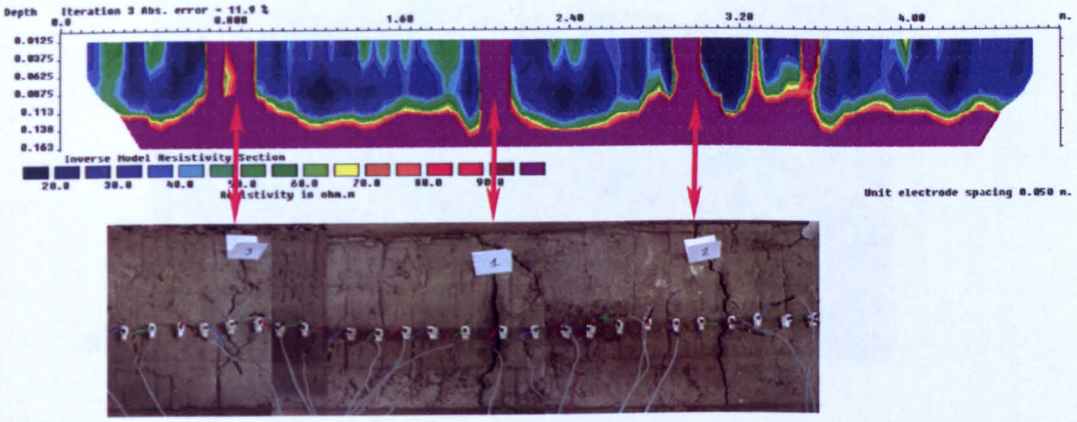

Figure 6.10 Inverted resistivity map with corresponding picture of the cracked surface.

The resistivity results seem to reflect well the real desiccation cracking by comparing them with visual observations of the clay model.

One of the assumptions, which has been considered during this study, is that horizontal cracks can be observed as a horizontal discontinuity, between two layers and in this case should result as high resistivity measurements detected above horizontal crack. It is however, difficult to verify this assumption as the resistivity artifact due to the tank boundaries and shown before on Figure 6.4 is also present. This hypothesis can be explained as the shielding or air insulation for the current to pass through the horizontal discontinuity in the homogeneous soil which is the natural obstacle for the electrodes installed above it. The results are the creation of electrical anomalies (Figure 6.11) as the average of the resistivity measurements are affected during the inversion process. It is different for the electrodes positioned outside the range of the horizontal crack length, because current can go underneath it and the resistivity can be measured as before.

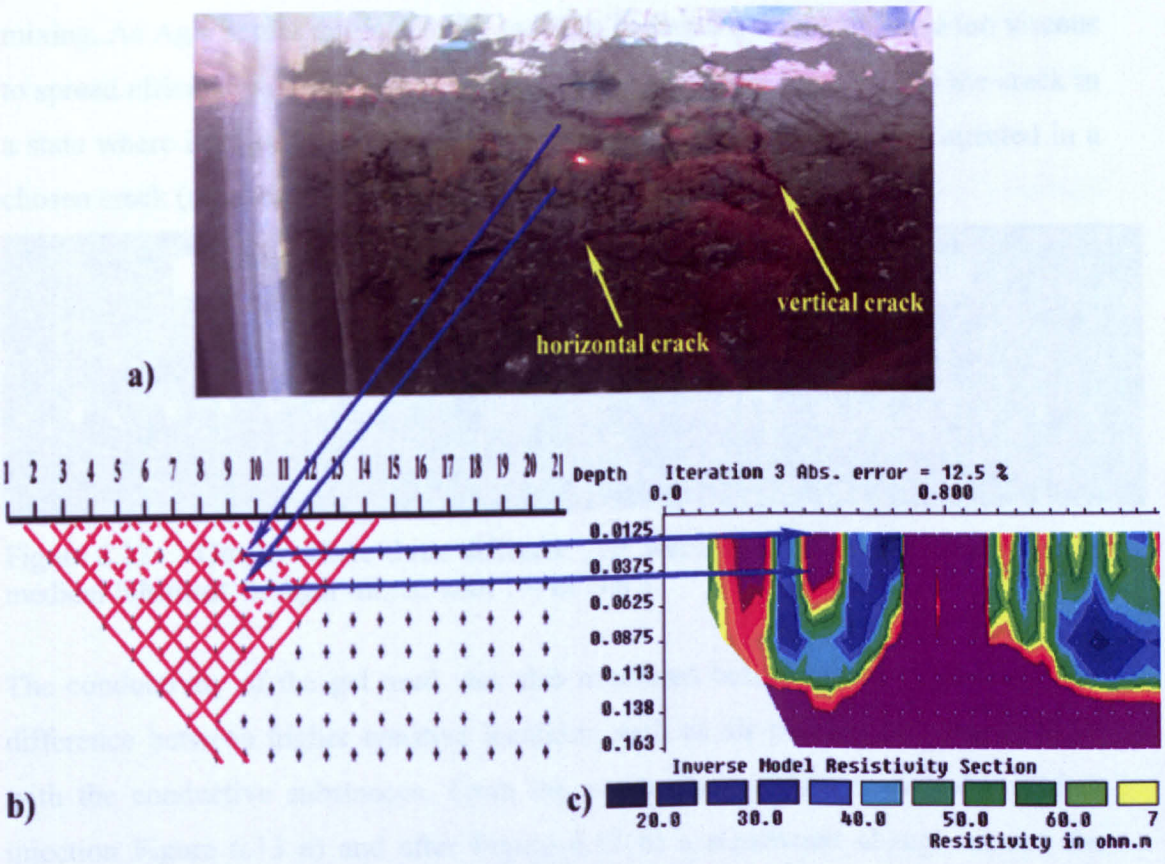

Figure 6.11 Proposed interpretation for horizontal crack detection. Example of two points on picture (a) corresponding to the measurements shown in the cross section (b) and inverted to the resistivity contour model (c).

6.1.5. USE OF VISCOUS TRACER FOR TIME DETECTION IMPROVEMENT.

The purpose of this experiment was to use a ''slow'' tracer, which can be injected into the cracks to improve the quality of the measurements, time related. The duration of the geo-electrical scans can be very long, as such it was very important to find a tracer which was viscous enough to allow time for the equipment to track the seepage of the tracer fluid through the cracks. Another requirement for the tracer was to be able to penetrate the cracks remaining on the walls without any absorption or adsorption by clay, which could significantly change the measurements. It was decided to use a gelatinous substance, chiefly used as a solid substrate to contain culture medium for microbiological work. This substance called Plate Agar at a concentration of 8 g/l, was first dissolved in hot water and 1% of NaCl was then added to rise its electrical conductivity from 0.02 to 18.6 µS/m. The Agar mixture with 1% of NaCl was selected because the viscosity can be adjusted during the

mixing. As Agar settles down at 46°C and then becomes a jelly substance too viscous to spread efficiently into the cracks it was very important to inject it into the crack in a state where it will flow freely, just after preparation. This tracer was injected in a chosen crack (number 3) in the experimental model (see Figure 6.12).

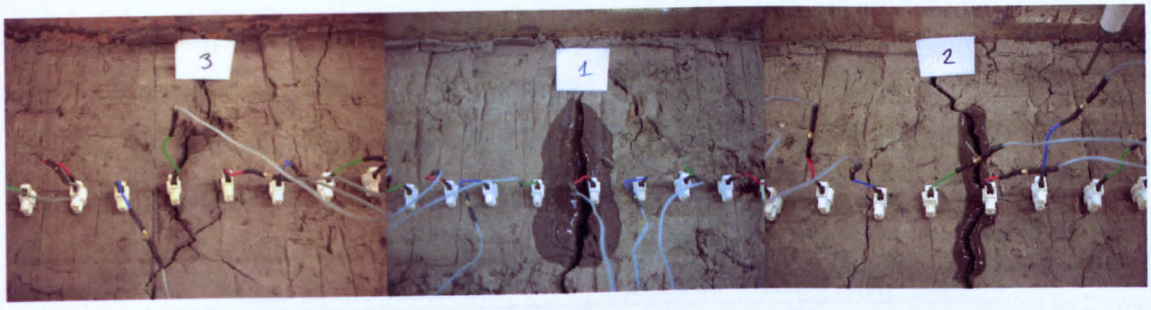

Figure 6.12 Cracks where three different gels were injected; 1. ultrasound gel, 2. medical lubricant, 3. Agar mixed with 1% of NaCl.

The conductivity of the gel used was also measured before injection, to check the difference between higher resistive locations such as air pockets and cracks filled with the conductive substances. From the comparison of two scans taken before injection Figure 6.13 a) and after Figure 6.13 b) a significant change around the crack can be observed.

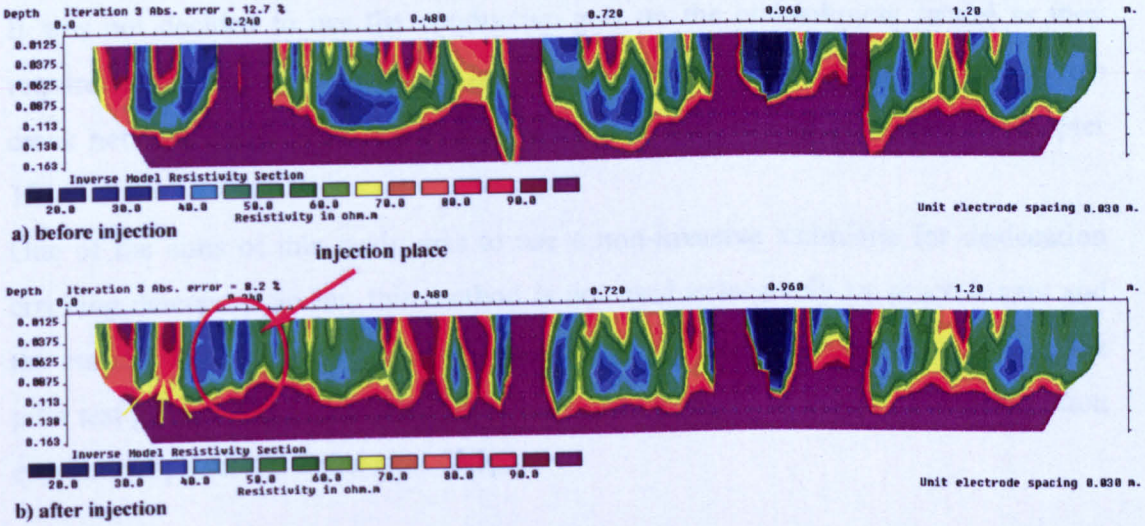

Figure 6.13 Inverted resistivity scans for plate agar mixed with 1% of NaCl: (a) before injection, (b) after injection.

The changes in the contour, from dark purple to deep blue as indicated by the circle on Figure 6.13 b), showed that resistivity of the soil has dramatically decreased, and that the injected substance has mostly penetrated all surrounding area. It can be also

seen that in the place where horizontal crack was formed, the deep purple colour started changing to a red line boundary indicated by yellow arrows on Figure 6.13 b), which could mean that air void was also filled with injected gel.

Additionally, two other viscous gels were tested: (i) ultrasound gel and (ii) medical lubricant during this study. Both gels were injected into remaining cracks number 1 and 2 on Figure 6.12. However, it was found that the mixture of plate agar with 1% of NaCl has the highest conductivity (Table 6.1). Thus, not such improvement was expected from the other gels.

Table 6.1 Comparison of the electrical conductivity.

Name of the substance	Electrical Conductivity [μS]
Ultrasound Gel	0.72
Medical Lubricant	0.18
Pure Agar	0.02
Agar mixed with 1% of NaCL	18.6

In summary, the pilot test presented in this Chapter, revealed a great capability of the miniature resistivity arrays for the detection of desiccation cracking. The growth and development for all vertical cracks, caused by the natural desiccation process, were efficiently mapped on the geophysical scans.

It was not decided to use the conductive gels on the embankment model as they required a post-mortem excavation in order to visually confirm their penetration into crack network. However, they could be part of future studies presented in Chapter 12.

One of the aims of this study was to use a non-invasive technique for desiccation cracking detection. So far, this method is not used extensively by practitioners and the current techniques are intrusive and disturb the embankment body. Hence, the pilot test provided very promising results that are going to be validated in desiccation experiment presented in the next Chapter.

CHAPTER 7

7. DESICCATION EXPERIMENT

7.1. INTRODUCTION

Moisture content conditions in the field are controlled by two mechanisms: infiltration or evaporation. The subsurface soil suction and moisture content profiles varying over time as the effect of infiltration and evaporation processes, are closely associated with the variation of the boundary conditions. The relatively well understood infiltration process, which results from natural precipitation, irrigation or pooling of surface runoff, can be described by analytical or numerical solutions to Richard's equation (Likos and Lu, 2003). Most of the existing models for predicting infiltration into the subsurface have been experimentally validated (Philip, 1969; Srivastava, 1991).

The evaporation process occurs in the form of liquid and vapour transport at depth and at the ground surface (Likos and Lu, 2003). Hence, it is more complex and difficult to predict. Moreover, when discontinuities in the form of cracking appear on the soil surface, it makes it even more challenging as an additional vapour transport takes place (evaporation from inside the cracks).

Under the field conditions, desiccation cracking of flood embankments is dependent not only on the geotechnical parameters of the soil, but also on the weather conditions, their location and ground water conditions. Accordingly, the evaporation process is dependent not only on the soil properties, such as: hydraulic conductivity, vapour diffusivity and the Soil Water Characteristic Curve, but also on the conditions described above.

The experimental study presented in this Chapter reveal the evaporation models which account for these combined soil-atmospheric related factors. Moreover, it investigates the nature, pattern and growth of desiccation cracking.

Presented experiment consists of three main phases: (i) desiccation with one weekly precipitation, (ii) desiccation with two weekly precipitations, and (iii) desiccation under extreme drying without precipitation. The first phase was carried out for 6

weeks, the second phase was carried out for 4 weeks and the last phase was carried out for 5 weeks. Over this period of time, the measurements of soil suction, moisture content, relative humidity, temperature inside the chamber were taken every 30 sec. Geophysical scans were taken by both resistivity arrays twice a day. Visual observation was followed by photographs taken of both slopes, crest and through the side windows. Any significant change observed in embankment behaviour was recorded and is presented in this Chapter.

7.2. PHASE ONE – DESICCATION WITH ONE WEEKLY PRECIPITATION

Following the installation of the sensors, one week of testing procedure was carried out in order to test the experimental set-up. Furthermore, it was observed that during this time all tensiometers reached the equilibrium with the soil. It was impossible to replicate exactly the natural conditions and temperature variations occurring on the field. Thus, the temperature inducing desiccation cracking was set to 20°C on the thermostat. Moreover, one weekly precipitation was introduced at the beginning of each week reaching the amount of 55 mm/m^2, which is equal to the averaged heavy rainfall recorded over the years in UK. It was found, that using the sprinkling system installed inside the chamber a time of six minutes was required to reach this amount of water.

A visual observation for the first few hours of the experiment showed, that the cracks started appearing on the surface immediately, after desiccation was induced. It can be clearly seen in Figure 7.1 and Figure 7.2 a few tiny cracks which created on the crest and on the upstream side of the embankment model.

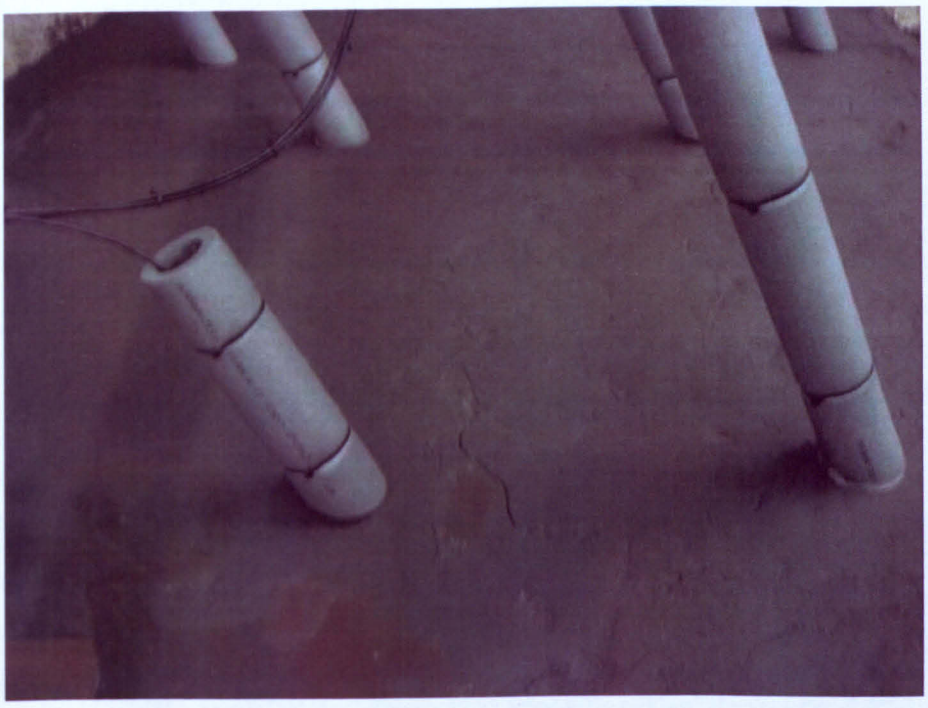

Figure 7.1 First cracks observed on the embankment.

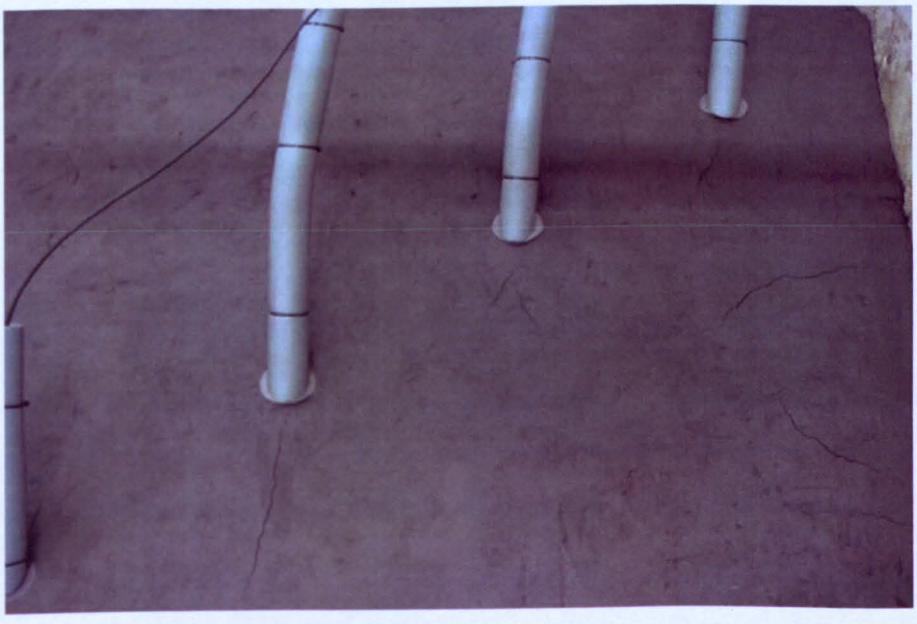

Figure 7.2 Cracks observed on the upstream side of the embankment.

During the first phase, the data logging system was continuously measuring and recording any change in the environment. The averaged recorded temperature varied between 18°C and 23°C (Figure 7.3).

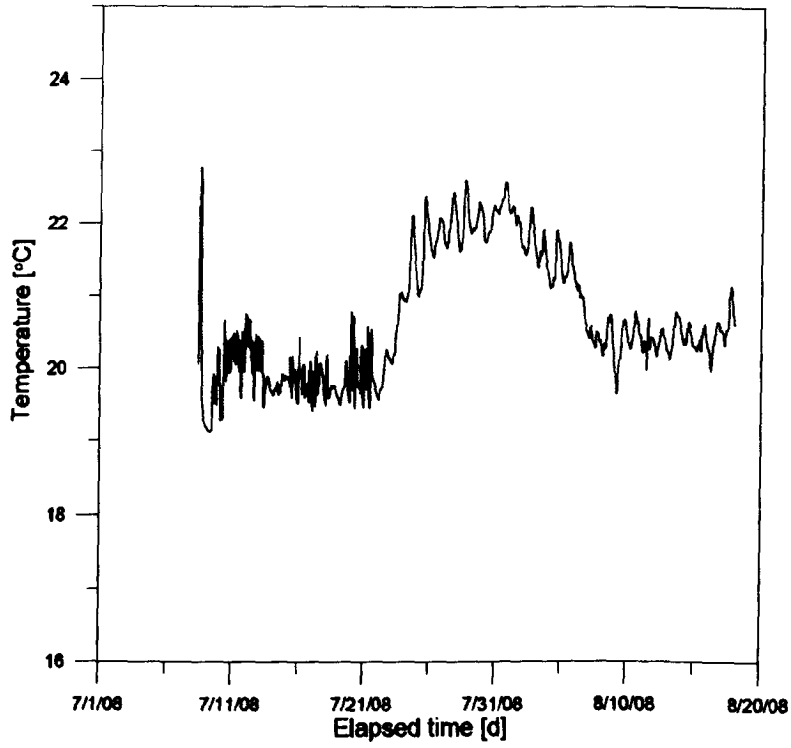

Figure 7.3 Averaged air temperature during the first phase of experiment.

At the same time Relative Humidity ranged between 40 and 70% (Figure 7.4).

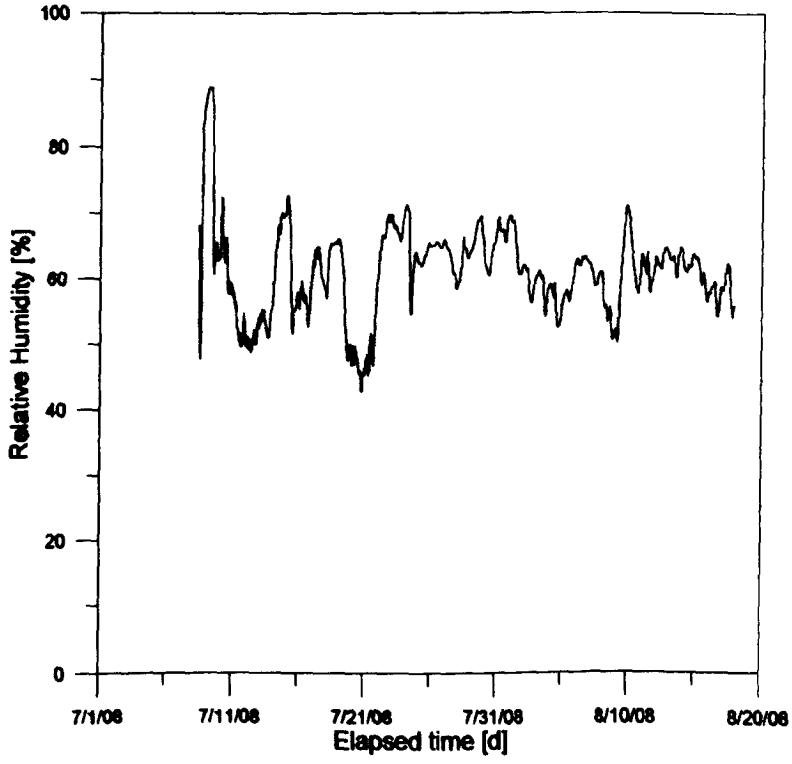

Figure 7.4 Averaged Relative Humidity during the first phase of experiment.

It was observed that during the rainfall the water accumulating on the crest of the model was disappearing inside the cracks, and was flowing out from the cracks on the slope. It has been also seen that water flowing on the slope surface, once reached the cracks edge, was flowing inside them. This matches the observation made by Cooling and Marsland (1954) and later by Dyer et al. (2007) about the distribution of the water flowing through interconnected crack network.

Under normal circumstances, when the soil is in equilibrium with water, clay swells when it is wet. However, the observed wide cracks (Figure 7.5) appearing after the first week of drying, stayed open even if the moisture content of the soil increased due to rainfall (Figure 7.6). More pictures of the first week of drying can be found in the Annex-A (Chapter 14).

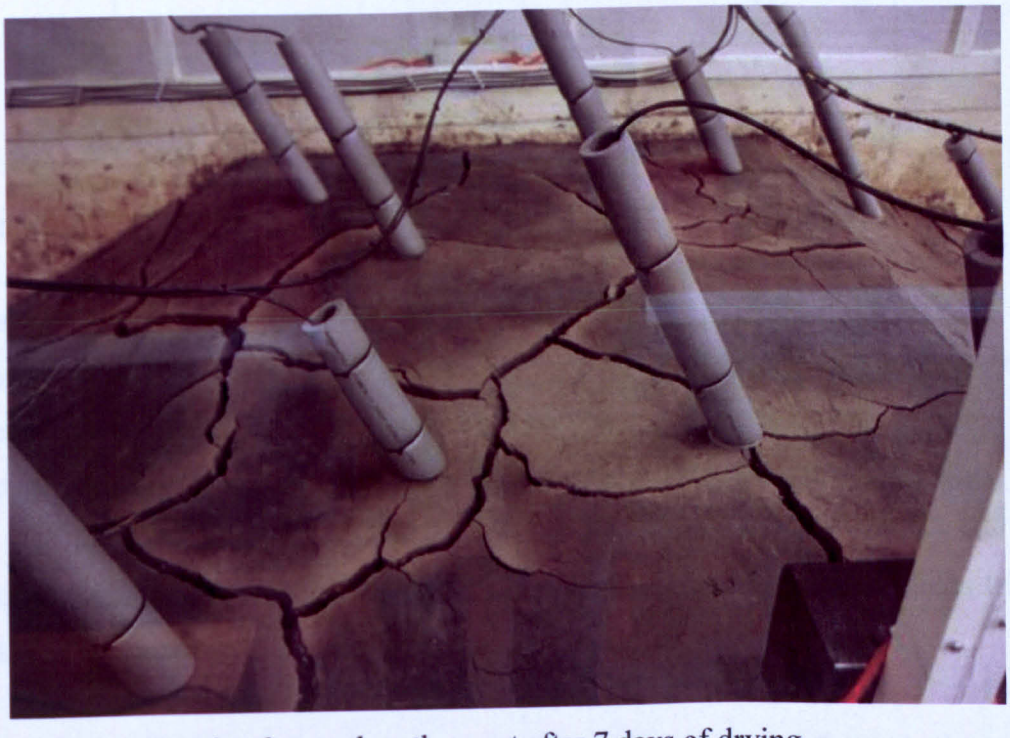

Figure 7.5 Cracks observed on the crest after 7 days of drying.

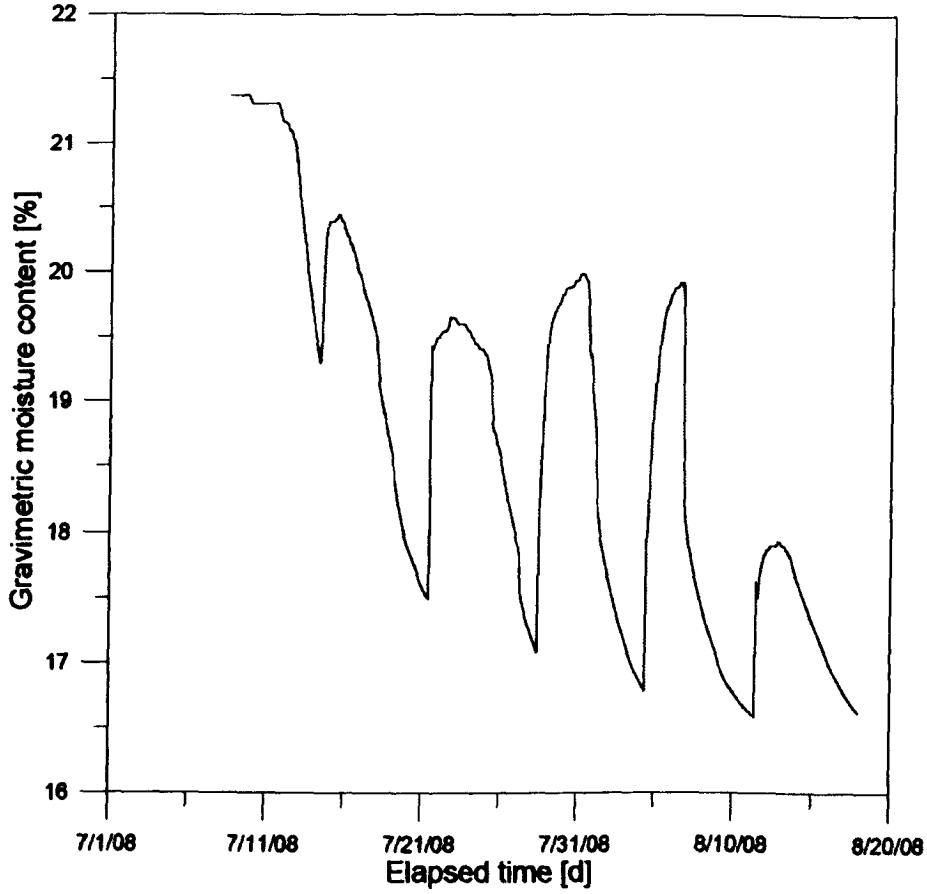

Figure 7.6 Recorded variations in moisture content at 20 cm depth.

It is assumed that an "additional evaporation" effect was taking place and did not allow the clay to swell. This effect can be described as the evaporation from fractured soil, where not only the surface is considered as the evaporation source but also the wide cracks and their walls are transmitting the water to the atmosphere.

This assumption has been confirmed in the observation of the measurements taken by the TDR sensors.

It can be clearly seen from the moisture content profiles (Figure 7.7) that in the upper part of embankment moisture content varied significantly.

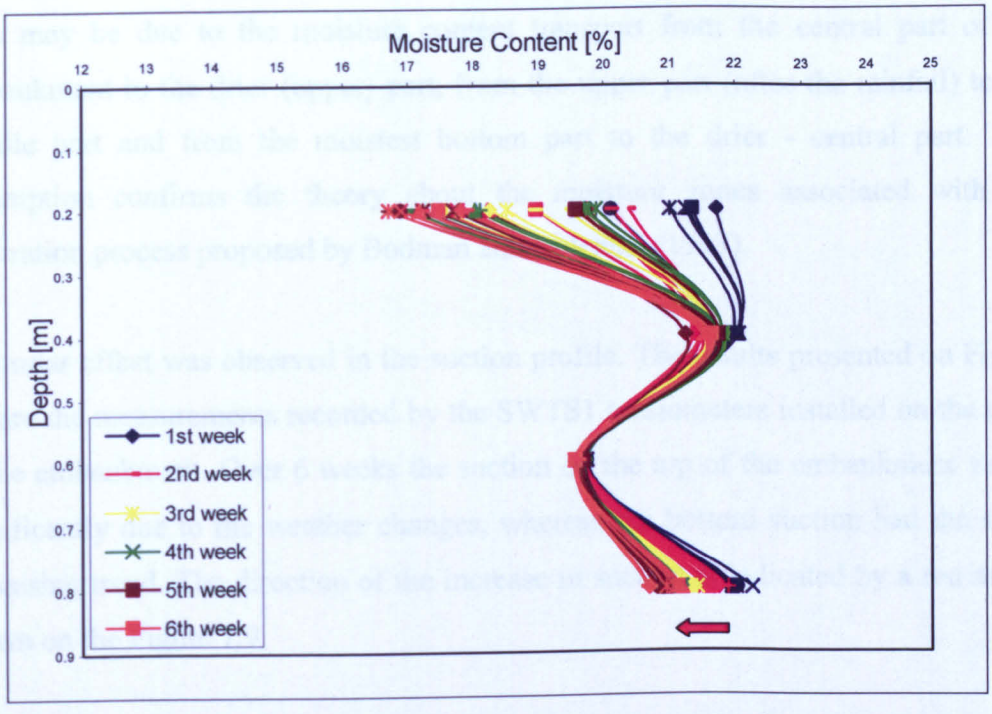

Figure 7.7 Moisture content profiles representative for first 6 weeks of experiment – 1 cycle of rainfall.

At the same time, a small decrease in the moisture content was recorded at the bottom of the model along with the moisture in the middle part remaining constant (Figure 7.8).

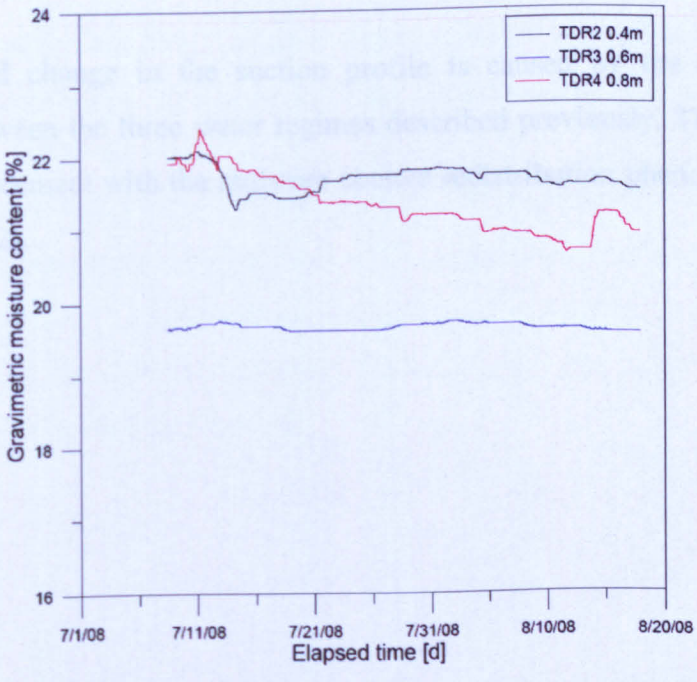

Figure 7.8 Gravimetric moisture content measured at lower parts.

This may be due to the moisture content transport from the central part of the embankment to the drier (upper) part, from the upper part (after the rainfall) to the middle part and from the moistest bottom part to the drier - central part. This assumption confirms the theory about the moisture zones associated with the infiltration process proposed by Bodman and Coleman (1943).

A similar effect was observed in the suction profile. The results presented on Figure 7.9 are the measurements recorded by the SWTS1 tensiometers installed on the crest of the embankment. Over 6 weeks the suction on the top of the embankment varied significantly due to the weather changes, whereas the bottom suction had the same increasing trend. The direction of the increase in suction is indicated by a red arrow shown on the Figure 7.9.

As it can be seen in the suction profiles, the suction in the middle of the model was almost constant with only a small increase. From the observations made during this phase of the experiment it can be noticed that the movements and changes of the suction are mainly dependent on the moisture content flow within the soil controlled by infiltration and evaporation processes described previously.

The observed change in the suction profile is caused by the moisture content transport between the three water regimes described previously. This observation is in a good agreement with the moisture content redistribution phenomenon described by Bear (1972).

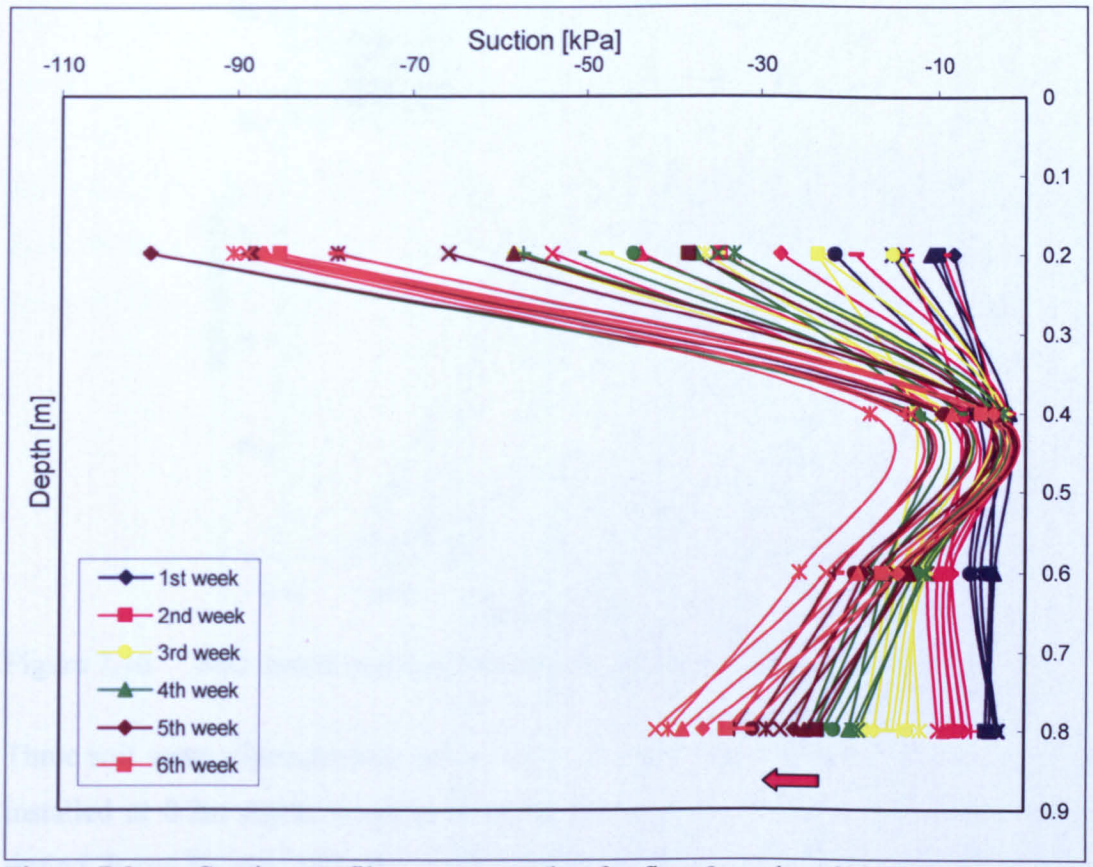

Figure 7.9 Suction profiles representative for first 6 weeks of experiment – 1 cycle of rainfall.

These results match the observations of matric suction recorded at different depths of the embankment model. In Figure 7.10, the measurements of soil matric suction at four different depths are presented.

It can be noticed from Figure 7.10 that for the upper tensiometer (0.2 m) a sharp drop in suction appears at constant intervals at the beginning of the experiment, whereas for the lower sensors a similar effect appeared at the end of this phase. This is due to the creation of the vertical cracking which allowed the water to penetrate the structure gradually with their growth.

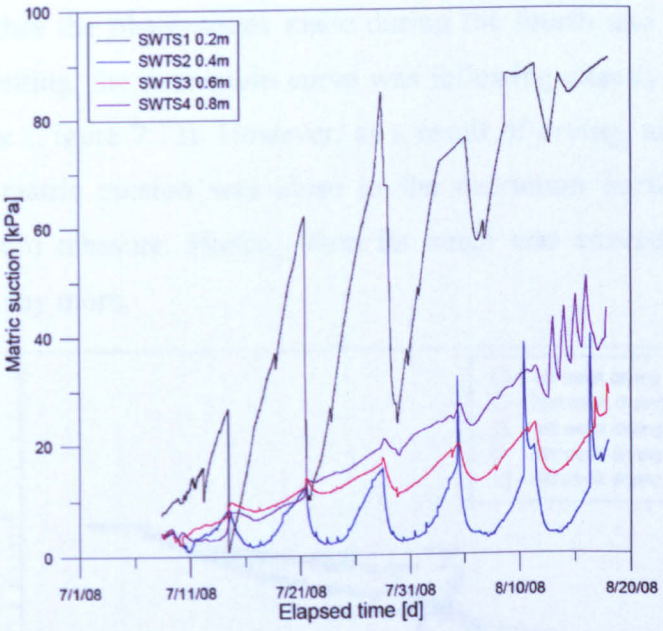

Figure 7.10 Soil matric suction measured at different depths from the crest.

Three soil water characteristic curves were obtained from the tensiometer and TDR installed at 0.2m depth in order to show the path that SWCC will follow during drying. It can be seen from the measurements presented in Figure 7.11 that after the rainfall, the same slope of desorption curve was obtained even when the soil volume changed as a result of wetting and drying.

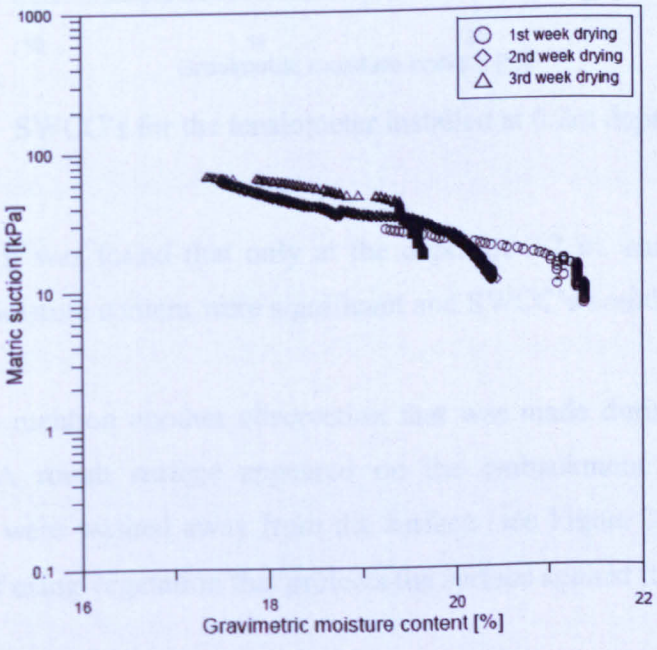

Figure 7.11 SWCC's for the tensiometer installed at 0.2m depth for the first three weeks.

This also matches the observations made during the fourth and fifth week of this phase. After wetting, the desorption curve was following exactly the same slope as observed before (Figure 7.12). However, as a result of drying, and lack of rainfall, the measured matric suction was close to the maximum suction value that the tensiometer could measure. Hence, when its range was exceeded, measurements were not taken any more.

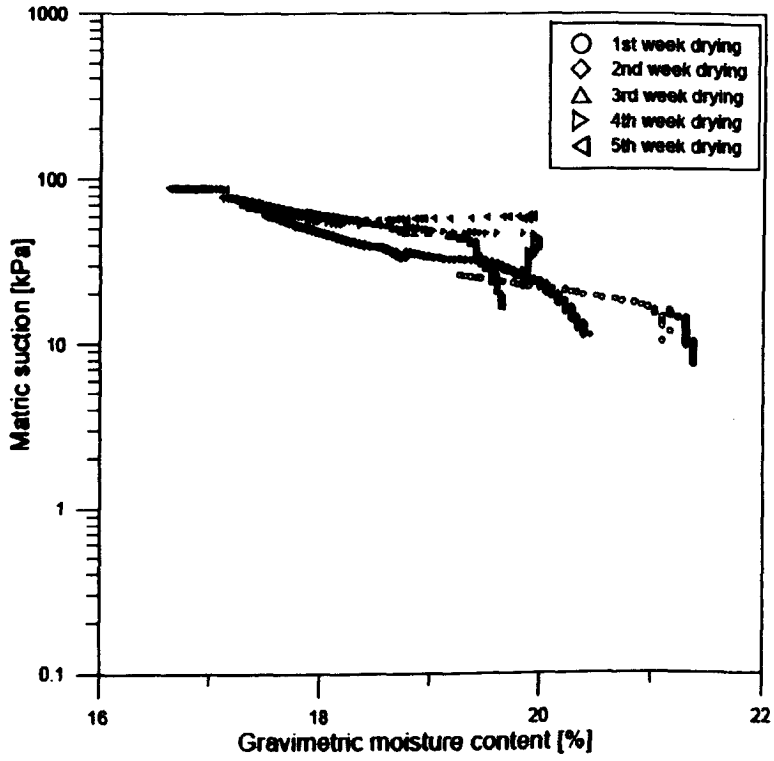

Figure 7.12 SWCC's for the tensiometer installed at 0.2m depth for the first five weeks.

Furthermore, it was found that only at the depth of 0.2 m, changes in matric soil suction and moisture content were significant and SWCC's could be obtained.

It is worth to mention another observation that was made during this phase of the experiment. A rough surface appeared on the embankment model, due to the particles that were washed away from the surface (see Figure 7.13). This raises the importance of using vegetation that protects the surface against its erosion.

Figure 7.13 Rough surface on the crest.

The measurements using resistivity arrays were taken every morning and every afternoon. Furthermore, additional scans were taken after the rainfall in order to map any changes in the embankment body. It was expected that water will remain in the cracks if they are not interconnected. Furthermore, in some types of soils swelling can be observed and hence self-healing of the cracks can take place. Thus, the scans after the rainfall were necessary to observe if this phenomenon would take place.

Two initial scans taken by the two arrays (α and β) after compaction confirmed that the embankment body is homogenous, and no cracking occurred since the construction was finished. The inversed resistivity models shown in Figure 7.14 and Figure 7.15 are the initial scans confirming that homogenous state was fully achieved.

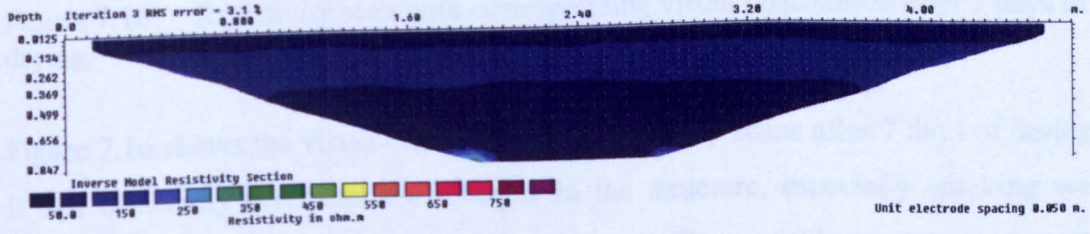

Figure 7.14 Inversed resistivity scan taken by section α before the experiment.

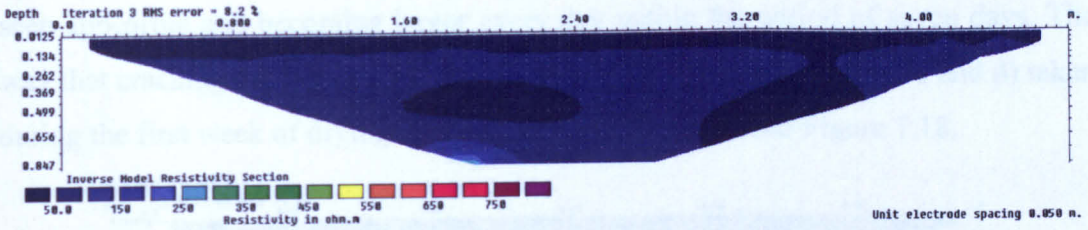

Figure 7.15 Inversed resistivity scan taken by section β before the experiment.

A deep blue colour on the picture represents very low resistivity (~50Ωm) and only small changes can be seen on the bottom of the model which might be due to the disturbance caused by the boundaries effect. A similar effect was observed in the pilot test presented in Chapter 6, where the disturbance at the bonduary was caused by the Perspex base of the flume tank.

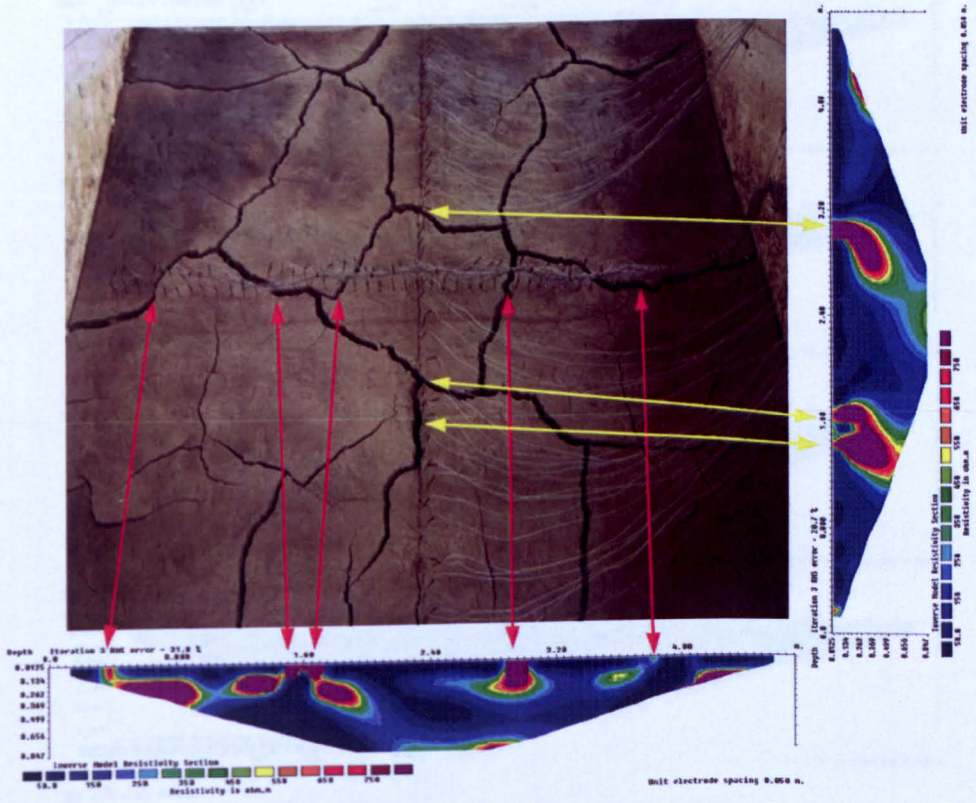

Figure 7.16 Resistivity scan with corresponding visual observation after 7 days of drying.

Figure 7.16 shows the visual observation and resistivity scans after 7 days of drying. It can be clearly seen that the changes in the structure, especially cracking was mapped by the two miniature resistivity arrays. Deep purple contours represent places with the high resistivity values such as air voids. These discontinuities were

seen appearing and becoming larger every day within the period of seven days. The way that cracking growth was mapped by the resistivity scans (section α and β) taken during the first week of drying is presented in Figure 7.17 and Figure 7.18.

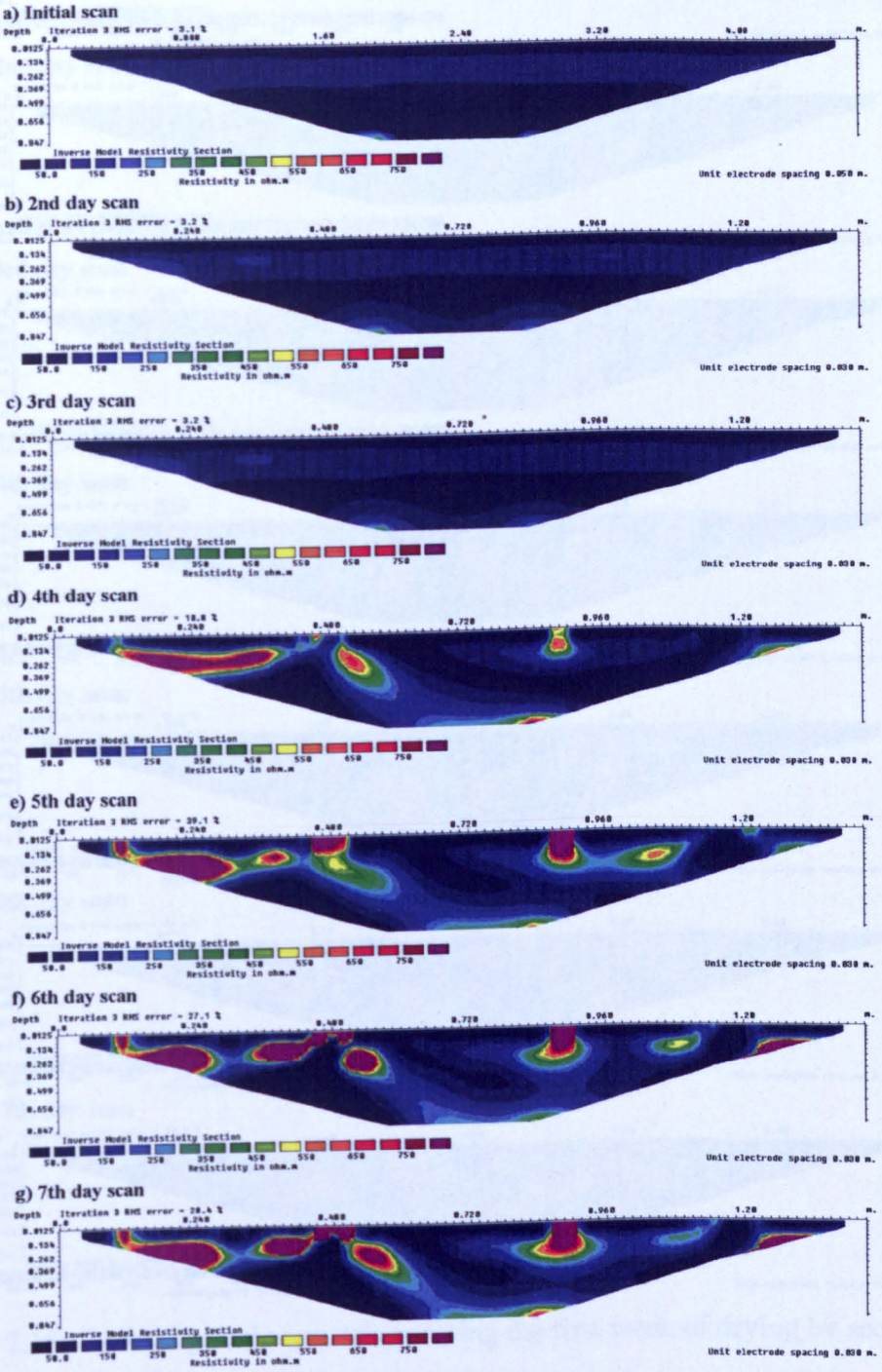

Figure 7.17 Geophysical scans taken during the first week of drying by section α.

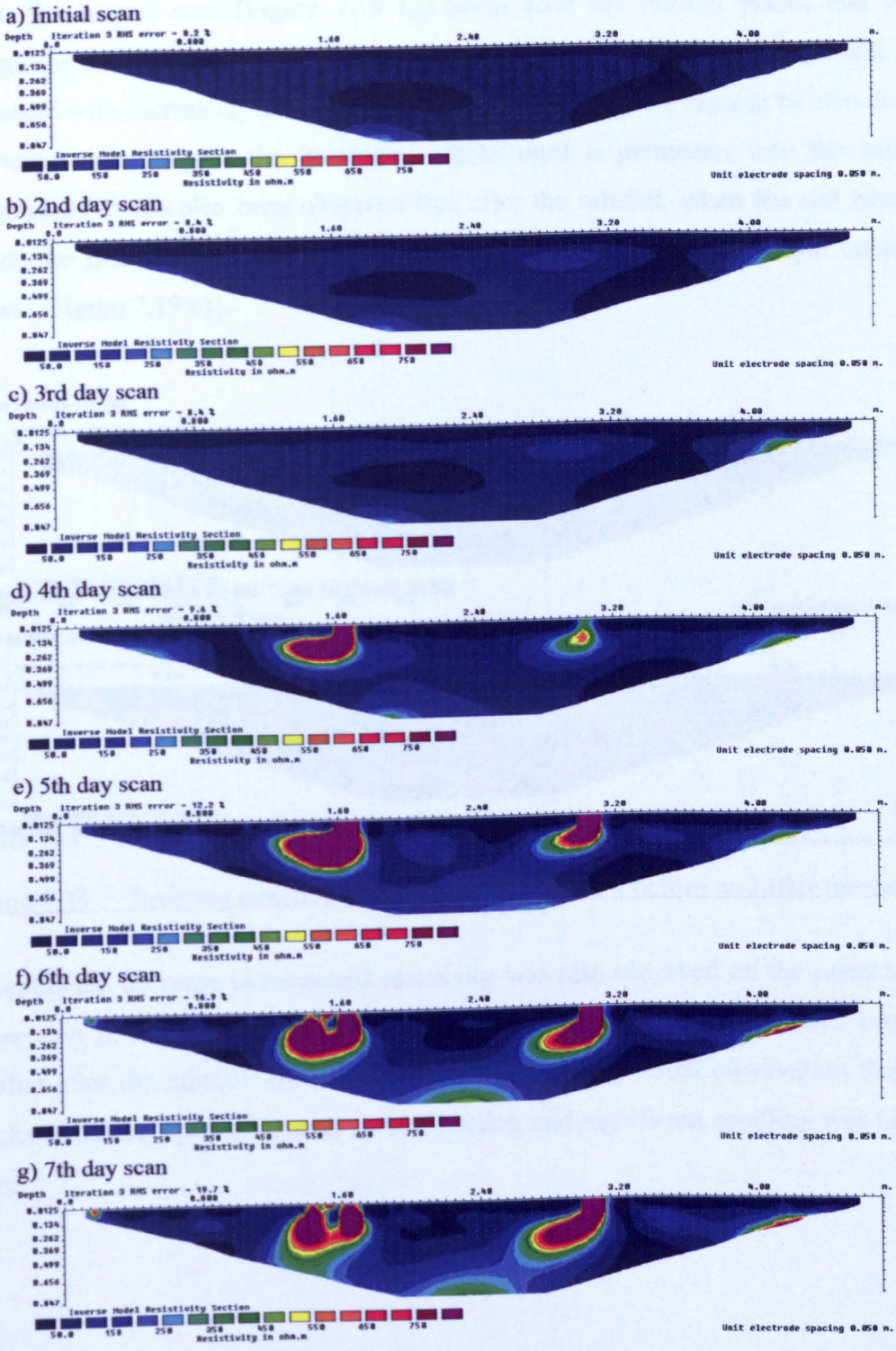

Figure 7.18 Geophysical scans taken during the first week of drying by section β.

The inversed resistivity scan taken before the rainfall was introduced on the embankment model. It can be clearly recognized where the places with high resistivity (deep purple colour) have widely grown after one week of drying.

From the second scan (Figure 7.19 b)) taken after the rainfall places that were recognised as highly resistive, became smaller as the conductivity of the soil had increased with increasing moisture content. It is believed, that this can be also due to the water remaining in the horizontal cracks until it permeates into the soil or evaporates. It has also been observed that after the rainfall, when the soil became moist, the measured resistivity values decreased [high resistivity purple contours shown Figure 7.19 a)].

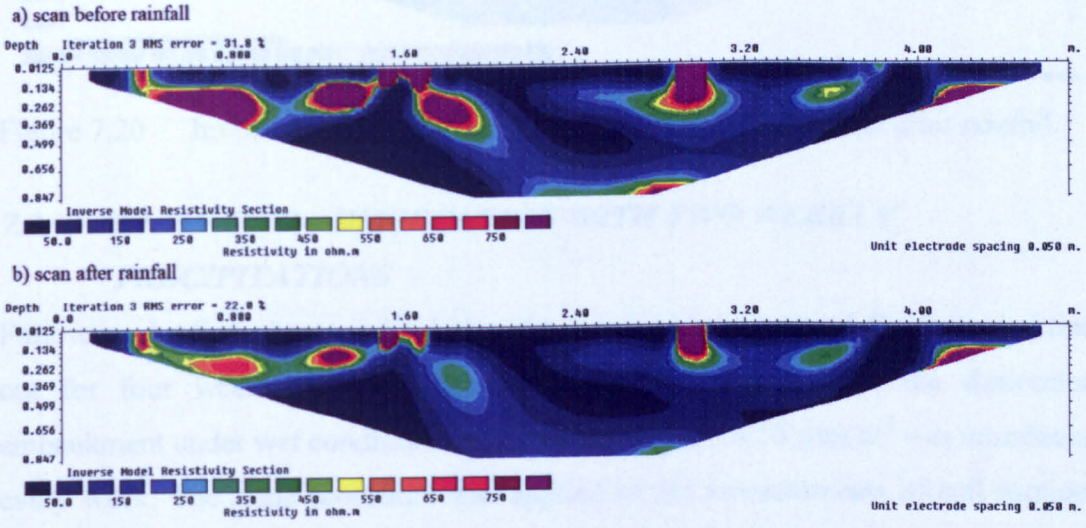

Figure 7.19 Inversed resistivity scan taken by section α before and after rainfall.

A significant decrease in measured resistivity was also observed on the scans taken by section β. It can be seen from Figure 7.20, that wide openings have become smaller after the rainfall. However, it was found during visual observation that the cracks remained opened. Hence, no self-healing and significant swelling was taking place.

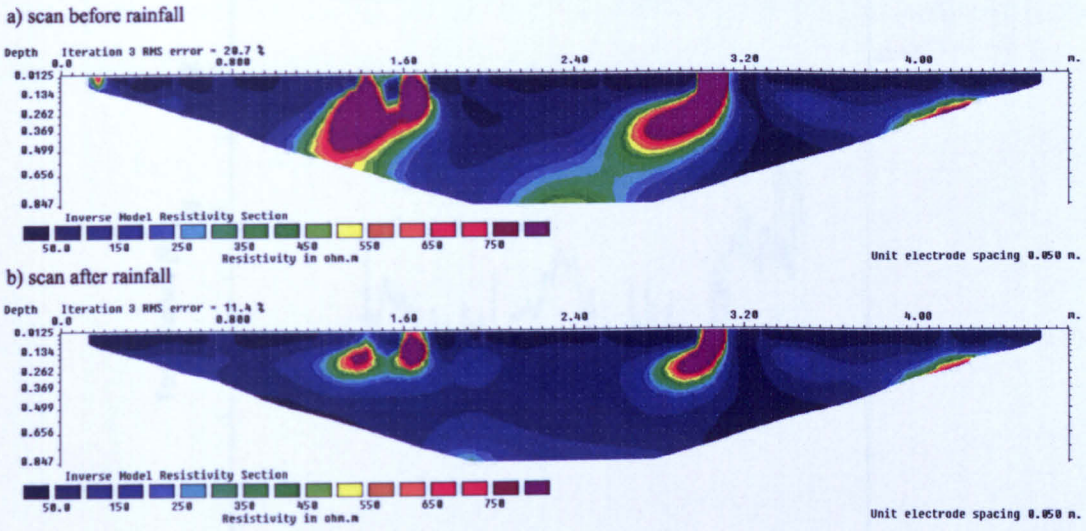

Figure 7.20 Inversed resistivity scan taken by section β before and after rainfall.

7.3. PHASE TWO – DESICCATION WITH TWO WEEKLY PRECIPITATIONS

Following the first phase of the desiccation experiment, a second phase was carried out for four weeks. In order to investigate the behaviour of the desiccated embankment under wet conditions an additional rainfall of 55 mm/m^2 was introduced every week. The same procedure was applied to the measurements of soil suction, moisture content, air temperature, Relative Humidity. All of them were taken with 30 sec intervals. Two geophysical scans were taken every day using the same arrays. Visual observations with photographs provided an extended evidence of the embankment behaviour.

The averaged recorded temperature varied between 19 °C and 22 °C. From the Figure 7.21, the temperature seemed to be much more stable than this observed during the first phase, which was probably due to more intensive rainfalls. Hence, the Relative Humidity recorded at the same time (Figure 7.22) looked much more stabilised.

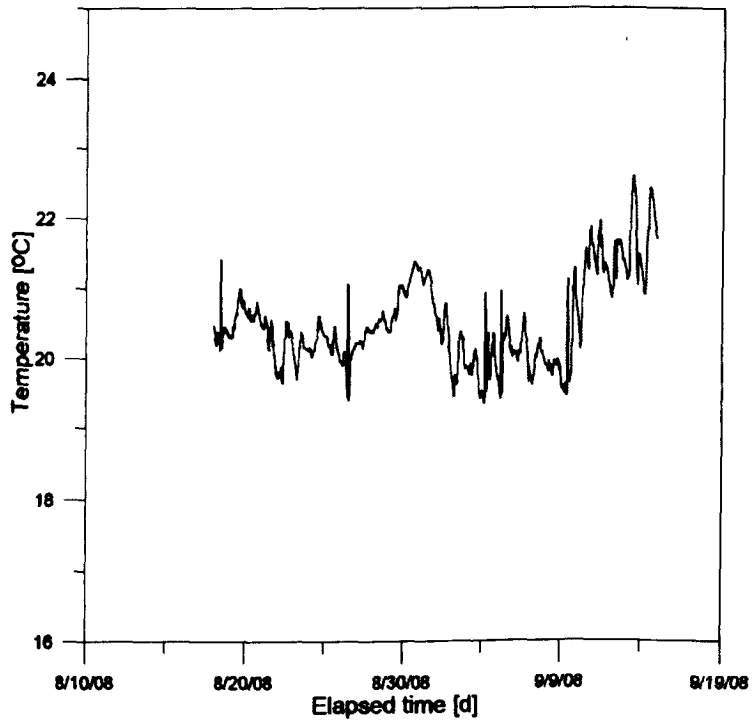

Figure 7.21 Averaged air temperature during second phase of experiment.

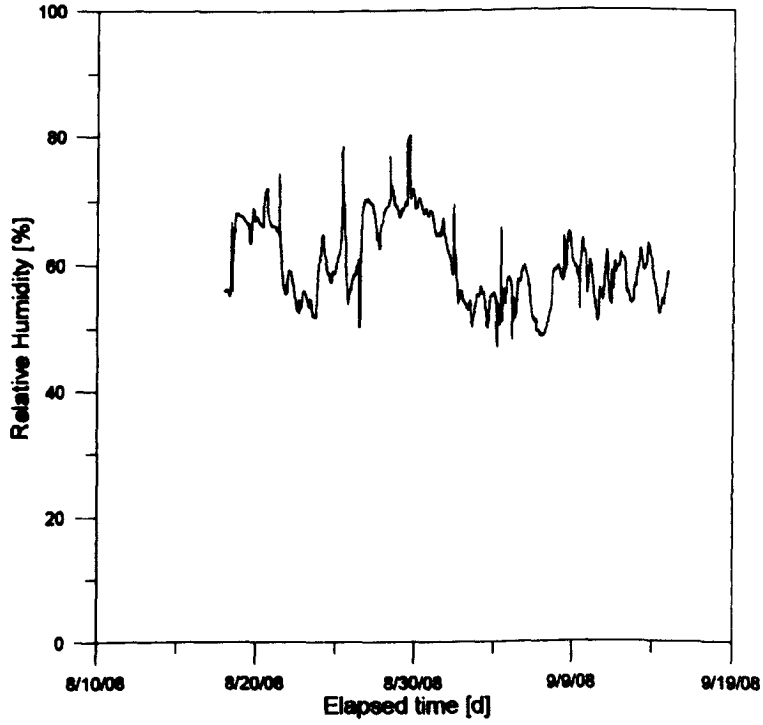

Figure 7.22 Averaged Relative Humidity during second phase of experiment.

Due to this intensive rainfall, an increase in moisture content was observed in the upper part of embankment (Figure 7.23).

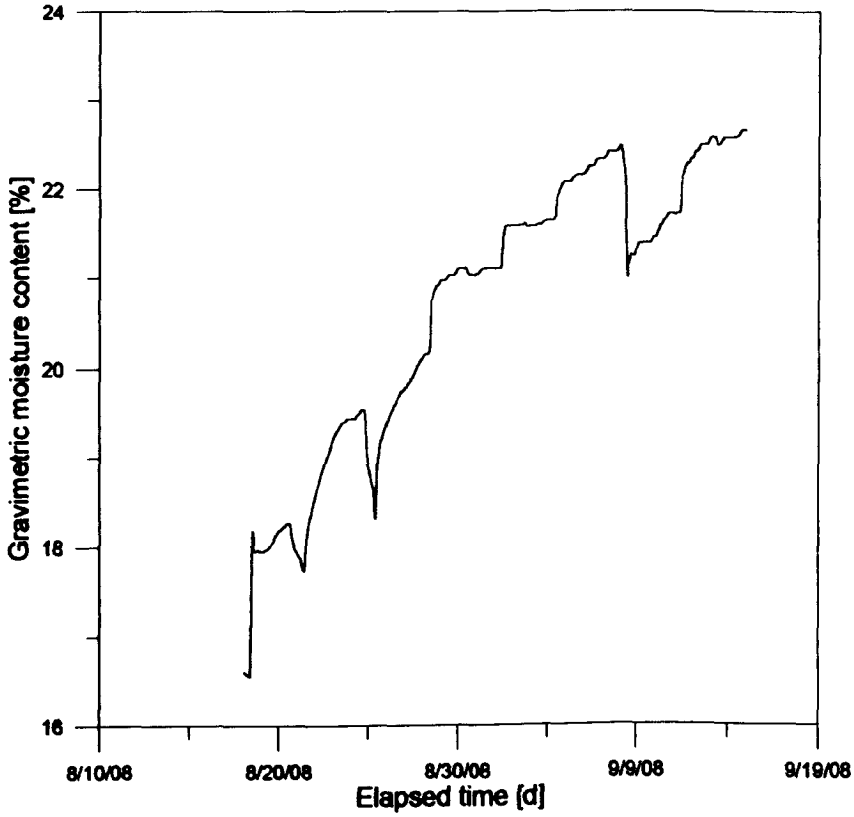

Figure 7.23 Moisture content increase recorded at 20 cm depth.

A few drops in the moisture content that can be seen in Figure 7.23, were due to the widely cracked upper layer very sensitive to any changes in the environment (drying and wetting).

It appears to be the same for the observations made on the moisture content profiles recorded within this period. Substantial variations in the upper layer were observed. At the same time, the moisture content in the lower parts remained constant (Figure 7.24).

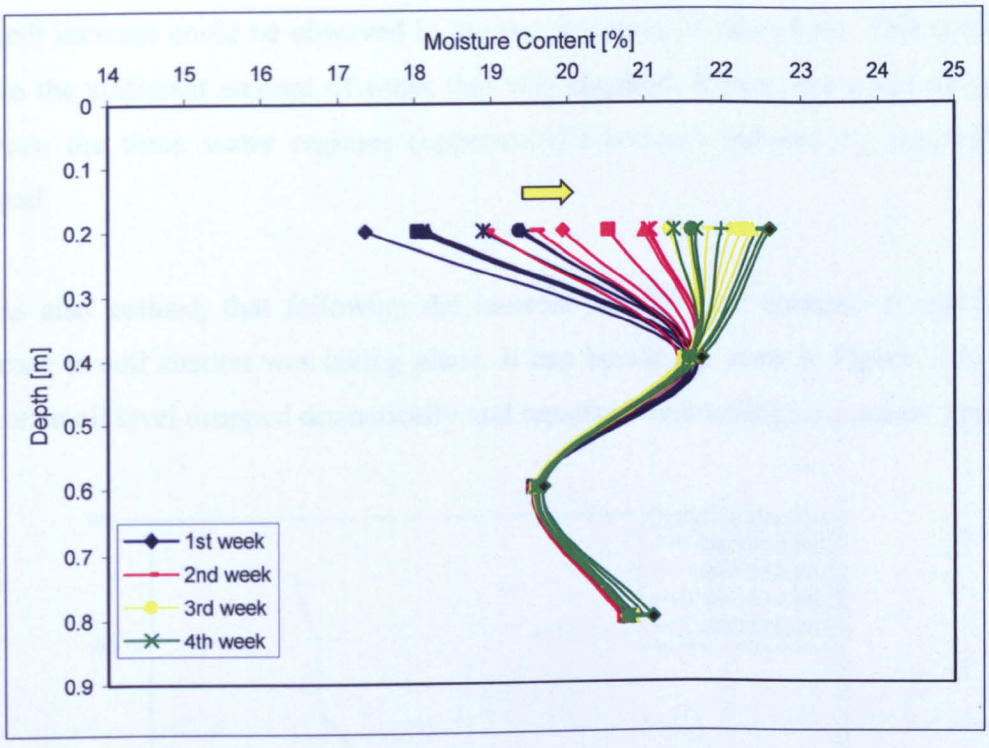

Figure 7.24 Moisture content profiles representative for 4 weeks of experiment – 2 cycles of rainfall.

This was later confirmed by the observation of the moisture content readings during experiment (Figure 7.25).

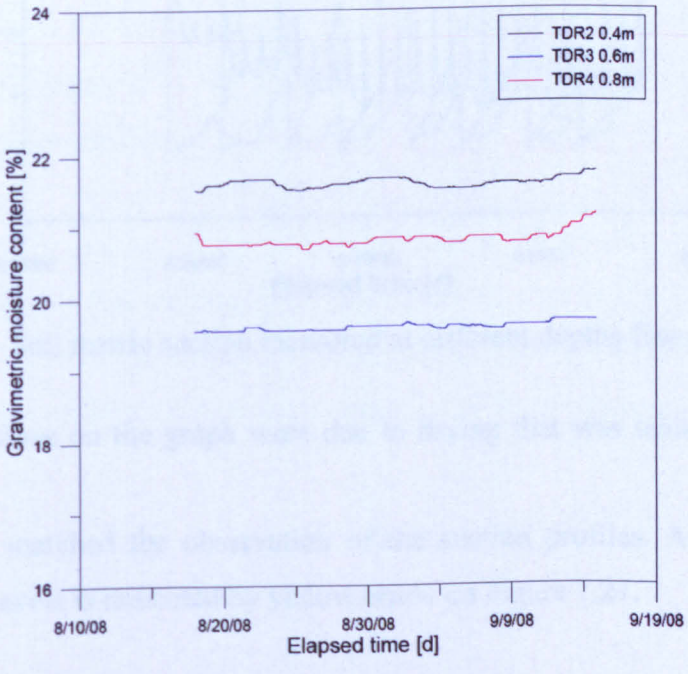

Figure 7.25 Gravimetric moisture content measured at lower parts of embankment model.

A small increase could be observed in the last few days of this phase. This could be due to the sufficient amount of water that was supplied. Hence, the water transport between the three water regimes (upper-middle-bottom) induced by desiccation, stopped.

It was also noticed, that following the increase of moisture content, a significant decrease in soil suction was taking place. It can be clearly seen in Figure 7.26 that suction at all level dropped dramatically and remained fluctuating in a narrow range.

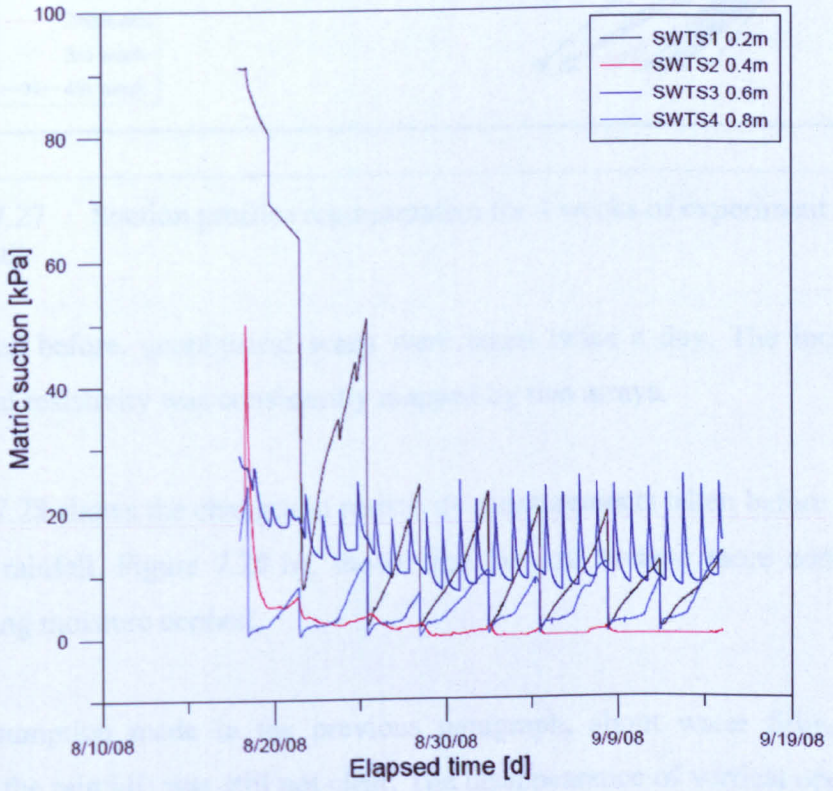

Figure 7.26 Soil matric suction measured at different depths from the crest.

Small fluctuations on the graph were due to drying that was taking place between rainfalls.

These results matched the observation of the suction profiles. A decrease of soil suction at all levels is indicated by yellow arrow on Figure 7.27.

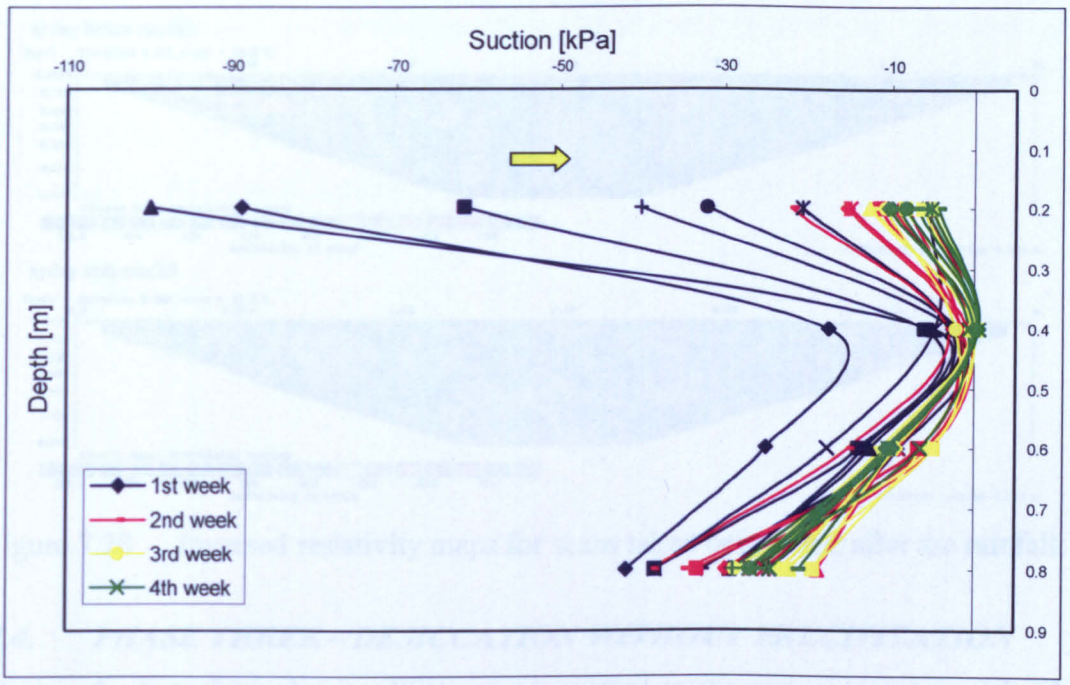

Figure 7.27 Suction profiles representative for 4 weeks of experiment – 2 cycles of rainfall.

As stated before, geophysical scans were taken twice a day. The increase in soil electrical resistivity was consistently mapped by two arrays.

Figure 7.28 shows the changes in resistivity measurements taken before and after the second rainfall. Figure 7.28 b), shows that the soil became more conductive with increasing moisture content.

The assumption made in the previous paragraph, about water filling the cracks (during the rainfall) was still not clear. The disappearance of vertical openings that is seen in Figure 7.28 b) can be also due to the cracks healing by fines washed from the surface. Hence, this these observations required further investigation.

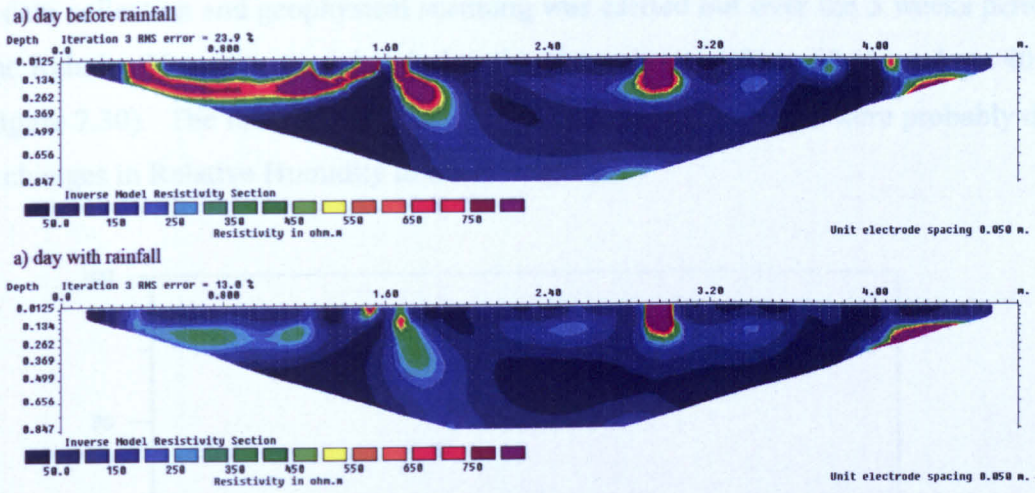

Figure 7.28 Inversed resistivity maps for scans taken before and after the rainfall.

7.4. PHASE THREE – DESICCATION WITHOUT PRECIPITATION

During the last phase dry conditions were applied to the experimental model. The embankment was only subjected to drying conditions in order to investigate its behaviour and how the desiccation process can influence the moisture content and suction of the soil. Hence, a temperature within the range of 20-23°C was kept inside the environmental chamber (Figure 7.29).

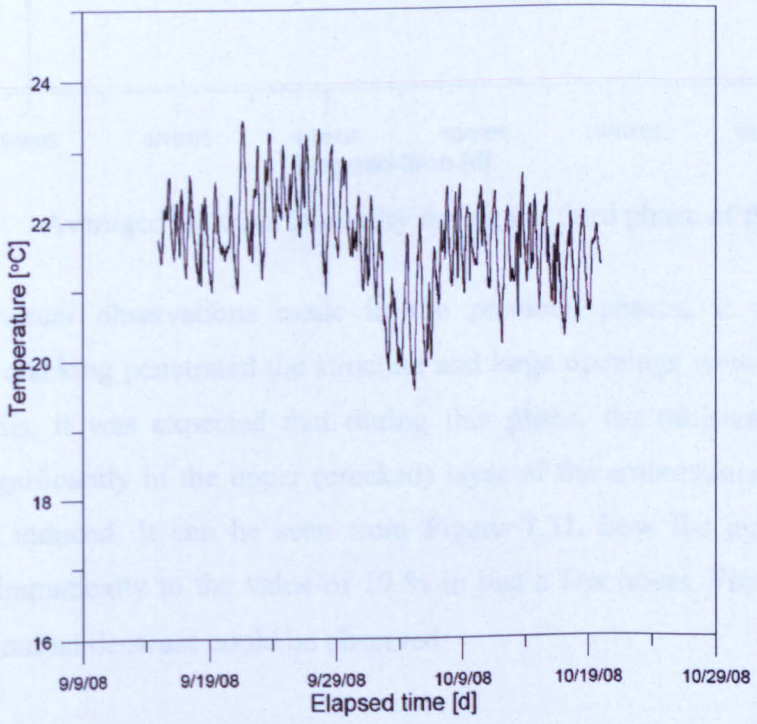

Figure 7.29 Averaged air temperature during third phase of experiment.

A data collection and geophysical scanning was carried out over the 5 weeks period. The Relative Humidity recorded during this time, dropped from 60 % to about 40 % (Figure 7.30). The few fluctuations that can be seen on the graph were probably due to changes in Relative Humidity in the laboratory.

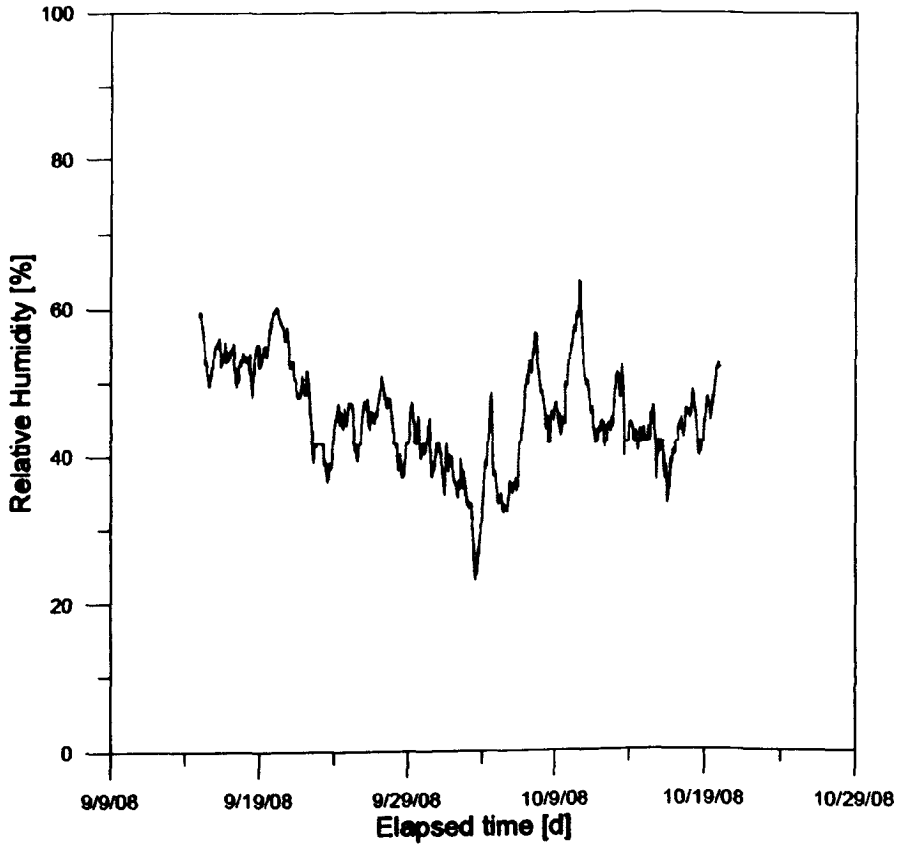

Figure 7.30 Averaged Relative Humidity during the third phase of the experiment.

From the visual observations made in the previous phases, it was seen that desiccation cracking penetrated the structure and large openings were created on the surface. Thus, it was expected that during this phase, the moisture content will decrease significantly in the upper (cracked) layer of the embankment model when drying was induced. It can be seen from Figure 7.31, how the moisture content decreased dramatically to the value of 19 % in just a few hours. From this point, a parabolic, gradual decrease could be observed.

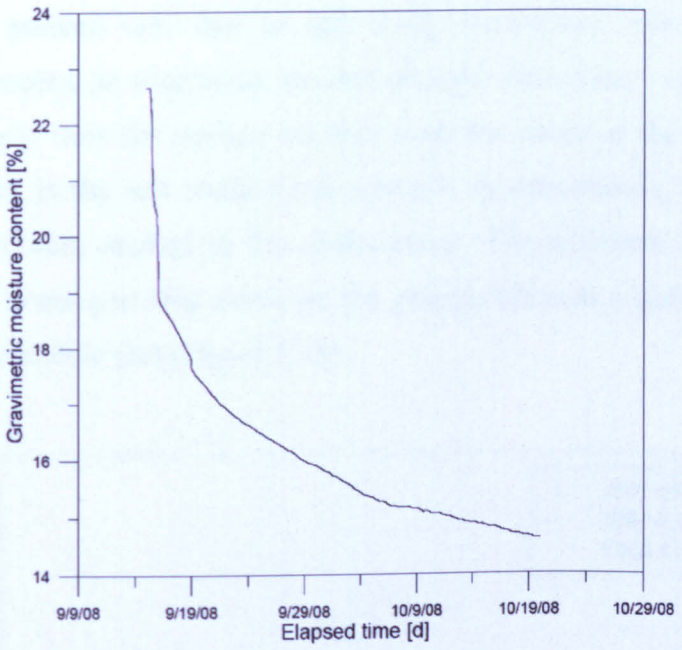

Figure 7.31 Moisture content recorded at 20 cm depth.

These results matched the moisture content profiles (Figure 7.32), where the shift in the upper layer could be observed. It was also expected that the embankment will dry out gradually at the lower depths as a result of the desiccation process.

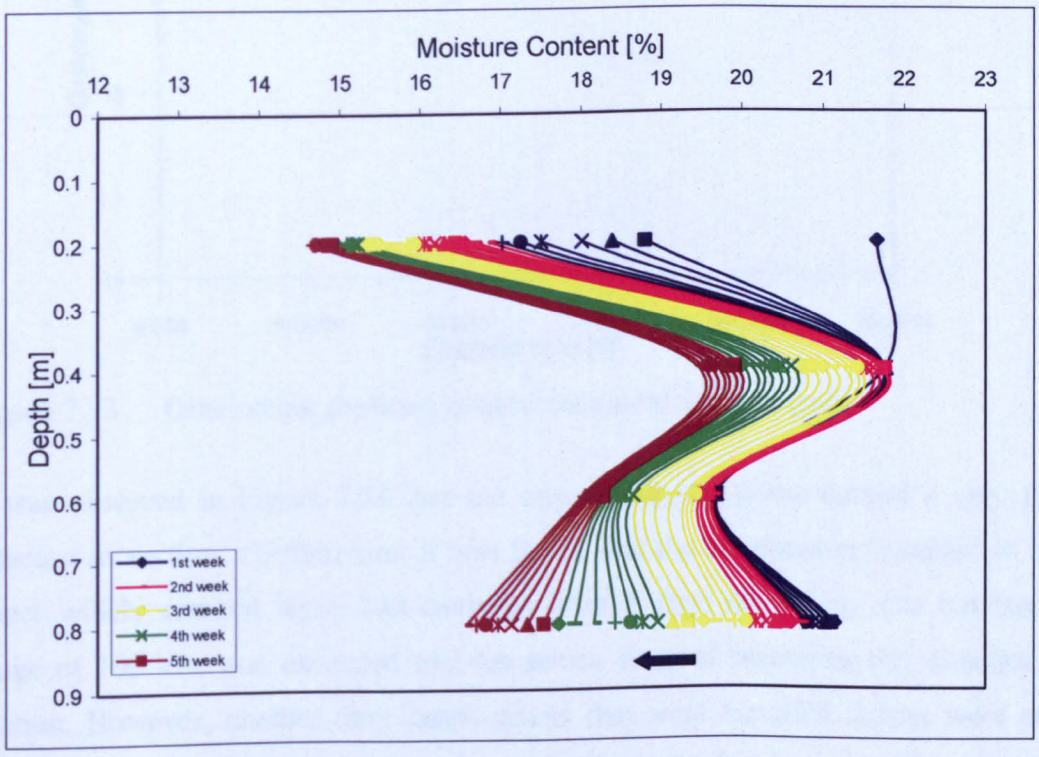

Figure 7.32 Moisture content profiles representative for 5 weeks of drying at 20°C – no rainfall.

It should be pointed out, that in this study desiccation was caused only by evaporation process, as vegetation was not present. Moreover, evaporation was not taking place only from the surface but also from the inside of the wide cracks. The water contained in the soil could move upwards or downwards, depending on the conditions that were applied to the environment. The moisture content decreased sharply in the lower part (red curve on the graph), whereas a gradual increase was observed in the middle part (Figure 7.33).

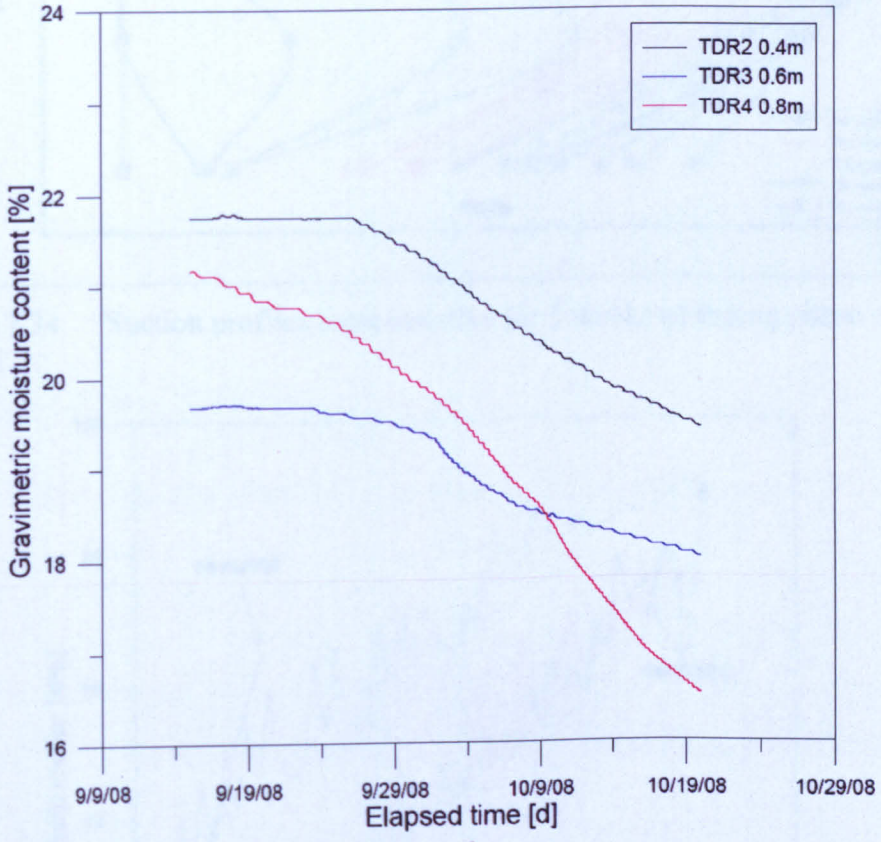

Figure 7.33 Gravimetric moisture content measured at lower parts.

It was observed in Figure 7.34 that the initiated drying phase caused a very fast increase in suction. Furthermore, it was found that the tensiometer installed in the upper widely cracked layer, had cavitated after 5 days of drying. The maximum range of 100 kPa was exceeded and the sensor stopped recording any changes in suction. However, another three tensiometers that were installed deeper were still working and the matric suction was measured (Figure 7.35).

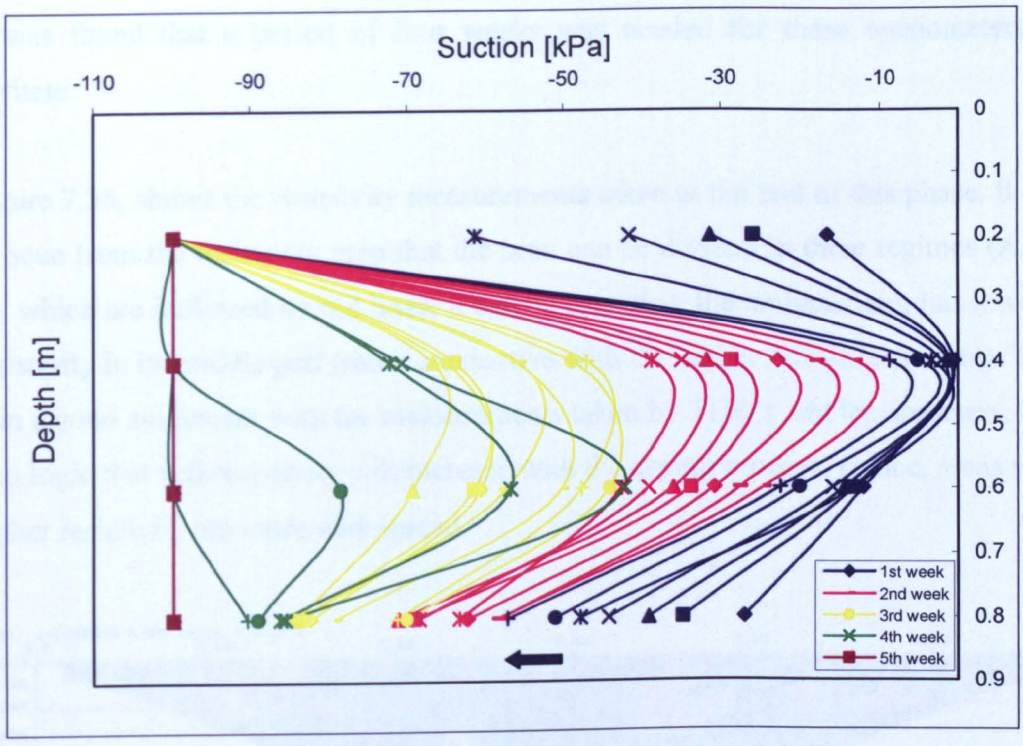

Figure 7.34 Suction profiles representative for 5 weeks of drying phase – no rainfall.

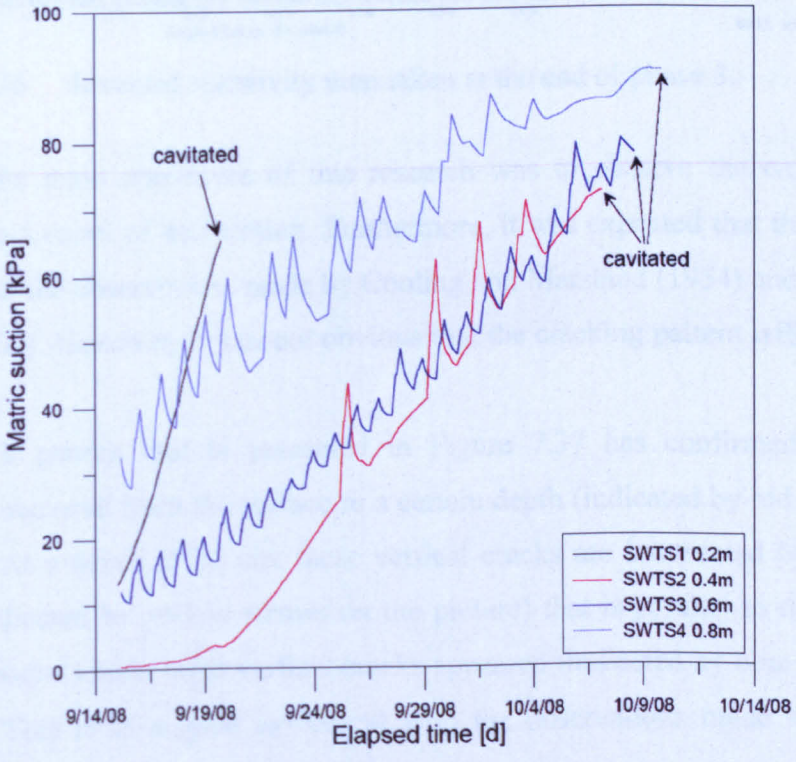

Figure 7.35 Matric suction measurements during the third phase of the experiment.

It was found that a period of four weeks was needed for these tensiometers to cavitate.

Figure 7.36, shows the resistivity measurements taken at the end of this phase. It can be seen from the resistivity map that the scan can be divided in three regimes (A, B, C), which are indicated by red lines. It can be seen that, the embankment has lower a resistivity in its middle part (more conductive with the higher moisture content). This is in a good agreement with the measurements taken by TDR's and tensiometers. It is also logic that soil resistivity will increase with the drying process. Hence, areas with higher resistivity are more widespread.

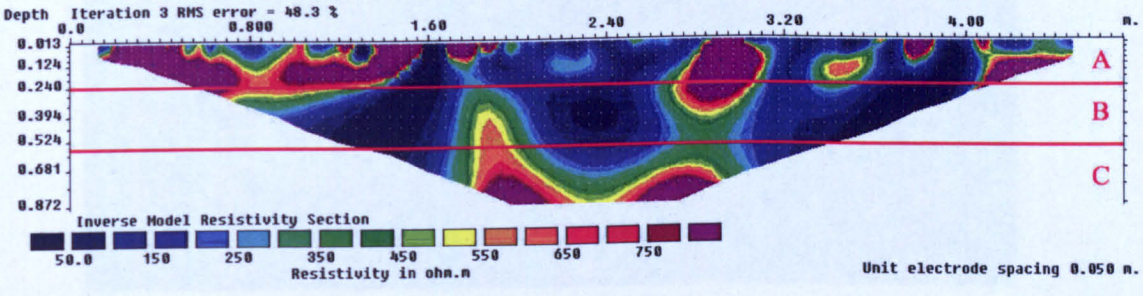

Figure 7.36 Inversed resistivity map taken at the end of phase 3.

One of the main objectives of this research was to observe the cracking pattern created as a result of desiccation. Furthermore, it was expected that this observation will match the observations made by Cooling and Marsland (1954) and later by Dyer et al. (2007). However, it was not obvious that the cracking pattern will appear in the same way.

The crack pattern that is presented in Figure 7.37 has confirmed that vertical cracking occurred from the surface to a certain depth (indicated by red arrows on the picture). At a depth of 25 cm, these vertical cracks are intersected by a horizontal crack (indicated by yellow arrows on the picture) that is parallel to the crest. From this horizontal crack, three vertical cracks appeared (indicated by blue arrows on the picture). This is in a good agreement with the observations made by Dyer et al. (2007).

Despite the fact that similar crack pattern was observed, it has to be noticed, that this particular observation is not common. Desiccation cracking depends on many factors (i.e.: type of the soil, weather conditions, water level, compaction, etc.) that can cause creation of different crack patterns.

Figure 7.37 Observed desiccation cracking inside embankment body.

Figure 7.38 Crack parallel to the slope.

The visual observation of the crack pattern has also validated the hypothesis proposed by Dyer et al. 2007, that horizontal crack could create in a parallel line to the shape of the embankment. It can be clearly seen from Figure 7.37 and Figure 7.38 that the horizontal crack followed the embankment's shape (marked by yellow line on the wall).

The results presented in this Chapter, confirmed that cracking may appear shortly after construction when desiccation process takes place. Furthermore, it was observed that the soil suction is controlled by the moisture movement within the soil. Various weather conditions applied to the experimental model revealed a quick response of the sensors to the changing soil-atmospheric interactions accounting for evaporation models observed previously by Likos and Lu (2003) on soil column. Hence, this experiment confirms the existing theories and the assumptions made previously. The potential of the geophysical measurements has to be acknowledged. The resistivity measurements were validated by visual observations. Although the depth of cracking was not manually measured, the observed crack pattern matched the observations made by Cooling and Marsland (1954) and later by Dyer et al. (2007).

The main aim of this study was to investigate the influence of desiccation fissuring on the stability of flood embankments. Hence, the next Chapter examines the stability of the embankment model subjected to flooding conditions.

CHAPTER 8

8. FLOODING EXPERIMENT

8.1. INTRODUCTION

Following the desiccation experiment presented in Chapter 7, the flooding experiment was carried out in order to investigate the behaviour of desiccation cracked embankment subjected to flooding conditions.

Studies carried out by Marsland and Cooling (1958), revealed a seepage of a specific nature during their Cofferdam test. It appeared during the test that rising water seeped through the rubbilised upper zone. Hence, the failure was initiated on the outward face leading to the embankment instability. However, the process of this specific failure is still not well understood. Hence, presented experiment was designed to investigate the nature of failure indicated by Marsland and Cooling (1958) and later by Dyer et al., (2007). In addition, the hypothesis given by Dyer et al., (2009) was also studied.

8.2. EXPERIMENTAL SET UP

The same set of sensors was used in this experiment. As described in Chapter 5 the function of tensiometers was to measure the suction of the soil. However, both types of tensiometers used in this research were optionally designed to measure positive pore water pressure. Hence, they could perform as piezometers. Moreover, there was not a special calibration required. It was only necessary to refill them with water if the cavitation took place. Thus, four tensiometers installed on the slope were refilled in order to provide reliable measurements.

It was observed that during the desiccation phase, a settlement and excessive shrinkage of the embankment model took place (Figure 8.1). Hence, a gap between the embankment and the flume walls appeared (Figure 8.2).

Figure 8.1 Size of settlement from the initial state.

Figure 8.2 Gap between embankment model and concrete flume.

In order to prevent any seepage along the walls, an expanding foam was used to fill the gap. In addition, cutting edges (see Figure 8.12 on page 174) were designed and attached to the sensors that were installed on the crest in order to prevent any erosion behind the sensors caused by scouring effect. It is worth mentioning that these cutting edges where previously tested in the small hydraulic flume and no scour was observed.

Data logger was programmed to take the readings every 5 seconds in order to measure immediately any changes in pore water pressure.

Figure 8.3 Embankment model with the experimental set up.

Furthermore, it was decided to use two miniature resistivity arrays (Figure 8.3) in order to be able detect any internal seepage and subsequent capillary wetting following flood.

8.3. EXPERIMENT

The initial geophysical scan taken before flooding, confirmed the state of the embankment model to be extremely dry. It can be seen from the Figure 8.4 that the measured electrical resistivity of 400-800 Ωm is a dominant value.

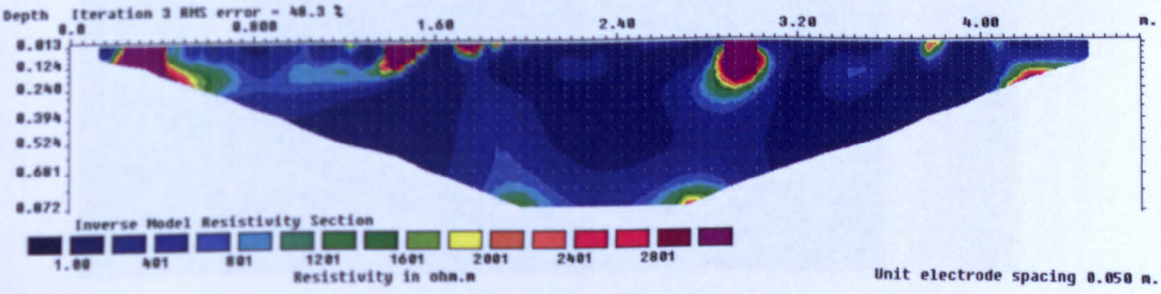

Figure 8.4 Inversed resistivity map taken by section α before flooding.

Following the geophysical scans, the upstream side was gradually filled with water (flow rate-60 l/min) to the level of the first tensiometer (Figure 8.5).

Figure 8.5 Channel filled with water to the level of the first tensiometer.

The pump was stopped and visual observation was carried out. As it can be seen from the Figure 8.6 no seepage was observed (after 1 hour) on the downstream side of the embankment. It was assumed that at this level, the model was impermeable and not affected by cracking.

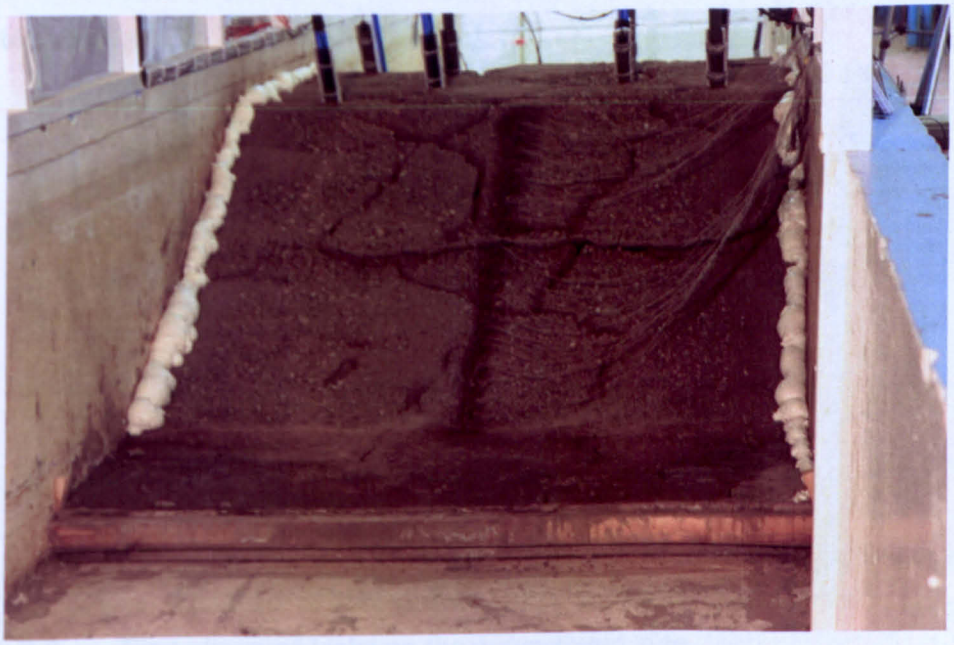

Figure 8.6 Downstream side of the embankment after one hour of flooding.

After 1 hour, the water level was raised again to the level of the third tensiometer and kept constant (Figure 8.7).

Figure 8.7 Upstream side of the embankment with the water level 20 cm below the crest.

It should be noticed that the pore water pressure increased with the increasing water level behind the embankment. Hence, the internal seepage could take place. Figure 8.8 shows the first local seepage occurring after 15 minutes at the bottom of the downstream slope. Figure 8.9 and Figure 8.10 show zoomed photographs of the reported seepage.

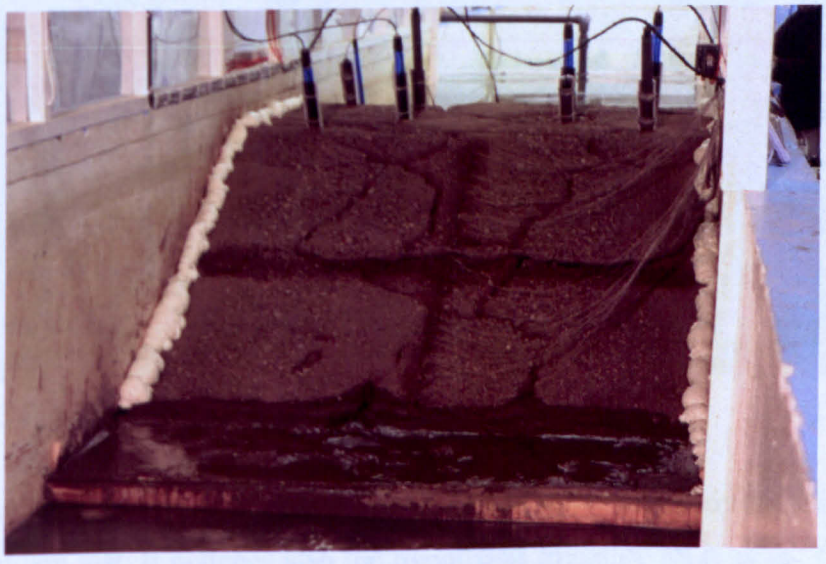

Figure 8.8 First observed leaks on the downstream side.

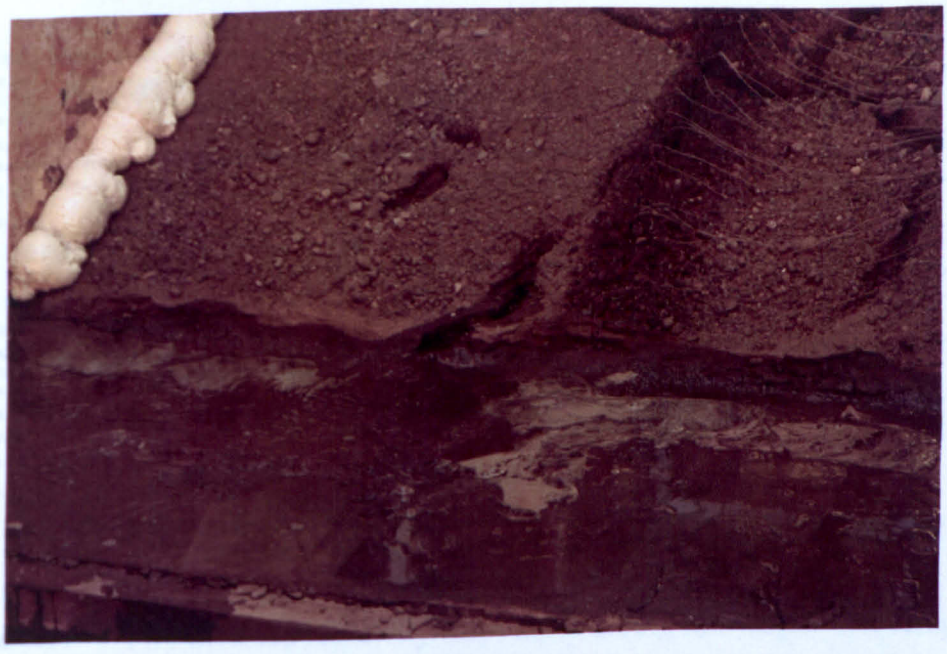

Figure 8.9 Local seepage.

Figure 8.10 Local seepage from the bottom of the slope.

These pictures validate the observation made by Marsland and Cooling (1958) during their Cofferdam test. It matches also the hypothesis given by Dyer et al., (2007) and Dyer et al., (2009) with a specific internal seepage.

It appears from the geophysical scans (Figure 8.11) that following the internal seepage the electrical resistivity decreased at the same time.

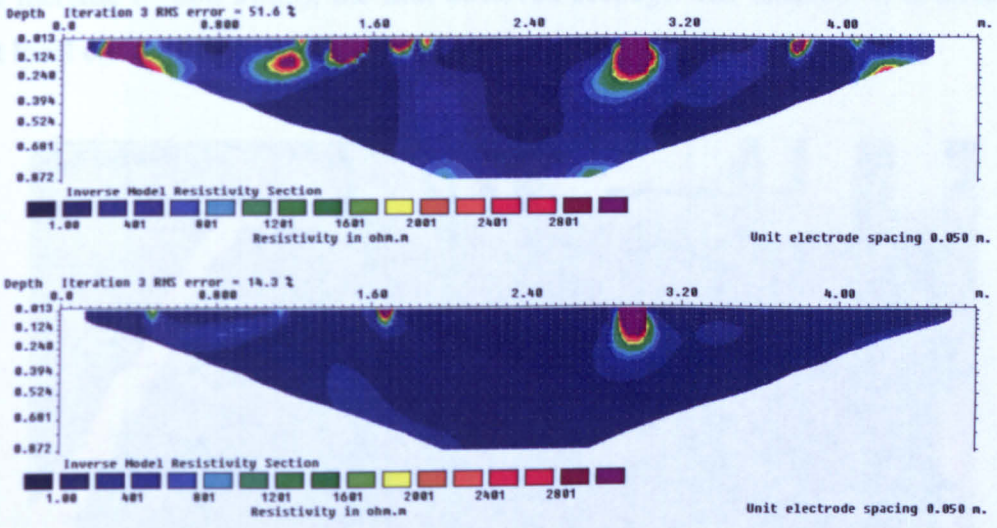

Figure 8.11 Two inversed resistivity maps taken during first stage of flooding.

The water level was subsequently raised up to the crest level (see Figure 8.12) in order to observe water activity through the surface fissures. The visual observations made at this stage, revealed some important findings. It was observed that water distributed by the surface cracks was either seeping inside them or flowing further up and filling other crack paths.

Figure 8.12 Water penetrating cracks on the crest.

When the water reached the crest edge on the downstream side, two leaks were observed from the fissured slope (Figure 8.13). After 4 hours with an increased flow

rate increase (~ 600 l/min), the first observed seepage was blocked. It is assumed, that local collapse took place and stopped the water flow.

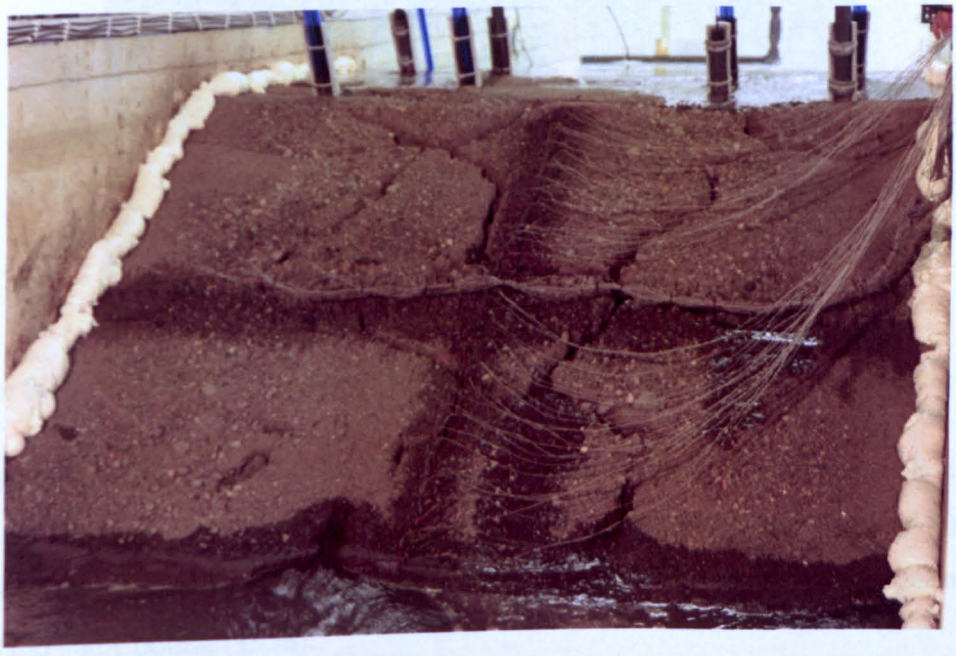

Figure 8.13 Overflowed crest.

The observations made during the first day of the experiment explored an important finding and provided some more understanding about the embankment behaviour. It was clearly seen, that erosion, softening and undercutting of the clay blocks were the major factors affecting the embankment model. Moreover, these factors were accompanied by localised failures and internal collapses. It was also noticed, that the settlement of transported sediment did not took place due to the rapid movements of seeping water. Thus, all fines were washed away from the cracks, and progressive erosion could be observed. It can be clearly seen on the Figure 8.14, that extensive internal erosion took place on the downstream slope.

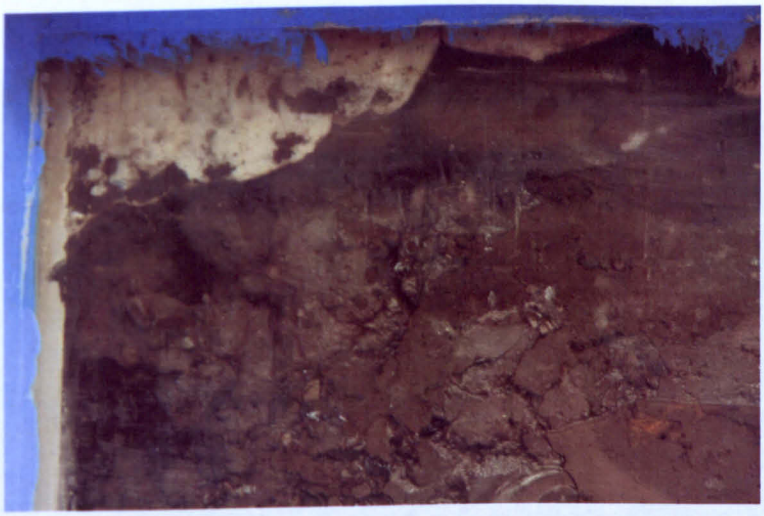

Figure 8.14 Eroded crack inside embankment close to the edge of the slope.

Another important observation that is mainly observed in non-cohesive soils can be seen on Figure 8.15. A phreatic line has created (indicated by red dashed line on Figure 8.15) within the rubblised zone which again validates findings explored by Marsland and Cooling (1958).

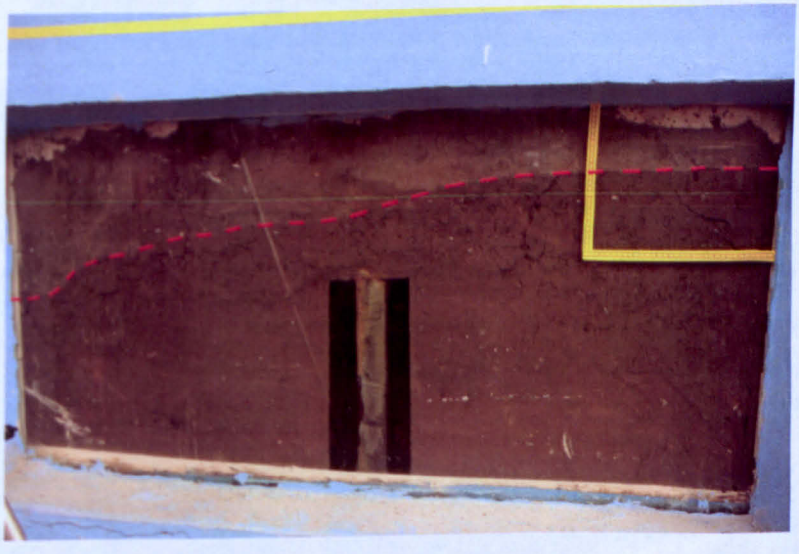

Figure 8.15 Observed phreatic zone.

It appeared from visual observation (after overtopping) shown on Figure 8.16 and Figure 8.17, that erosion took place in one half of the crest as well as on the downstream side of the embankment. The other half was sealed by the sediment according to the water flow direction. Moreover, a 5 cm increase in erosion depth was measured every day.

Figure 8.16 Eroded slope and the half crest.

Figure 8.17 5 cm deep cracks on the crest edge after first day of flooding.

It can be seen on Figure 8.18 that due to very intensive overtopping conditions two flow paths have created on the downstream slope.

Figure 8.18 Eroded slope with the two flow paths visible in the middle of the slope.

Erosion takes place where overtopping conditions are present. Moreover, it was believed that for specific types of soil, such as stiff clays the embankment will remain stable, even when the water head above the crest is significant. Thus, it was decided to increase the water head of about 10 cm in order to increase the hydrodynamic forces on the downstream slope. A wooden barrier was installed across the flume and sealed using expanding foam (Figure 8.19).

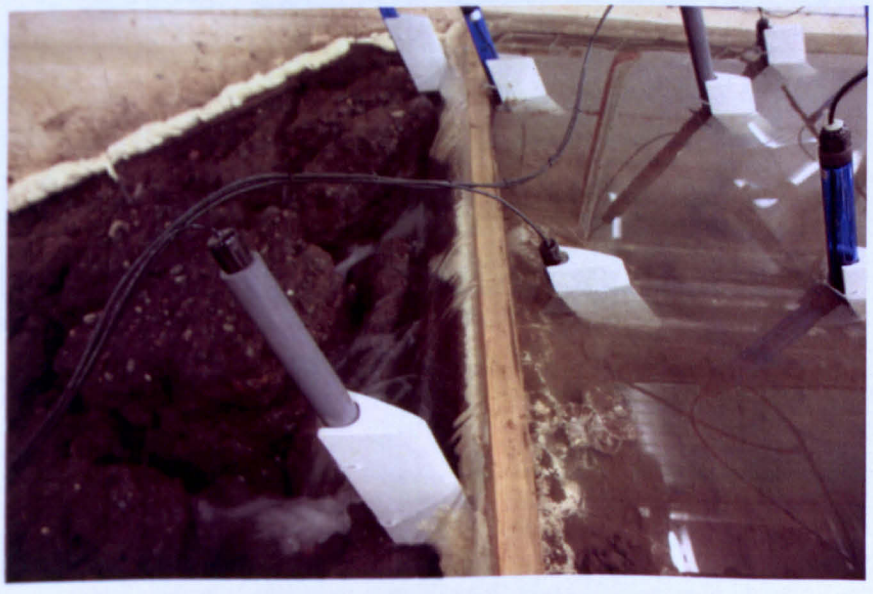

Figure 8.19 Increased water head with the wooden barrier.

It can be seen in Figure 8.20, Figure 8.21 and Figure 8.22 that a small crack appeared on the block of clay followed by collapse.

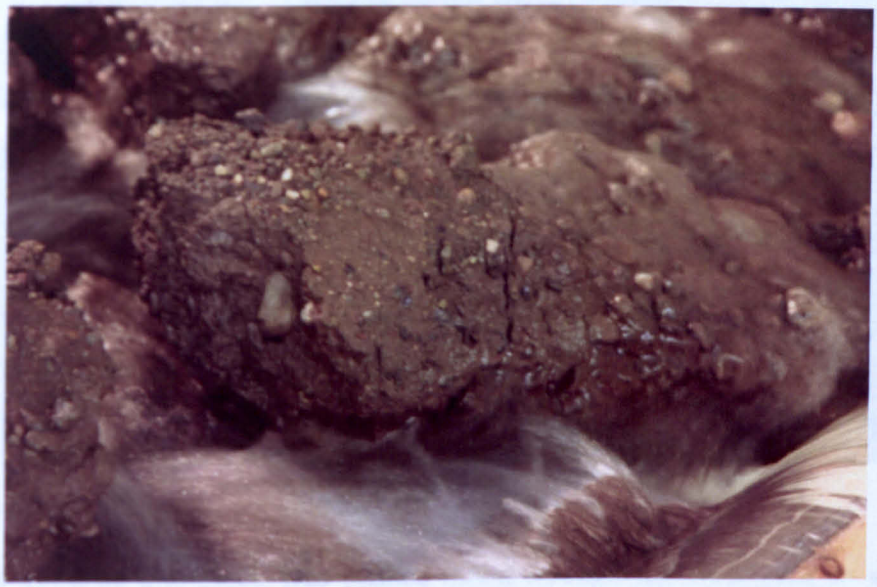

Figure 8.20 Undercutting of clay block.

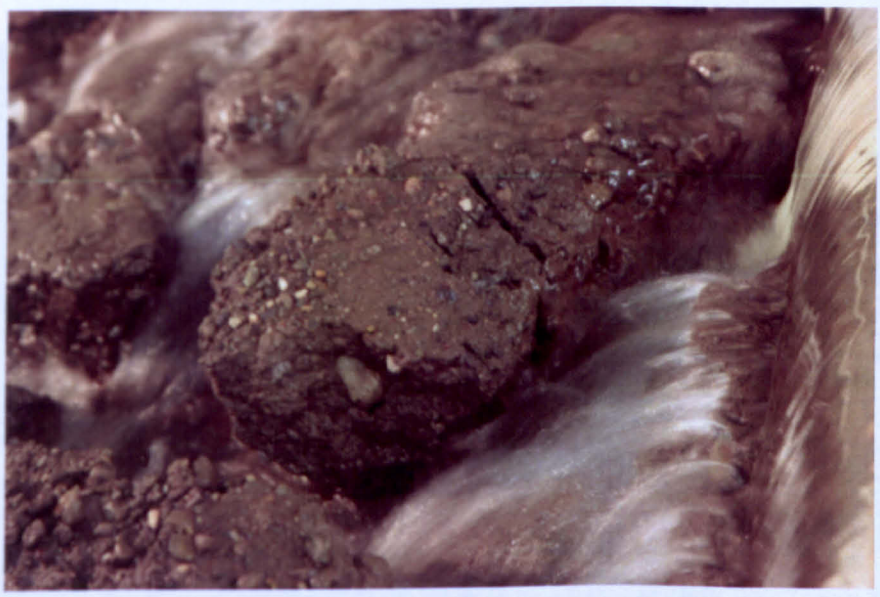

Figure 8.21 Visible crack in collapsing block.

Figure 8.22 Collapsing clay block.

After the collapse this block was pushed down through the flow path by dragging forces to be finally washed away (Figure 8.23 and Figure 8.24).

Figure 8.23 Pushed away clay block.

Figure 8.24 Visible small collapse in the clay block.

It has been found that the soil at all levels became fully saturated after a period of about 7 days (see Figure 8.25). After this period the response from the moisture content probes was only caused by small variations in the water level during flooding.

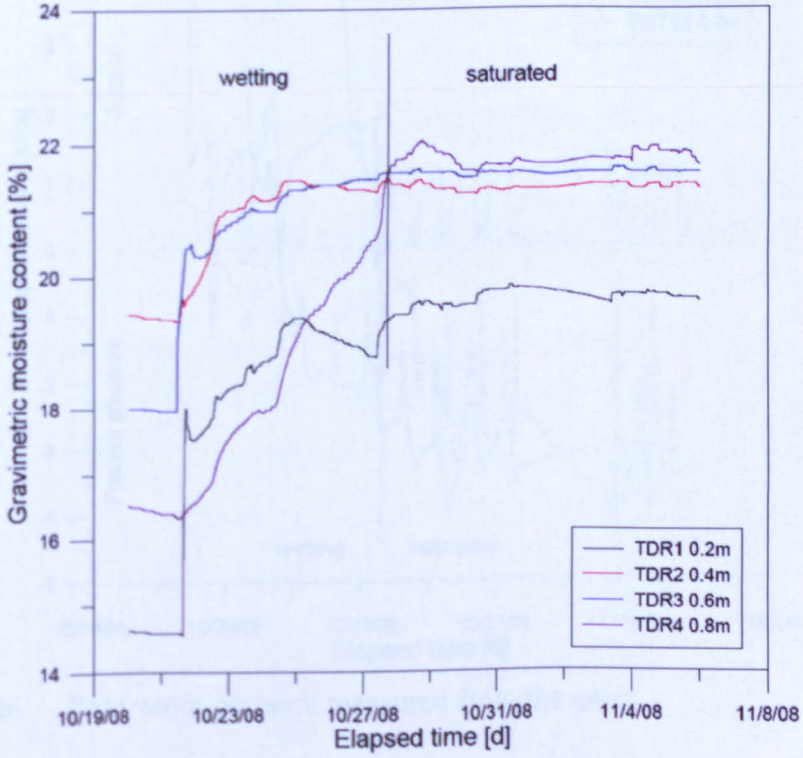

Figure 8.25 Moisture content readings during flooding.

It can be seen on Figure 8.25, that there is an evident limit where the readings of moisture content at all depths are not significantly increasing, but only fluctuate in a small range.

A sharp increase of the moisture content was observed at the bottom part of the embankment model, whereas a gradual increase is noticed at other levels. Moreover, the moisture content at corresponding levels increased, due to the water pressure increase with depth (see Figure 8.25).

This observation is in good agreement with the pore water pressure readings recorded on the crest and on the slope (see Figure 8.26 and Figure 8.27). The increase of the pore water pressure was followed by the wetting front that was penetrating the embankment model. From the point where the saturated state can be observed, changes in pore water pressure are only due to the water level changes above the embankment (see Figure 8.26 and Figure 8.27). Furthermore, it can be also noticed from the Figure 8.26, that a different time was needed for the tensiometers to be refilled again since they cavitated.

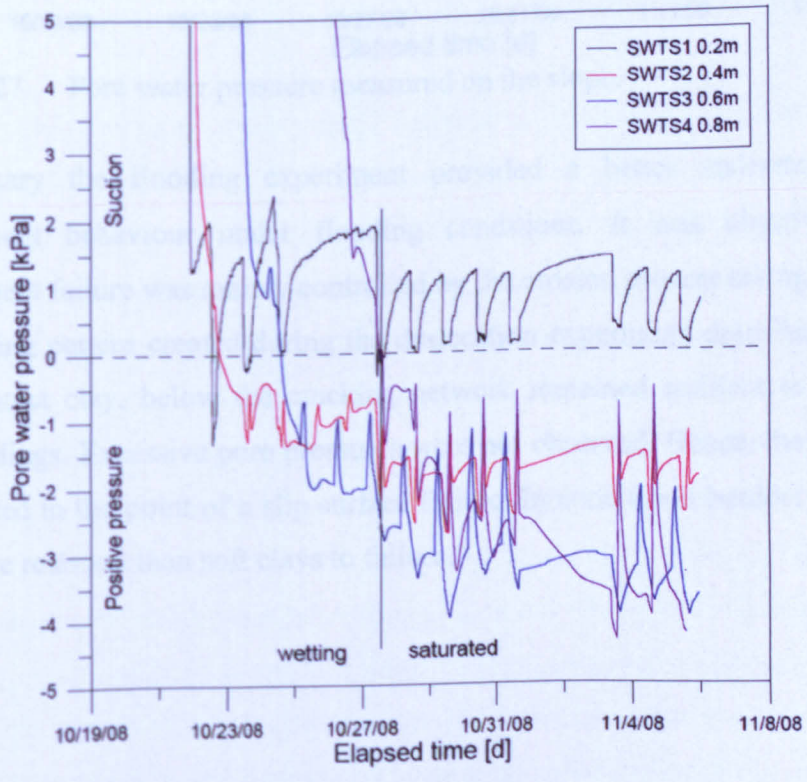

Figure 8.26 Pore water pressure measured from the crest.

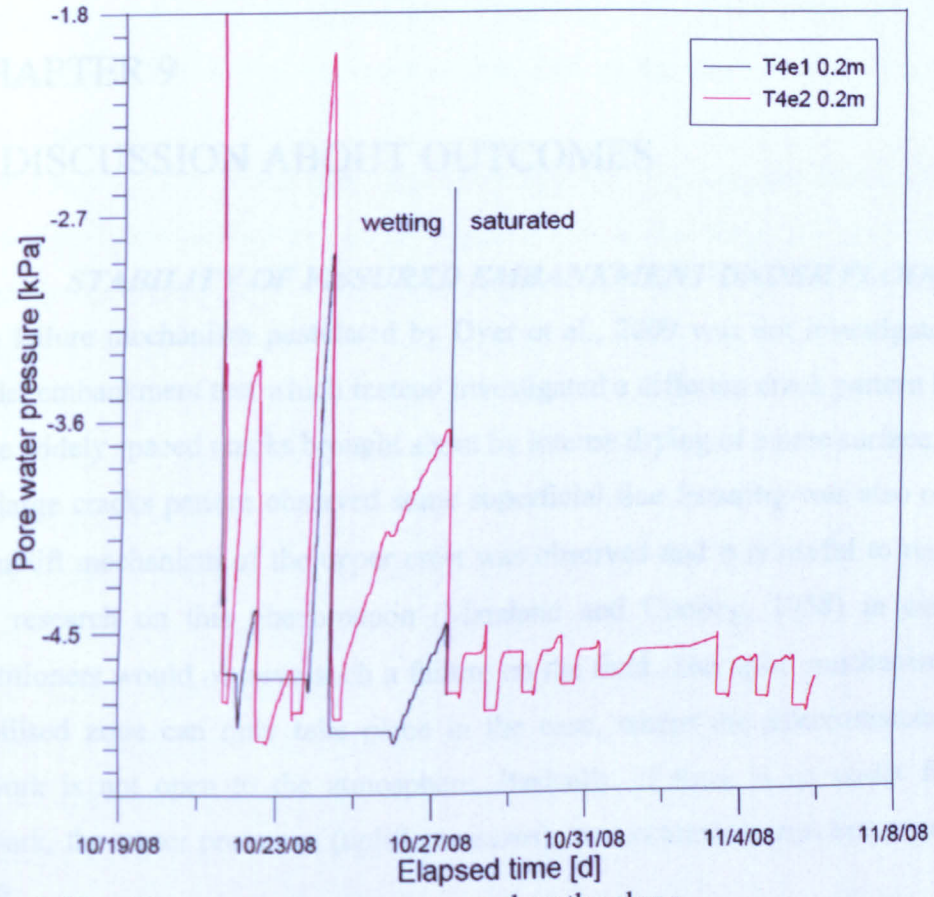

Figure 8.27 Pore water pressure measured on the slope.

In summary the flooding experiment provided a better understanding about embankment behaviour under flooding conditions. It was observed that the embankment failure was mainly controlled by the erosion process taking place within the cracking pattern created during the desiccation experiment described in Chapter 7. The intact clay, below the cracking network remained resilient to erosion and flood loadings. Excessive pore pressures were not observed. Hence, the stability was not affected to the point of a slip surface failure. In conclusion boulder clay seemed to be more resistant than soft clays to failure.

CHAPTER 9

9. DISCUSSION ABOUT OUTCOMES

9.1. STABILITY OF FISSURED EMBANKMENT UNDER FLOODING

The failure mechanism postulated by Dyer et al., 2009 was not investigated in the model embankment test which instead investigated a different crack pattern based on large widely spaced cracks brought about by intense drying of a bare surface. Despite the large cracks pattern observed some superficial fine fissuring was also observed. No uplift mechanism of the upper crest was observed and it is useful to remind the past research on this phenomenon (Marsland and Cooling, 1958) in case other practitioners would observe such a failure on the field. The uplift mechanism of the rubbilised zone can only take place in the case, where the interconnected crack network is not open to the atmosphere. Basically, if there is no outlet from the network, the water pressures (uplift pressures) can accumulate and hence cause the uplift.

It is worth mentioning an earlier study undertaken by Cooling and Marsland (1954) where an uplift mechanism of a different nature is presented. The failure mode proposed by Cooling and Marsland (1954) relates to underseepage and excessive pore water pressures mobilising in the pervious layer which is covered on the landward side by the less pervious layer of sand. Under high water heads, "boils" and "springs" may develop near the landward toe of the embankment. This, can then lead to complete failure of the embankment as the toe of the embankment may be undermined, especially cases when it becomes violent and widespread.

Another, more recent study carried out by Van et al., (2005) showed that the uplift mechanism and uplift pressures were due to the excessive pore water pressures in the underlying sandy gravel. Hence, it resulted in the flotation of the overlying alluvium in the marsh and complete collapse of the flood defence. Theoretically, if the sand layer is incompressible and completely open to the river, and the overlying layer on the landward side is impervious, then the pressure in the sandy gravel layer becomes equal to the river and every rise in the water level in the river will result in the increase of the pressure in the permeable layer.

The uplift mechanism mentioned above was observed on the landward side of the embankment close to the toe and was followed by the shallow slip of unsupported back slope.

In this study it was found that when the rubbilised soil becomes fully saturated the pore water pressure can be closely equal to this in the river, but not significantly excessive (see Chapter 8). Hence, every rise in the water level in the river channel will result in the increase of the pressure in the permeable layer that was created during desiccation. Marsland and Cooling (1958) observed the increase in pore water pressure into the fissured zone in much the same way as if the core had been covered with the gravel blanket.

Even though, embankments are usually made of cohesive soils to provide maximum impermeability, it is believed that where the soft deposits are used, these pressures can be more dangerous as the soil strength will reduce to zero. At the moment, the effect of excessive pore water pressures revealed by Marsland and Cooling (1958) is still not fully understood. It is more likely that the excess pore pressure would be caused by a combination of changes in static and dynamic pressures. In this case, as it was observed during the flooding experiment presented in Chapter 8, only dragging forces can be considered as the factors playing major role in the embankments failure.

The observation made by Marsland and Cooling (1958) about the water flow through the fissured zone was validated by the experiment described in Chapter 8.

Water flow in clayey embankments is always neglected as they are constructed as impermeable and homogenous structures. The observation of pore water pressure during the flooding experiment has provided valuable insight into embankment behaviour.

It can be seen from both Figure 9.1 and Figure 9.2 that there was no significant increase in pore water pressure measured by tensiometers and even after raising the water head above the embankment and increasing the flow rate the changes were not crucial.

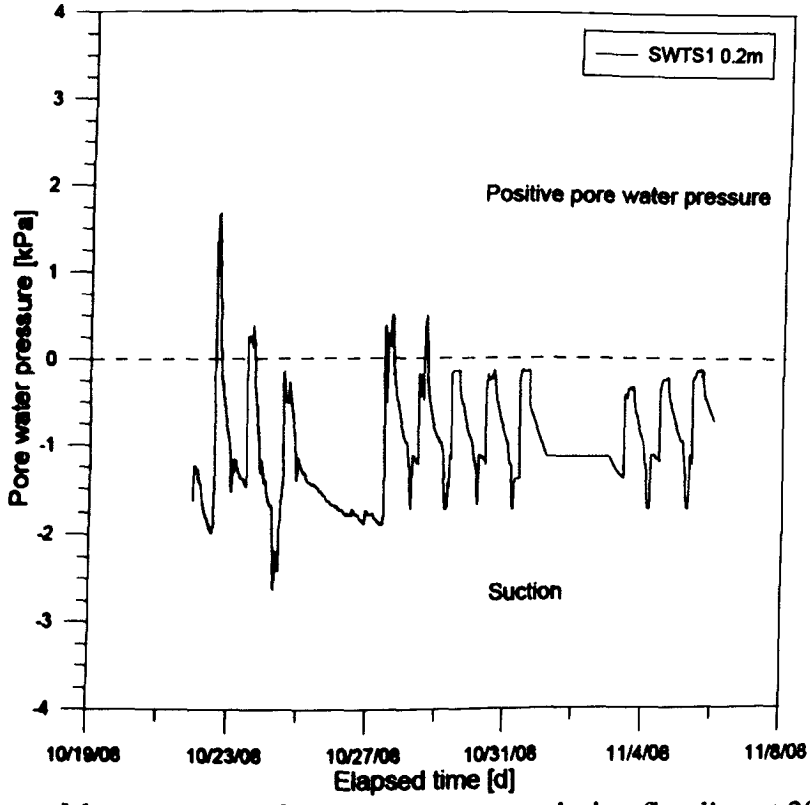

Figure 9.1 Measurements of pore water pressure during flooding at 20 cm depth.

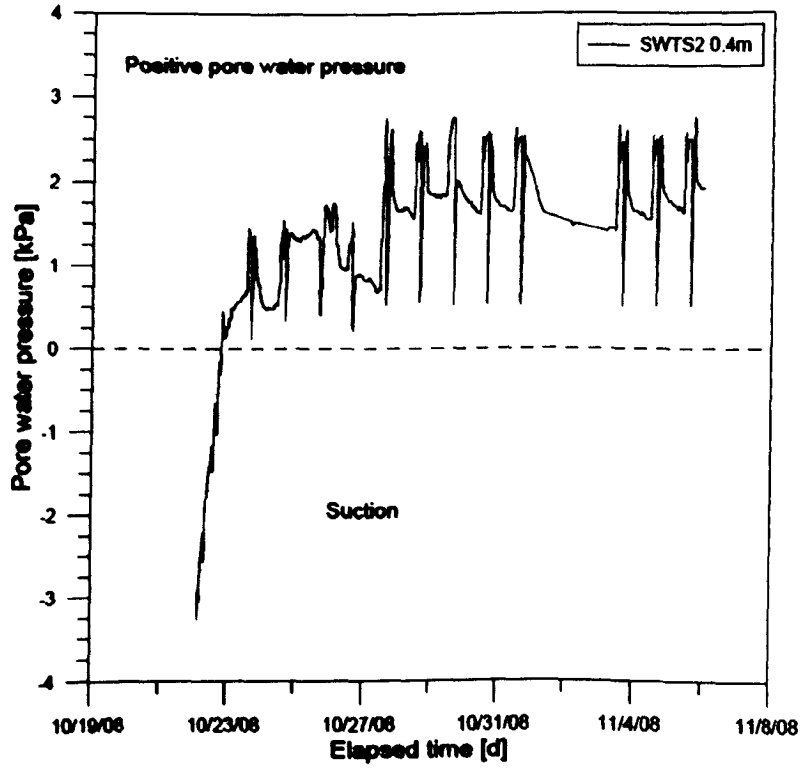

Figure 9.2 Measurements of pore water pressure during flooding at 40 cm depth.

The reduction in mass permeability caused by fissuring was observed immediately as piping appeared soon at the bottom of the embankment when the flooding was at its highest level but not overtopping. The flow of water through the fissured soil in the laboratory didn't lead to slope instability but more as a superficial erosive process rather than a real breach initiation. There appeared to be no major disruptive forces and specifically differences in hydrostatic pressure across individual soil blocks that would have led to rapid failure because the hydraulic gradient through a heavily-fissured embankment has a relatively steady slope. There was heavy seepage and as such a significant loss of the water-retaining function of the flood embankment.

It was observed that during flooding the flowing water progressively eroded the embankment to a depth where the clay was intact. Hence, the intact clay remained resilient to the water and still cohesive. A good example of comparative resistance of intact and fissured clay similar to this observed during model test is the embankment in Easington, East Yorkshire investigated by Marsland (1957). The laboratory study brought some more explanations about this failure mentioned in Chapter 1. It also, gives a light on what might have happened in 1957.

9.2. SOIL PROPERTIES

Another important issue which must be highlighted is the properties of the soil used in laboratory studies and classified as stiff clay with the undrained shear strength varying from 121 kN/m^2 to 152 kN/m^2 and dry density 1.948 Mg/m^3 (see Chapter 4). The results of the soil surveys along the Thames estuary in 1953 revealed the variable nature of marsh soils, peats, peaty clays and silty clays overlaying the sand and gravel stratum (Marsland, 1968). The measured dry density of the marsh clay that was used for construction was found to be 1.6 Mg/m^3 with the undrained shear strength varying between 9.57 kN/m^2 to 14.36 kN/m^2 (classified as very soft clay, BS5930:1990). This indicates the weakness of the soil that was subjected to the unexpected high flood in 1953 and it is the low shear strength which probably had a significant role in the type of embankment instability which occurred.

Marsh clays (soft clays) led to more catastrophic failures than the one observed during the laboratory test. Such failures were due to the poor geomechanical properties of the soil used for construction.

Soft soils are usually much more sensitive to reductions in shear strength when they are in contact with water. Especially these, affected by highly fissured upper layer deteriorated structures, (Cooling and Marsland, 1958), are more liable to any changes in moisture content and pore water pressures. As a consequence, their strength is reduced to the minimum.

Stiff clays, such as "Boulder clay" as used in this study appear to be more resilient to erosion as a result of overtopping, primarily due to their undrained shear strength which is significantly higher than that of soft clays.

The soil properties analysis such as plasticity index and linear shrinkage can give some indications about the extent of cracking which can occur in clayey embankments as the cracking is directly linked with the shrinkage of the soil. However, this cannot be considered as determinant for the embankments assessment as the cracking is also dependent on factors that are not directly linked to soil properties (weather conditions, size of the structure, water regime and type of vegetation).

9.3. DETERMINATION OF SOIL WATER CHARACTERISTIC CURVE

Although, three different methods were used to determine SWCC for the soil used, a good match between all of them can be noticed. Moreover, the valuable results were obtained from the measurements that were based on relatively small clay samples (different sizes of samples were used for each method, see Chapter 2). The comparison between water retention curves obtained from the laboratory tests and embankment model is presented in Figure 9.3.

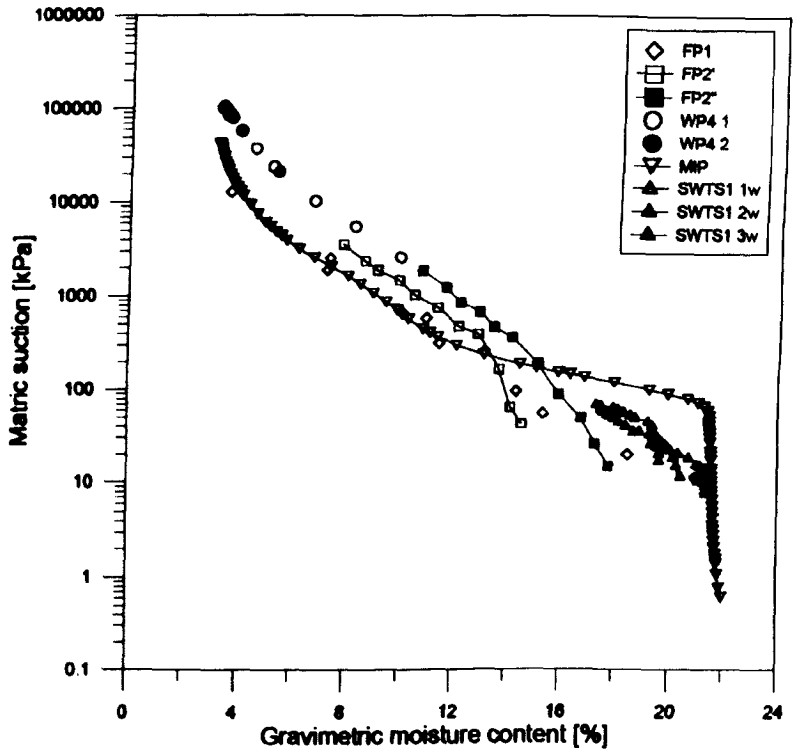

Figure 9.3 SWCC's for all tests.

It can be clearly seen on the Figure, that the relationship between soil suction and moisture content measured by sensors on the scaled embankment model matches exactly the same desorption curve prior to soil drying. It is rare that four techniques (filter paper, MIP, WP4 and tensiometer) involving three different measuring and deterministic methods (indirect, deterministic and direct) will provide such interesting results. Moreover, due to the lack of such observation in the literature, it makes it even more unique and valuable.

The water-retention curves obtained from different tests were also compared with the existing constitutive models describing the Soil Water Characteristic Curve. A van Genuchten model (van Genuchten, 1980) and two recently developed models: modified van Genuchten model proposed by Zhou and Yu (2005) and modified Fredlund and Xing model proposed by Fredlund and Xing (1994) were used in order to find the best water-retention distribution for the results obtained in this study (see Figure 9.4).

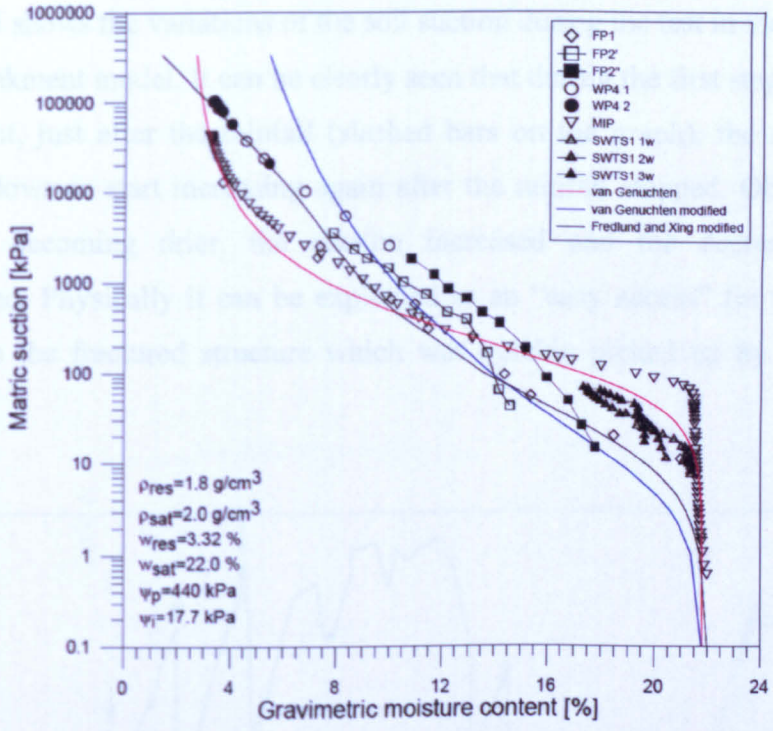

Figure 9.4 Experimental results compared with constitutive models.

9.4. MONITORING AND MEASURING THE EXTENT OF FINE FISSURING

The monitoring and measuring of the extent of fine fissuring in the field using visual inspection is the first step in identifying the degree of cracking. This must be carefully done and the difference between superficial and internal fissuring has to be recognised. The attention is required during the assessment as some cracks can be due to the localised settlement of the embankment or shallow slip of the slope. Hence, a tension crack creates which is usually longitudinal in its nature.

9.5. MONITORING AND MEASURING THE DEPTH OF CRACKING USING SUCTION AND MOISTURE CONTENT PROBES

The direct measurement of soil suction gives an indication about the depth of the cracking. This happens when the cracking front reaches the level of installed sensor. The "live suction" is closely linked with the extent of the cracking within the zone where the cracks are present. The fast changes and fluctuations in suction readings due to rainfall can indicate the degree of cracking, but only within the localised zone.

Figure 9.5 shows the variations of the soil suction during the test in the upper layer of the embankment model. It can be clearly seen that during the first stage of the drying experiment, just after the rainfall (slashed bars on the graph), the suction sharply dropped down to start increasing again after the rainfall stopped. Obviously, as the soil was becoming drier, the suction increased and the decrease was more accentuated. Physically it can be explained as an "easy access" for the percolating water into the fractured structure which was quickly picked up by the measuring sensor.

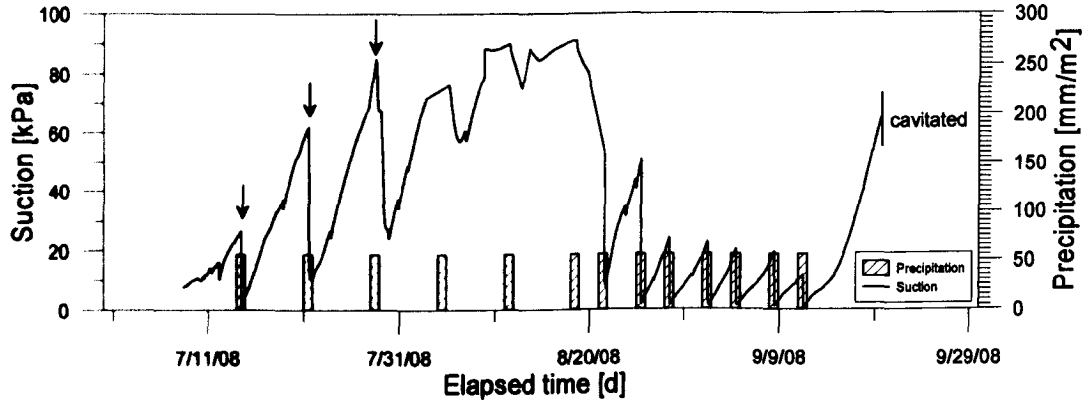

Figure 9.5 Suction variations at 20 cm.

For the sensor installed at 40 cm depth shown on Figure 9.6 it can be seen that this sharpen decrease in suction started appearing after four weeks. This means that the progressive vertical cracking has reached this depth and allowed the water to percolate deeper and spread around.

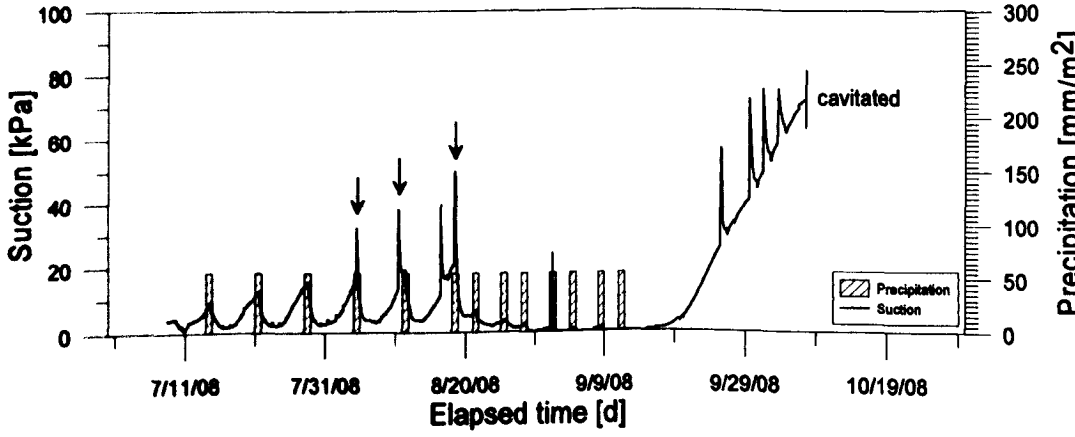

Figure 9.6 Suction variations at 40 cm.

Investigation of the soil suction profiles (Figure 9.7) recorded before and after the rainfall revealed a good agreement with the interpretation given by Jennings (1961). A depth of cracking can be simply estimated from the soil suction profiles measured before and after the rainfall (see Figure 9.8).

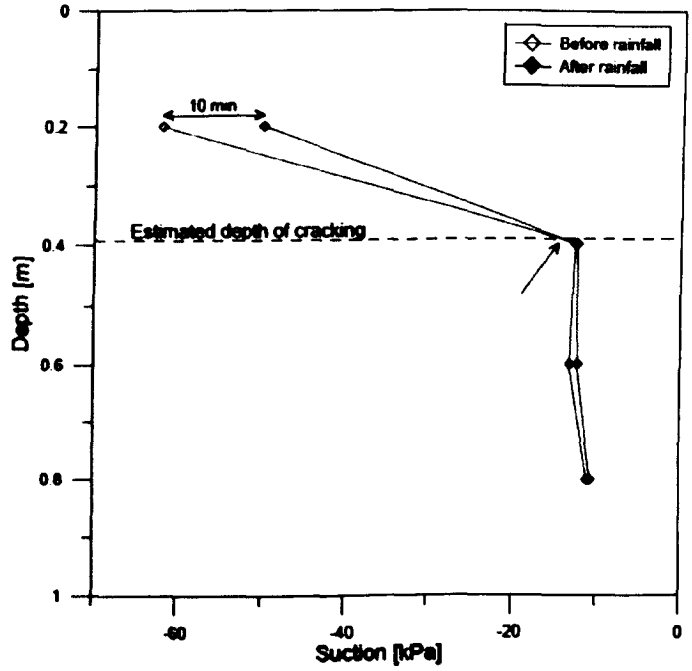

Figure 9.7 Soil suction profiles before and after the rainfall indicating depth of cracking.

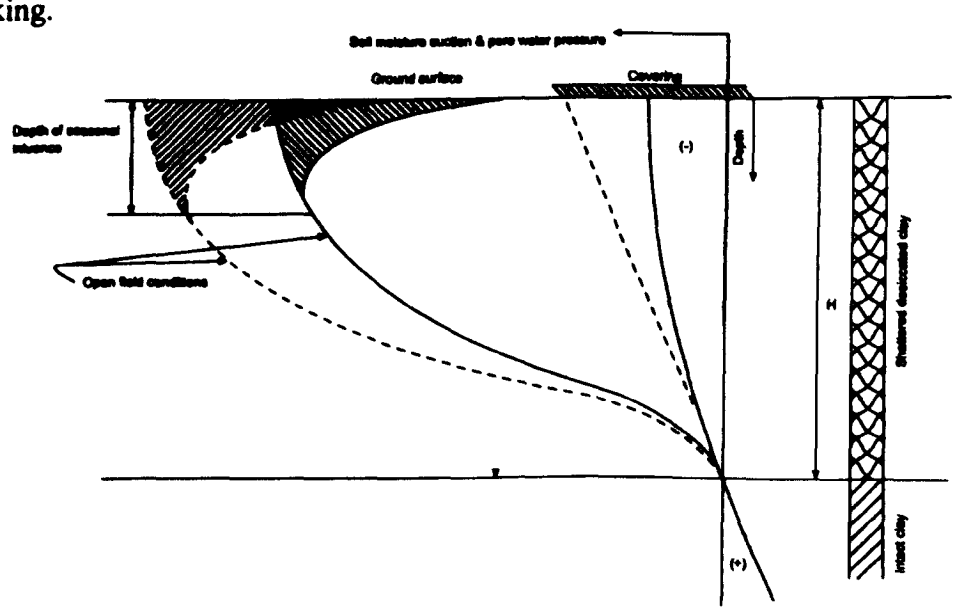

Figure 9.8 Soil suction in desiccated clay under seasonal variations (after Jennings, 1960).

It can be clearly seen on Figure 9.7 and Figure 9.8 that there is an evident point where the two suction profiles, before and after the rainfall, merge at the boundary between intact and desiccated clay.

The measurements of the moisture content are different to those of the suction presented above. Figure 9.9 shows the response of the upper sensor to the moisture changes due to the water entering the cracks, whereas the moisture content measured at lower depth remained stable (Figure 9.10).

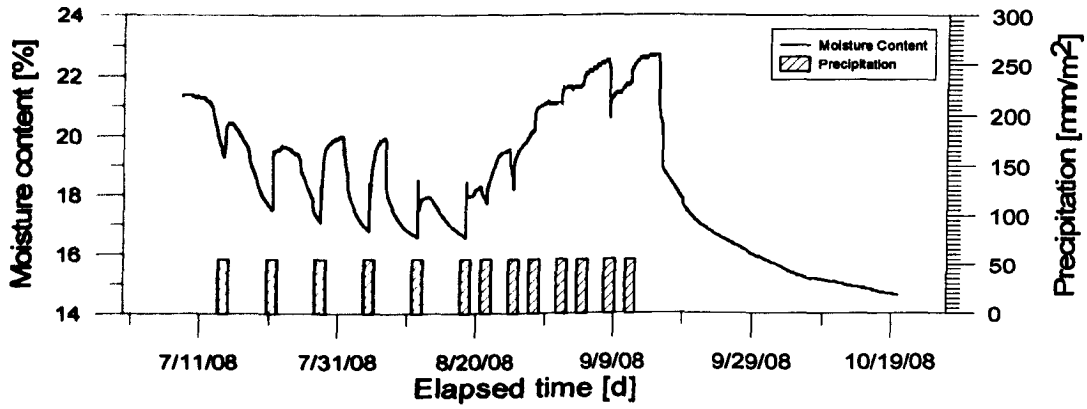

Figure 9.9 Moisture content variations at 20 cm.

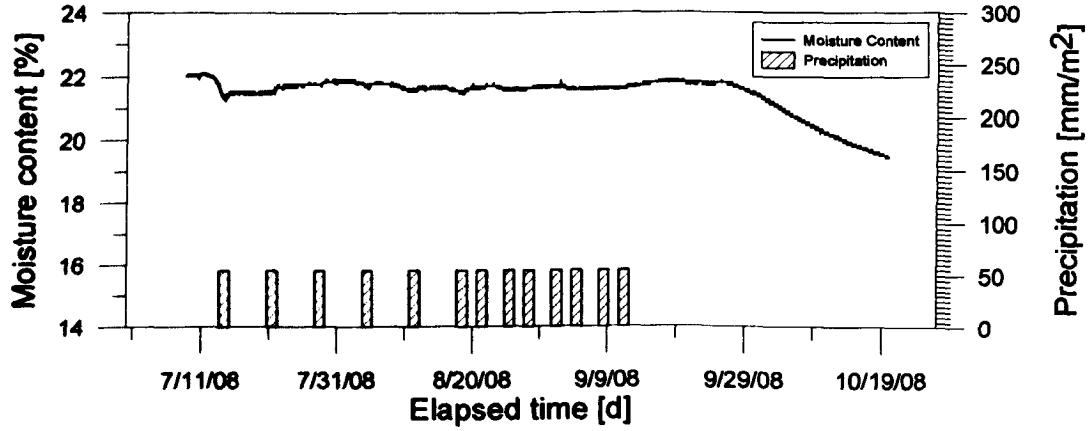

Figure 9.10 Moisture content variations at 40 cm.

It can be concluded from the results presented above that suction probes are more sensitive to the creation of fissured zones than moisture content probes. They seem to be reliable tools in desiccation cracking detection.

However, the suction measurements are constricted to the area where the soil is in contact with ceramic cup. This makes this method very limited, as a distributed system will be needed for a long term monitoring.

9.6. EMBANKMENTS INSPECTIONS

In many cases, cracking of the embankments is neglected by the engineers. It is difficult to assess embankments when the vegetation is abundant. Also some other potential and dangerous symptoms of embankments instability are ignored i.e.: tension cracking along the slope due to the settlement.

Adequate Environment Agency departments should pay more attention to the training of the specialists who are responsible for the condition assessment and somehow for human lives. To conclude this point it is strongly recommended to run high quality and intensive training course, where experienced engineers will give an overview about different conditions of soil structures. The Magnetic Conductivity survey and Resistivity arrays survey for a more detailed assessment can be a useful tool in terms of cracking and anomalies detection along the structure of the embankment.

9.7. CHARACTERISTICS OF DESICCATION CRACKING

Based on the results presented in this research the following comments can be made about development and depth of desiccation fissuring for flood embankments constructed from medium or highly plastic clayey fill material.

- Desiccation fissuring can occur after a relatively short period of time within 2 years of construction.
- If the embankment is constructed during hot summers and not protected against drying, fissuring can occur after few hours during construction.
- Desiccation fissuring is more likely to occur in areas of poor grass cover but not exclusively.
- Desiccation fissuring typically extends to a depth of 60 cm below the surface (crest or side slopes) but can penetrate to a depth of 100 cm.
- Desiccation fissures generally propagate perpendicular from the drying surface (crest surface or side slopes) and can bifurcate into lateral fissuring at a depth of 30 cm that can result in an orthogonal network of desiccation fissures. The orthogonal network of fissures would allow lateral internal

seepage beneath the surface of the embankment, which according to infiltrometer tests data results in a permeability similar to coarse sand or gravel.

- It should be pointed out that the desiccation cracks observed in the embankment model were wider and coarser than those previously observed at or near the surface of flood embankments (Dyer et al., 2009) with the exception of two major cracks observed in 2006 during studies at Thorngumbald. Although, the embankment is affected by wide and coarse cracks a tiny superficial cracking can be still present (see Figure 9.11).
- Even so the model test provided a valuable insight into the onset and development of desiccation cracks for an embankment, which could be used in future to inform researchers for larger scale embankment studies such as those carried out in the USA (via HR Wallingford).
- Observations made during model tests have shown that desiccation cracking started appearing after 4 hours of drying at a relatively low suction (around 5 kPa). Even, after one week of drying, when the embankment was extensionally cracked, the suction was oscillating around 10 kPa.

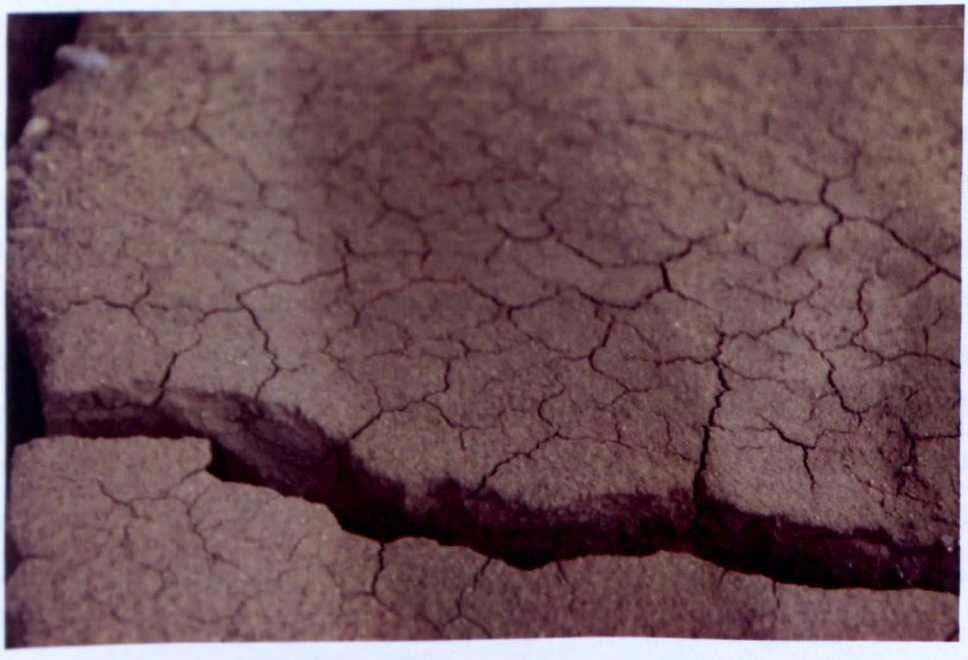

Figure 9.11 Superficial cracking observed on the crest.

Field and laboratory results indicate that desiccation fissuring can take place within a relatively short period of time after construction for medium or highly plastic clay fills. The resulting desiccation fissuring can typically extend to a depth of 60 cm. However the crucial factor is the onset of an orthogonal pattern of fissures that allows lateral seepage of flood water. This has been observed to take place within a depth of 30 cm. The relatively homogeneous fill material is then transformed into a rubblised layer of desiccated blocks of clay. Double ring infiltrometer tests show that the mass permeability of the desiccated fill material can increase to the level of a coarse sand or gravel.

9.8. USE OF GEOPHYSICS IN CRACKING DETECTION

This experimental study has shown that a miniature geo-electrical method using resistivity arrays can be used as non-invasive method for the detection of desiccation cracks. All the major vertical cracks, which have been visually observed at the surface of the clay model, have been recorded by the resistivity equipment and displayed using the 2 dimensional contour model. Despite the limitations of the method explained before, the vertical cracking network detected by the miniature resistivity arrays has been identified and validated by visual observations.

Assumptions were made about the detection of horizontal cracks that could be hampered by the insulating property of air related to crack continuity. It is also very important to remember that electrical resistivity images are the outcome of data processing (i.e. they are based on apparent resistivity values) and for this reason they must not be interpreted as a direct representation of the field situation, but rather as a guide for qualitative estimation of the electrical resistivity distribution in the soil model. The limitation of the method was the geometry of the electrodes and boundary effects that will be necessary to investigate further to fully map the structure of the cracks also along the horizontal pattern in the future experiments on the embankment in Thorngumbald.

CHAPTER 10

10. REMEDIAL MEASURES

10.1. INTRODUCTION

The characterisation of the nature of desiccation fissuring and the associated failure mechanism is very well known since the research carried out by Marsland (1961) and Marsland (1968). Apart from this characterisation, another important issue to address is to identify potential remedial solutions or best practice to minimise the extent of fissuring. So far, this issue has not been addressed in the scientific literature. Thus, the insight gained during this study into the desiccation fissuring provides some guidance to the potential solutions.

10.2. PROPOSED REMEDIAL MEASURES

To limit, prevent and cure fissuring, revised remedial solutions were elaborated, and are listed below:

- Injections of polymers – once the cracking of the embankment is identified, it is considered to inject the polymers (i.e. this supplied by URETEC) inside embankment body, to decrease the permeability of the structure, prevent any further cracking and to increase the strength of the structure. However, only "soft" injection has to be considered in case of the potential destruction of the construction during injection. It is proposed to use the polymers which can penetrate inside embankment body, spread inside cracking network and expand to fill in the small and the big gaps.

- Spraying of the lime/cement suspension or gels on the embankment surface – the purpose is the same as above. It is just a different technique which may be use for curing the embankment cracking.

- Rubblised layer mixing with polymers, lime or cement – when the depth of the cracking is not bigger than available for mixing heavy machines, it can be considered to mix the upper layer with the polymers, lime or cement to decrease permeability of the cracked layer.

- Berm – the construction of a berm on the landward side of an embankment is only an effective measure if the slip circle is contained within the embankment or extends only a shallow distance below the embankment. The construction of a berm may significantly reduce the risk of failures associated with water filled wide fissures. The design of a berm should be carried out by an experienced geotechnical engineer. The height of a berm can be 40 % to 50% of the embankment height.

- Replacement with clay or clayey silt – this method is based on the removing of deteriorated layer and replacing it with the clay or clayey silt. It is suggested to remove the top soil along with fissured clay to a minimum 50 cm below the top of the intact clay. During dry seasons, the exposed soil must be covered by waterproof sheet in order to protect it against drying. Material with the proper consistency can be then placed and compacted in layers. At least 60 cm of top soil is required on the top of the restored structure. The top soil has to be placed as soon as the compaction works are finished. The best would be to carry out these works in 10 m sections.

- Replacement with Hoggin – the procedure consists of removing all the top soil from the fissured area, then digging out the fissured zone of the embankment, extending the excavation work to a minimum of 20-30 cm below the zone. Then the removed material is replaced by hoggin. In order to place and compact the hoggin, it is suggested to follow the Specifications for Highway Works. The removed fissured material can be used to form a berm on the landward face.

- Granular crest – if a granular material is poured into the clay, this reduces the plasticity of the clay and therefore its tendency to fissure. The treatment consists of rolling and harrowing a thick layer of graded granular material into the crest of the embankment. Layers are added until a dense granular surface is produced. Clay below the treated layer will still be subject to fissuring, but there will be little or no wide fissures at the surface.

- Geotextiles and Geogrids – fissuring occurs when the negative water pressure induced by desiccation exceeds the strength of the material. Under normal circumstances the negative porewater pressure will not exceed the strength of a geotextile or geogrid since the selected geotextile or geogrid depends on the system adopted and on the dimensions of the embankment. Wide fissures are not able to transfer across the geotextile or geogrid and their extent is therefore limited. On the contrary, fine fissures are unaffected by the presence of a geotextile or geogrid and are likely to occur to the same extent.

Before considering one of the proposed remedial solutions, the best available technique for cracking detection must be considered in order to localise the extent of fissuring. From the experience, gained during this project, the best technique is non-invasive geophysical scanning which is able to give very quick view of the embankment body and localize the extent and the depth of the cracking.

CHAPTER 11

11. CONCLUSIONS

The aim of the study was to examine the effects of fine fissuring of clay fills on the geotechncial stability and breach initiation for flood defence embankments. This was one of the key factors identified by Cooling and Marsland (1953) as causing embankment failure in the 1953 North Sea Floods that inundated vast tracts of land in Essex and Kent with loss of life.

In particular, it aimed to investigate how the desiccation and fissuring of clay embankments affects the long-term performance by:

- monitoring and measuring the extent of fine fisusring in the field using visual inspection, analysis of soil properties such as plasticity/shrinkage and Soil Water Retention Curve,
- monitoring of the extent of fine fissuring on the examined embankment model using visual observation,
- measuring changes in moisture content and suction profiles during: dry, wet and extremely dry conditions,
- investigating the state of desiccation through the Soil Water Characteristic Curve and comparing the results obtained from four different measuring and empirical methods,
- investigating a non-invasive geophysical method for cracking initiation and detection,
- investigating the use of soil instrumentation to detect the extent of desiccation fissuring,
- monitoring the behaviour of fissured embankment model under flooding conditions using visual observation and geophysics,

- measuring the reduction in mass permeability caused by fissuring and further investigate the flow of water through fissured soil in the laboroatry that could lead to slope instability and breach initiation.

The fulfilment of each of these aims related to the experimental results and findings is explained in the following sections.

11.1. DEPTH AND PATTERN OF DESICCATION FISSURING IN THE FIELD

The results from field investigations confirm that desiccation fissuring occurs to a depth of typically 60 cm within the outer surface of a flood embankment constructed from clay fill and can occur within 2 years of construction. In some cases desiccation cracking can effectively penetrate the structure to a depth of more than 1.0 m. The critical condition occurs when desiccation creates an interconnected network of sub-vertical and sub-horizontal fissures that increases the mass permeability of the fill material to that of coarse sand or gravel and hence allows rapid seepage of flood water through the surface layer of the embankment (crest and side slopes).

11.2. ASSESSMENT OF DESICCATION OF CLAY FROM LABORATORY TESTS

The small scale desiccation tests carried out using three different methods showed very good agreement with the soil water characteristic curve obtained from embankment model. This suggests that for this soil the effects of sample geometry on the Soil Water Characteristic Curve are not significant. Thus, it is possible to assess the possibility of desiccation occurring in an embankment by using small scale tests which allow the determination of the Soil Water Characteristic Curve.

11.3. MEASURING THE EXTENT OF DESICCATION CRACKING

Laboratory results confirm that desiccation fissuring can transform homogenous material into interconnected network of cracks. This can occur to a depth of typically 40-60 cm within the outer surface of a flood embankment and can be initiated within relatively short period after construction. This is directly dependent on the

geotechnical properties of the soil, weather conditions and water regime inside and around the structure. It has been proved during laboratory studies that horizontal cracking forms horizontal discontinuities which are perpendicular to the embankment shape. The embankment model that has been tested in the laboratory was not covered by the grass and the nature of cracking can be different when there is the top soil and vegetation. In the soft clays cracking process can occur faster, as the soft soil is prone to loose its strength and retaining water, whereas the stiff clays will still remain intact.

Tensiometers were found to be a useful tool in monitoring of desiccation fissuring, as they were sensitive to the creation of fissured zone. Although, the measurements were localised around the sensor cup (pointwise measurements), they seemed to be reliable tools in desiccation cracking detection. For this reason, an extended network of sensors to cover the embankment will be needed.

As a proof of concept, the laboratory model data obtained in this study must now be used with a geotechnical stability model taking into account the 3 zones of different suction profiles and a head of water corresponding to the height of the embankment.

11.4. GEOPHYSICAL MEASUREMENTS OF THE EXTENT OF DESICCATION FISSURING

The potential benefits provided by restivity surveys needs to be fully acknowledged. It proved to be a useful tool for detecting the presence of cracks and the extent of cracking below the surface. This merits further research in the field. An ICE R&D and Scottish Executive Enabling Fund project is already underway.

11.5. FAILURE MECHANISM OF THE EMBANKMENT MODEL

The failure mechanism was different from that observed by Cooling and Marsland (1954). The soil used in the model test was much more strengthened than the one investigated by Cooling and Marsland (1958), and later proposed by Dyer et al., (2009). This led to the resistance of the clay blocks, which were still in contact with the intact clay.

The evidence from the laboratory tests is that, because the hydraulic gradient through a heavily-fissured embankment has a relatively steady slope, there appeared to be no major disruptive forces (and specifically differences in hydrostatic pressure) across individual soil blocks that would have led to rapid failure. Obviously there was heavy seepage and as such a significant loss of the water-retaining function of the flood embankment. The hydro-dynamic forces need to be better understood and need some further investigation.

In general some of the limitations of the test can be recognised (i.e.: larger desiccation cracking due to absence of vegetation, soil/concrete interface on the sides). Positive outcomes need to be highlighted (detection of cracks by restivity, accurate soil suction/moisture content profiles, almost unique observations of the breaching of desiccated clay embankment with numerous: –time, rate, physical features, etc). In future other researchers can make use of these results to model breach growth.

Even so the results clearly demonstrate that breaching of a flood embankment constructed from clay soil is controlled by the weakness in the embankment construction (such as highly permeable underlying strata) or deterioration (such as desiccation) and not the classical Bishop's slope failure. The classical slope instability is rarely recorded for clay flood embankments except during the construction phase when the underlying soil may be too weak to initially support the embankment (as it occurred for the new embankment at Thorngumbald). In the future, fault trees and corresponding fragility curves need to focus on potential weakness that could lead to breach initiation and avoid the misconception that classical slope failure is a primary failure mode during a flood event.

These findings as part of the ongoing research into flood embankments since the mid 1990's should also feed into an improved asset condition survey methodology. Flood engineers should survey with a geotechnical and geophysical check list (soil properties, suction and moisture sensing, resistivity/conductivity) and attribute

meaningful ratings that really indicate the contribution to a likely failure taking place, not only visually. This result alone justifies the research project.

CHAPTER 12

12. RECOMMENDATIONS FOR FUTURE STUDIES

The following recommendations are proposed for future study in order to investigate new "Detection tracers" in the form of gels to fill in the fine fissuring network of flood defense embankments and monitor their location. Four different detection Geophysical techniques used will govern the choice of the tracer fluid properties. Ultimately, these tracers associated with a proper subsurface detection technique and thermographic sensing could be used for general maintenance strategies for earth dams as the fissuring network that can appear during the desiccation process can lead to deep erosion inside the structure and partial collapse. The innovative aspect of the proposed future work is either to turn a "repair grout" into a tracer or use a gel that could be finally detected by the scanning equipment and that must have a curing time to turn into a solid mould inside the cracks reducing the permeability of the embankment and improving its integrity.

The proposed future study can be divided into two main tasks:

- Task A: Laboratory studies
- Task B: Field investigation

The plan is to advance progressively in the development / implementation / verification / validation / application of the different features of proposed grouts, tracers and geophysical techniques accounting for increasing their suitability and widespread applications. The final goal is to have a new improved scanning technique that can be used for different approaches related to desiccation cracking of the soil structures.

12.1. TASK A: LABORATORY STUDIES

This task relates to the investigation of tracers and grouts that will be used to improve the scanning of desiccation cracked soils. In particular it will investigate the properties (viscosity, conductivity) of available tracers and grouts (KELLER). This

part of work will have a close link with the undertaken research that was carried out in this direction at Strathclyde University. Furthermore, the construction of clay models such as one presented by Sentenac and Zielinski (2009) should be considered. The clay models will be subjected to extreme drying conditions in order to create naturally formed crack patterns. In addition, the tracers and grouts that have been previously tested will be injected into the separate clay models. The miniature resistivity and thermography will be used in order to detect expected improvement.

12.2. TASK B: FIELD STUDIES

Laboratory findings need to be validated on the naturally cracked existing embankment, thus it is proposed to undertake a similar work at the flood embankment in Thorngumbald (Paull Holme Strays near Humber Estuary, Kingston upon Hull), that was previously investigated (Dyer et al., 2007) and indicated as a highly fissured embankment.

In parallel, the aim will be to investigate the correlation between the geophysical measurements and the measurements of soil suction and moisture content at Thorngumbald embankment. This will be done by direct measurements of the soil suction (tensiometers) and moisture content (TDR's) at different depths of the embankment. At the same time, geophysical measurements will be taken at the location of installed sensors.

CHAPTER 13

13. REFERENCES

ASTM Standard D4404 – 84, 2004 (2004), Standard test method for determination of pore volume and pore volume distribution of soil and rock by mercury intrusion porosimetry. Tech. rep., ASTM International, West Conshohocken, PA 2004, DOI: 10.1520/D4404-84R04

Abu-Hassanein, Z., Benson, C., Blotz, L., (1996), Electrical resistivity of compacted clays. Journal of Geotechnical Engineering., 122 (5), pp. 397-406.

Ahmed, S., Lovell, C., Diamond, S., (1974), Pore sizes and strength of compacted clay. Geotechnical Engineering Division., 100 (4), pp. 407-425.

Aitchison, G., (1965), Moisture equilibria and moisture changes in soils beneath covered areas. A symposium in print. Editor, Aitchison, G.D., Australia, Butterworths.

Aitchison, G. D., Richards, B. G., (1969), The fundamental mechanics involved in heave and soil moisture movement and the engineering properties of soils which are important in such movement. In: Second International Research and Engineering Conference on Expansive Clay Soils, Texas A & M Press.

Akroyd, T., (1964), Laboratory testing in soil engineering. Soil Mechanics Ltd.

Aubeny, C., Lytton, R., (2004), Shallow slides in compacted high plasticity clay slopes. Journal of geotechnical and geoenvironmental engineering., 130 (7), pp. 717-727.

Aung, K., Rahardjo, H., Leong, E., Toll, D., (2001) Relationship between porosimetry measurement and soil-water characteristic curve for unsaturated residual soil. Geotechnical and Geological Engineering., 19, pp. 401-416.

Barker, R., (1997), Electrical imaging and its application in engineering applications. Modern physics in Engineering Geology. Geological Society Engineering. Special Publication., 12, pp. 37-43.

Benson, C., Gunter, J., Boutwell, G., Trautwein, S., Berzanskis, P., (1997), Comparison of four methods to assess hydraulic conductivity. Journal of Geotechnical and Geo-Environmental Engineering, 123 (10), pp. 929-937.

Bear, J., (1972), Dynamics of fluids in porous media., American Elsevier, Environmental Science Series.

Benson, C., Zhai, H., Wang, X., (1994), Estimating hydraulic conductivity of compacted clay liners. Journal of Geotechnical Engineering., 120 (2), pp. 366-387.

Bishop, A., (1959), The principle of effective stress. Teknisk Ukeblad I Samarbeide Med Teknikk, 106 (39), pp. 859-863.

Bishop, A., (1960), The measurement of pore pressures in the triaxial test. Pore Pressure and Suction in Soils. Conference organized by the British National Society of the International Society of Soil Mechanics and Foundation Engineering at the Institution of Civil Engineers held on March 30th and 31st, 1960.

Black, W. P. M., Croney, D., (1958), Field studies of the movement of soil moisture. Road research technical report no. 41., Department of Scientifc and Industrial Research. Road Research Laboratory.

Bodman, G. B., Coleman, E.A., (1943), Moisture and energy conditions during downward entry of water into soils., Soil Science Society American Proceedings, 8, pp. 116-122.

BS1377-2:1990, British Standards. Methods of test for: Soils for civil engineering purposes - part 2: Classification tests.

BS5930:1999, British Standards. Code of practice for site investigations.

BS8004:1986, British Standards. Code of practice for foundations.

Bulut, R., Lytton, R., Wray, W., (2001), Soil suction measurements by filter paper. Proceedings of Geo-Institute Shallow Foundation and Soil Properties Committee Sessions at the ASCE 2001 Civil Engineering Conference., 1, pp. 243-261.

Cameron, D., Walsh, P., (1984), Damage to buildings on clay soils. Technical report. Australian Council of National Trusts, Melbourne.

Cardoso, R., Romero, E., Lima, A., Ferrari, A., (2007), A comparative study of soil suction measurement using two diferent high-range psychrometers. Springer Proceedings in Physics. Experimental Unsaturated Soil Mechanics., 112, pp. 79-93.

Chandler, R., Crilly, M., Montgomery-Smith, G., (1995), A low-cost method of assessing clay desiccation for low-rise buildings. discussion. Proceedings of the Institution of Civil Engineers. August., 108, pp. 135-136.

Chandler, R., Gutierrez, C., (1986), The flter-paper method for suction measurement. Géotechnique, 36 (2), pp. 265-268.

Coleman, J., (1962) Stress/strain relations for partially saturated soil. Géotechnique, 12 (4), pp. 348-356.

Cooling, L., Marsland, A., (1954), Soil mechanics of failures in the sea defence banks of Essex and Kent. ICE Conference on the North Sea Floods of 31 January / 1 February 1953.

Crilly, M., Chandler, R., (1993), A method for determining the state of desiccation in clay soils. Tech. rep., Building Research Establishment.

Croney, D., Coleman, J., (1960), Pore pressure and suction in soil. Pore pressure and suction in soils. Conference organized by the British National Society of the International Society of Soil Mechanics and Foundation Engineering at the Institution of Civil Engineers held on March 30th and 31st, 1960.

Cui, Y., Tang, A., Mantho, A., De Laure, E., (2008), Monitoring field soil suction using miniature tensiometer. Geotechnical Testing Journal., 31 (1), pp. 95-100.

Croney, D., Coleman, J.D., Black, W.P, (1958), Movement and distribution of water in soil in relation to highway design and performance. Highway Research Board special report., Issue: 40, pp. 226-252.

Dane, J., Topp, G., (2002), Methods of soil analysis. Part 4. Technical Report, Soil Science Society of America, Madison, Wisconsin.

Daniel, D., (1989) In-situ hydraulic conductivity test for compacted clay. Journal of Geotechnical Engineering., 115 (9), pp. 1205-1226.

Delage, P., Lefebvre, G., (1984), Study on the structure of a sensitive Champlain clay and of its evolution during consolidation. Canadian Geotechnical Journal., 21, pp. 21-35.

Delage, P., Pellerin, M., (1984), Influence de la lyophilisation sur la structure d'une argile sensible du quebec. Clay mineralogy., 19, pp. 151-160.

Delage, P., Romero, E., Tarantino, A., (2008), Recent developments in the techniques of controlling and measuring suction in unsaturated soils. Proceedings

of the first European Conference on Unsaturated Soils, E-UNSAT 2008, Durham, UK 1, pp. 33-52.

Delta-T Devices, User Manual for ThetaProbe. Soil moisture sensor. Type ML2x.

Delta-T Devices, User Manual for the RH and Air Temperature sensors. Types RHT2nl and AT2.

Depountis, N., H. C., Davies, M., (1999), The application of miniaturised electrical imaging in scaled centrifuge modelling of pollution plume migration. Proceedings 2nd BGS International Geoenvironmental Engineering Conference., 1, pp. 214-221.

Diamond, S., (1970), Pore size distribution in clays. Clay mineralogy., 18, pp. 7-23.

Driscoll, R., (1983), The influence of vegetation on the swelling and shrinking of clay soils in Britain. Géotechnique., 33 (6), pp. 93-105.

Durner, W., Or, D., (2005), Soil water potential measurement., Encyclopedia of Hydrological Sciences. Edited by M.G. Anderson. John Wiley & Sons, Ltd.

Dyer, M., (2004), Performance of food embankments in England and Wales. Proceedings of the institution of Civil Engineers. Water Management. December 2004, Issue WM4, pp. 177-186.

Dyer, M., (2005), Further tests on the fissuring of clay fill at the Thorngumbald flood embankment. In: Proceedings International symposium on advanced experimental unsaturated soil mechanics, Trento, Italy.

Dyer, M., Utili, S., Zielinski, M., (2009), Field survey of desiccation fissuring of food embankments. Proceedings of the Institution of Civil Engineers. Water Management. June 2009, Issue WM3, pp. 221-232.

Dyer, M., Utili, S., Zielinski, M., (2007), Influence of the desiccation fine fissuring on the stability of food embankments. UFMO UR11., FRMRC Research Report.

Eigenbrod, K., (2003), Self-healing in fractured fine-grained soils. Canadian Geotechnical Journal., 40 (2), pp. 435-449.

ELE (2006) H-60 Field Inspection Vane Tester. Operating Instructions.

Fredlund, D., (1964), Comparison of soil suction and one-dimensional consolidation characteristics of a highly plastic clay, National Research Council Technical Report No.245, Division of Building Reserach, Ottawa, Canada, pp. 26.

Fredlund, D., Morgenstern, N., (1977), Stress state variables for unsaturated soils. Journal of Geotechnical Engineering Division., 103, pp. 447-466.

Fredlund, D., Rahardjo, H., (1993), Soil mechanics for unsaturated soils. John Wiley & Sons Inc., New York.

Fredlund, D., Xing, A., (1994), Equations for the soil-water characteristic curve. Canadian Geotechnical Journal., 31, pp. 521-532.

Fredlund, G., (2006), Unsaturated soil mechanics in engineering practice. Journal of Geotechnical and Geoenvironmental Engineering., 132 (3), pp. 286-321.

Gardner, W.R., (1937), A method of measuring the capillary tension of soil moisture over a wide moisture range. Soil Science Society of America Journal., 43 (4), pp. 277-283.

Gardner,W.R., (1956), Calculation of capillary conductivity from pressure plate out-flow data. Soil Science Society of America Proceedings., 20, pp. 317-320.

Ghosh, R., (1980), Estimation of soil-moisture characteristics from mechanical properties of soils. Soil Science Journal., 130 (2), pp. 60-63.

Glendinning, S., Hall, J., Manning, L., (2009), Asset-management strategies for infrastructure embankments. Proceedings of the ICE – Engineering Sustainability, 162 (2), pp. 111 – 120.

Godio, A., Bottino, G., (2001), Electrical and electromagnetic investigation for landslide characterisation. Physics and Chemistry of the Earth., 26 (9), pp. 705-710.

Gourley, C., Schreiner, H., (1995), Field measurements of soil suction. First International Conference on Unsaturated Soils, UNSAT '95, Paris, 6-8 September.

Grifths, D., Barker, R., (1993), Two-dimensional resistivity imaging and modelling in areas of complex geology. Journal of Applied Geophysics., 29 (3-4), pp. 211-226.

Grifths, D., Barker, R., (1994), Electrical imaging in archeology. Journal of Archeological Science., 21, pp. 153-158.

Grifths, F., Joshi, R., (1989), Change in pore size distribution due to consolidation of clays. Géotechnique., 39 (1), pp. 159-167.

Guan, Y., (1996), The measurement of soil suction. Ph.D. thesis, University of Saskatchewan. Saskatoon. Canada.

Guan, Y., Fredlund, D., (1997), Direct measurement of high soil suction. Proceedings, 3rd Brazilian Symposium on Unsaturated Soils, NSAT'97, Rio de Janeiro, Brazil 2, pp. 543-550.

Gupta, S., Larson, W., (1979), Estimating soil-water retention characteristics from particle size distribution, organic matter percent, and bulk density. Water Resources Research Journal., 15 (6), pp. 1633-1635.

Harrison, B., Blight, G., (2000), A comparison of in-situ soil suction measurements in unsaturated soils for Asia. Proceedings of the Asian Conference on Unsaturated Soils. Singapore., 1, pp. 281-285.

Highway Agency, (2006) Specification for highway works. earthworks. series 600. Technical Report, Highways Agency.

Hird, C.C. Marsland, S. S. A., (1978), The development of centrifuge models to study the influence of uplift pressures on stability of a food bank. Géotechnique., 28 (1), pp. 85-106.

HR Wallingford, (2004), Reducing the risk of embankment failure under extreme conditions. Report 1: Good practice review. DEFRA/EA Report, Environment Agency, Bristol.

Hudacsek, P., Bransby, M., (2008), Centrifuge modelling of embankments subject to seasonal moisture changes. 1st ISSMGE International Conference on Transportation Geotechnics, Nottingham, UK, September 2008.

Jennings, J., (1960) A revised effective stress law for use in the prediction of the behaviour of unsaturated soils. Pore Pressures and Suction in Soils. Conference organized by the British National Society of the International Society of Soil Mechanics and Foundation Engineering at the Institution of Civil Engineers held on March 30th and 31st, 1960.

Jennings, J., J.B., B., (1962), Limitations to the use of effective stresses in partly saturated soils. Géotechnique., 12 (2), pp. 125-144.

Juang, C., Holtz, R., (1986a), Fabric, pore size distribution and permeability of sandy soils. Journal Geotechnical Engineering. 112 (9), pp. 855-868.

Juang, C., Holtz, R., (1986b), A probabilistic permeability model and pore size density function. International Journal of Numerical and Analytical Methods in Geomechanics., 10, 543f553.

Kawai, K., Karube, D., Kato, S., 2000. The Model of Water Retention Curve Considering Effects of Void Ratio. *In*: Rahardjo, H., Toll, D.G., Leong, E.C.(Eds.), Unsaturated Soils for Asia. Balkema, Rotterdam, p.329-334.

Kayyal, M., (1995), Effect of the moisture evaporative stages on the development of shrinkage cracks in soils. Unsaturated Soils. Sols Non Saturés.

Konrad, J., Ayad, R., (1997), Desiccation of a sensitive clay: field experimental observations. Canadian Geotechnical Journal., 34, pp. 929-942.

Lataste, J., Sirieix, C., Breysse, D., Frappa, M., (2003), Electrical resistivity measurement applied to cracking assessment on reinforced concrete structures in civil engineering. Independent Non-destructive Testing and Evaluation., 36, pp. 383-394.

Leong, E., Rahardjo, H., (1997), Review of soil-water characteristic curve equations. Journal of geotechnical and geoenvironmental engineering., 123 (12), pp. 1106-1117.

Leong, E., Tripathy, S., Rahardjo, H., (2003), Total suction measurement of unsaturated soils with a device using the chilled-mirror dew-point technique., Géotechnique., 53 (2), pp. 173-182.

Leong, E., Widiastuti, S., Lee, C., Rahardjo, H., (2007), Accuracy of suction measurement. Technical note., Géotechnique., 57 (6), pp. 547-556.

Lu, N., Likos, W., (2002), Filter paper technique for measuring total suction., Transportation Research Record: Journal of the Transportation Research Board. 1786/2002, pp. 120-128.

Lu, N., Likos, W., (2003), Filter paper column for measuring transient suction profiles in expansive clay., Transport Research Board 2003, Annual Meeting, CD-ROM.

Lu, N., Likos, W., (2004), Unsaturated soil mechanics. Wiley.

Marshall, T., (1958), A relationship between permeability and size distribution of pores. Journal of soil science., 9, pp. 1-8.

Marsland, A., (1957), The design and construction of earthen food banks. Journal Institution of Water Engineers., 11 (3), pp. 236-258.

Marsland, A., (1968), The shrinkage and fissuring of clay in food banks. Internal report no. 39/68. Building Research Station.

Marsland, A., Cooling, L., (1958), Tests on full scale clay food bank to study seepage and the effects of overtopping. internal report no. c562. Building Research Station.

Marsland, A., Randolph, M., (1978), A study of the variations and effects of pore water pressures in the pervious strata at Crayford Marshes. Géotechnique., 28 (4), pp. 435-464.

McCarter, W., (1984), The electrical resistivity characteristics of compacted clays. Géotechnique., 34, pp. 263-267.

McKeen, R., (1981), Suction studies: Filter paper method. Design of airport pavements for expansive soils. final report (no. dot/faa/rd-81/25). Tech. rep., U.S. Department of Transportation, Federal Aviation Administration, Systems Research and Development Service, Washington, DC.

McKeen, R., (1985), Validation of procedures for pavement design on expansive soils. Final report, U.S. Department of Transportation, Washington, DC.

Meilani, I., Rahardjo, H., Han, K., Leong, E., (2002), Mini suction probe for matric suction measurement. Canadian Geotechnical Journal., 39 (6), pp. 1427-1432.

Mitchell, J., (1962), Components of pore water pressure and their engineering significance. Clays and Clay Minerals: Proceedings of the Conference, Pergamon Press, Symposium Publications Division.

Mongiovi, L., Tarantino, A., (2003), Calibration of tensiometers for different measurement of matric suction. Géotechnique., 53 (1), pp. 137-141.

Morris, P., Graham, J., D.J., W., (1992), Cracking in drying soils. Canadian Geotechnical Journal., 29 (2), pp. 263-277.

Muraleetharan, K., Granger, K., (1999), The use of miniature pore pressure transducer in measuring matric suction in unsaturated soils. Geotechnical Testing Journal., 22 (3), pp. 226-234.

Navaneethan, T., Sivakumar, V., Wheeler, S., Doran, I., (2005), Assessment of suction measurements in saturated clays. Proceedings of the Institution of Civil Engineers. Geotechnical Engineering. January 2005, Issue GE 1, pp. 15-24.

Ng, C., Zhan, L., Bao, C., Fredlund, D., Gong, B., (2003), Performance of an unsaturated expansive soil slope subjected to artificial rainfall infiltration. Géotechnique., 53 (2), pp. 143-157.

Nguyen, F., Garambois, S., Jongmans, D., Pirard, E., Loke, M.H., (2005), Image processing of 2d resistivity data for imaging faults. Journal of Applied Geophysics., 57 (4), pp. 260-277.

Olayinka, A., Weller, A., (1997), The inversion of geoelectrical data for hydrogeological applications in crystalline basement areas of Nigeria. Journal of Applied Geophysics., 37, pp. 103-115.

Padfeld, C., Schofeld, A., (1983), Development of centrifugal models to study the influence of uplift pressures on stability of a food bank. Géotechnique., 33 (4), pp. 57-66.

Peck, R., (1969), Advantages and limitations of the observational method in applied soil mechanics. Géotechnique., 19 (2), pp. 171-187.

Penman, A., (1956), A field piezometer apparatus. Géotechnique., 6 (2), pp. 57-65.

Philip, J.R., (1969), Theory of infiltration. Advances in Hydroscience., 5, pp. 215-296.

Picarelli, L., Urciuoli, G., Mandolini, A., Ramondini, M., (2006), Softening and instability of natural slopes in highly fissured plastic clay shales. Natural Hazards and Earth System Sciences., 6, pp. 529-539.

Prapaharan, S., Altschaef, A., Dempsey, B., (1985), Moisture curve of compacted clay: mercury intrusion method. Journal of Geotechnical Engineering., 111 (9), pp. 1139-1142.

Ravina, I., (1983), The influence of vegetation on moisture and volume changes. Géotechnique., 33 (6), pp. 151-157.

Reginato, R., van Bavel, C., (1962), Pressure cell for soil cores. Soil Science Society of America Journal., 26, pp. 1-3.

Richards, L., (1941), A pressure membrane extraction apparatus for soil suction. Soil Science., 51 (5), pp. 377-386.

Richards, B., Peter, P., Emerson, W., (1983), The effects of vegetation on the swelling and shrinking of soils in Australia. Géotechnique., 33 (2), pp. 127-139.

Ridley, A., (1993), The measurement of soil moisture suction. Ph.D. thesis, Imperial College, London.

Ridley, A., Brady, K.C., Vaughan, P., (2003a), Field measurement of pore water pressures. TRL Report. Highways Agency.

Ridley, A., Burland, J., (1999), Use of the tensile strength of water for the direct measurement of high soil suction. discussion. Canadian Geotechnical Journal., 34, pp. 604-614.

Ridley, A., Dineen, K., Burland, J., Vaughan, P., (2003b), Soil matrix suction: some examples of its measurement and application in geotechnical engineering. Géotechnique., 53 (2), pp. 241-253.

Ridley, A., Marsland, F., Patel, A., (1998), Tensiometers: their design and use for civil engineering purposes. Proceedings 1st International Conference on Site Characterisation. Atlanta 2, pp. 851-856.

Ridley, A., McGinnity, B., Vaughan, P., (2004), Role of pore water pressures in embankment stability. Proceedings of the Institution of Civil Engineers. Geotechnical Engineering. October 2004, Issue GE4, pp. 193-198.

Ridley, A., Wray, W., (1996), Suction measurement: theory and practice. A state of-the-art-review. Proceedings 1st International Conference of Unsaturated Soils, Paris 3, pp. 1293-1322.

Romero, E., (1999), Characterisation and thermo-hydro-mechanical behavior of unsaturated boom clay: An experimental study. Ph.D. thesis, Universitat Politècnia de Catalunya, Barcelona.

Romero, E., Gens, A., Lloret, A., (1999), Water permeability, water retention and microstructure of unsaturated boom clay. Engineering Geology., 54, pp. 117-127.

Romero, E., Simms, P., (2008), Microstructure investigation in unsaturated soils: A review with special attention to contribution of mercury intrusion porosimetry and environmental scanning electron microscopy. Geotechnical and Geological Engineering., DOI 10.1007/s10706-008-9204-5, pp. 1-23.

Sai, J., Anderson, D., (1990), Field hydraulic conductivity tests for compacted soil liners. Geotechnical Testing Journal., 13 (3), pp. 215-225.

Samouëlian, A., Cousin, I., Richard, G., Tabbagh, A., Bruand, A., (2003), Electrical resistivity imaging for detecting soil cracking at the centimetric scale. Soil Science Society of America Journal., 67 (5), pp. 1319-1326.

Sentenac, P., Zielinski, M., (2009), Clay fine fissuring monitoring using miniature geo-electrical resistivity arrays. Journal of Environmental Geology. DOI:10.1007/s12665-009-0017-5 online

Simms, P., Yanful, E., (2001), Measurement and estimation of pore shrinkage and pore distribution in a clayey till during soil-water characteristic curve tests. Canadian Geotechnical Journal., 38, pp. 741-754.

Simms, P., Yanful, E., (2002), Predicting soil-water characteristic curves of compacted plastic soils from measured pore-size distributions. Géotechnique., 52 (4), pp. 269-278.

Sivakumar Babu, G., Gartung, E., (2001), Methodology for prediction of desiccation of clay liners. Clay Science for Engineering. Balkema, Rotterdam.

Skempton, A., (1960), Efective stress in soils, concrete and rock. Pore Pressures and Suction in Soils. Conference organized by the British National Society of the International Society of Soil Mechanics and Foundation Engineering at the Institution of Civil Engineers held on March 30th and 31st, 1960.

Smethurst, J., Clarke, D., Powrie, W., (2006), Seasonal changes in pore water pressure in a grass-covered cut slope in London clay. Géotechnique., 56 (8), pp. 523-537.

Srivastava, R., Yeh, T.C.J., (1991), Analytical solutions for one-dimensional, transient infiltration toward the water table in homogeneous and layered soils. Water Resources Research., 27 (5), pp. 753-762.

Stark, T., Eid, H., (1997), Slope stability analyses in stiff fissured clays. Journal of geotechnical and geoenvironmental engineering., 123 (4), pp. 335-343.

Tabbagh, J., Samouëlian, A., Cousin, I., (2007), Numerical modelling of direct current electrical resistivity for the characterisation of cracks in soils. Journal of Applied Geophysics., 62 (4), pp. 313-323.

Take, W., Bolton, M., (2001), The use of centrifuge modelling to investigate progressive failure of overconsolidated clay embankments. Centrifuge and Constitutive Modelling: Two extremes, Ascona, Switzerland, Springman S.M.(ed.).

Take, W., Bolton, M., (2002), A new device for the measurement of negative pore water pressures in centrifuge models. International Conference on Physical Modelling in Geotechnics, St. John's. Rotterdam: Balkema.

Take, W., Bolton, M., (2004), Tensiometer saturation and reliable measurement of soil suction. Géotechnique., 54 (3), pp. 229-232.

Tarantino, A., (2003) Panel report: Direct measurement of soil water tension. Proceedings 3rd International Conference on Unsaturated Soils.

Tarantino, A., Mongovi, L., (2003), Calibration of tensiometer for direct measurement of matric suction. Géotechnique., 53 (1), pp. 137-141.

Terzaghi, K., (1943), Theoretical soil mechanics. Wiley, New York.

Tezel, O., Özçep, F., (2003), Relationships of electrical resistivity and geotechnical parameters. 3rd International Conference on Earth Sciences and Electronics, Proceedings, ed. By O.N.Uçan and A. M. Albora 1, pp. 137-146.

Tinjum, J., Benson, C., Blotz, L., (1997), Soil-water characteristic curves for compacted clays. Journal of geotechnical and geoenvironmental engineering., 123 (11), pp. 1060-1069.

Trandafr, A., Gomi, T., (2008), Monitored and simulated variations in matric suction during rainfall in a residual soil slope. Environmental Geology., 55, pp. 951-961.

Trast, J., Benson, C., (1995), Estimating field hydraulic conductivity of compacted clay. Journal of Geotechnical Engineering., 121 (10), pp. 736-739.

UMS User Manual for INFIELD7C. Handheld measuring device. UMS, Germany.

UMS User Manual for SWT4e Tensiometer. UMS, Germany.

UMS User Manual for SWTS1 Self-refling Tensiometer. UMS, Germany.

Van, M.A., Koelewijn, A.R., and Barends, F.B.J., (2005), Uplift Phenomenon: Model, Validation, and Design. International Journal of Geomechanics., 5 (2), June 2005, pp. 98-106.

van Genuchten, M., (1980), A closed-form equation for predicting the hydraulic conductivity of unsaturated soils. Soil Science Society of America Journal., 44, pp. 892-898.

Vatsala, A., Srinivasa Murthy, B., (2003), Suction in compacted states. Discussion. Géotechnique., 53 (9), pp. 839-841.

Washburn, E., (1921), Note on a method of determining the distribution of pore sizes in a porous material. Proceedings of the National Academy of Sciences., 7, pp. 115-116.

Wendling, S., Meiÿner, H., (2001), Soil water suction and compaction influence on desiccation cracks of mineral liners. Clay Science for Engineering. Balkema, Rotterdam.

Williams, P., (1982), The surface of the Earth, an introduction to geotechnical science. Longman Inc., New York.

Wu, T., Randolph, B., Huang, C.S., (1993), Stability of shale embankments. Journal of geotechnical engineering., 119 (1), pp. 127-146.

Yoshida, S., Adachi, K., (2001), Influence of the distribution of soil suction on crack patterns in farmlands. Clay Science for Engineering. Balkema, Rotterdam.

Zhou, J., You, J.-l., (2005), Influences affecting the soil-water characteristic curve. Journal of Zhejiang University, Science 6A(8), pp. 797-804.

CHAPTER 14

14. ANNEXES

14.1. ANNEX A - FIGURES

14.1.1. CRACKS RECORDED DURING INSPECTION AT THORNGUMBALD

14.1.1.1. New embankment - cracks on the crest

Figure 14.1 Cracks on the crest.

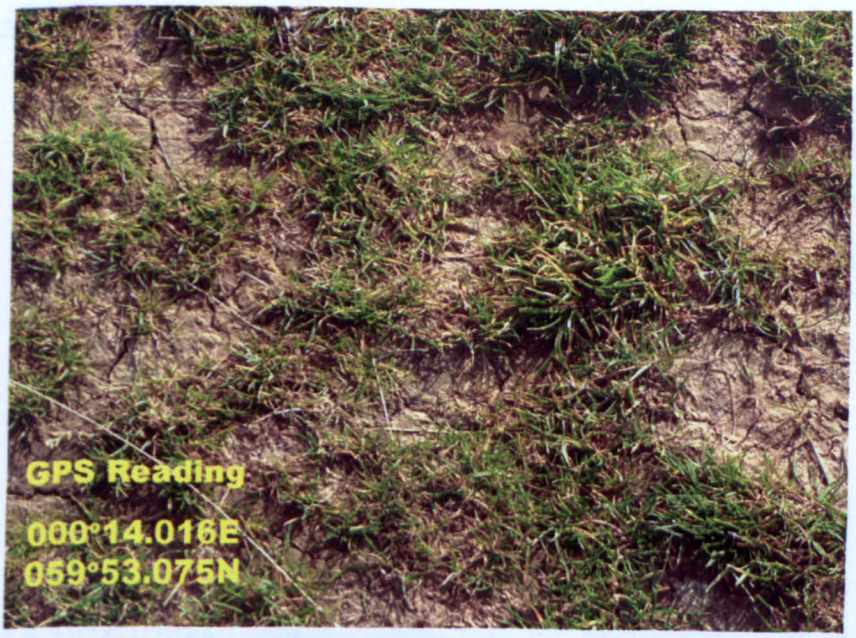

Figure 14.2 Cracks on the crest.

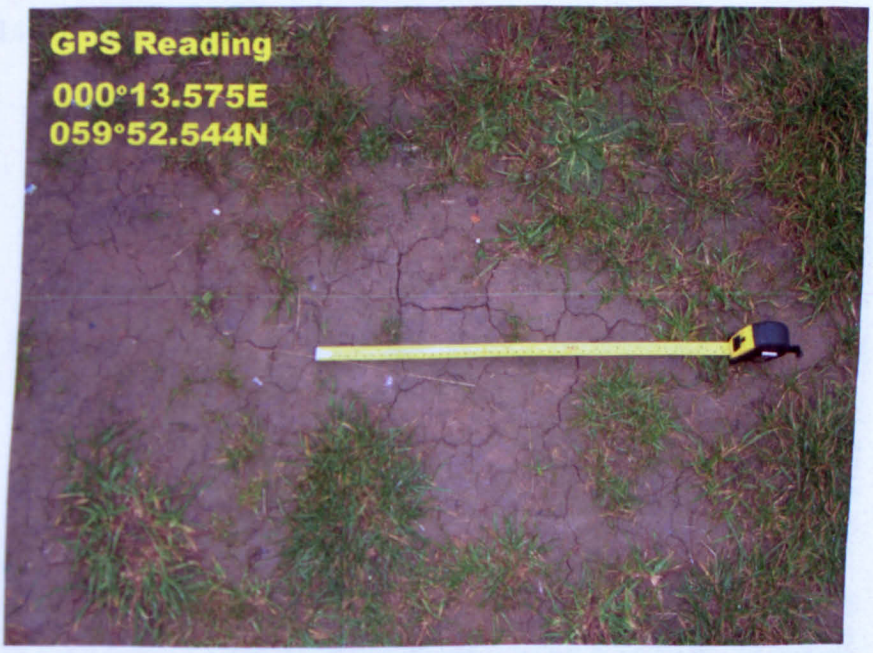

Figure 14.3 Cracks on the crest.

14.1.1.2. New embankment - cracks on the slope

Figure 14.4 Crack on the slope.

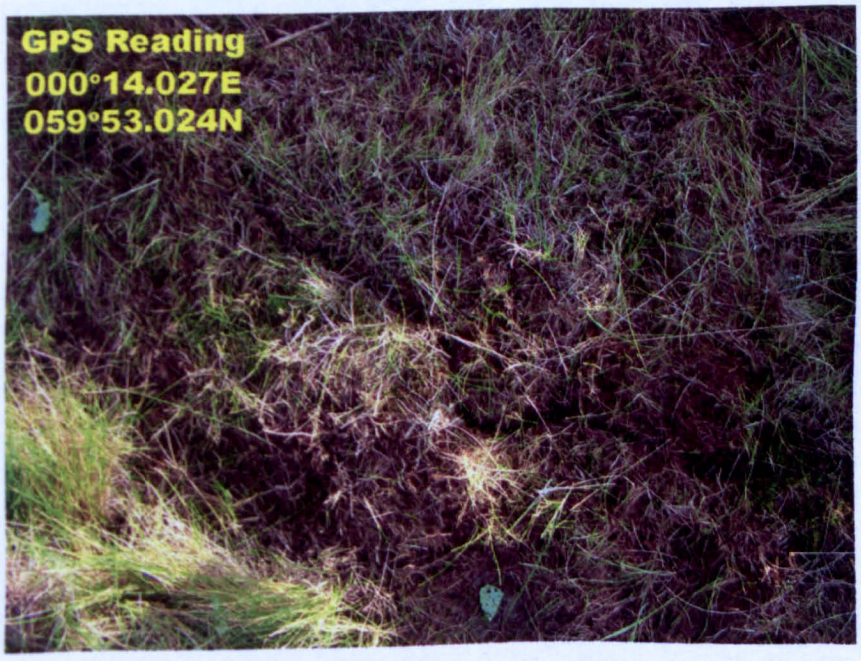

Figure 14.5 Crack on the slope.

Figure 14.6 Crack on the slope with the length.

14.1.2. HAND EXCAVATION ON THE NEW EMBANKMENT

Figure 14.7 Hand excavation on the new embankment.

Figure 14.8 Hand excavation on the new embankment.

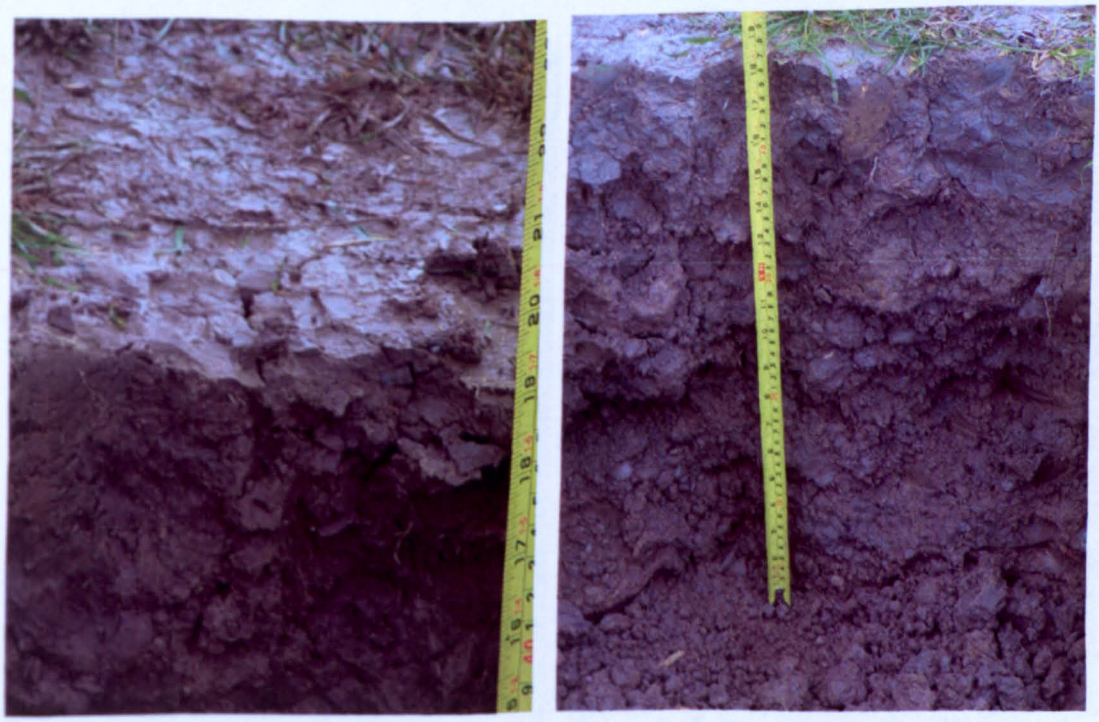

Figure 14.9 Observed cracks in trench excavated along the new embankment.

14.1.3. HAND EXCAVATION ON THE HISTORIC EMBANKMENT

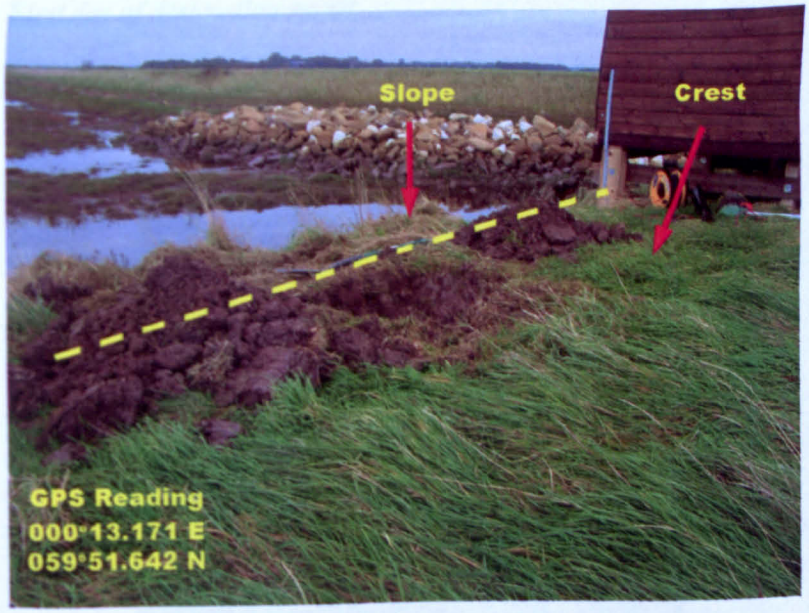

Figure 14.10 Trial trench on the old embankment.

Figure 14.11 Left picture - vertical crack (depth-300mm), right picture - crack network (depth-400mm).

14.1.4. CRACKING GROWTH DURING FIRST WEEK OF DRYING

14.1.4.1. First day of desiccation phase

Figure 14.12 Downstream side of the embankment.

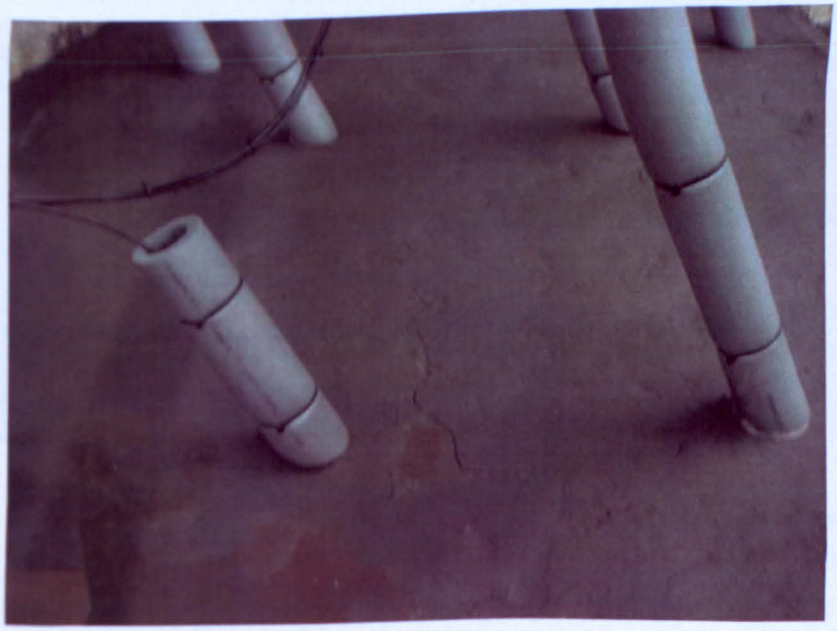

Figure 14.13 Crest of the embankment.

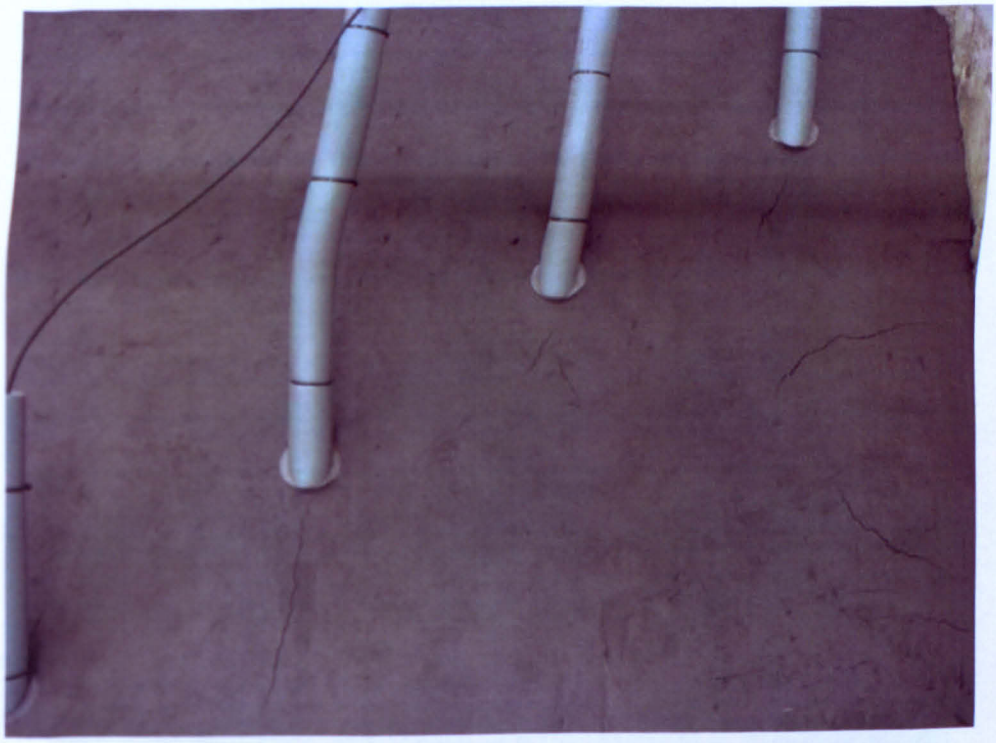

Figure 14.14 Upstream side of the embankment.

14.1.4.2. Second day of desiccation phase

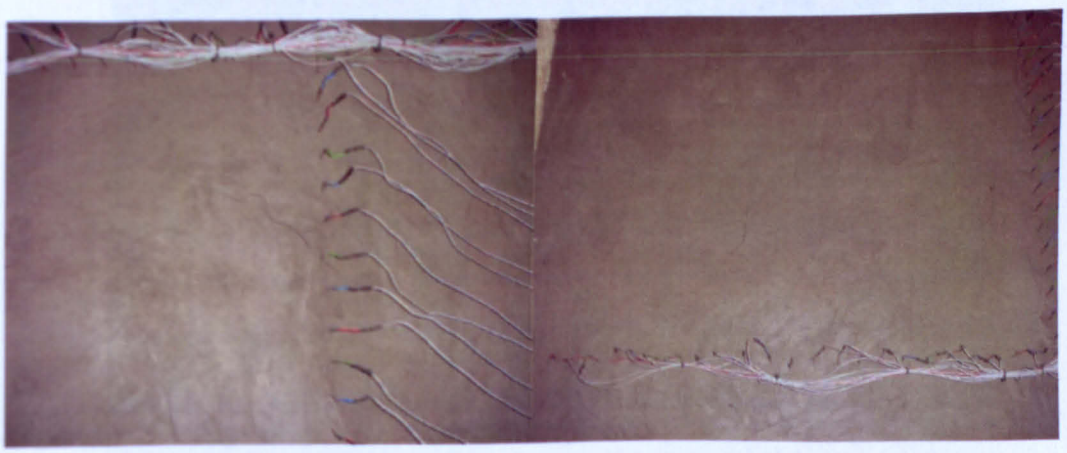

Figure 14.15 Downstream side of the embankment.

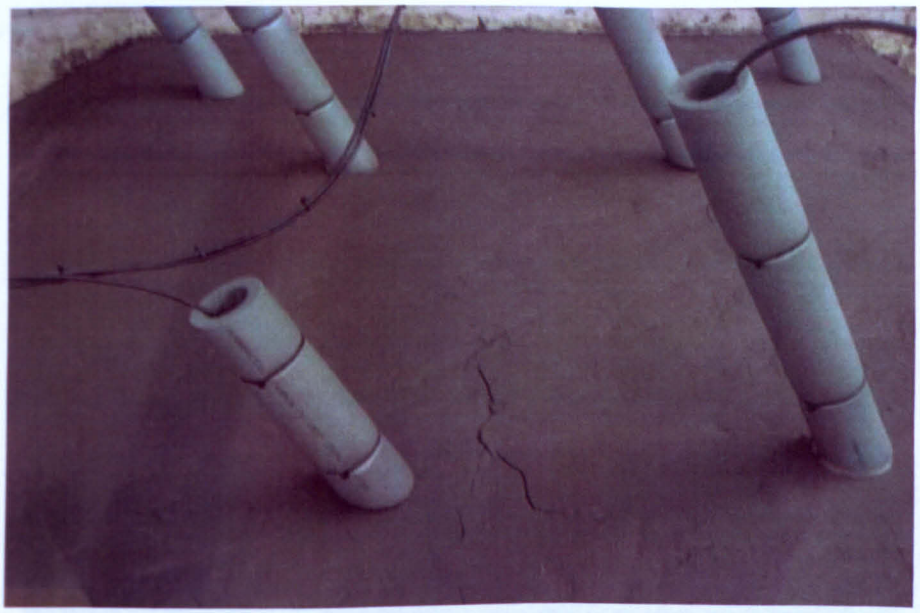

Figure 14.16 Crest of the embankment.

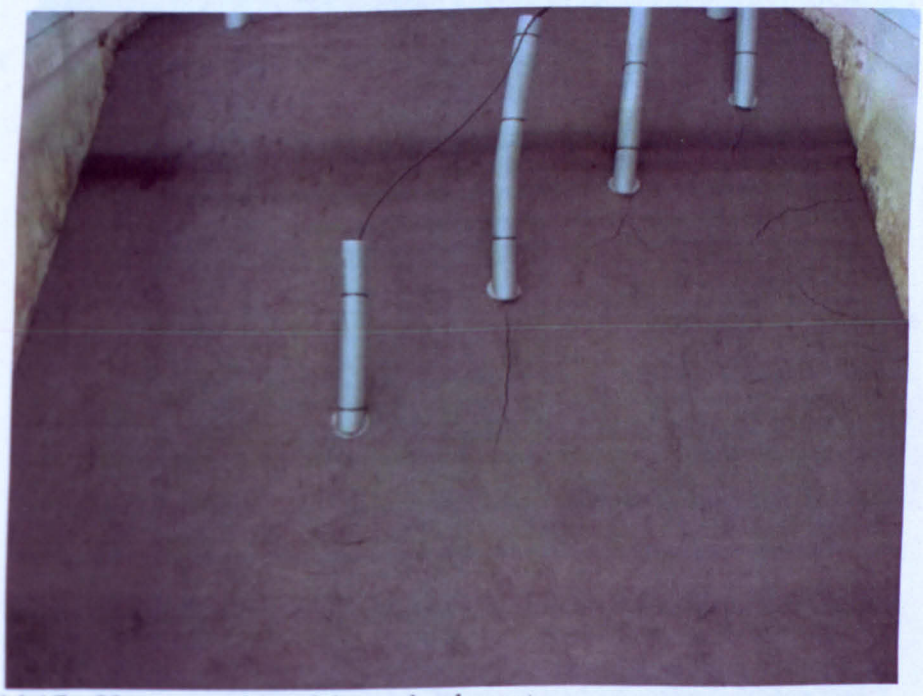

Figure 14.17 Upstream side of the embankment.

14.1.4.3. Third day of desiccation phase

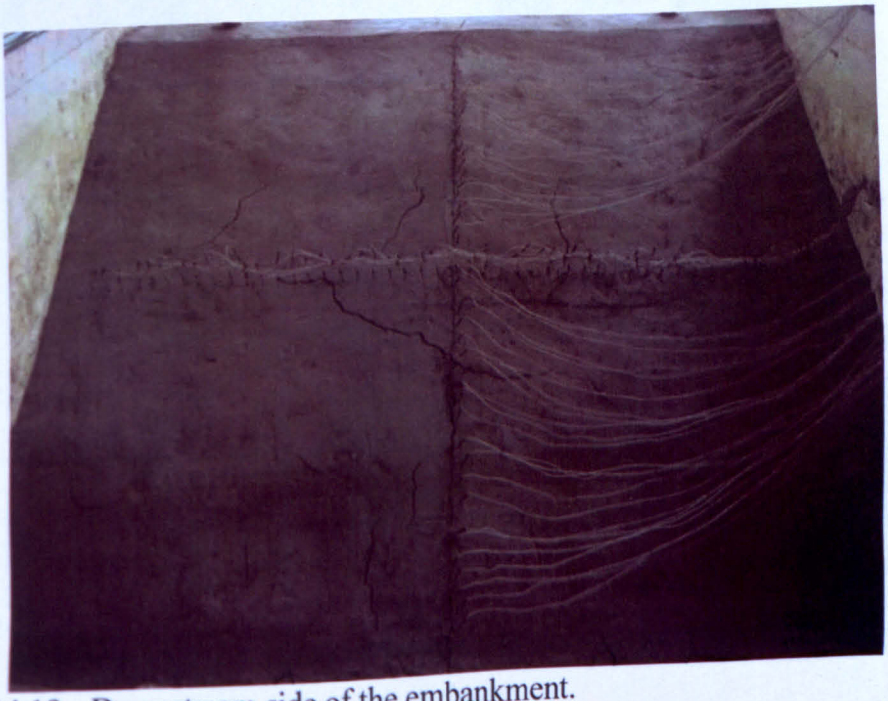

Figure 14.18 Downstream side of the embankment.

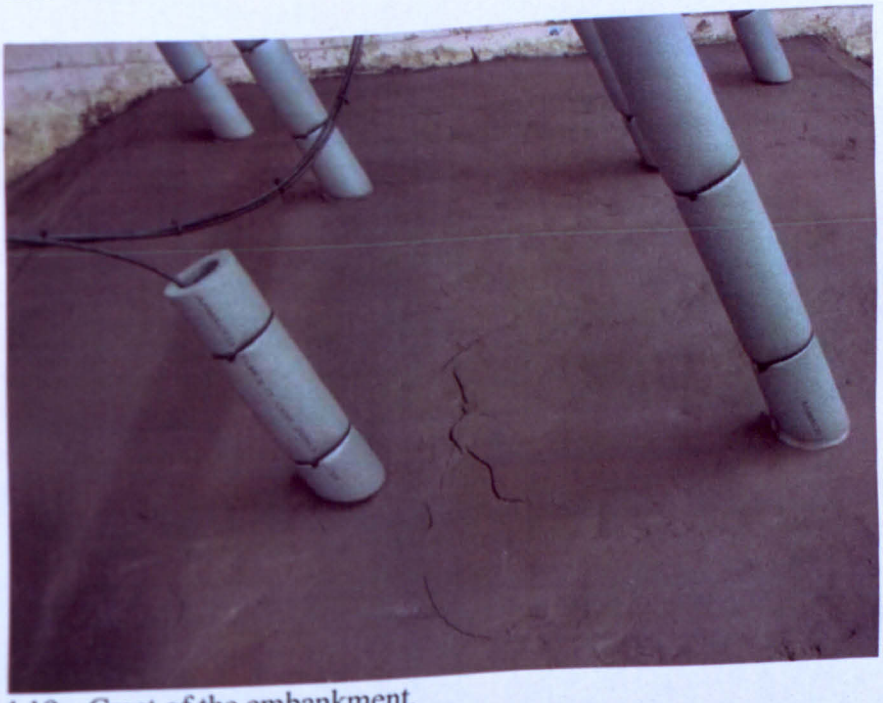

Figure 14.19 Crest of the embankment.

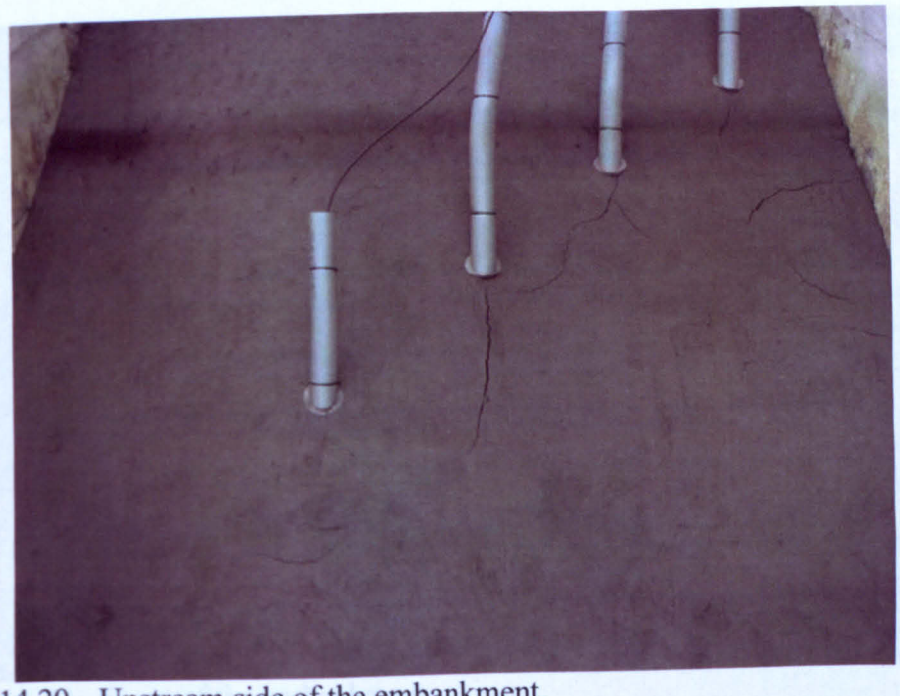

Figure 14.20 Upstream side of the embankment.

14.1.4.4. Fourth day of desiccation phase

Figure 14.21 Downstream side of the embankment.

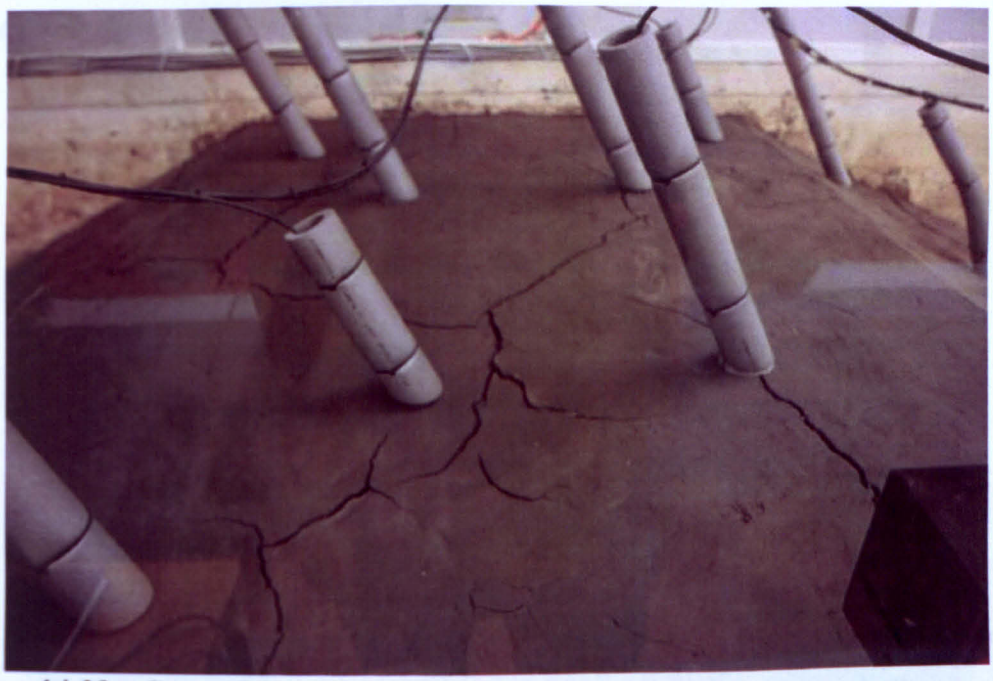

Figure 14.22 Crest of the embankment.

Figure 14.23 Upstream side of the embankment.

14.1.4.5. Fifth day of desiccation phase

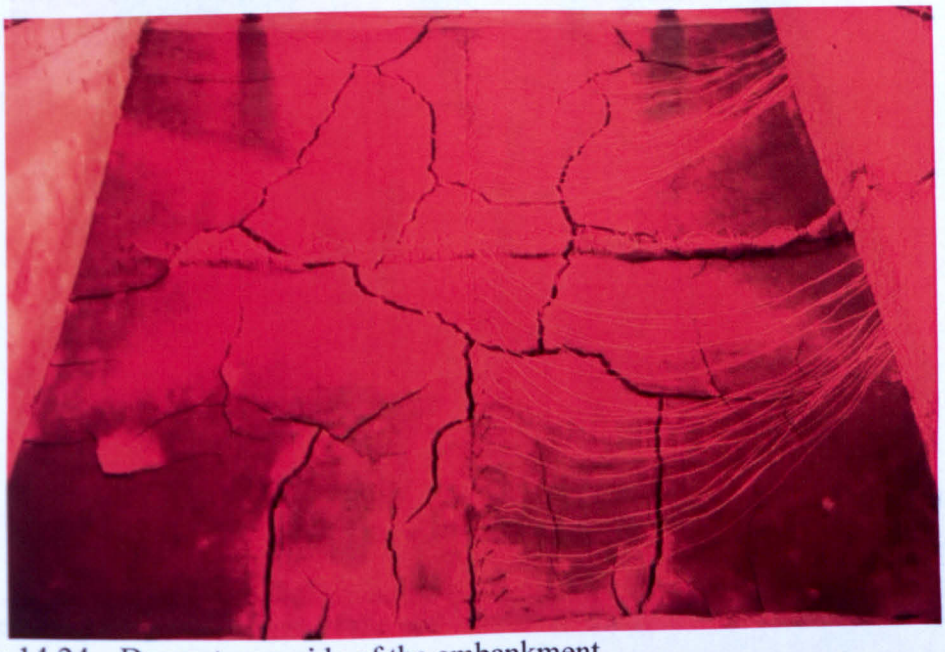

Figure 14.24 Downstream side of the embankment.

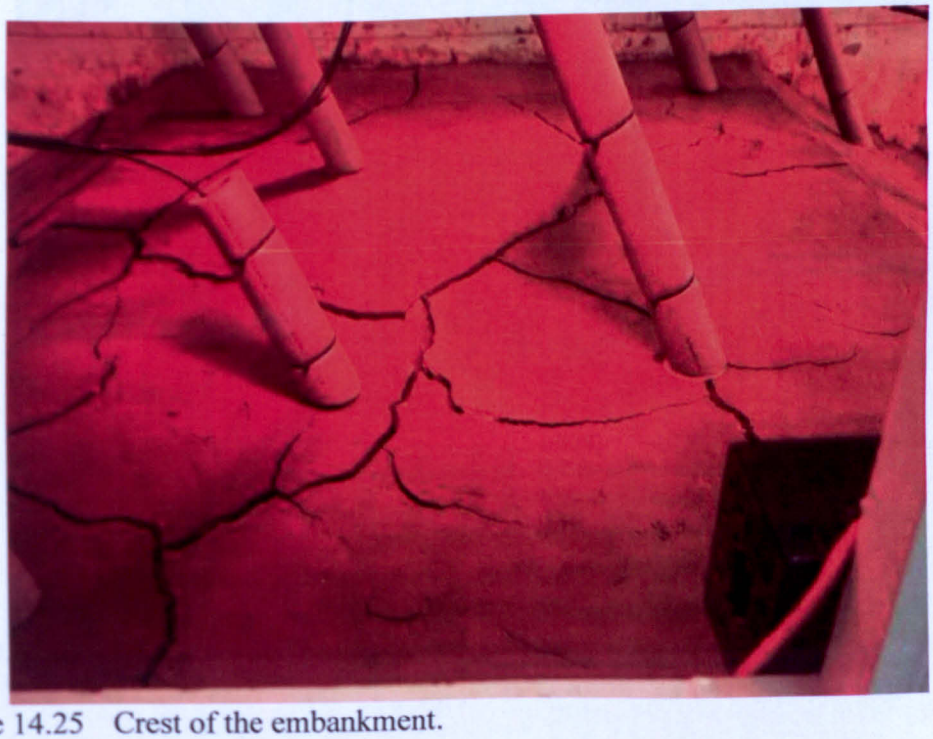

Figure 14.25 Crest of the embankment.

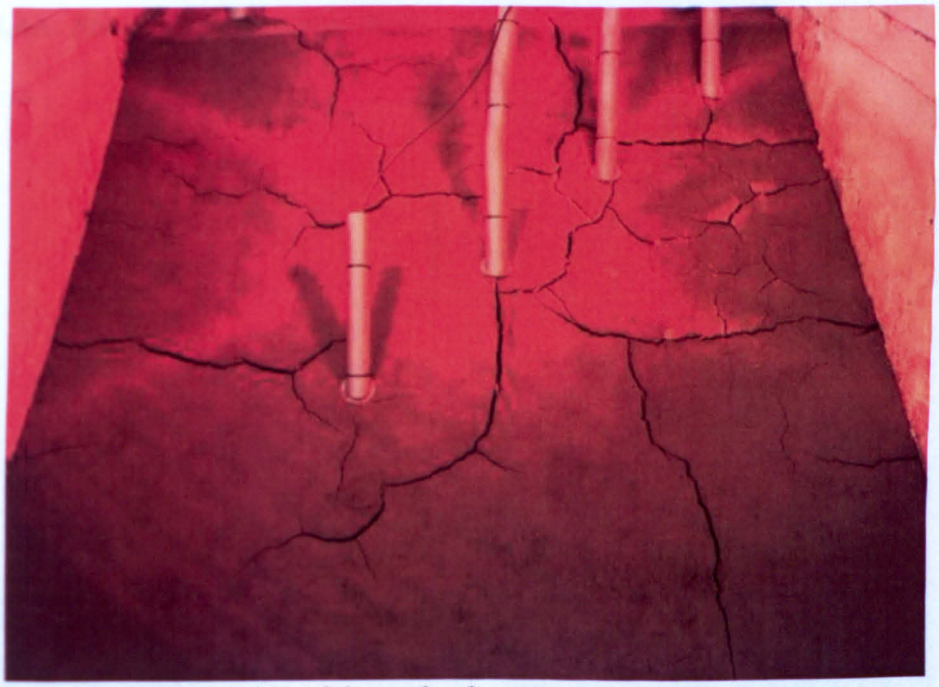

Figure 14.26 Upstream side of the embankment.

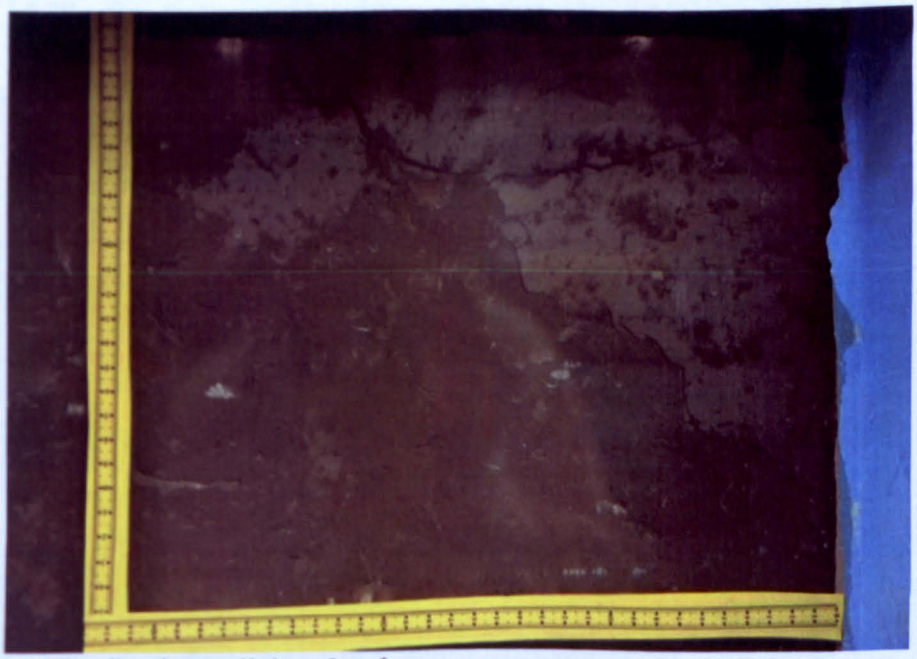

Figure 14.27 Crack parallel to the slope.

14.1.4.6. Sixth day of desiccation phase

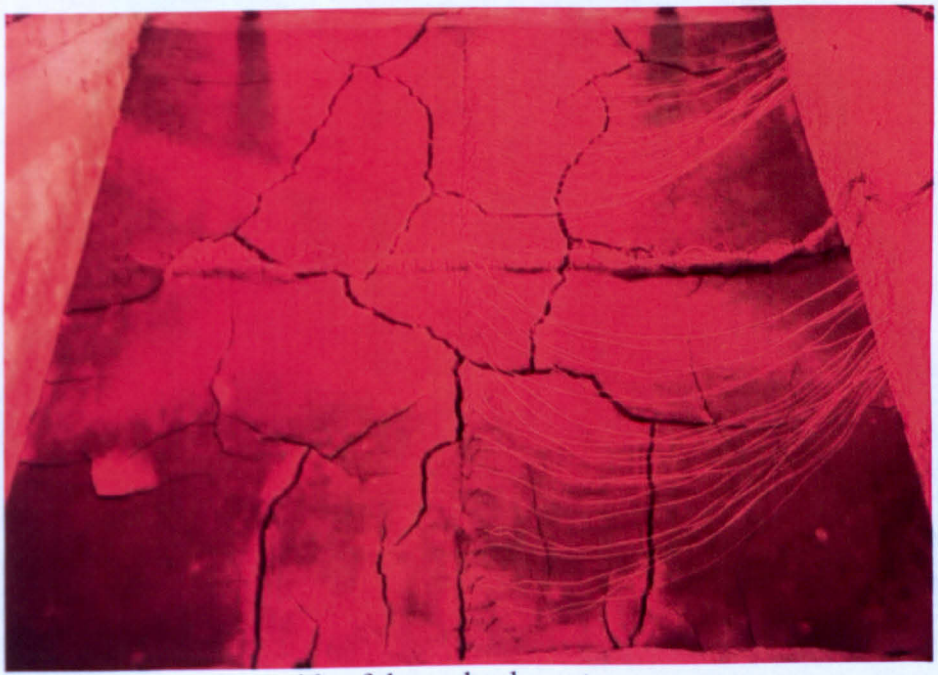

Figure 14.28 Downstream side of the embankment.

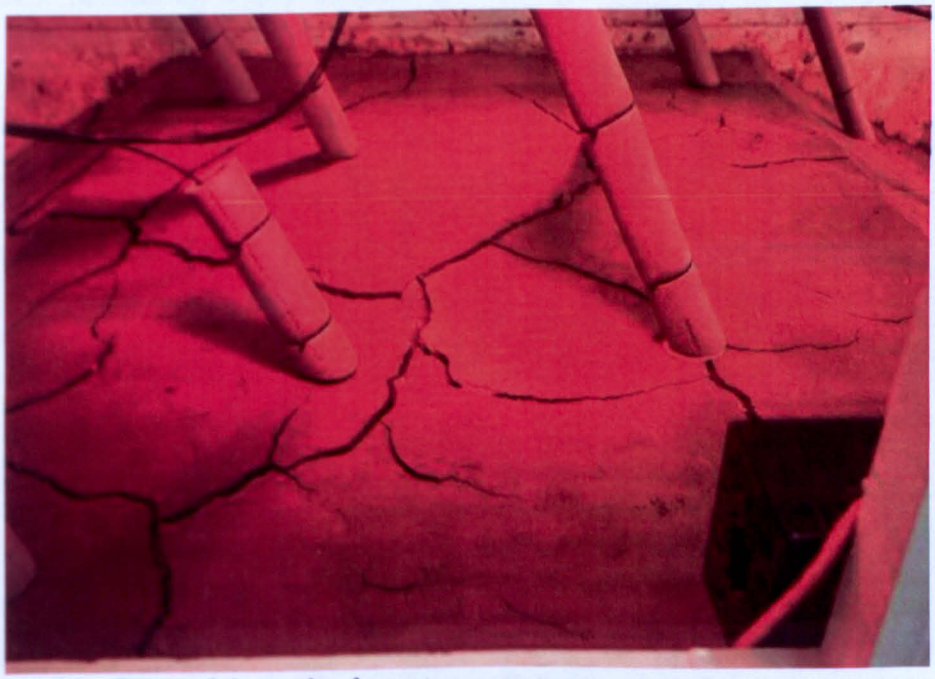

Figure 14.29 Crest of the embankment.

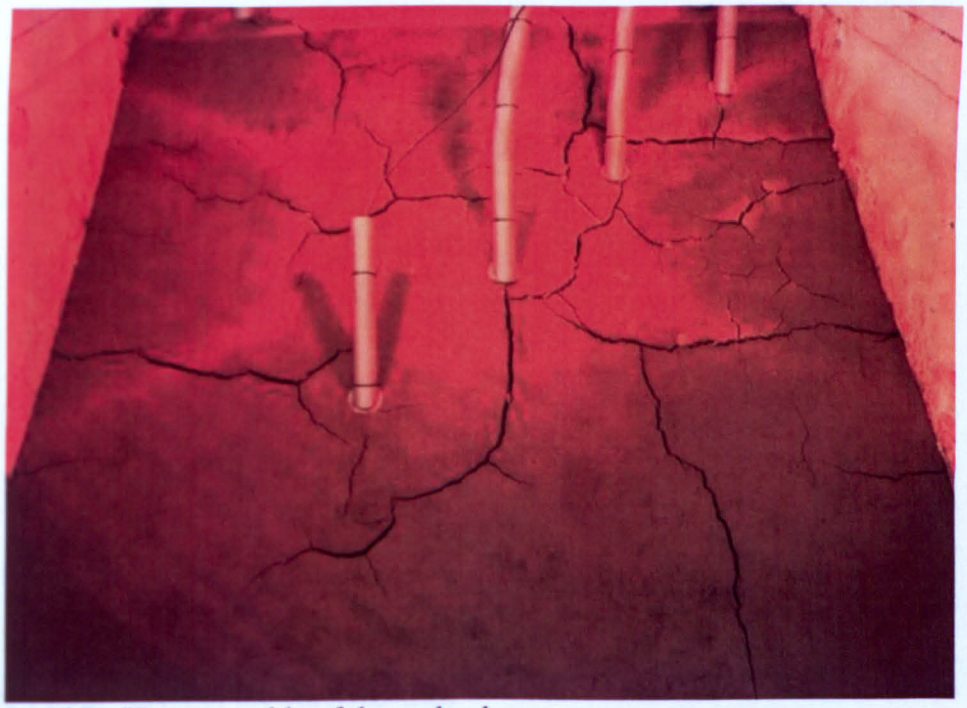

Figure 14.30 Upstream side of the embankment.

14.1.4.7. Seventh day of desiccation phase

Figure 14.31 Downstream side of the embankment.

Figure 14.32 Crest of the embankment.

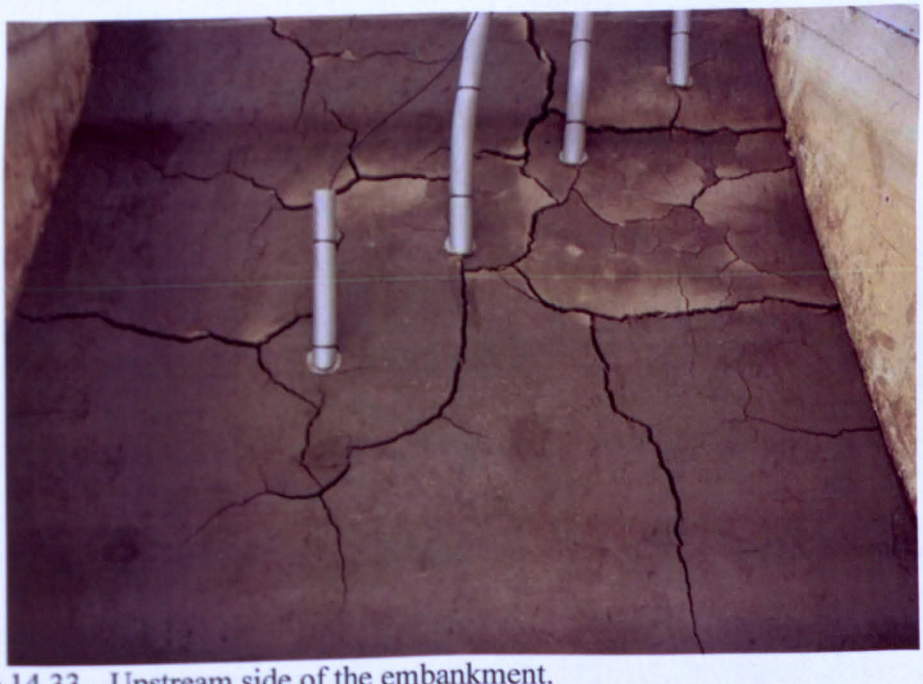

Figure 14.33 Upstream side of the embankment.

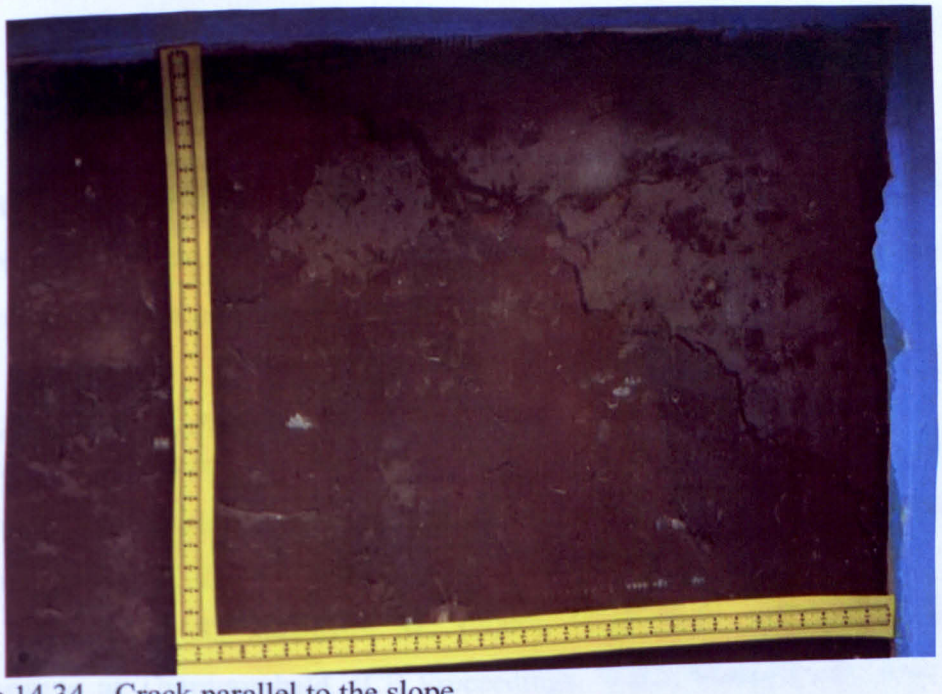

Figure 14.34 Crack parallel to the slope.

14.2. ANNEX B - LIST OF PUBLISHED PAPERS RELATED TO PRESENTED RESEARCH

A part of this thesis has led to three journal publications four conference papers and four research reports. The full list of publications is presented below. The copies of the Journal Papers are attached at the end of this paragraph.

14.2.1. JOURNAL PAPERS

Zielinski, M., Sentenac, P., McCloskey, G., Dyer, M., (2009), Desiccation cracking detection using resistivity array. Under review. ICE Proceedings. Geotechnical Engineering. GE-D-09-00068

Dyer, M.R., Utili, S., **Zielinski, M.,** (2009), Field study into fine desiccation fissuring at Thorngumbald. ICE Proceedings. Water Management. June 2009, Issue WM3, pp.221-232

Sentenac, P., and **Zielinski, M.,** (2009), Clay fine fissuring monitoring using miniature geo-electrical resistivity arrays. Journal of Environmental Geology. DOI:10.1007/s12665-009-0017-5 online

14.2.2. CONFERENCE PAPERS

Zielinski, M., Romero, E., Sentenac, P., Sanchez, M., (under review), Comparison of four methods for determining the soil water retention curve. Fifth International Conference on Unsaturated Soils. UNSAT 2010, Barcelona, Spain, 2010.

Zielinski, M., Sentenac, P., (under review), Desiccation Cracking in Flood Defences and its Detection Using Miniature Resistivity Array. 6th International Congress on Environmental Geotechnics., New Dehli, India, 2010.

Zielinski, M., Sentenac, P., Utili, S., Dyer, M., (2008), Influences of the weather changes on the desiccation fissuring propagation and stability of flood embankments. 11th Baltic Sea Geotechnical Conference, Gdansk (Poland), Vol. 2, pp. 647-655

Utili, S., Dyer, M., Redaelli, M. & **Zielinski, M.,** (2008), Desiccation fissuring induced failure mechanisms for clay levees. 10th Int. Symp. on Landslides and Engineered Slopes, ISSMGE, Xian (China), pp. 1309-1314.

Utili, S., Dyer, M.R., **Zielinski, M.**, (2008), Failure mechanisms and ultimate resistance of earth flood embankment with attention to desiccation fissuring. Canadian Society for Civil Engineering Annual Conference, Quebec city (Canada), CD-ROM, paper TR-502

Redaelli, M., Dyer, M., Utili, S. and **Zielinski, M.**, (2007) 'Flood embankments reliability rating'. ISL in China

14.2.3. RESEARCH REPORTS

Piontkowitz, T., Verhagen, H.J., Verheij, H., Mai Cao, T., Dassanayake, D., Roelvink, D., Utili, S., **Zielinski, M.**, Kont, A., Ploompuu, T. (2009), EroGRASS - Failure of Grass Cover Layers at Seaward and Shoreward Dike Slopes. Design, Construction and Performance. First Interim Research Report. www.kyst.dk/erograss

Zielinski, M., Sentenac, P., Dyer, M., (2009), Influence of the desiccation fine fissuring on the stability of flood embankments. Laboratory Testing. Department of Civil Engineering, Strathclyde University. FRMRC EPSRC grant GR/S76304/01, Report UR14, http://www.floodrisk.org.uk/

Utili, S., **Zielinski, M.**, Dyer, M., (2008), Failure modes and breach initiation. Report to the Environment Agency, Grant SC050059. Civil Engineering Department, Strathclyde University.

Dyer, M., Utili, S., **Zielinski, M.**, (2007), Influence of the desiccation fine fissuring on the stability of flood embankments. Department of Civil Engineering, Strathclyde University. FRMRC EPSRC grant GR/S76304/01, Report UR11, http://www.floodrisk.org.uk/